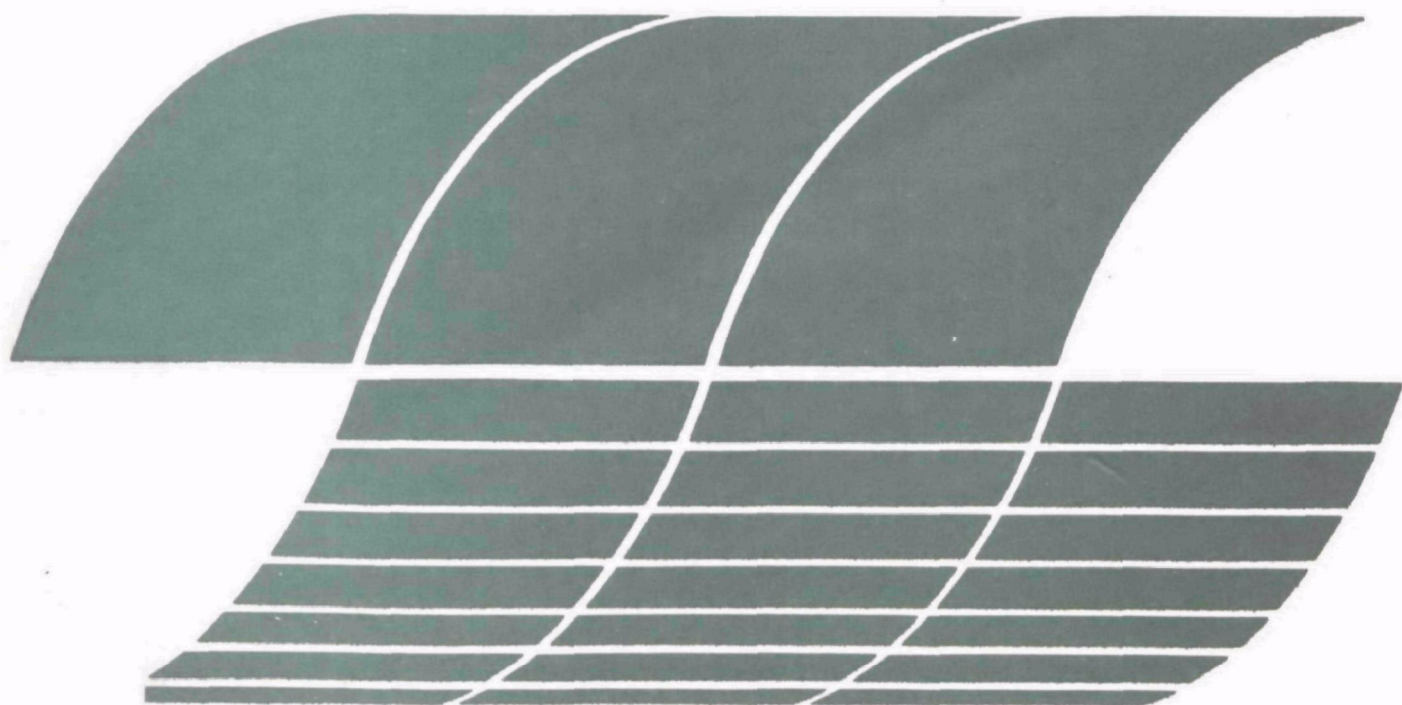




Electrostatic Precipitators for Collection of High Resistivity Ash

Interagency
Energy/Environment
R&D Program Report



RESEARCH REPORTING SERIES

Research reports of the Office of Research and Development, U.S. Environmental Protection Agency, have been grouped into nine series. These nine broad categories were established to facilitate further development and application of environmental technology. Elimination of traditional grouping was consciously planned to foster technology transfer and a maximum interface in related fields. The nine series are:

1. Environmental Health Effects Research
2. Environmental Protection Technology
3. Ecological Research
4. Environmental Monitoring
5. Socioeconomic Environmental Studies
6. Scientific and Technical Assessment Reports (STAR)
7. Interagency Energy-Environment Research and Development
8. "Special" Reports
9. Miscellaneous Reports

This report has been assigned to the INTERAGENCY ENERGY-ENVIRONMENT RESEARCH AND DEVELOPMENT series. Reports in this series result from the effort funded under the 17-agency Federal Energy/Environment Research and Development Program. These studies relate to EPA's mission to protect the public health and welfare from adverse effects of pollutants associated with energy systems. The goal of the Program is to assure the rapid development of domestic energy supplies in an environmentally-compatible manner by providing the necessary environmental data and control technology. Investigations include analyses of the transport of energy-related pollutants and their health and ecological effects; assessments of, and development of, control technologies for energy systems; and integrated assessments of a wide range of energy-related environmental issues.

EPA REVIEW NOTICE

This report has been reviewed by the participating Federal Agencies, and approved for publication. Approval does not signify that the contents necessarily reflect the views and policies of the Government, nor does mention of trade names or commercial products constitute endorsement or recommendation for use.

This document is available to the public through the National Technical Information Service, Springfield, Virginia 22161.

EPA-600/7-79-189

August 1979

Electrostatic Precipitators for Collection of High Resistivity Ash

by

D.H. Pontius, P.V. Bush, and W.B. Smith

**Southern Research Institute
2000 Ninth Avenue, South
Birmingham, Alabama 35205**

**Contract No. 68-02-2193
Program Element No. EHE624**

EPA Project Officer: Leslie E. Sparks

**Industrial Environmental Research Laboratory
Office of Energy, Minerals, and Industry
Research Triangle Park, NC 27711**

Prepared for

**U.S. ENVIRONMENTAL PROTECTION AGENCY
Office of Research and Development
Washington, DC 20460**

EXECUTIVE SUMMARY

This research program included as principal objectives the comparison of various types of electrode systems for charging fine, high-resistivity dusts, the investigation of techniques for charging high resistivity dusts in a high current density corona system, performance of a laboratory scale study to determine the technical feasibility of selected charging systems, and finally the design, fabrication and testing of a $0.47 \text{ m}^3/\text{sec}$ (1000 acfm) pilot-scale precharger applicable to a two-stage system for electrostatic precipitation of high resistivity particulate materials. As a preliminary step, the literature was reviewed for indications of previous attempts to control back corona resulting from the presence of high resistivity dust in an electrostatic precipitator. Limited theoretical and experimental investigations were carried out to eliminate impracticable techniques and to develop novel approaches to the solution of the problem. This work resulted in the derivation of a new three-electrode particle charging device (precharger) upon which further developments in this project were based.

The general concept of the three-electrode precharger is that a properly biased, open mesh screen electrode placed near the grounded plate electrode in a wire plate system will serve to remove a large portion of the ions resulting from back corona, while permitting a reasonably high primary corona current to pass. This concept was tested in a small laboratory device, where it was found that back corona effects could be controlled sufficiently well to permit charging of dusts having electrical resistivity above 10^{12} ohm-cm to levels that could be achieved for low and moderate resistivity dusts ($<5 \times 10^{10} \text{ ohm-cm}$) in a conventional corona geometry.

As a consequence of the laboratory scale work, a pilot scale system was designed and fabricated for testing at a gas volume flowrate of approximately 1000 ACFM. The tests performed on that device demonstrated good charging results, but also revealed the necessity for improvements in the mechanical design. Hence a second generation, ruggedized version of the $0.47 \text{ m}^3/\text{sec}$ charger was designed, constructed and tested. Charging results remained consistent with those of previous tests.

Used with a modified conventional pilot-scale ESP as a second stage (collector) the precharger was tested as a part of a two-stage system. Measurements of particle size distributions and mass loadings at the inlet and outlet of the system showed overall collection efficiency above 90% when operated at a specific collection area of $25.2 \text{ m}^2/\text{m}^3/\text{sec}$ ($128 \text{ ft}^2/1000 \text{ acfm}$) where the dust resistivity was above 10^{12} ohm-cm .

These tests indicate the feasibility of making substantial size reductions, with concomitant economic savings, in the fabrication of electrostatic precipitators applied to the collection of high resistivity dusts.

This report has been submitted in fulfillment of Contract No. 68-02-2193 by Southern Research Institute under the sponsorship of the U. S. Environmental Protection Agency. This report covers a period from September 30, 1976 to July 31, 1978, and work was completed as of September 30, 1978.

CONTENTS

Executive Summary	i
Figures	iv
Tables	x
Acknowledgements	xi
1. Introduction	1
2. Summary and Recommendations	5
Laboratory studies	5
Pilot scale program	6
Recommendations	6
3. Preliminary Studies	8
Description of three-electrode concept	8
Bench-scale tests	9
Laboratory scale precharger	17
Electrode geometry studies	21
4. Pilot Scale Precharger	43
Initial pilot test program	43
Installation of automatic screen voltage control	67
Pilot tests at IERL/RTP	70
Summary of tests results	75
Second generation pilot precharger	77
5. Charged Particle Collector	87
6. Engineering and Cost Analysis	99
Estimated costs of full scale precharger --	
collector systems	99
Comparisons of costs with conventional precipitators	105
References	112
Appendices	
A. Investigation of alternate methods	A-1
B. Theoretical study of space charge effects	B-1
C. Precharger	C-1
D. Collector	D-1

FIGURES

<u>Number</u>	<u>Page</u>
1 Apparatus used for preliminary evaluation of three-electrode corona geometry concept.	10
2 Current as a function of time for each electrode. Corona discharge electrode is at -25 kV, and screen electrode is at -9 kV. Dust laden air is injected at 1.2 l/min.	11
3 Current as a function of time for each electrode. Corona electrode is at -25 kV. The screen electrode is at 8.5 kV, which is below the magnitude of potential required to accept ions resulting from back corona at the plate. Screen voltage was shifted momentarily to -9 kV at $t = 6$ min.	13
4 Current as a function of time for corona discharge electrode and plate electrode as a function of time, with dust injection. Screen electrode was removed, and voltage is -25 kV. Losses to oven walls account for current difference.	14
5 Current as a function of time for each electrode, with corona discharge electrode at -22 kV. The screen electrode was initially set at 8.5 kV, and reduced to 8.0 kV after 30 min. running time.	15
6 Current for each electrode in the three-electrode system. The vertical dashed lines denote times at which voltage changes were made to the values indicated. Initially the discharge electrode voltage was 15 kV and the screen voltage was 8 kV.	16
7 Laboratory scale precharger assembly in the three-electrode configuration.	18
8 Bare plate I-V characteristics at ambient and at 130°C with corona electrode-to-plate spacing = 8.89 cm.	19
9 Comparison of the I-V characteristics of the three-electrode configuration with grid-to-plate spacings of 1.0 and 2.5 cm. The corona electrode-to-plate spacing = 8.89 cm, temperature = 130°C, and the grid current = 0 μ A.	20

<u>Number</u>		<u>Page</u>
10	Test results of a three-electrode charger used for back corona suppression. Temperature = 125°C, corona electrode-to-plate spacing = 8.9 cm, grid electrode-to-plate spacing = 2.6 cm, and dust loading $\approx 3.4 \text{ g/m}^3$	22
11	Test results of a three-electrode charger used for back corona suppression. Temperature = 125°C, corona electrode-to-plate spacing = 8.9 cm, grid electrode-to-plate spacing = 2.6 cm, and dust loading $\approx 3.4 \text{ g/m}^3$	23
12	Test results of a three-electrode charger used for back corona suppression. Temperature = 130°C, corona electrode-to-plate spacing = 8.9 cm, grid electrode-to-plate spacing = 2.6 cm, and dust loading $\approx 6.8 \text{ g/m}^3$	24
13	Comparison of theoretical and experimental I-V characteristics for a wire-plate configuration with 11 cm plate width and 9 cm electrode separation.	26
14	Comparison of theoretical and experimental I-V characteristics for a wire-plate configuration with 11 cm plate width and 3 cm electrode separation.	27
15	Comparison of theoretical and experimental I-V characteristics for a wire-plate configuration with 11 cm plate width and 2 cm electrode separation.	28
16	Comparison of theoretical and experimental I-V characteristics for a wire-plate configuration with 5.5 cm plate width and 5 cm electrode spacing.	29
17	Comparison of theoretical and experimental I-V characteristics for a wire-plate configuration with 2.75 cm plate width and 9 cm electrode separation.	30
18	Comparison of theoretical and experimental I-V characteristics for a wire-plate configuration with 2.75 cm plate width and 2 cm electrode separation.	31
19	Ratio of apparent to actual plate width used to provide best theoretical fit for various values of plate width to electrode separation ratio.	32
20	Electrical characteristics of a parallel wire-plate corona electrode system for five values of electrode spacing. Plate width is 11 cm, and wire diameter is 0.25 mm.	33

<u>Number</u>		<u>Page</u>
21	Electrical characteristics of a parallel wire-plate corona electrode system for five values of electrode spacing. Plate width is 5.5 cm, and wire diameter is 0.25 mm.	34
22	Electrical characteristics of a parallel wire-plate corona electrode system for five values of electrode spacing. Plate width is 2.75 cm, and wire diameter is 0.25 mm.	35
23	Electrical characteristics of a parallel wire-plate corona electrode system for five values of electrode spacing. Plate width is 11 cm, and wire diameter is 0.79 mm.	36
24	Electrical characteristics of a parallel wire-plate corona electrode system for five values of electrode spacing. Plate width is 5.5 cm, and wire diameter is 0.79 mm.	37
25	Electrical characteristics of a parallel wire-plate corona electrode system for five values of electrode spacing. Plate width is 2.75 cm, and wire diameter is 0.79 mm.	38
26	Total corona current for fixed length of barbed wire discharge electrode as a function of separation between barbs.	40
27	Corona current per disc for a discharge electrode consisting of discs at various spacings with axes aligned.	41
28	Comparison of I-V characteristics for a 0.02 cm wire, a barbed wire and an array of disc discharge electrodes. The passive electrode is a 14 cm diameter cylinder for all three curves.	42
29	View of the pilot scale charger on its side.	44
30	View of the pilot scale charger electrode configuration.	45
31	Corona current vs. corona voltage characteristics for the precharger with the screen voltage adjusted to maintain zero screen current.	46
32	Results of the dust loading characterization at the pre-charger inlet with the sandblasting gun at 138 Pa (20 psi) . . .	47
33	Results of the dust loading characterization at the pre-charger inlet with the sandblasting gun at 138 Pa (20 psi) . . .	48
34	Results of the dust loading characterization at the pre-charger inlet with the sandblasting gun at 138 Pa (20 psi) . . .	49

<u>Number</u>		<u>Page</u>
35	Results of the dust loading characterization at the pre-charger inlet with the sandblasting gun at 138 Pa (20 psi) . .	50
36	Back corona suppression test results. Test conditions were: $T = 130^{\circ}\text{C}$, $\% \text{H}_2\text{O} = 1.2$ (by volume), average gas volume flowrate = $.71 \text{ m}^3/\text{sec}$ ($1500 \text{ ft}^3/\text{min}$), dust loading = 1.88 g/m^3 , MMD = $25 \text{ }\mu\text{m}$, $E = 3.26 \times 10^5 \text{ V/m}$, and $Nt = 1.4 \times 10^{13} \text{ sec/m}^3$	51
37	Back corona suppression test results. Test conditions were: $T = 130^{\circ}\text{C}$, $\% \text{H}_2\text{O} = 1.2$ (by volume), average gas volume flowrate = $.71 \text{ m}^3/\text{sec}$ ($1500 \text{ ft}^3/\text{min}$), dust loading = 1.88 g/m^3 , MMD = $25 \text{ }\mu\text{m}$, $E = 2.72 \times 10^5 \text{ V/m}$, and $Nt = 1.3 \times 10^{13} \text{ sec/m}^3$	52
38	Back corona suppression test results. Test conditions were: $T = 130^{\circ}\text{C}$, $\% \text{H}_2\text{O} = 1.2$ (by volume), average gas volume flowrate = $.71 \text{ m}^3/\text{sec}$ ($1500 \text{ ft}^3/\text{min}$), dust loading = 1.88 g/m^3 , MMD = $25 \text{ }\mu\text{m}$, $E = 2.61 \times 10^5 \text{ V/m}$, and $Nt = 8.8 \times 10^{12} \text{ sec/m}^3$	53
39	Back corona suppression test at 130°C , $1.2\% \text{ H}_2\text{O}$, $\rho = 1.2 \times 10^{12} \Omega\text{-cm}$, $j = 9.4 \times 10^5 \text{ nA/m}^2$, and the dust loading = 1.88 g/m^3 . .	55
40	Corona current vs. corona voltage for clean and dirty electrodes at 130°C , $1.2\% \text{ H}_2\text{O}$, and $\rho = 1.2 \times 10^{12} \Omega\text{-cm}$. Grid current was held to zero for these measurements.	56
41	Back corona suppression test and Q/m measurement at 75°C , $1.2\% \text{ H}_2\text{O}$, $\rho = 1.4 \times 10^{12} \Omega\text{-cm}$, $j = 9.4 \times 10^5 \text{ nA/m}^2$, dust loading = 1.88 g/m^3 , and $Q/m = 9.6 \times 10^{-6} \text{ C/g}$	57
42	Back corona suppression test and Q/m measurement at 100°C , $1.2\% \text{ H}_2\text{O}$, $j = 9.4 \times 10^5 \text{ nA/m}^2$, dust loading = 1.88 g/m^3 , and $Q/m = 3.0 \times 10^{-6} \text{ C/g}$	60
43	Corona current vs. corona voltage for clean and dirty electrodes at 100°C and $1.2\% \text{ H}_2\text{O}$. Grid current was maintained at zero for these measurements.	61
44	Back corona suppression test at 75°C , $1.2\% \text{ H}_2\text{O}$, $\rho = 1.4 \times 10^{12} \Omega\text{-cm}$, $j = 9.4 \times 10^5 \text{ nA/m}^2$, ash injection at 276 Pa (40 psi) and manual rapping	62
45	Back corona suppression test and Q/m measurement at 75°C , $1.2\% \text{ H}_2\text{O}$, $\rho = 1.4 \times 10^{12} \Omega\text{-cm}$, $j = 9.4 \times 10^5 \text{ nA/m}^2$, ash injection at 276 Pa (40 psi), pneumatic rapping at 552 Pa and $Q/m = 8.7 \times 10^{-6} \text{ C/g}$	63

<u>Number</u>		<u>Page</u>
46	Back corona suppression test at 100°C, 1.2% H ₂ O, $j = 9.4 \times 10^{-5}$ nA/m ² , ash injection at 414 Pa (60 psi) and pneumatic rapping at 552 Pa (80 psi)	64
47	Corona current vs. corona voltage for clean and dirty electrodes at 100°C and 1.2% H ₂ O. Grid current was held to zero for these measurements.	65
48	Back corona suppression test and Q/m measurement at 100°C, 1.2% H ₂ O, $j = 9.4 \times 10^{-5}$ nA/m ² , ash injection at 345 Pa (50 psi) pneumatic rapping at 552 Pa (80 psi) and Q/m = 2.86×10^{-7} C/g.	66
49	Schematic diagram of the electronic circuit designed to provide automatic adjustment of the precharger screen voltage in response to changes in the primary corona current.	69
50	Back corona suppression test with T = 93°C, flowrate = 5.19 m ³ /sec, and mass loading = 1.0 g/m ³ . The Q/m value obtained in this test is 1.36×10^{-6} C/g.	71
51	Current-voltage characteristics for the precharger clean and dirty at 93°C.	72
52	Back corona suppression test with T = 107°C, flowrate = 5.19 m ³ /sec, and mass loading = 1.0 g/m ³	73
53	0.47 m ³ /sec (1000 acfm) precharger assembly.	77
54	I-V curves of the downstream collector section with dirty wires and plates, no dust flow, and 149°C (300°F).	79
55	I-V curves of sections 1 and 2 of the downstream collector with dirty 2.5 cm mesh discharge electrodes, dirty plates, no dust flow, and 149°C.	80
56	I-V curves of sections 3 and 4 of the downstream collector with dirty wires, dirty plates, no dust flow and 149°C.	81
57	Precharger corona electrode I-V curve with the grid current held at zero, temperature = 158°C, and gas flowrate = 0.47 m ³ /sec (1000 acfm).	82
58	Optical particle counter measurement system.	84
59	Number of counts vs. particle diameter as observed with the Climet optical particle counter for the three conditions: 1 - precharger off and collector off, 2 - precharger off and collector on, and 3 - precharger on and collector on . . .	85

60	The current-voltage characteristic of five 0.64 cm diameter wires spaced 9.5 cm from a grounded plate with a wire-to-wire spacing = 3.81 cm.	88
61	The current-voltage characteristics of 0.32 cm diameter wires spaced 9.5 cm from a grounded plate at three wire-to-wire spacings.	89
62	Comparison of electrical behavior for various types of corona discharge electrodes. The wires are in arrays of five in parallel, spaced at 3.8 cm.	91
63	Small pilot scale precipitator assembly.	92
64	I-V characteristics of section 1 of the downstream collector with no gas flow and ambient conditions.	93
65	I-V characteristics of section 2 of the downstream collector with no gas flow and ambient conditions.	94
66	I-V characteristics of section 3 of the downstream collector with no gas flow and ambient conditions.	95
67	I-V characteristics of section 4 of the downstream collector with no gas flow and ambient conditions.	96
68	I-V characteristics of section 1 through 4 of the pilot scale downstream collector at ambient conditions. The two gas passages in each section were electrically connected for these tests.	97
69	Theoretical collection efficiency of the pilot scale precharger-collector combination, plotted as a function of particle diameter. Charging parameters are $Nt = 8.63 \times 10^{12}$ sec/m ³ , $E_p = 3.15 \times 10^5$ V/m and $T = 348^\circ\text{K}$. These data correspond to charging experiments where the dust resistivity was greater than 10^{11} Ω -cm.	103

TABLES

<u>Number</u>		<u>Page</u>
1	EAA data analysis for the following test conditions: $T = 75^{\circ}\text{C}$, $\% \text{H}_2\text{O} = 1.2\%$ (volume), $\rho = 1.4 \times 10^{12} \Omega\text{-cm}$, $j_{\text{precharger}} = 9.4 \times 10^5 \text{ nA/m}^2$, $E_{\text{collector}} = 2 \text{ kV/cm}$, dust loading = 1.88 g/m^3	58
2	Test conditions for which successful back corona suppression was maintained.	68
3	Estimated performance of the pilot scale precharger- collector system.	102
4	Cold ESP cost model.	106
5	Hot ESP cost model.	108
6	Cold SO_3 conditioned ESP cost model.	109
7	Detailed average costs for new cold ESP.	110
8	Comparison of average costs for electrostatic precipitators collecting high resistivity fly ash.	111

ACKNOWLEDGEMENTS

Technical assistance in the design of an automatic grid voltage control circuit was provided by Mr. W. J. Steele and Mr. R. N. Coker. Precharger fabrication was accomplished principally by Mr. R. H. Leopard, under the supervision of Mr. T. D. Hughes. Lodge-Cottrell Operations, Dresser Industries, Inc. provided design assistance in connection with the ruggedized version of the 1000 ACFM precharger.

The work of Mr. G. Ramsey and Mr. B. Daniel of IERL in helping with the testing program is appreciated. Finally, we gratefully acknowledge the continued encouragement and assistance of Dr. L. E. Sparks.

SECTION 1

INTRODUCTION

The presence of high resistivity particulate material in an electrostatic precipitator tends to degrade the collection efficiency of the system by reducing the rate of particle charging. The problem occurs as a result of a phenomenon known as "back corona", which arises from electrical breakdown in the dust layer on the precipitator collection plates. Breakdown of the dust layer leads to localized field effects capable of producing ionization of gas molecules near the breakdown sites. Under these conditions, corona discharges occur at both the corona wire and the grounded plate electrode, resulting in a bipolar ion current throughout most of the space between electrodes. When both positive and negative ions are present the particle charging mechanisms become ineffective, leading to very poor performance of the ESP.

The electric field strength in the dust layer on precipitator collection plates depends upon the electrical resistivity of the dust and the current density passing through it. The thickness of the layer is not a primary factor. Thus, electrical breakdown and the consequent back corona can occur even where only an extremely thin dust layer exists. It has been demonstrated that mechanical cleaning by rapping, scraping or brushing cannot provide a clean enough metal surface to prevent back corona. It is therefore unrealistic to attempt to defeat the effects of high resistivity dust by application of mechanical plate cleaning techniques.

Several approaches have been developed to deal with the high resistivity problem in conventional precipitators. Among these are the use of chemical additives, operation of precipitators at elevated temperatures and the use of extraordinarily large collecting surfaces relative to the gas volume flowrate. There are, however, disadvantages associated with each of these methods. The use of chemical additives entails the expense of providing an injection system, as well as the cost of maintaining a regular supply of the reagent to be used. Operation of a precipitator at elevated temperature (350°C to 450°C) presents engineering difficulties due to thermal stresses and materials considerations. Insulation costs for "hot-side" precipitators increase the capital outlay required relative to the expense of installing a conventional ESP. The use of a very large specific collection area (SCA, ratio of total collecting plate area to total gas volume flowrate) is a fairly reliable approach, since the overall effect of back corona is to reduce the efficiency of an ESP. But, for a given application, the installation cost of an ESP is roughly proportional to the value of the SCA. Thus, each of the techniques currently employed for the collection of high resistivity dusts by electrostatic precipitation entails substantial installation or operating costs above those associated with the collection of dusts having moderate electrical resistivity.

The principal objective of this project was to investigate possible solution to the problems associated with the precipitation of high resistivity particulate matter and to evaluate the results in terms of applicability to the control of industrial air pollution. The work is based on previous studies of particle charging with regard to the development of an effective two-stage electrostatic precipitator system.¹

In a two-stage system the charging and collecting functions are separated inasmuch as it is possible. The first stage, or precharger, is operated at a relatively high current density to provide a dense ion field for effective particle charging. The precharger is, physically, a relatively small part of the system, so it is possible to resort to unusual and relatively expensive techniques for controlling back corona in the precharger without incurring prohibitively high costs for the system as a whole. The second stage of the system serves as a particle collector. The desirable operating parameters in the collector are high electric field strength and low, uniform, ion current density at the plate electrodes. The high field provides for maximum migration velocity, and the low current density permits operation below the threshold for back corona. Operation at zero current density is impractical, since collection of reentrained particles may require some additional charging in the collecting stage.

The focus of this research work has been on the development of an effective precharger. Several approaches were examined and compared theoretically and experimentally with regard to feasibility of controlling the effects of back corona in an environment where the ion current density was well above the threshold for back corona. As a result of this investigation a three-electrode system was devised, which, after preliminary study, appeared to be superior to the other concepts under consideration. Laboratory scale tests of the three-electrode system supported the preliminary work, and led to the development of a small pilot scale precharger capable of handling a gas flow-rate of $0.47 - 0.94 \text{ m}^3/\text{sec}$ (1000 - 2000 acfm).

Tests of the pilot scale precharger were carried out at Southern Research Institute and at the U.S. Environmental Protection Agency's Industrial Environmental Research Laboratory at Research Triangle Park, North Carolina. The results of these tests showed that the precharger could attain charge levels on high resistivity particles ($>10^{12} \text{ ohm-cm}$) comparable to those achieved for particles of moderate resistivity ($<5 \times 10^{10} \text{ ohm-cm}$) in a conventional ESP. Measurements of collection efficiency, using a wire-plate device for the collector stage, showed a marked improvement in efficiency with the precharger energized, compared with operation of the collector alone.

Since the precharger was designed to demonstrate the feasibility of the concept under consideration, durability was not emphasized in the design. Thus, having shown that the three electrode precharger could perform well with high-resistivity dust, the program was concluded by designing and testing an improved device. The new precharger was made more ruggedly, and all insulating materials were removed from regions through which the dust laden gas could flow. Results of the tests were favorable. Charging results were consistent with those achieved by the first pilot precharger. By using closely-spaced wires and screen discharge electrodes in the collector stage

to maintain low current densities, it was possible to achieve a collection efficiency above 90% with a collection area less than $25.6 \text{ m}^2/\text{m}^3/\text{sec}$. ($130 \text{ ft}^2/1000 \text{ ACFM}$) for dust having electrical resistivity greater than 10^{12} ohm-cm .

SECTION 2

SUMMARY AND RECOMMENDATIONS

LABORATORY STUDIES

An investigation of electrode designs and methods for overcoming back corona was carried out, with the objective of developing a two-stage electrostatic precipitator system capable of collecting high resistivity dusts with greater efficiency than can be achieved by conventional precipitators. Several alternative approaches were subjected to limited theoretical and experimental studies. Among the ideas considered were heated passive electrodes, a novel technique for injecting liquid or gaseous chemical reagents directly into the active corona region and various electrode geometries and energization schemes. The most promising approach appeared to be a three-electrode geometry in which a screen electrode is used to trap ions originating from a back corona discharge, thus preventing those ions from interfering in the particle charging process.

The electrode arrangement in the new system consists of parallel plates, between each pair of which is a corona discharge electrode (a barbed wire in the prototype system), and a pair of open mesh screens, each located in a plane parallel to a plate and much closer to the plate than to the corona wire. The screen electrodes are energized at a voltage having the same polarity, but much lower magnitude than the potential of the corona wire. Ions originating at the corona wire are thus deflected away from the metallic part of the screen, and pass through the holes on the way to the plate electrode. When high resistivity dust is introduced into the system some small fraction of the particles will be deposited on the plate electrode, and back corona can be generated as in a conventional system. The ions originating from the back corona discharge are, however, attracted to the screen electrode. Since most of those ions are trapped by the screen, they are not permitted to interfere with the normal particle charging processes in the principal gas stream. The back corona effects are thus controlled. No back corona discharge occurs at the screen electrode because virtually none of the primary corona current is accepted by the screen.

After the principal features of the three-electrode system were tested in a bench scale mock-up, a small laboratory scale device was designed and fabricated for the purpose of evaluating control of back corona and high resistivity particle charging effectiveness in a realistic configuration. In the laboratory scale precharger Teflon spacers and insulators were used to maintain the electrodes in their proper relative positions. The device was exposed to redispersed fly ash heated sufficiently to raise the resistivity

above 10^{12} ohm-cm. Measurements of charge to mass ratio were made on particles that had passed through the energized precharger. The results compared favorably with calculated values based on primary corona current only, ignoring back corona. That is, the charging effectiveness of the device was similar to what would be expected for an ash having low resistivity in a conventional wire-plate corona system.

PILOT SCALE PROGRAM

In the next phase of the investigation a larger scale precharger was constructed for testing in combination with an existing pilot scale electrostatic precipitator, which could be used as a downstream collector following the precharger. The system was designed to handle approximately $0.71 \text{ m}^3/\text{sec}$ (1500 acfm) of simulated flue gas. Included was an automatic control circuit for the voltage applied to the screen electrodes. When the precharger was brought into operation with high resistivity ($\sim 10^{12} \Omega \text{ cm}$) dust loading the effects of the screen electrodes in controlling back corona were clearly evident. The primary corona current could be maintained at a constant level as the screen current fluctuated over a wide range in response to the back corona current. Charging measurements made on particles sampled on the exit side of the precharger indicated a charge to mass ratio of the order of $2 \times 10^{-6} \text{ C/g}$. Comparisons were made between the performance of the system in particle collection with the precharger energized versus the results obtained with the precharger turned off. Conditions in the downstream collector were maintained as similar as possible for comparative tests. Collection efficiency was markedly improved by action of the precharger over what could be achieved by the downstream collector alone.

Because of mechanical problems in the precharger a second, ruggedized version was designed and fabricated. The duct dimensions and electrical spacings were kept the same as in the original device. The testing program for this device was similar to that described in the above paragraph. Results of collection efficiency measurements made by use of optical particle counters and mass trains showed improvements in collection efficiency with the precharger on equivalent approximately to doubling the specific collection area of the ESP serving as the downstream collector, in comparison with similar measurements made on the ESP operating alone. In particular, collection efficiencies above 90 per cent were recorded for the two-stage system operating at an SCA of 128 on a dust having resistivity of approximately $10^{12} \Omega \text{ cm}$. The efficiency for the ESP alone under the same conditions was measured at about 70%.

RECOMMENDATIONS

Further developments are required in order to demonstrate that the two-stage concept can be applied successfully to the requirements of industries and utilities. The precharger must be complemented by an optimal collecting device. The small pilot scale system should be tested on an actual pollution source where electrical resistivity is a problem, and a larger scale system should be designed and tested to ensure that a practical scale-up is feasible.

Further fundamental studies are also in order to determine whether the concept can be modified in any way to provide still better particle charging, and to explore the applicability of such a system to a variety of air pollution control problems.

SECTION 3

PRELIMINARY STUDIES

In order to evaluate various alternative techniques for counteracting back corona and space-charge effects in a high current density corona field, preliminary theoretical studies and limited laboratory tests were carried out. Among the more promising of the concepts considered in detail were heated passive electrodes, introduction of chemical conditioning material through a porous passive electrode, and injection of chemicals directly into the active corona region at the discharge electrode. The general premise for this study was that extraordinary means for the control of back corona could be used in a particle charging device, which could serve as the first stage in a two-stage electrostatic precipitator (ESP) system. Since saturation charging is generally reached within a distance of a few inches at ordinary gas velocities in an ESP the particle charging device, or precharger, would be, physically, only a small part of the overall two-stage system. Thus the costs of application of special techniques or materials in the precharger might be more than offset by the reduction in collecting area required in the second stage (collector) of the system, due to the enhanced charge on the particles.

In the course of the investigation a novel approach to the control of back corona was developed. The new concept was based on the use of a third electrode, whose purpose was to act as a sink for ions generated as a result of back corona. Because this technique appeared to comprise a more practicable approach to the solution of the back corona problem, it was given precedence for further research, and an application for patent was initiated (U.S. Serial Number 882,673, dated March 2, 1978). The results of preliminary work done on the other approaches, mentioned in the above paragraph, are summarized in Appendix A.

DESCRIPTION OF THREE-ELECTRODE CONCEPT

The basic idea underlying the three-electrode corona system is to capture the ions resulting from back corona near their source, rather than attempting to prevent back corona from occurring. Two of the electrodes used in the system are the conventional corona discharge and passive electrodes. The third is a screen electrode placed near the passive electrode.

Separate power supplies are provided for the corona discharge and screen electrodes. The passive electrode is set at ground potential. Consider, for example, a two electrode system where the corona discharge electrodes is at a high negative potential with respect to the grounded passive electrode. Now, locate an equipotential surface near the passive electrode and insert a conducting screen coincident with that equipotential surface. If the screen voltage is set equal to the original potential on the surface the electric field will be practically undisturbed on comparison with the original field. Only the

non-zero thickness of the wires in the screen will cause very localized modifications to the field. A corona current originating at the discharge electrode will be distributed such that a fraction of the total current equal to the ratio of open area to total surface of the screen will reach the passive electrode. The remainder of the current will be intercepted by the screen.

Now, if the potential on the screen electrode is made more negative the field near the screen will become distorted in such a way that negative ions from the discharge electrode will be repelled from the screen wires and forced toward the open area, through which they can proceed to the plate. If we introduce high resistivity particulate material into the system it is certain that depositions will occur on both the plate and the screen electrodes. Since negative ions from the discharge electrode are being repelled by the screen it must have a lower current density than the plate, and hence corona from the screen electrode would probably not occur. If back corona occurs, the positive ions from the passive electrode would be attracted to the screen electrode, where many would be captured and removed from the system. If most of the positive ions resulting from back corona can be captured by the screen electrode, the ion field between the screen and the discharge electrode would be essentially unipolar, providing an effective particle charging region.

BENCH-SCALE TESTS

Experimental tests were run to verify the basic concepts involved in the three-electrode system discussed in the preceding paragraphs. The apparatus used was as shown in the schematic diagram, Figure 1. The system was enclosed in an oven maintained at 150°C, and a continuous flow of redispersed fly ash was introduced. The current for each electrode was monitored separately. (Discrepancies in current sums can be accounted for by losses to the oven walls.) Effectiveness of the concept is interpreted in terms of the relative magnitudes of the three current measurements. When back corona occurs the plate current should rise significantly. If the screen grid is effective in removing ions resulting from back corona, there should be a rise in screen current consistent and commensurate with the rise in plate current, and the discharge electrode current should remain nearly constant.

Figure 2 shows the results of an experiment where the behavior was near that predicted. After an overall initial drop in current at all electrodes (cause uncertain, possibly because of development of a space charge) back corona apparently set in rapidly. The plate current rose from 50 μA to 350 μA in about six minutes. The screen current increased quite consistently from about 5 μA to 250 μA . The corona discharge current rose also, but by less than 50%, compared with a seven-fold increase in plate current. A disturbing aspect of the experiment is that there appears to be no tendency toward approaching a steady-state operating condition. The average current density at the plate was very high, however, being well over 1000 nA/cm^2 .

In a second experiment, the negative voltage on the screen was reduced by about 6% so that the screen tended to repel positive ions and accept negative ions. The behavior of the system was virtually inverted, in agreement with theoretical expectations. The screen current was opposite from its direction in the previous experiment, and with the apparent onset of back

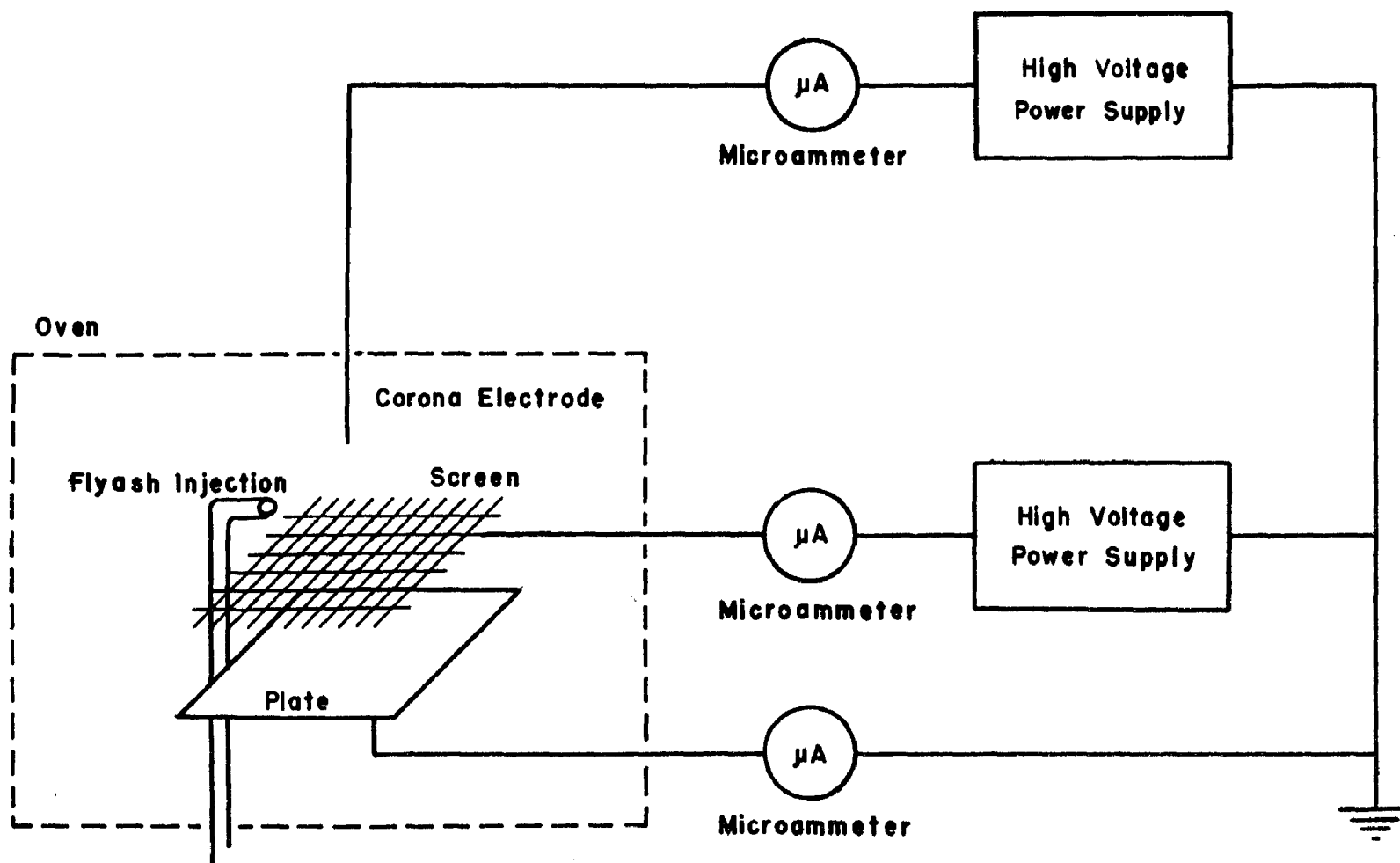


Figure 1. Apparatus used for preliminary evaluation of three-electrode corona geometry concept.

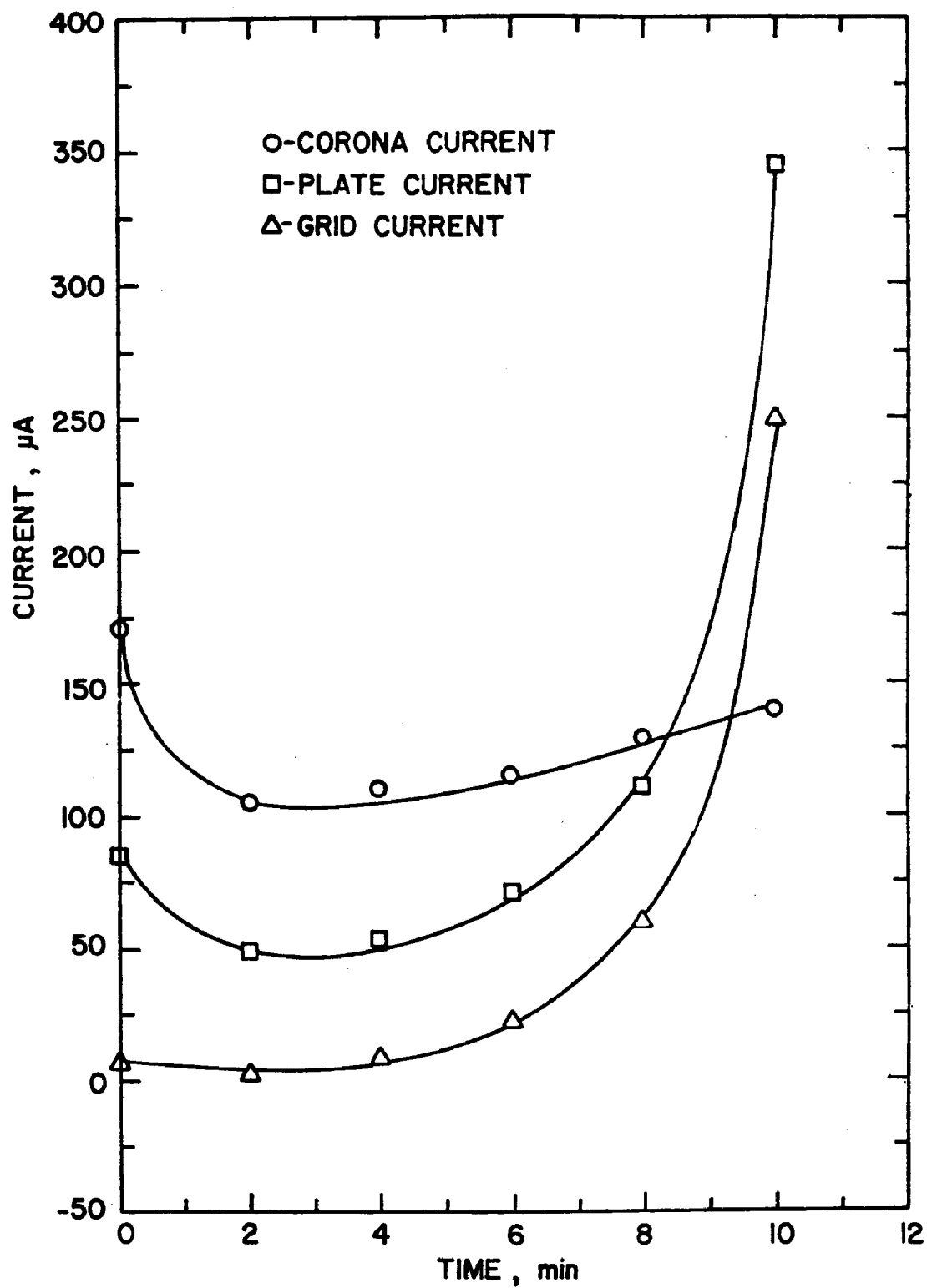


Figure 2. Current as a function of time for each electrode. Corona discharge electrode is at -25 kV, and screen electrode is at -9 kV. Dust laden air is injected at 1.2 l/min.

corona, the plate and discharge electrode currents rose together, while the screen current remained constant. These effects are shown in Figure 3.

Figure 4 shows the system behavior with the grid electrode removed, which is quite similar to the result depicted in Figure 3. The rate of increase in current as back corona apparently develops is approximately the same in the two experiments.

Another experiment in which the screen voltage was adjusted to accept positive ions repeated the results obtained in the first. This test was of longer duration. Again, the screen and plate currents increased simultaneously, as shown in Figure 5. After about 30 minutes sparking occurred between the screen and plate, forcing a reduction in screen voltage. When that adjustment was made the screen and plate currents continued to increase consistently but a more rapid increase in primary corona current also occurred.

The experiments performed with a three-electrode corona system thus indicated possible utility under some conditions where back corona is present. The additional degree of freedom resulting from the addition of a third electrode might complicate electrical control of the system. Improved behavior may be achieved by optimizing screen wire spacing and screen-to-plate separation. In a more realistic system the current density at the plate would be more uniform than in a point-plane apparatus. Under such conditions the peak current density would be smaller, and back corona effects easier to control.

Further tests of the three-electrode concept were carried out in order to investigate the possibility of operating at steady-state conditions after the onset of back corona. The discharge electrode was a sharp point, spaced 3 cm from a plate electrode. A wire screen electrode, 84% open area and 0.62 cm wire spacing was located parallel to the plate electrode at a distance of 1.0 cm.

The experiment progressed as shown in Figure 6. Fly ash was injected over the plate in a dry oven at a temperature of 150°C. With 15kV on the discharge electrode and 8kV on the screen, a sharp rise in both screen and plate current occurred after approximately 4 minutes. After about 8 minutes the screen and plate currents had risen by a factor of about 8, and occasional sparking occurred. A relatively small change in the current at the discharge electrode occurred. At this time the screen voltage was reduced to 7.8kV. At $t = 10$ min. the screen voltage was further reduced to 6.5kV and the corona discharge electrode voltage was reduced to 13kV. During the following 20 minutes the primary corona current remained essentially constant, and the current at both of the other electrodes drifted slowly toward a steady value.

Finally, at $t = 30$ min., the discharge electrode voltage was returned to its original value of 15kV. The primary corona current rose slightly and the current at the other two electrodes settled to a lower value, approximately three times the discharge electrode current.

Throughout the experiment the screen current followed the variations in the plate current quite consistently, indicating that ions resulting from back

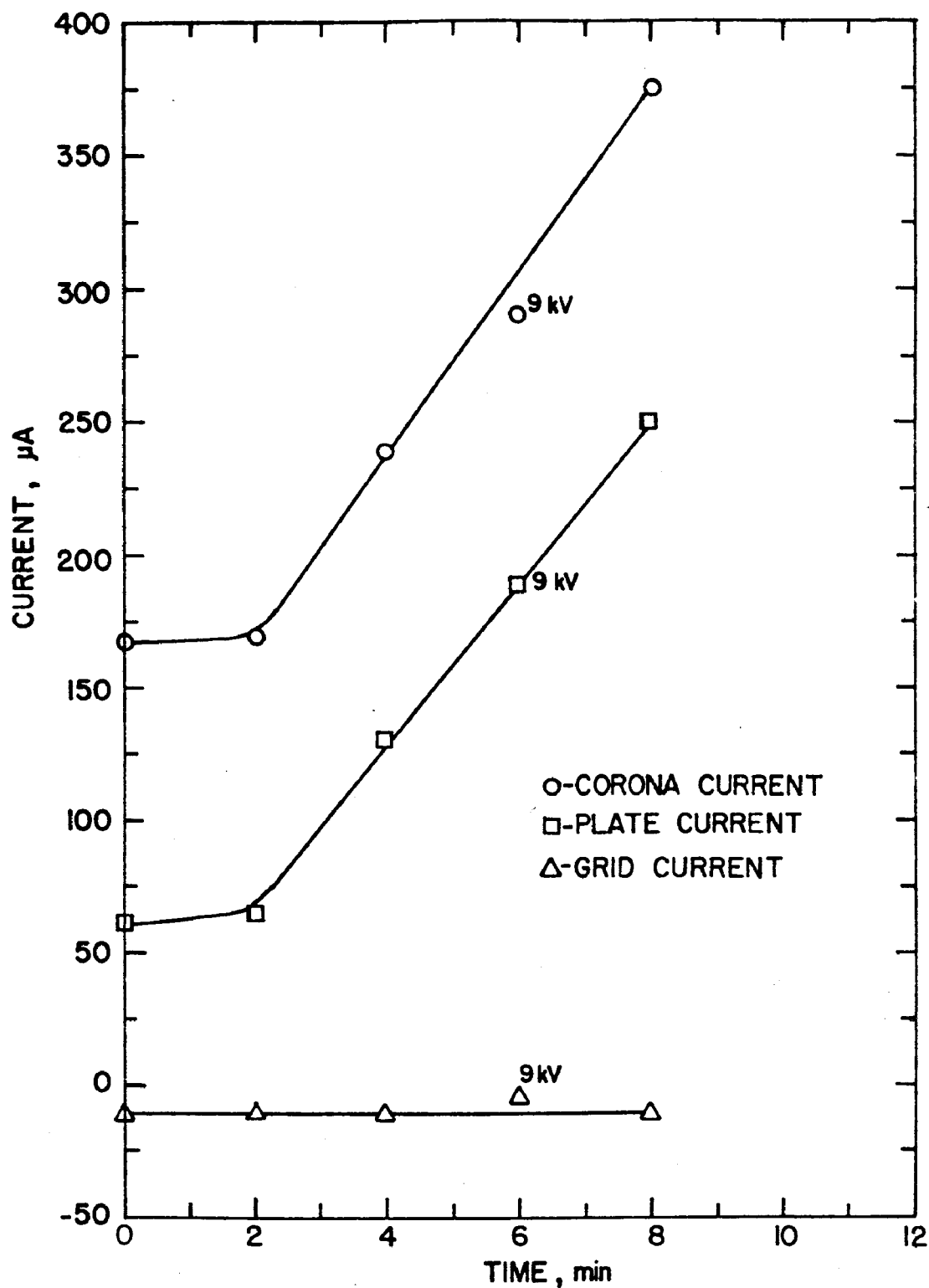


Figure 3. Current as a function of time for each electrode. Corona electrode is at -25 kV. The screen electrode is at 8.5 kV, which is below the magnitude of potential required to accept ions resulting from back corona at the plate. Screen voltage was shifted momentarily to -9 kV at $t = 6$ min.

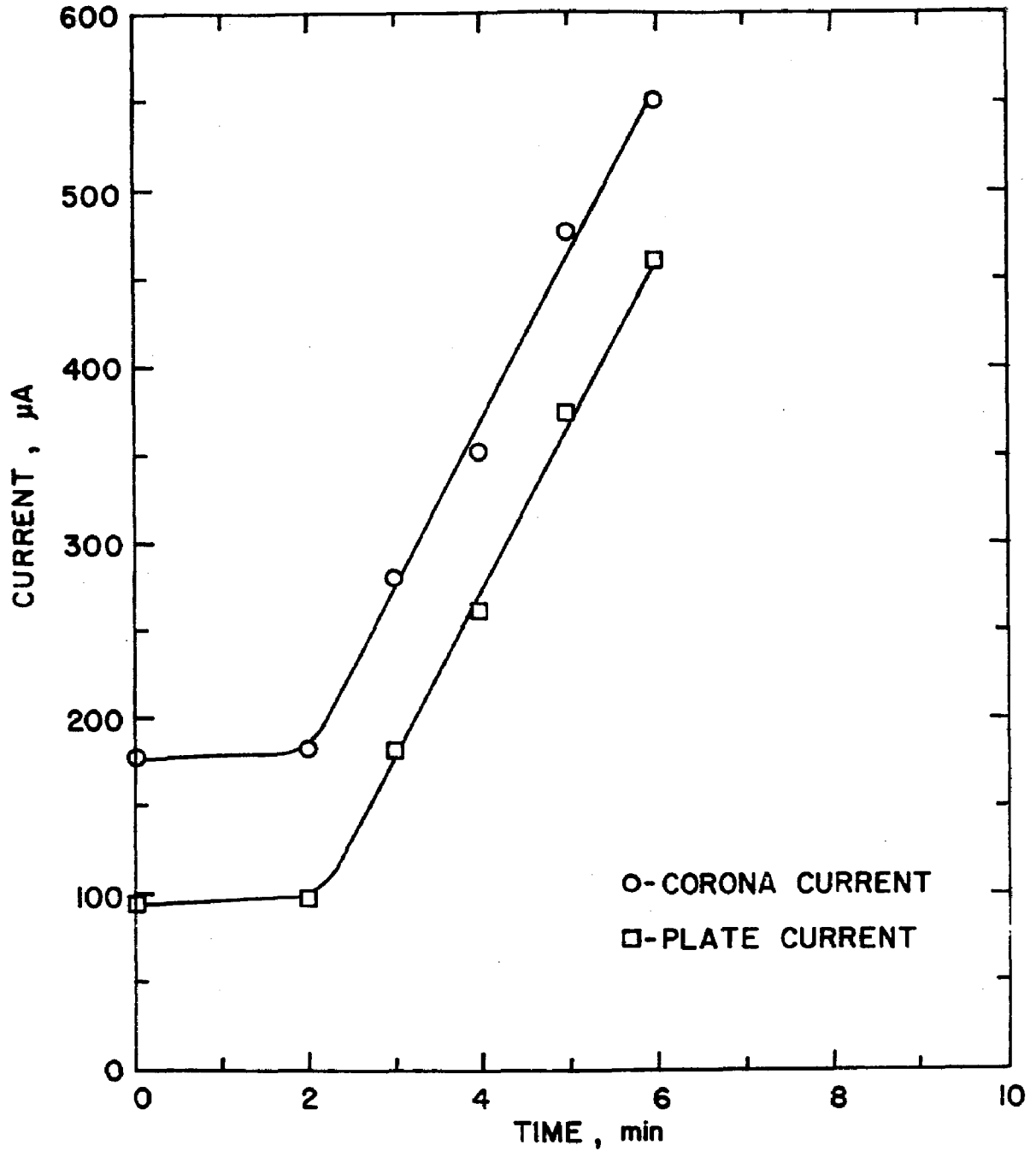


Figure 4. Current as a function of time for corona discharge electrode and plate electrode as a function of time, with dust injection. Screen electrode was removed, and voltage is -25 kV. Losses to oven walls account for current difference.

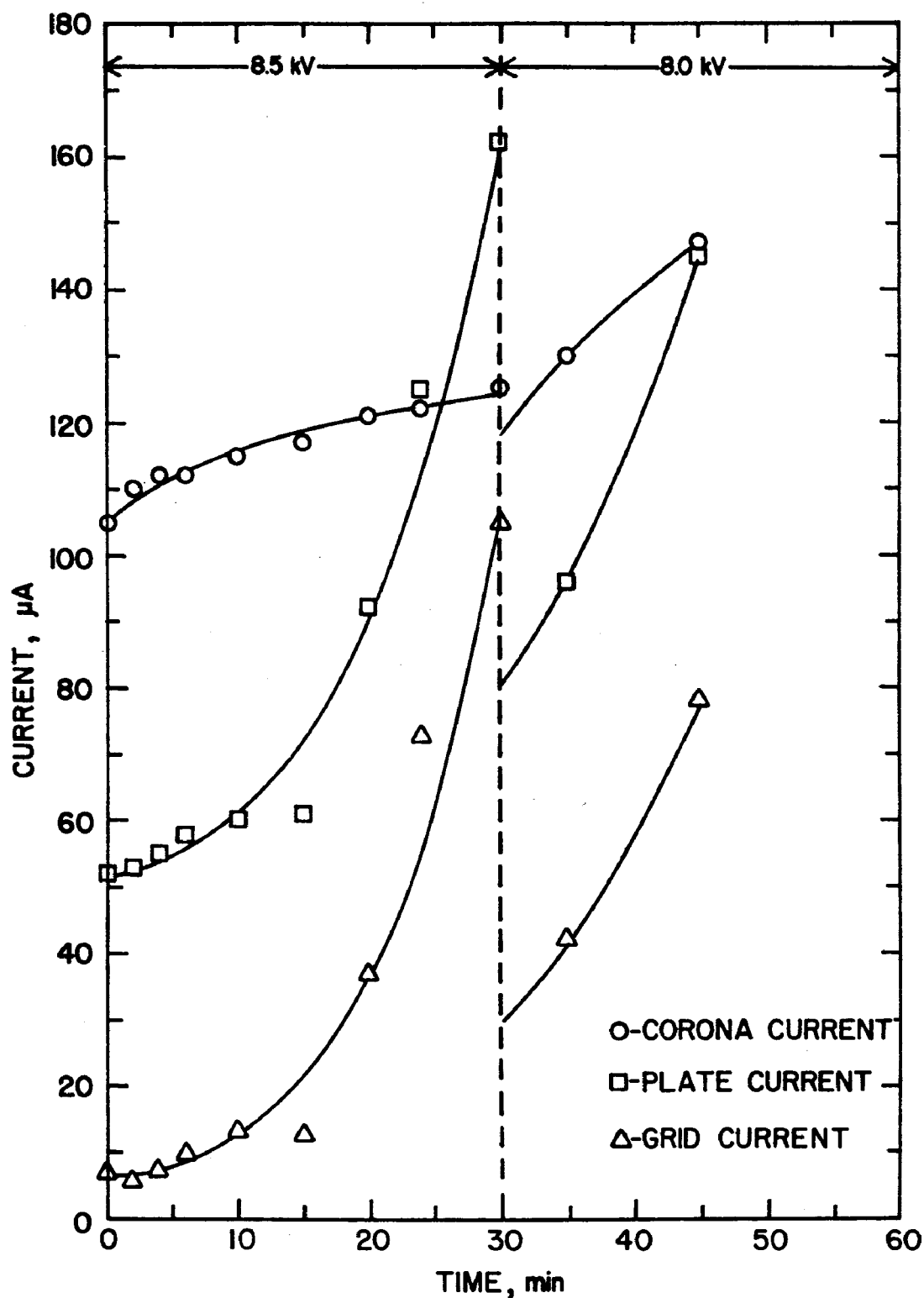


Figure 5. Current as a function of time for each electrode, with corona discharge electrode at -22 kV. The screen voltage was initially set at 8.5 kV, and reduced to 8.0 kV after 30 min. running time.

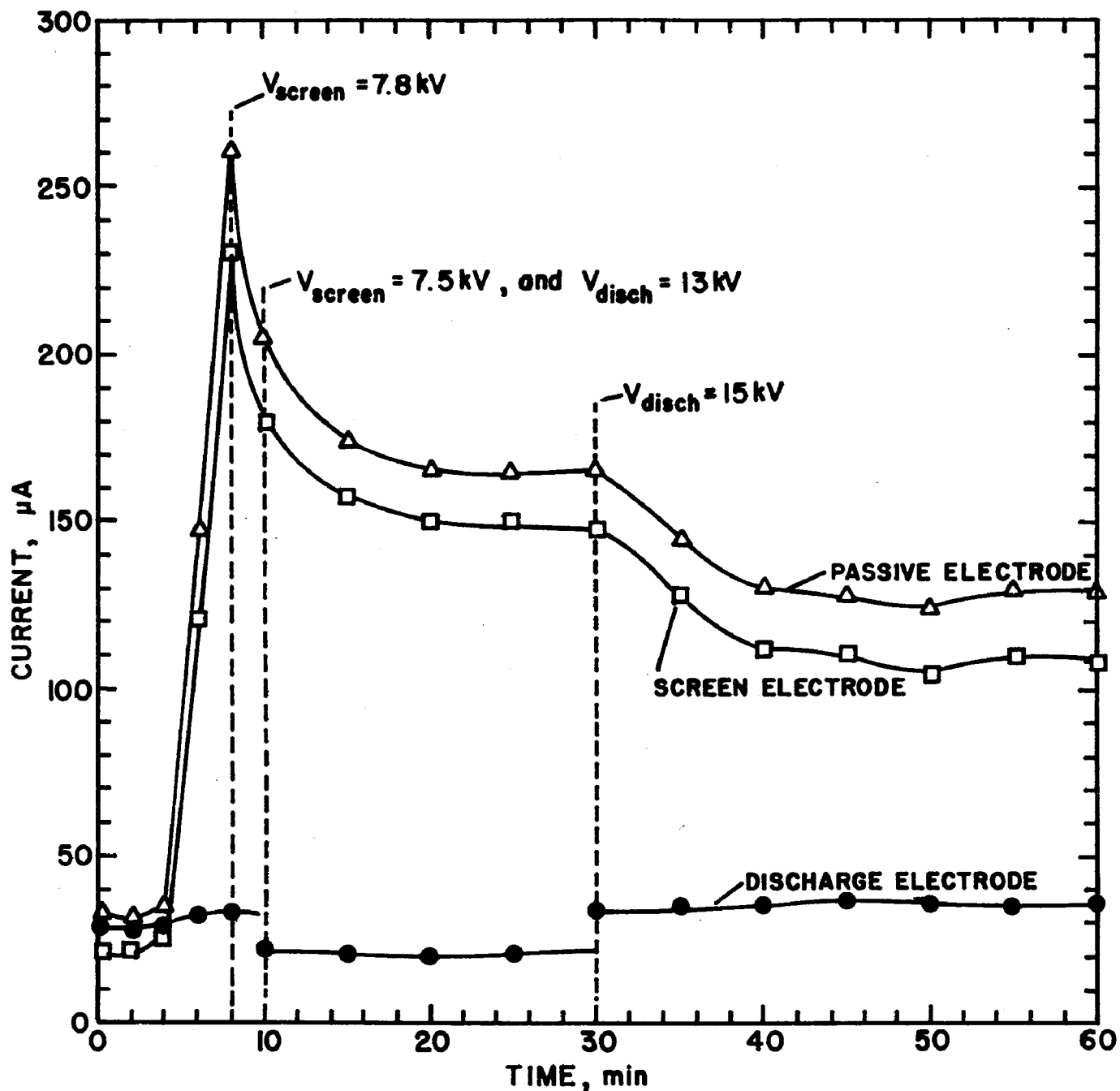


Figure 6. Current for each electrode in the three-electrode system. The vertical dashed lines denote times at which voltage changes were made to the values indicated. Initially the discharge electrode voltage was 15 kV and the screen voltage was 8 kV.

corona were intercepted by the screen electrode. Variations in current levels show a strong dependence upon the voltage applied to the screen electrode.

LABORATORY SCALE PRECHARGER

In order to examine the three-electrode concept in a more realistic configuration a small laboratory scale device was designed in a parallel wire-plate arrangement. A photograph of the precharger is shown in Figure 7. The height of the plates in this device is about 30 cm (12 in.), the enclosure is made of Teflon to isolate the electrodes from external effects. The plate-to-plate and screen-to-plate spacings were made variable so that the effects of changing those parameters could be examined. The screen electrodes were perforated plates with 0.635 cm hexagonal openings (79% open area).

After preliminary current-voltage (I-V) measurements were made at ambient conditions, the precharger assembly (Figure 7) was installed in the test section of an existing dry wall pilot scale electrostatic precipitator in order to evaluate its performance under conditions of elevated temperature and dust loading. The effect of elevated temperature (130°C) is indicated in Figure 8. The increase in current is probably a direct result of the increased mobility of ions at higher temperatures.

The three-electrode system with a corona electrode-to-plate spacing of 8.89 cm and a screen electrode-to-plate spacing of 1.0 cm was the initial precharger configuration studied under conditions of both high temperature and dust loading. The current-voltage relationships for this geometry, when subjected to a dust loading of approximately 3.5 g/m³ of redispersed fly ash (resistivity of $\sim 10^{13}$ Ω -cm) at 130°C, revealed that back corona was not controlled. The occurrence of back corona is indicated by a significant rise in the plate current. If the screen electrode is effective in removing ions resulting from back corona, there should be a similar rise in the screen current, and the discharge electrode current should remain nearly constant. Failure to suppress back corona also occurred in an experiment with the corona electrode-to-plate spacing reduced to 3.81 cm and all other parameters held constant.

The performance of the system seems to be quite sensitive to the position of the screen relative to the other electrodes. The screen-to-plate separation was increased from 1.0 cm to 2.5 cm, with the corona electrode-to-plate separation held at 8.89 cm. The difference in I-V characteristics at the two spacings is shown in Figure 9. With a dust loading of approximately 3.4 g/m³ of redispersed fly ash and at a temperature of 130°C this configuration controlled back corona temporarily until the screen voltage required to maintain a constant discharge electrode current exceeded the value obtainable with the screen electrode power supply. Similar results had been encountered in the intermediate stages of the earlier investigation of the three-electrode system.

Investigation of the three-electrode geometry laboratory scale charger continued under various conditions. Tests were conducted at 125°C or 130°C. In all cases, the corona electrode-to-plate separation was held at 8.89 cm, and the grid electrode-to-plate spacing was 2.6 cm. The corona electrode

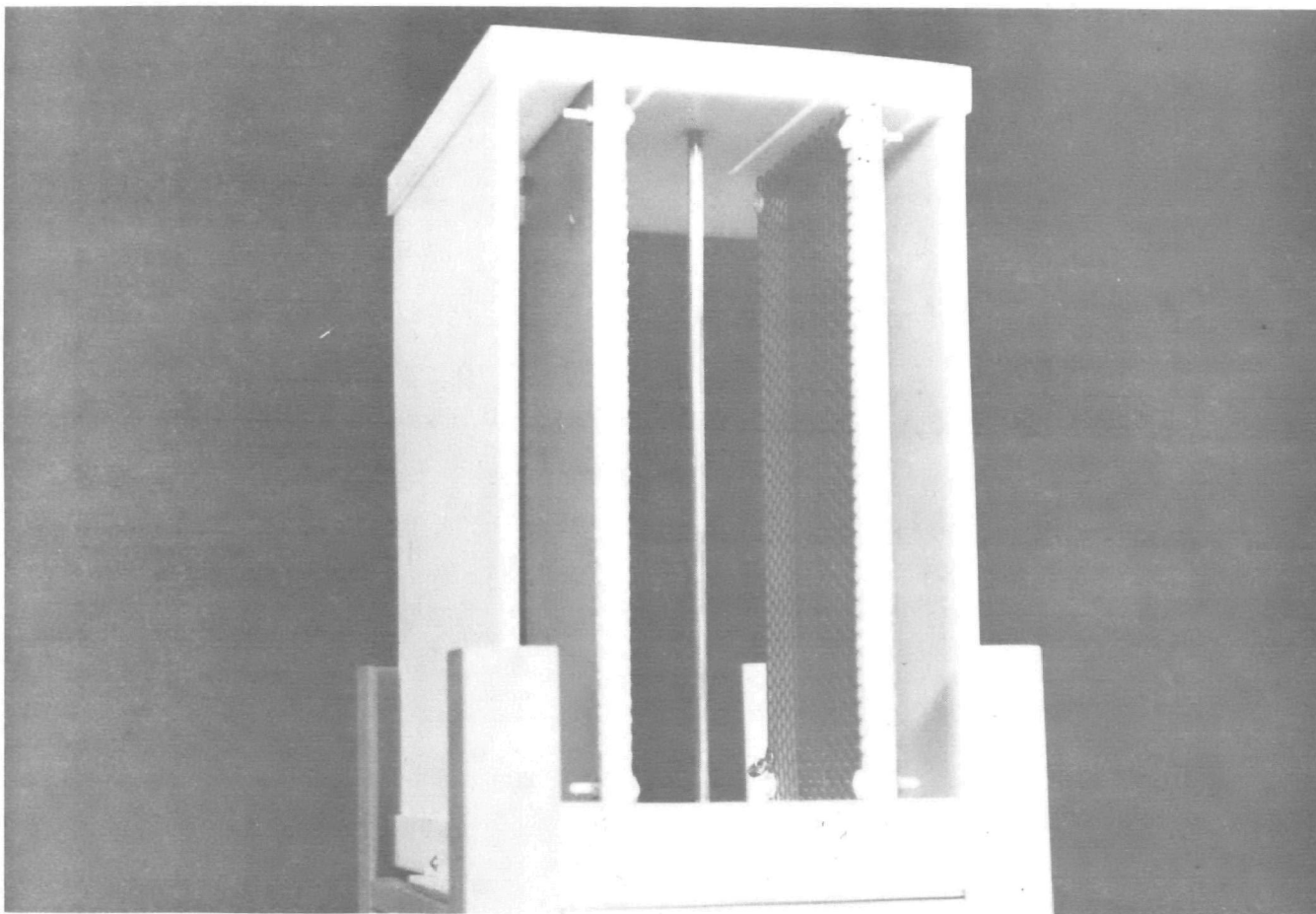


Figure 7. Laboratory scale precharger assembly in the three-electrode configuration.

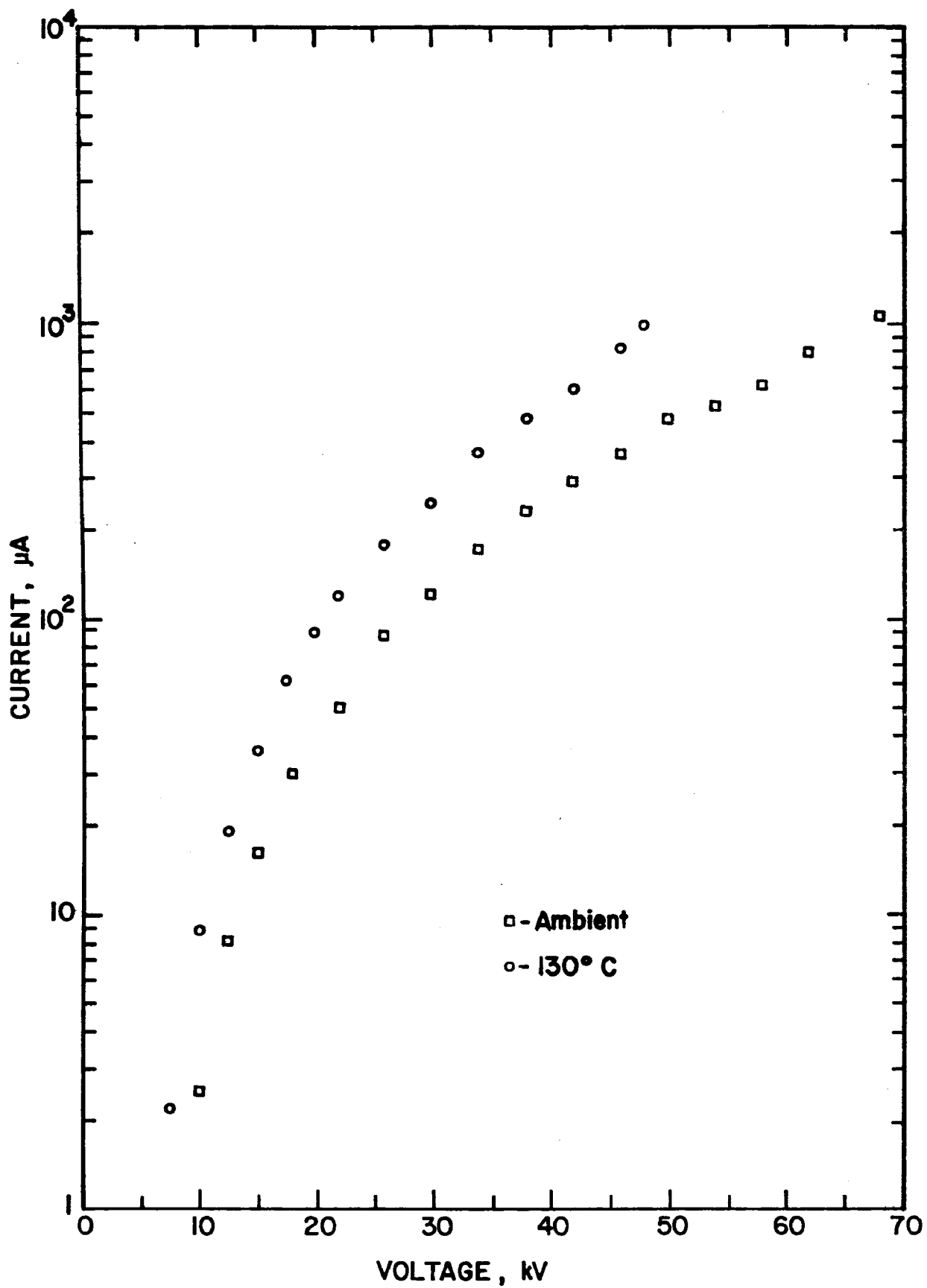


Figure 8. Bare plate I-V characteristics at ambient and at 130°C with corona electrode-to-plate spacing = 8.89 cm.

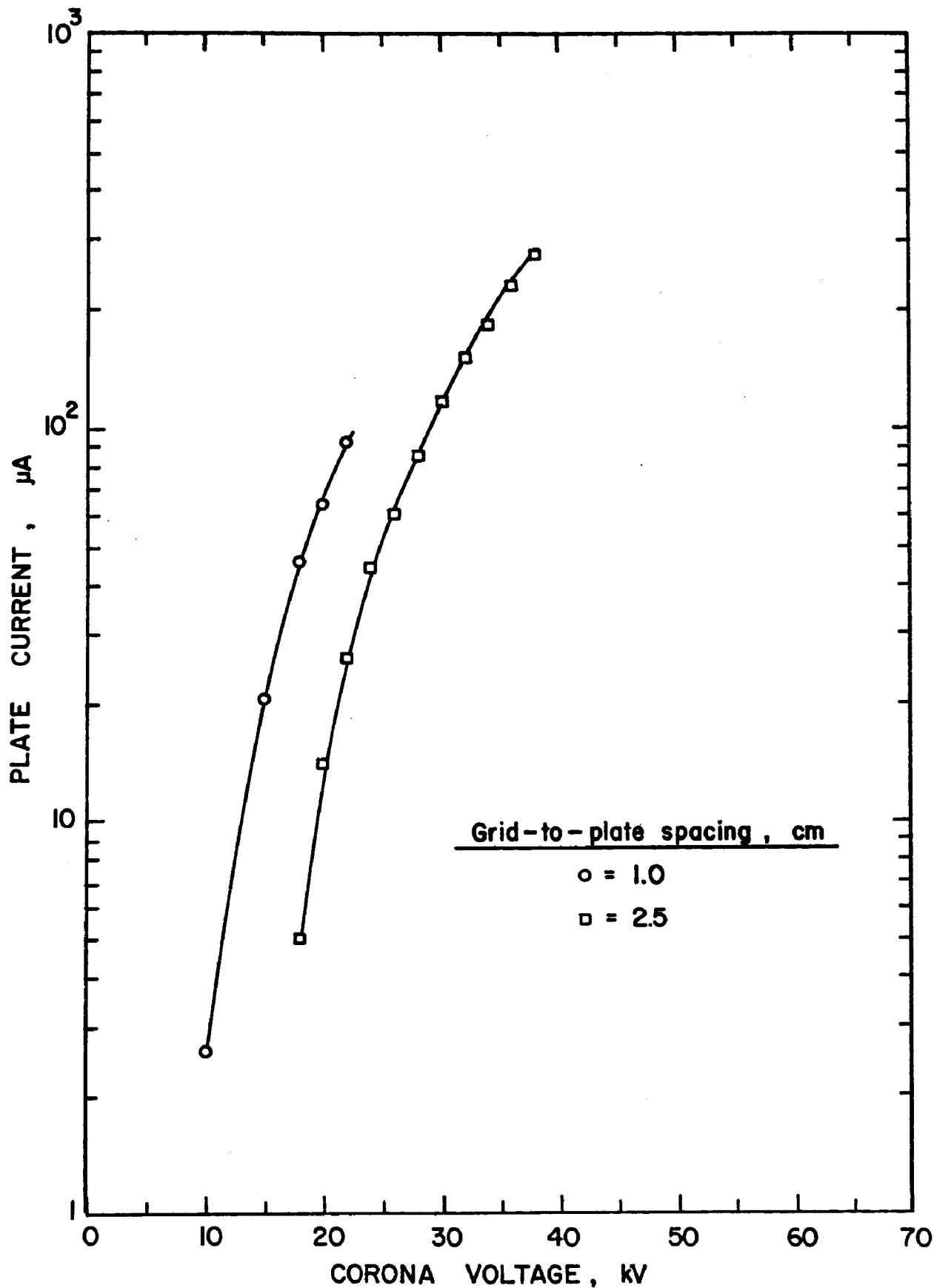


Figure 9. Comparison of the I-V characteristics of the three-electrode configuration with grid-to-plate spacings of 1.0 and 2.5 cm. The corona electrode-to-plate spacing = 8.89 cm, temperature = 130°C, and the grid current = 0 μ A.

used was a 0.028 cm diameter stainless steel wire and the grid electrodes used were perforated plates with 79% open area.

Figure 10 shows the results of one test where the charger was subjected to a dust loading of approximately 3.4 g/m^3 at a temperature of 125°C . The charger grids and plates were continually rapped with pulsed solenoids at a rapping frequency of 2 sec^{-1} . Back corona is evident in the sharp increase in the plate current. The grid voltage was adjusted throughout the experiment to maintain the corona current at its initial value. In this case, the grid electrode effectively suppressed the back corona for the duration of the test. The random fluctuations in the grid and plate currents could be a result of uneven dust feeding, an effect related to the rapping of plates and grids, or some combination of the two.

A series of experiments was conducted which included a determination of the charging effectiveness, as well as the back corona suppression capability of the laboratory scale charger. The particle charging measurements were made by collecting fly ash on an isolated silver filter which was placed immediately downstream from the charger. The filter was connected to an electrometer so that the integrated charge could be monitored for a sample of fly ash which had passed through the charger. The collected fly ash was then weighed and the charge/mass ratio was calculated.

An example of the results of an experiment in which the charging effectiveness measurement was made is shown in Figure 11. In this test, a dust loading of 3.4 g/m^3 and a temperature of 125°C were the conditions under which the charger was operated. The corona discharge electrode current was held constant throughout the test, indicating successful back corona suppression. The charge/mass (Q/m) ratio obtained in this experiment was $4.35 \times 10^{-5} \text{ C/g}$. This compares to a Q/m value of less than $1 \times 10^{-6} \text{ C/g}$ obtained in previous experiments with a conventional wire-plate precharger at a similar dust loading and a comparable resistivity.

The dust loading was increased to approximately 6.8 g/m^3 and the above experiment was performed with all other parameters the same. The results (Figure 12) show much higher grid and plate currents. The corona electrode current began to increase after eight minutes, which indicates an increasing difficulty to suppress the back corona generated at this higher dust loading.

ELECTRODE GEOMETRY STUDIES

The general electrode configuration used in the laboratory scale studies proved successful in achieving control of back corona, but only limited work was done in seeking an optimum geometry. Thus, as a preliminary step leading to the design of a pilot scale device, a combined theoretical and experimental investigation was made in order to provide a data base for selecting design parameters.

A computer simulation comparing the electrical performance of wire-plate corona systems having a wide range of geometric parameters was successfully employed to provide a set of theoretical current-voltage characteristics which

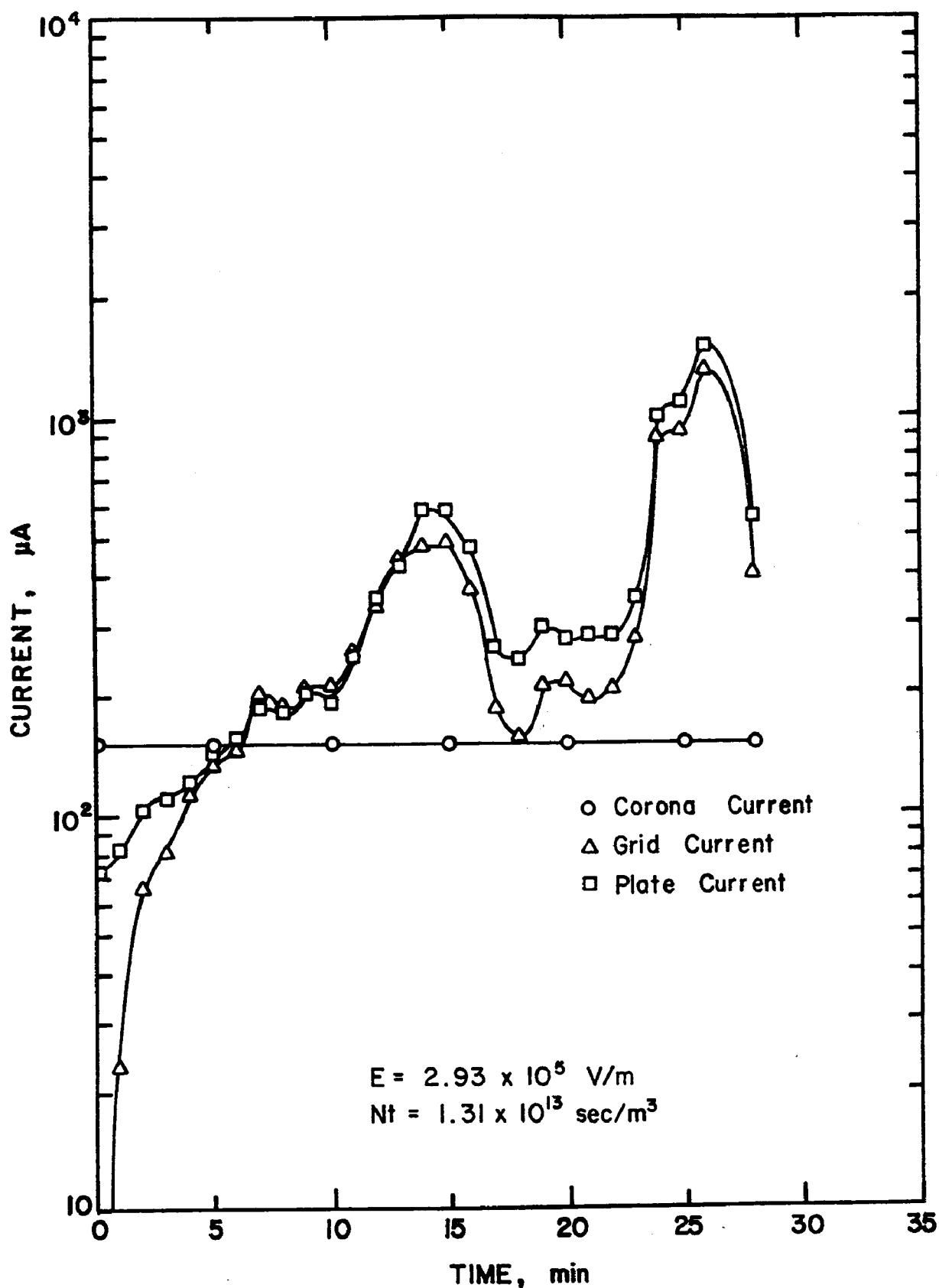


Figure 10. Test results of a three-electrode charger used for back corona suppression. Temperature = 125°C , corona electrode-to-plate spacing = 8.9 cm, grid electrode-to-plate spacing = 2.6 cm, and dust loading $\approx 3.4 \text{ g/m}^3$.

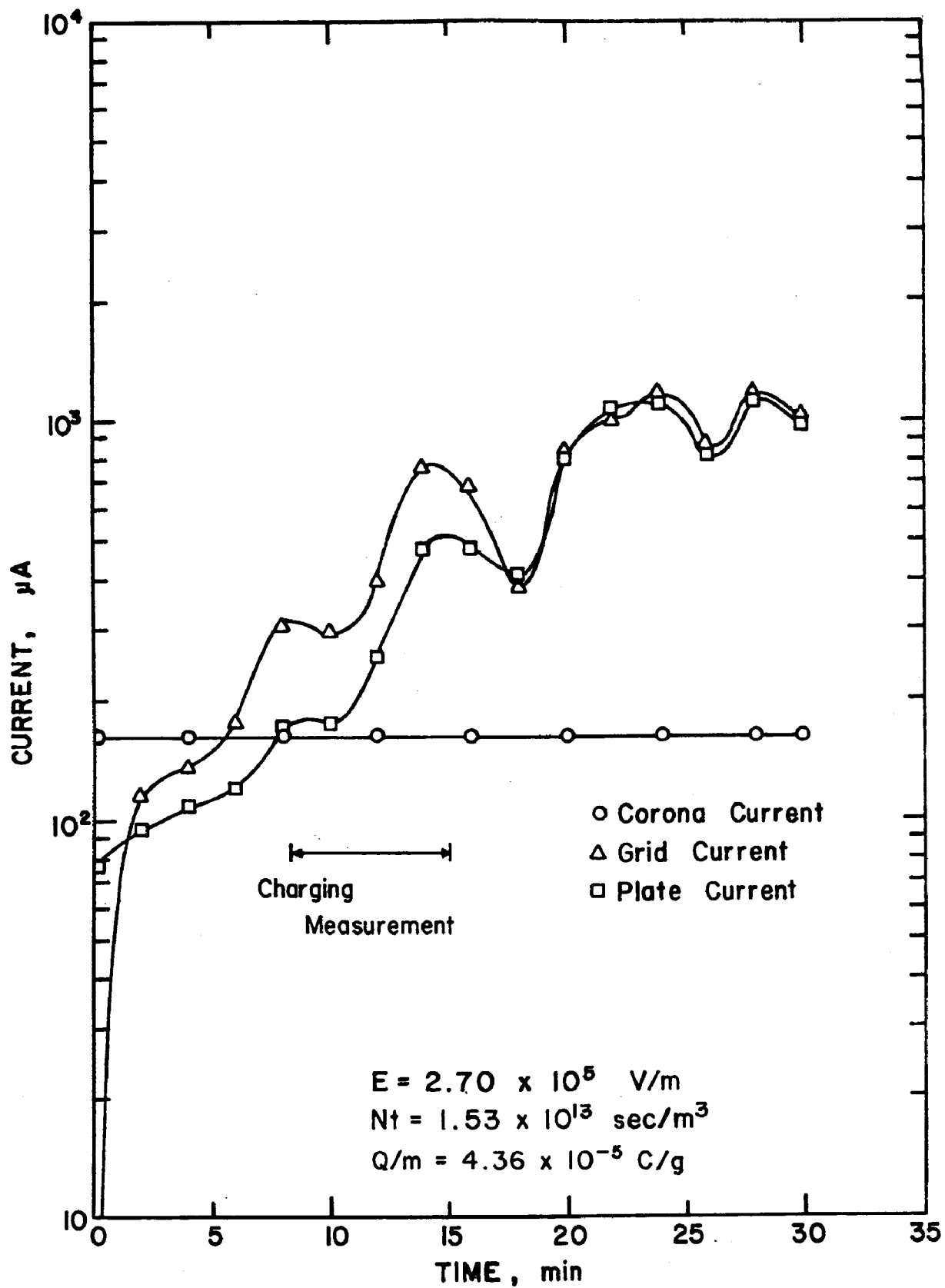


Figure 11. Test results of a three-electrode charger used for back corona suppression. Temperature = 125°C, corona electrode-to-plate spacing = 8.9 cm, grid electrode-to-plate spacing = 2.6 cm, and dust loading $\approx 3.4 \text{ g/m}^3$.

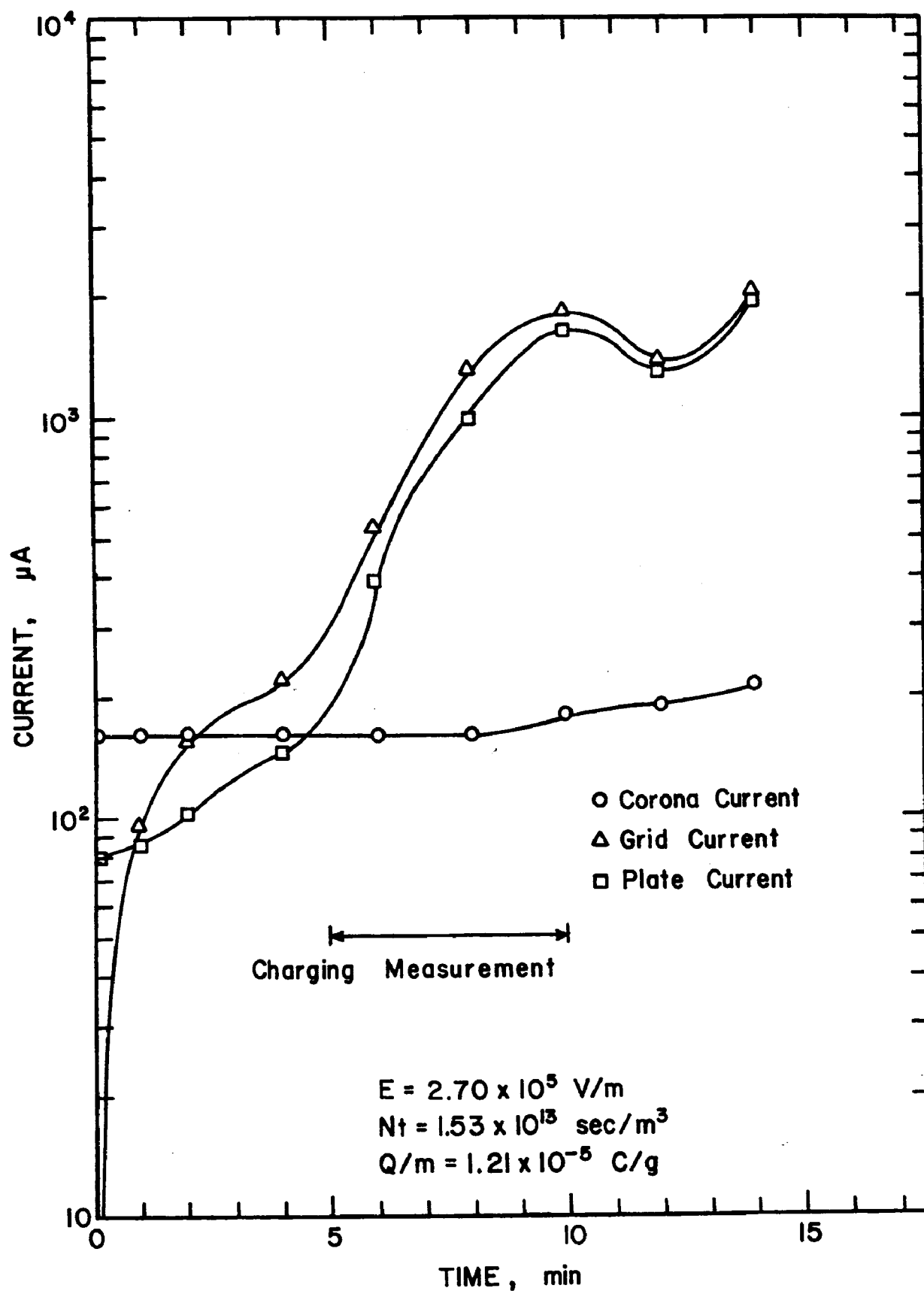


Figure 12. Test results of a three-electrode charger used for back corona suppression. Temperature = 130°C , corona electrode-to-plate spacing = 8.9 cm, grid electrode-to-plate spacing = 2.6 cm, and dust loading $\approx 6.8 \text{ g/m}^3$.

match a set of experimental electrical measurements obtained from a single laboratory setup. In order to find a theoretical current-voltage curve which would match a particular experimental result, the effective plate width was adjusted. Other geometric parameters including wire-to-plate spacing and wire diameter remained fixed at actual experimental values. An ion mobility of 2.4×10^{-4} meter²/volt-second was used in the simulation and coincides with previous experimental determinations of mobility. Figures 13 through 18 present the results of matching theoretical and experimental electrical characteristics for six wire-plate configurations. The decreasing accuracy of the theoretical curve fits as the current increases may result from variations in the ion mobility due to the changing electric fields which were not accounted for in the computer model. The ratio of the effective plate width to the actual plate width was compared with the ratio of the actual plate width to the wire-to-plate separation, as shown in Figure 19. This curve was used to predict the effective plate widths required to match the theoretical and experimental current-voltage curves for two wire-plate geometries for which experimental data existed. The effective plate widths which produced the best fits to the experimental curves differed by 0% and 20% from the predicted values. Thus, an approximate computer model may be obtained for any wire-plate configuration by using the effective plate width indicated in Figure 19.

The I-V characteristic of a wire-plate system with a single wire discharge electrode is not strongly dependent upon plate width. The sparkover voltage becomes smaller, however, if the plate width is reduced to less than approximately the wire-plate separation. Figures 20 through 25 are an experimentally generated family of curves for wire-plate corona systems. In general a drop in maximum current occurs, often sharply, as the wire-plate separation is increased beyond the distance equal to the plate width.

Discharge Electrodes

In order to produce large electric field strengths necessary for corona generation, field lines must converge strongly at the corona discharge electrode. A very thin wire thus serves effectively as a discharge. But in applications in a severe environment a fine corona wire does not have the structural strength to perform for long periods of time.

Barbed wire electrodes have been employed in many electrostatic precipitators in order to provide an electrode with both good structural strength and strong field convergence regions for good corona production. Since each barb serves as a corona point, a maximum corona current can be achieved by using as large a number of points as possible. If, however, the barbs are too closely spaced an interference will occur which can reduce the total corona current in the following manner: convergence of electric field lines at a corona point causes a reduction in field strength on the discharge electrode a short distance away from the corona point. Upon inception of a corona current the transverse component of the current causes a further reduction in field in the region outside the corona on the discharge electrode due to the space charge associated with the corona current. In a linear array of corona points, it would thus be possible for a corona discharge to occur only at every other point if the points are too closely spaced.

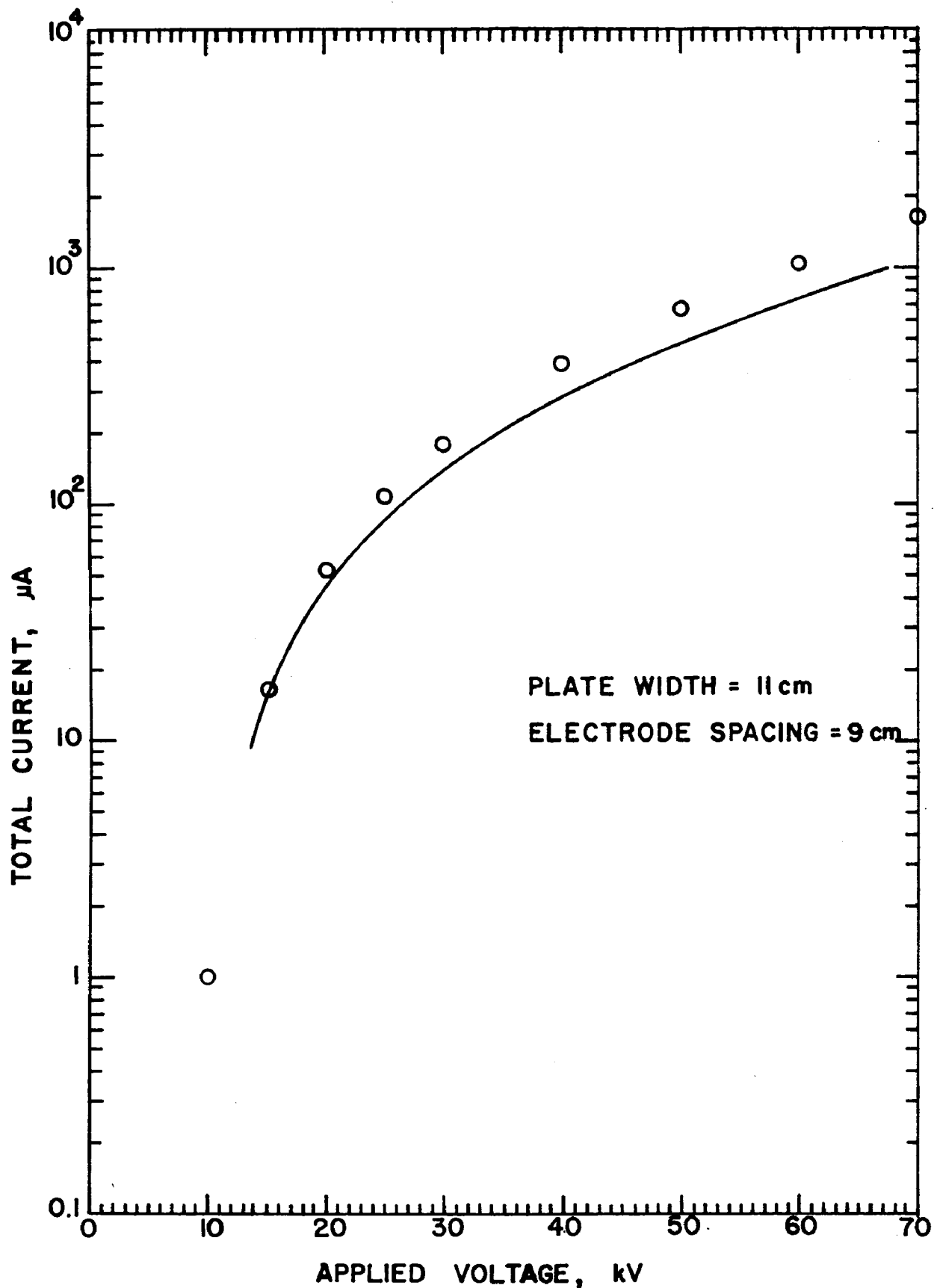


Figure 13. Comparison of theoretical and experimental I-V characteristics for a wire-plate configuration with 11 cm plate width and 9 cm electrode separation.

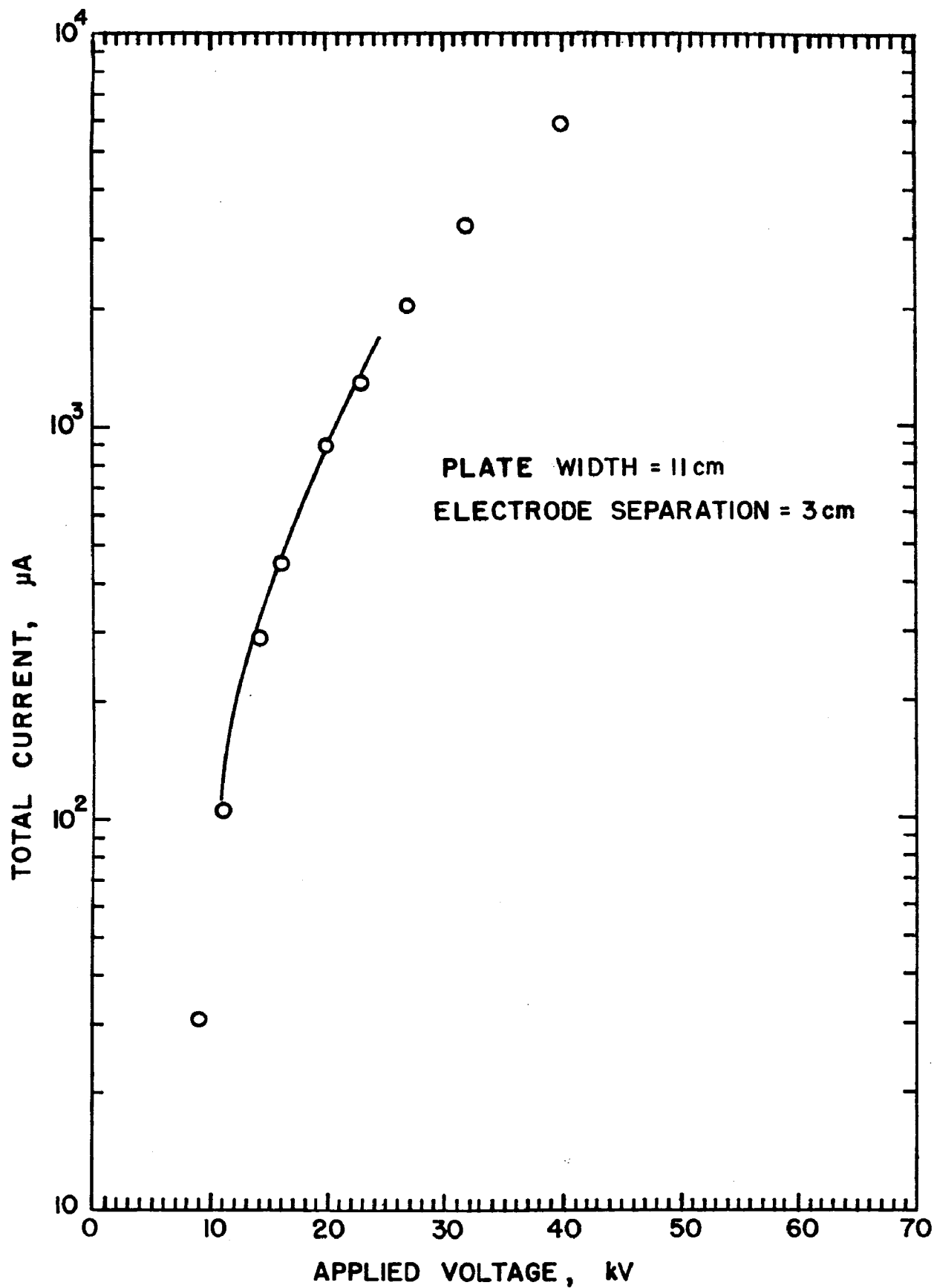


Figure 14. Comparison of theoretical and experimental I-V characteristics for a wire-plate configuration with 11 cm plate width and 3 cm electrode separation.

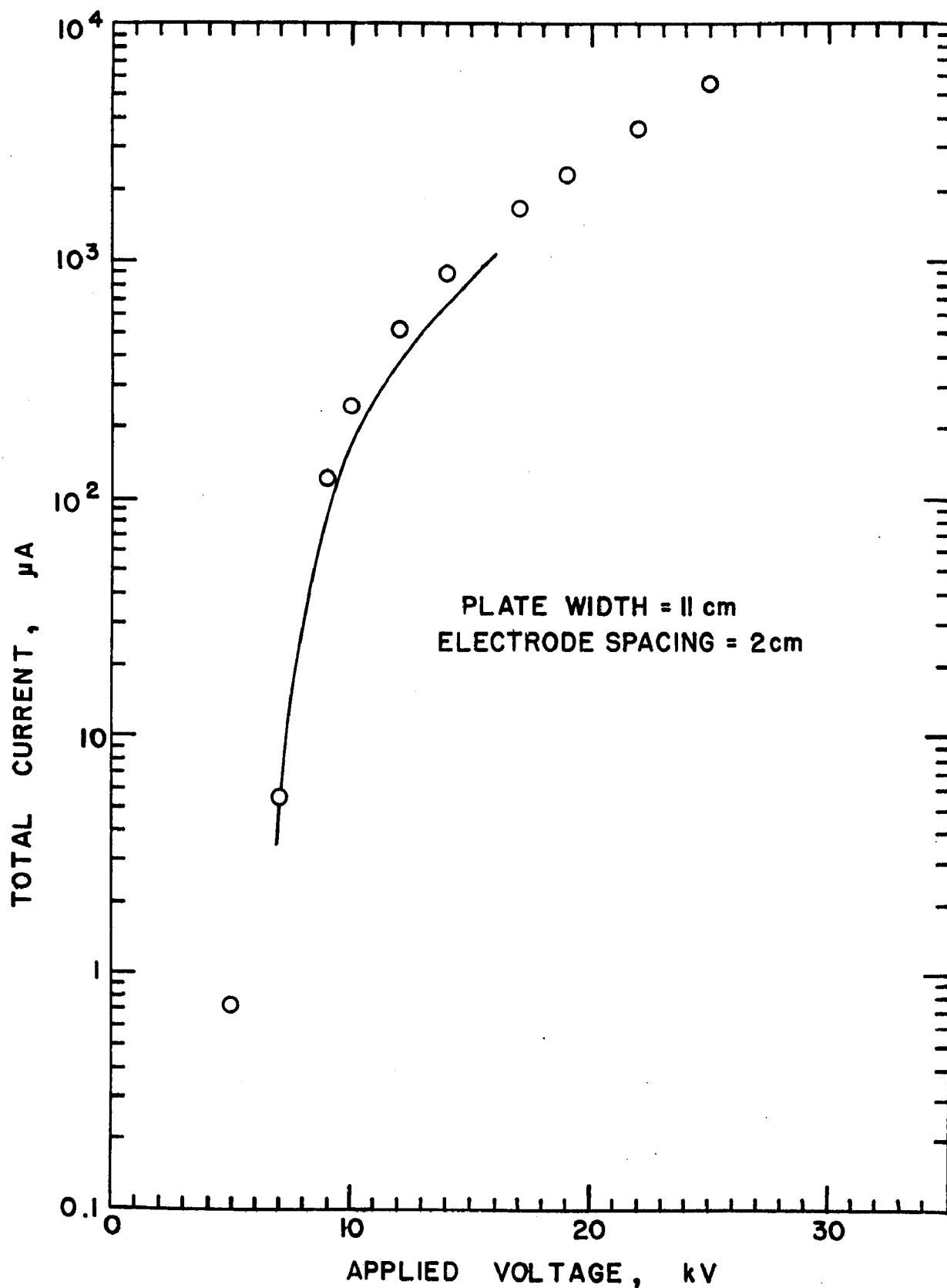


Figure 15. Comparison of theoretical and experimental I-V characteristics for a wire-plate configuration with 11 cm plate width and 2 cm electrode separation.

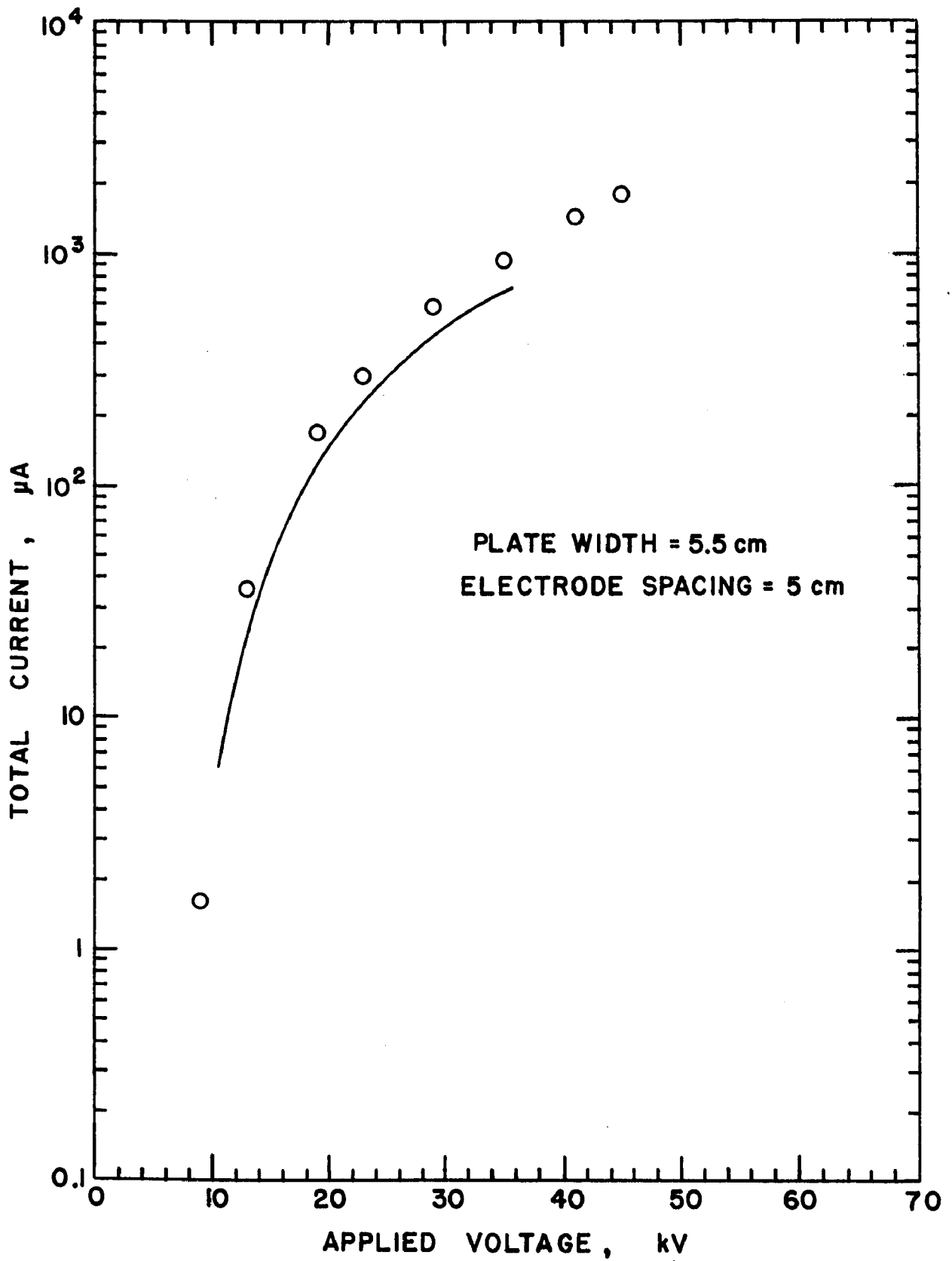


Figure 16. Comparison of theoretical and experimental I-V characteristics for a wire-plate configuration with 5.5 cm plate width and 5 cm electrode spacing.

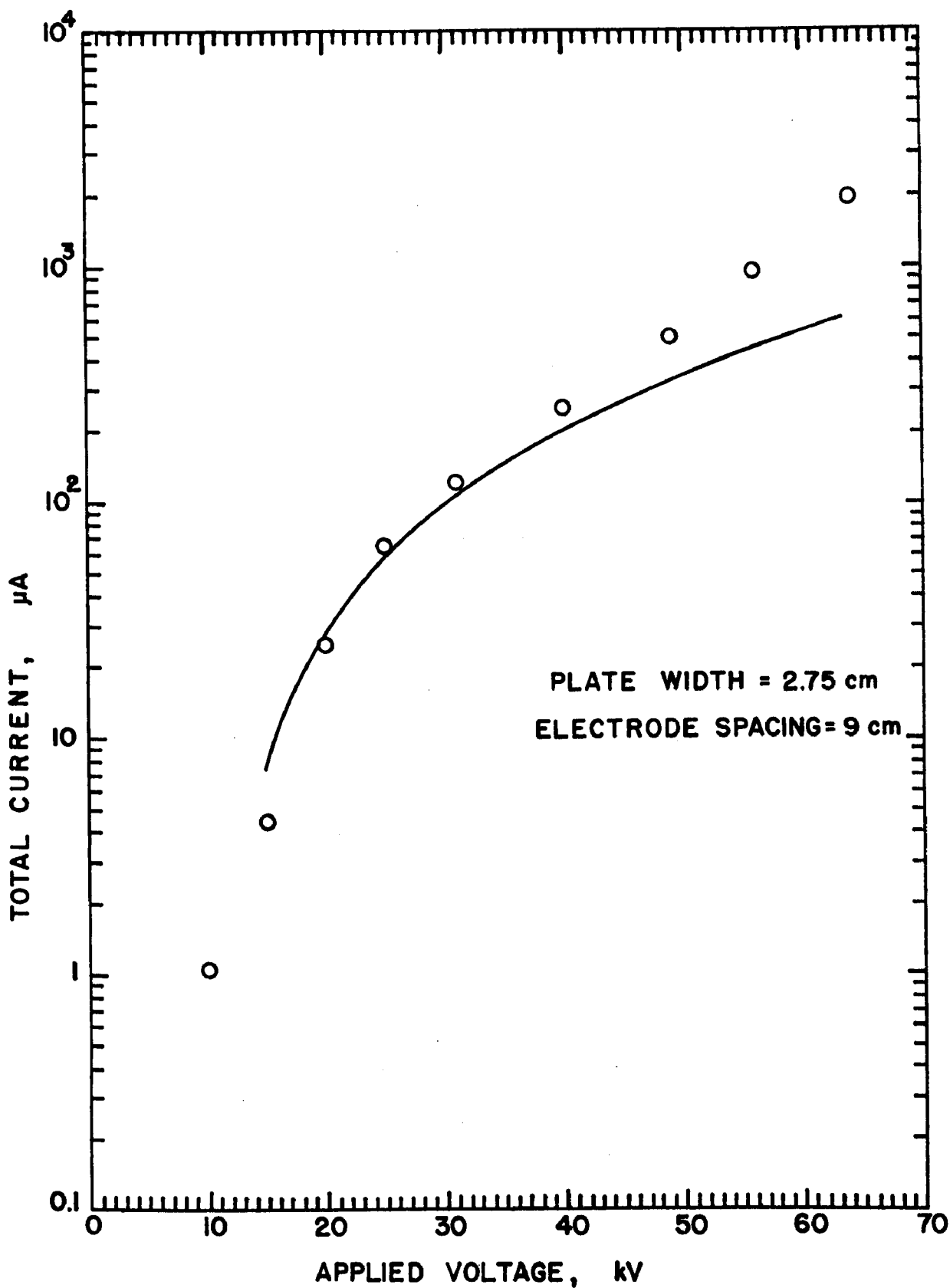


Figure 17. Comparison of theoretical and experimental I-V characteristics for a wire-plate configuration with 2.75 cm plate width and 9 cm electrode separation.

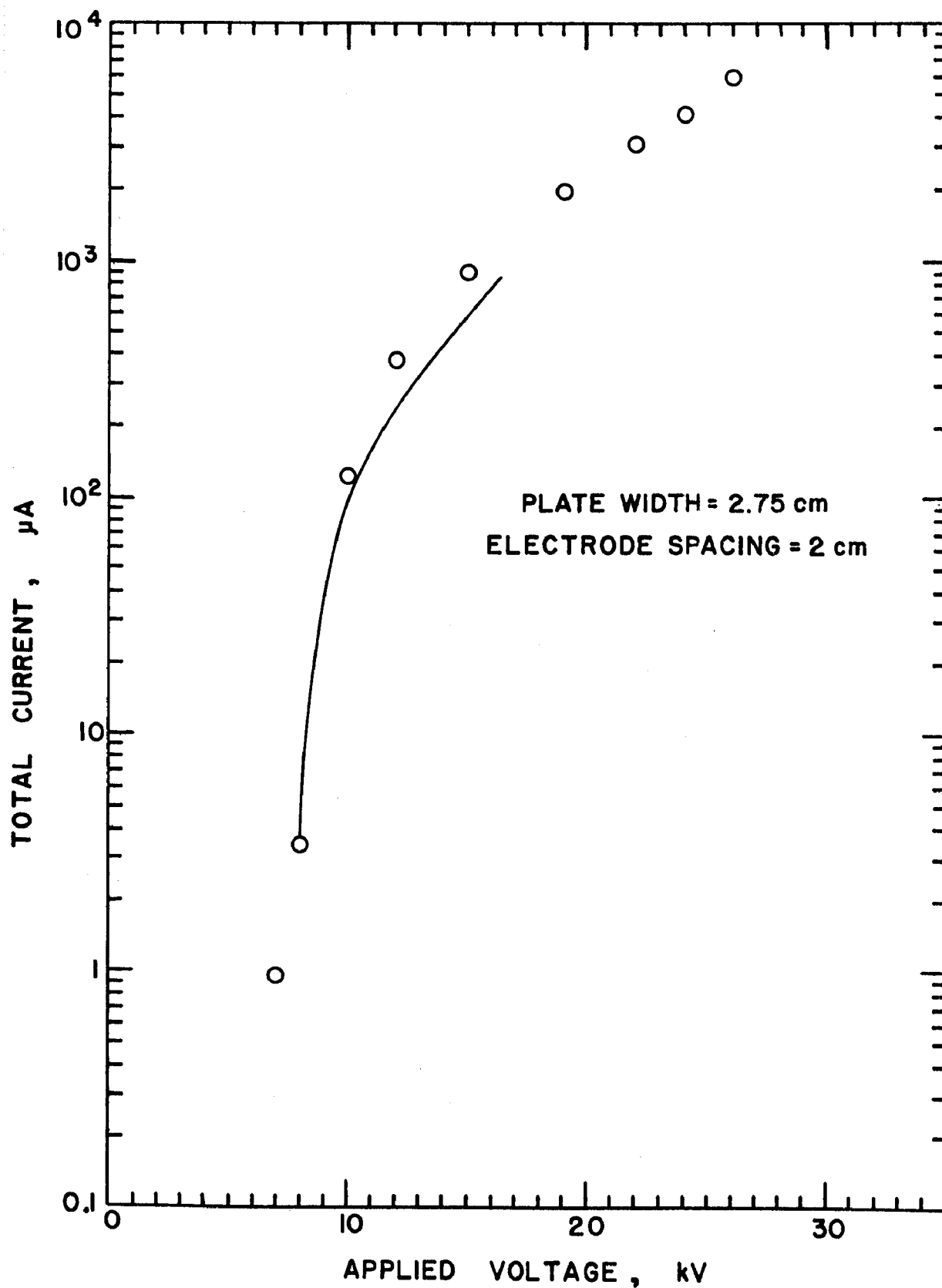


Figure 18. Comparison of theoretical and experimental I-V characteristics for a wire-plate configuration with 2.75 cm plate width and 2 cm electrode separation.

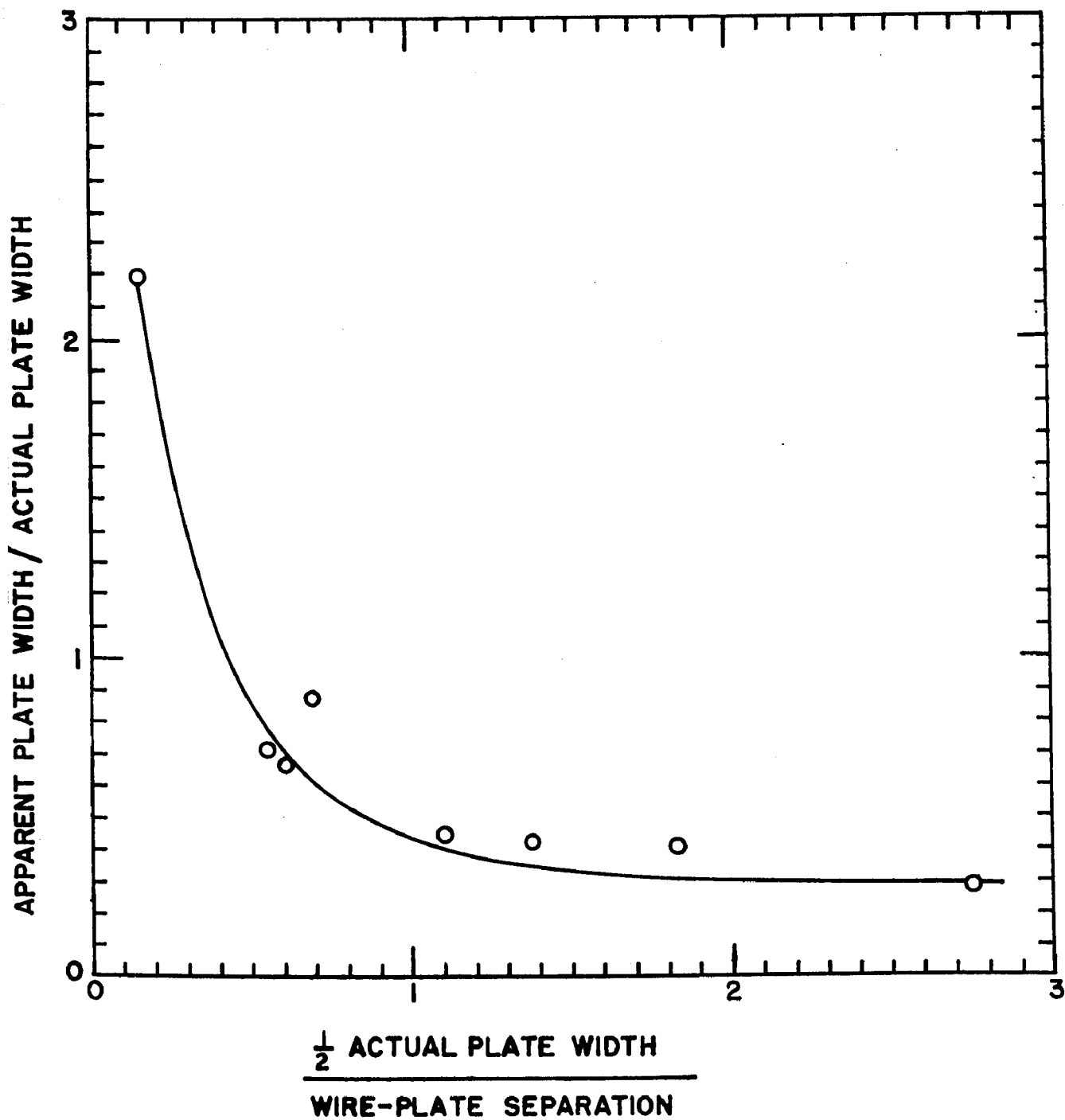


Figure 19. Ratio of apparent to actual plate width used to provide best theoretical fit for various values of plate width to electrode separation ratio.

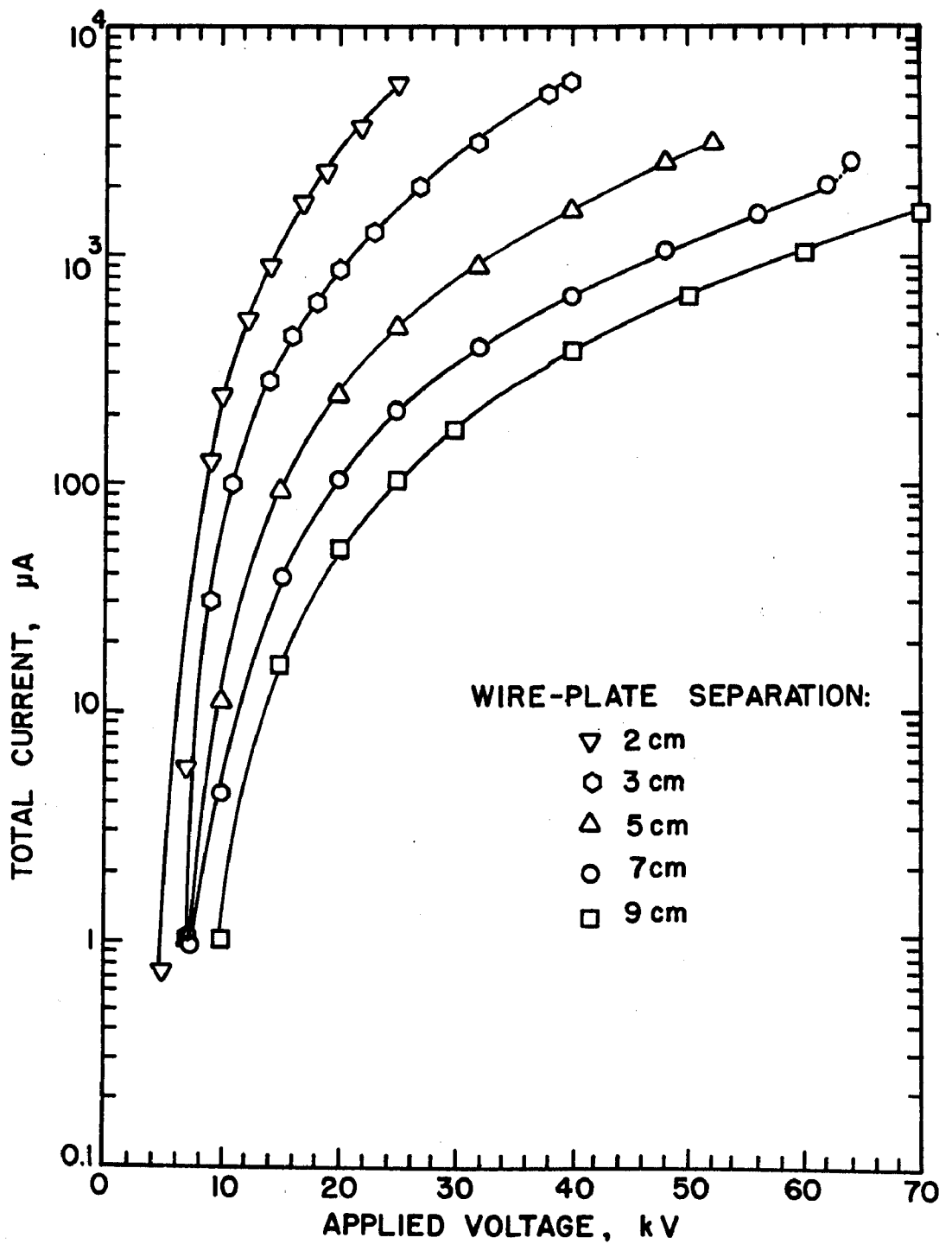


Figure 20. Electrical characteristics of a parallel wire-plate corona electrode system for five values of electrode spacing. Plate width is 11 cm, and wire diameter is 0.25 mm.

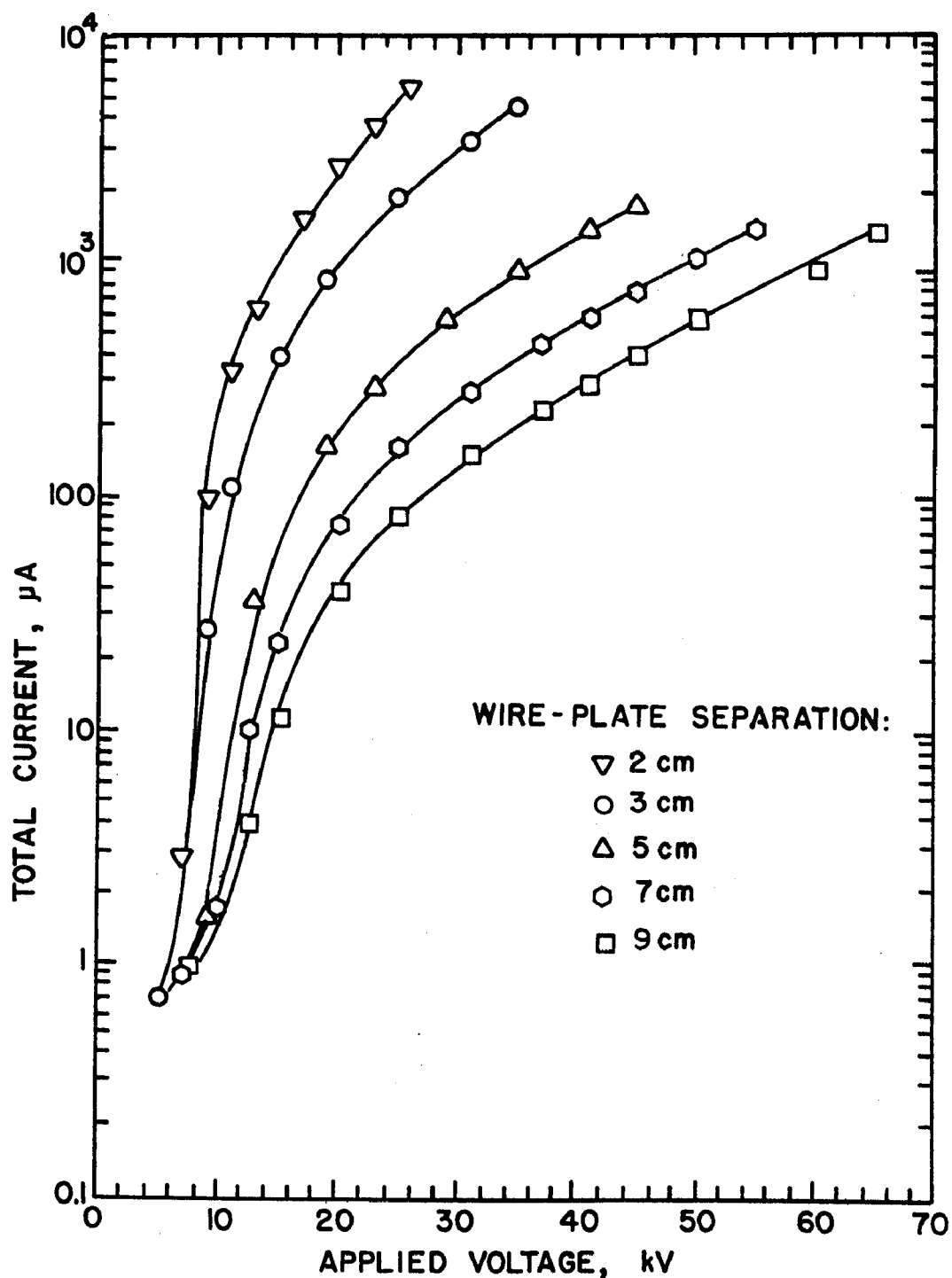


Figure 21. Electrical characteristics of a parallel wire-plate corona electrode system for five values of electrode spacing. Plate width is 5.5 cm, and wire diameter is 0.25 mm.

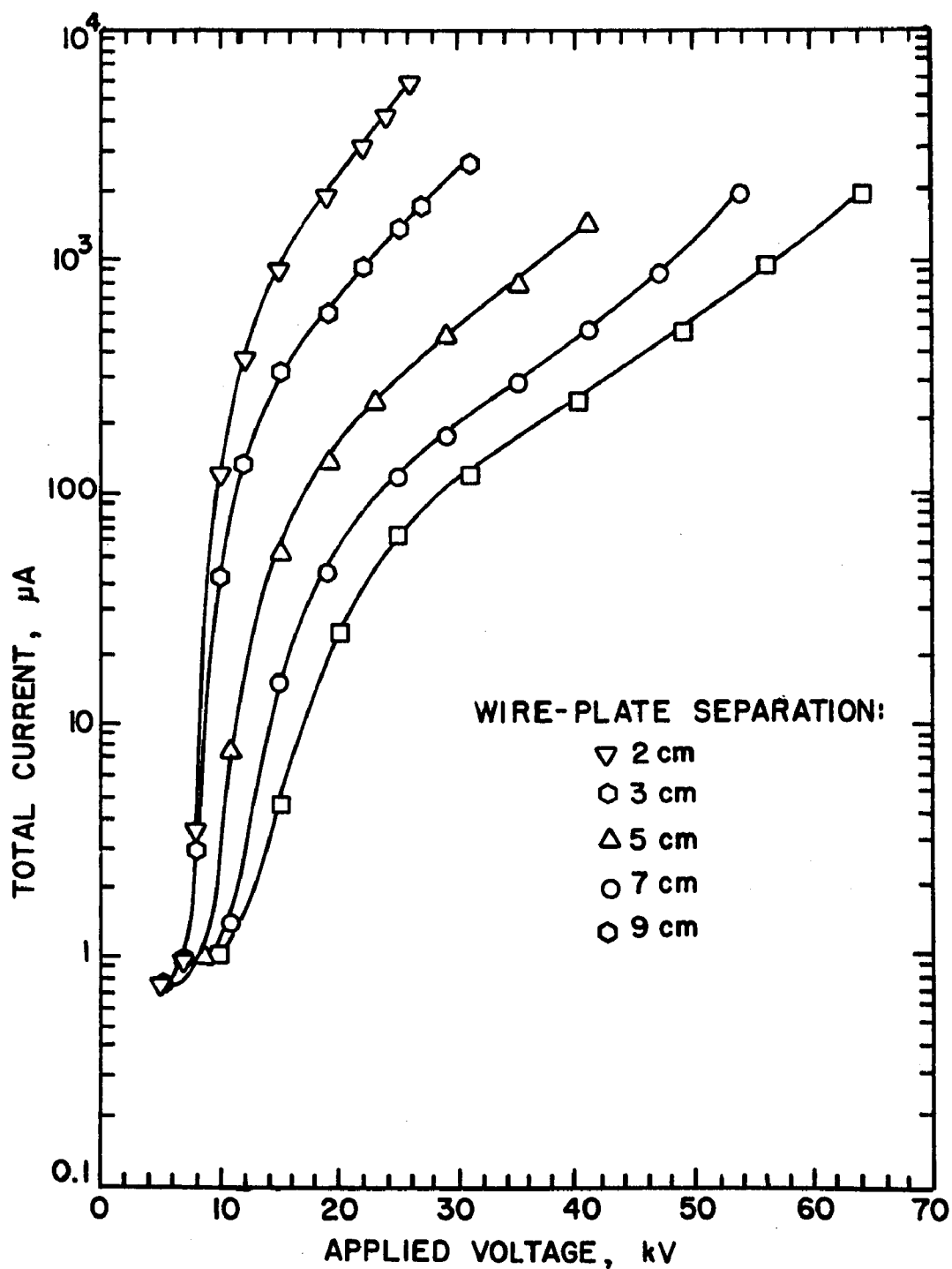


Figure 22. Electrical characteristics of a parallel wire-plate corona electrode system for five values of electrode spacing. Plate width is 2.75 cm, and wire diameter is 0.25 mm.

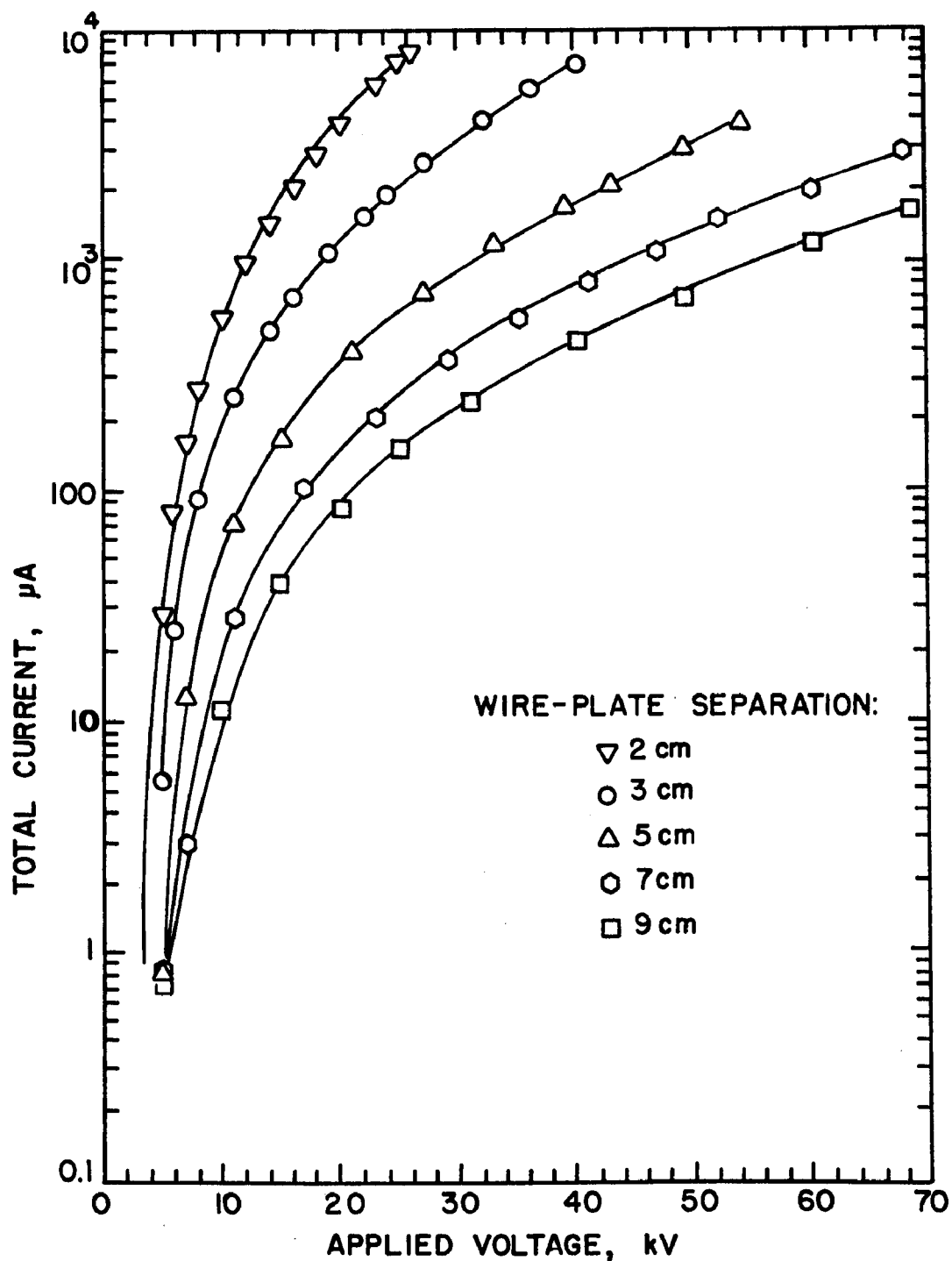


Figure 23. Electrical characteristics of a parallel wire-plate corona electrode system for five values of electrode spacing. Plate width is 11 cm, and wire diameter is 0.79 mm.

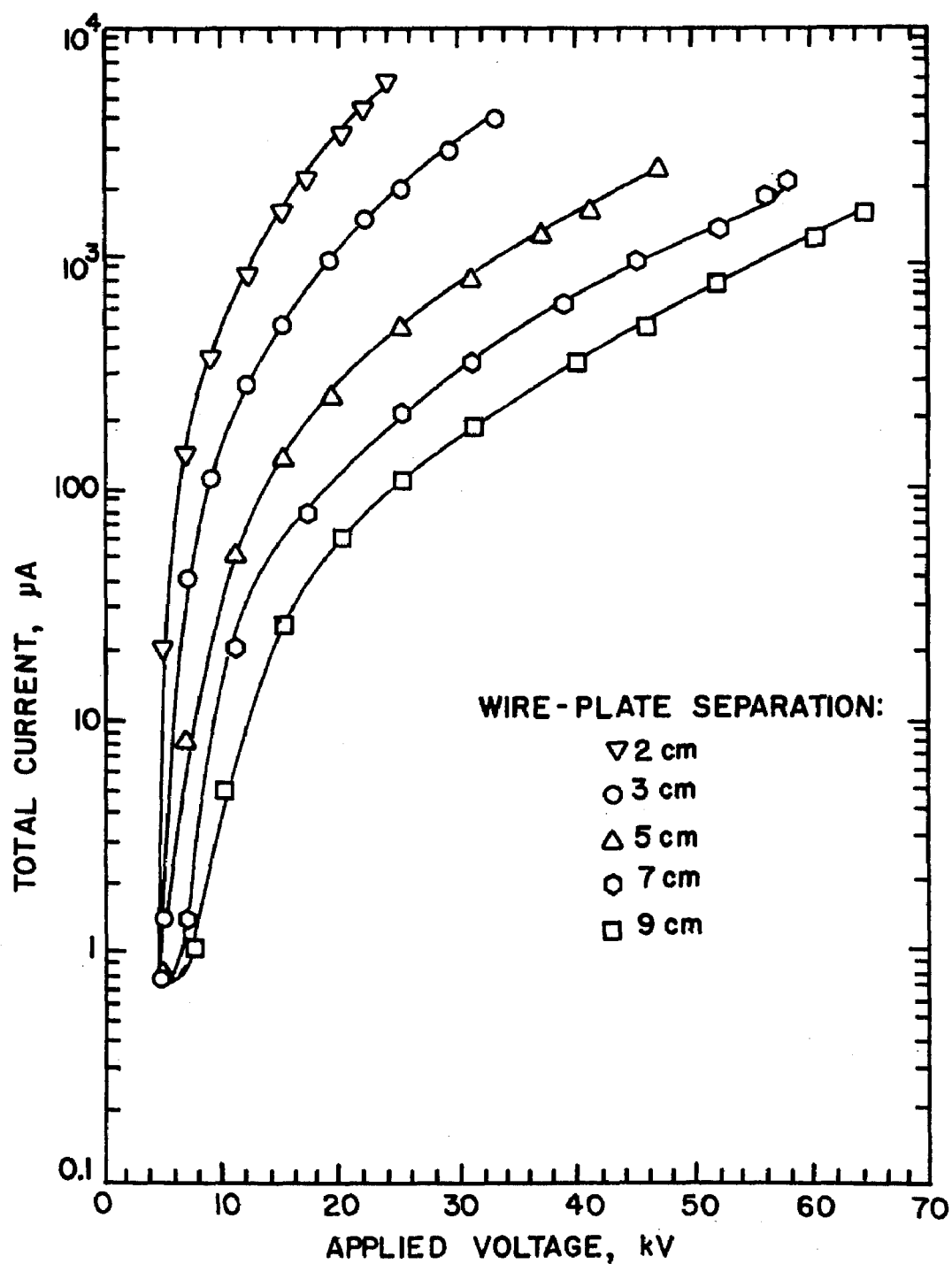


Figure 24. Electrical characteristics of a parallel wire-plate corona electrode system for five values of electrode spacing. Plate width is 5.5 cm, and wire diameter is 0.79 mm.

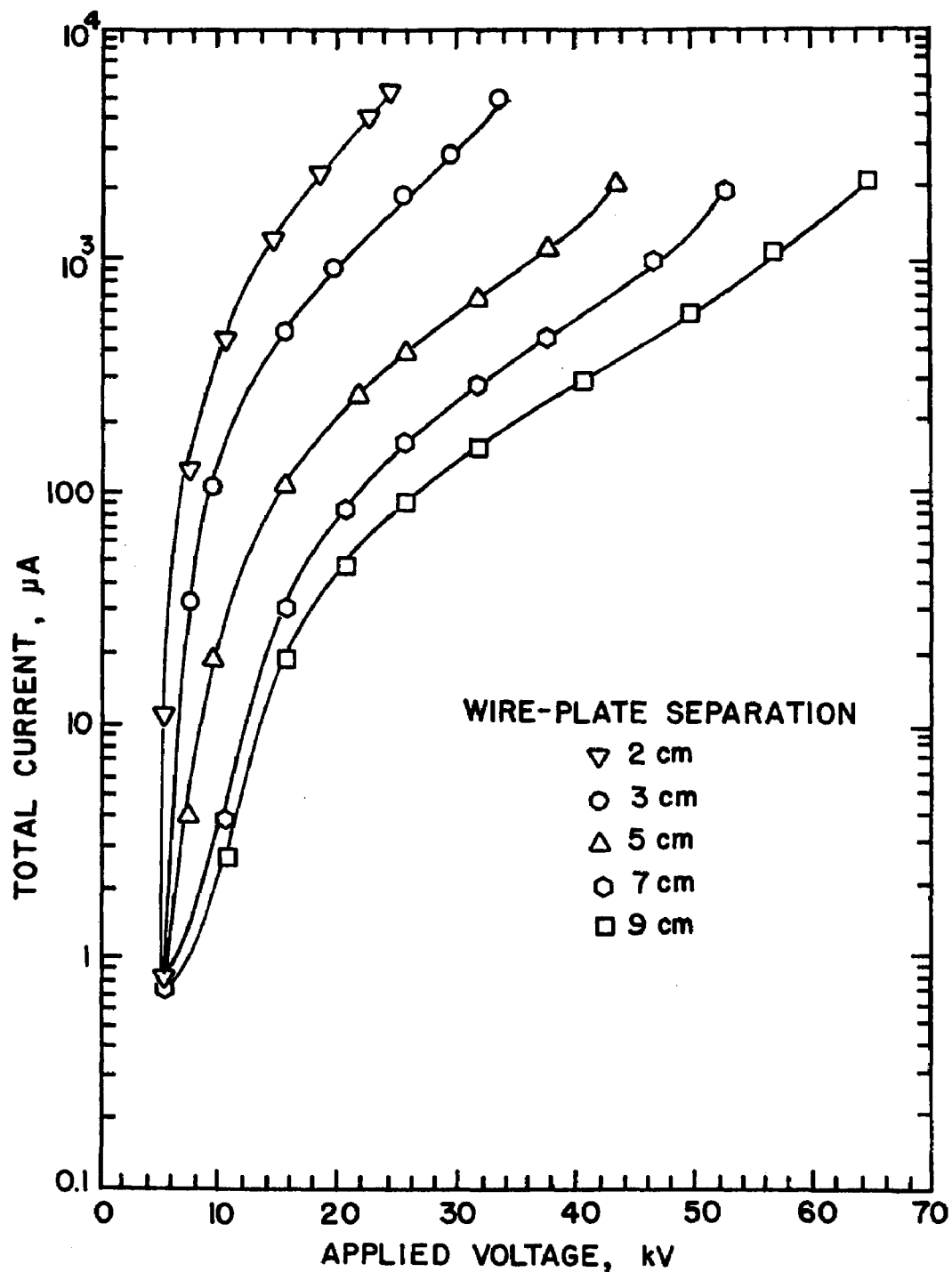


Figure 25. Electrical characteristics of a parallel wire-plate corona electrode system for five values of electrode spacing. Plate width is 2.75 cm, and wire diameter is 0.79 mm.

As the corona points on a barbed wire electrode are brought closer together, it would therefore be expected that the total corona current per unit length of electrode would increase to some maximum value. Bringing the points closer together would force a quenching of the corona on alternate points, thus reducing the total current. This conjecture has been borne out by experiment, as shown in Figure 26. A barbed wire electrode along the axis of a 14 cm diameter cylindrical conductor was used as a corona discharge electrode. A maximum total corona current is found for a barb spacing of approximately 0.7 cm.

A similar effect is shown in Figure 27 for a discharge electrode made up of a set of discs spaced along a rod on the cylinder axis. In this example the current per disc is plotted as a function of the disc separation distance. The rapid change in current per disc where the separation is close is similar to the barbed wire results.

The number of possible configurations for discharge electrodes is practically limitless; however, most can be derived from a set of sharp points or sharp edges supported by a rigid structure. Since many discharge electrode structures are complicated geometrical figures or contain discontinuities at the surface analytical treatment is generally impracticable. Comparative empirical studies using a fixed passive electrode offer the best means of evaluating discharge electrode types.

Among those tested, including helix, ribbon, barbed wire and disc electrodes those producing the greatest total current were barbed wire and stacked-disc electrodes. Figure 28 shows a comparison of these two types, along with a straight wire electrode. Sharpedged discs, 5 cm in diameter and spaced approximately 5 cm apart produced the largest total current. The barbed wire electrode also exhibits better performance than the straight wire. The barbed wire also has the advantage of causing less obstruction to the flow of gas through the system than does a system of disc electrodes.

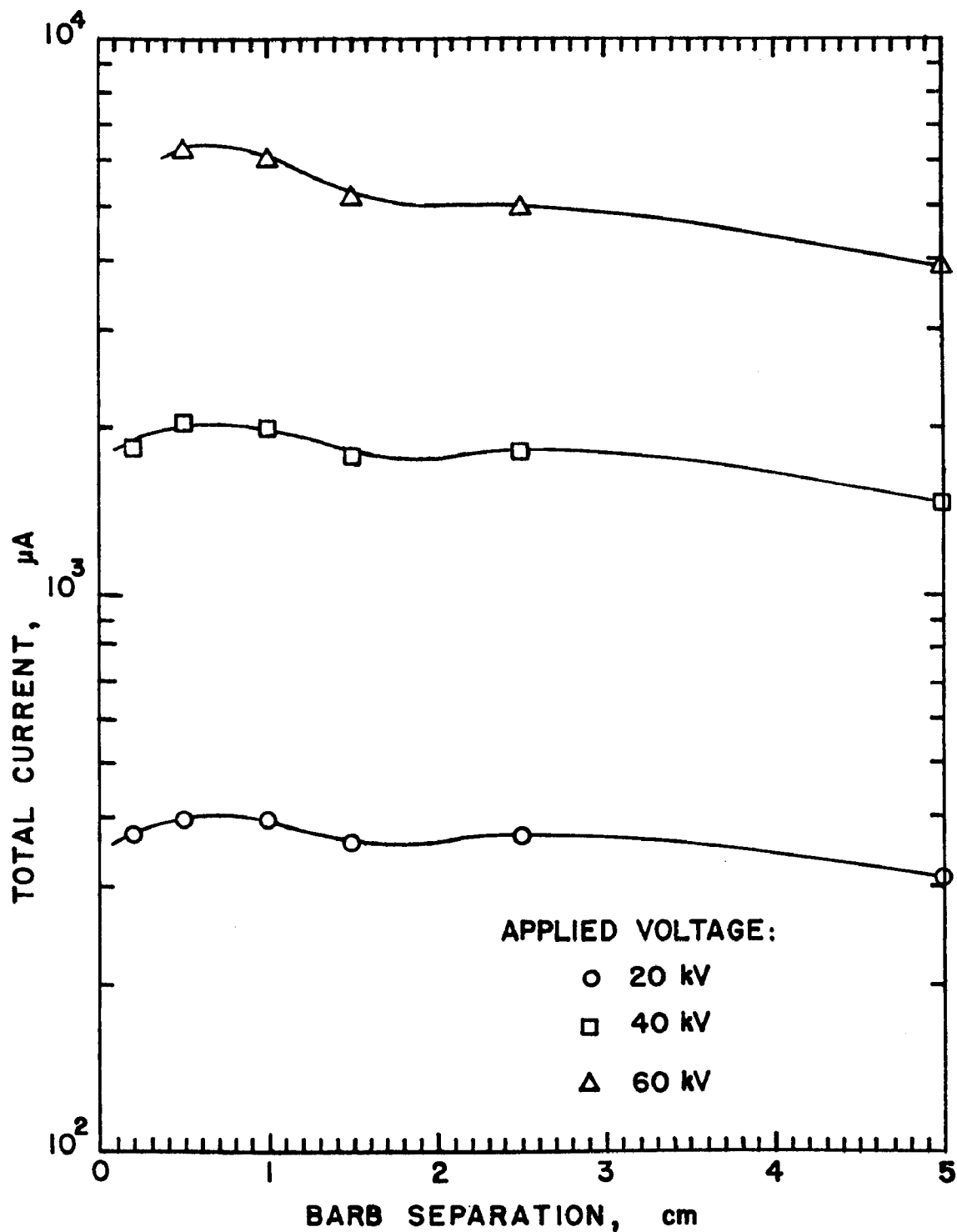


Figure 26. Total corona current for fixed length of barbed wire discharge electrode as a function of separation between barbs.

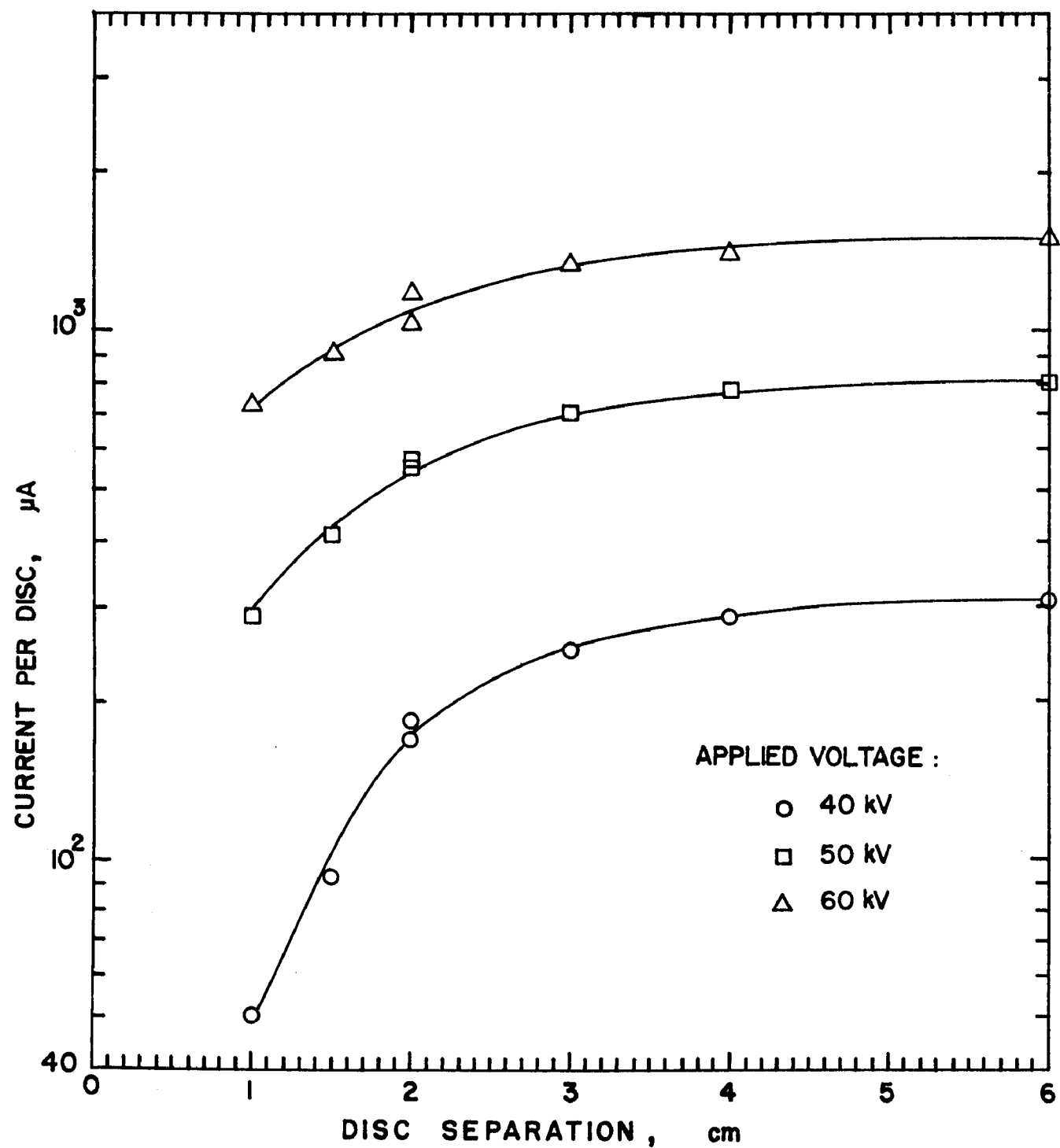


Figure 27. Corona current per disc for a discharge electrode consisting of discs at various spacings with axes aligned.

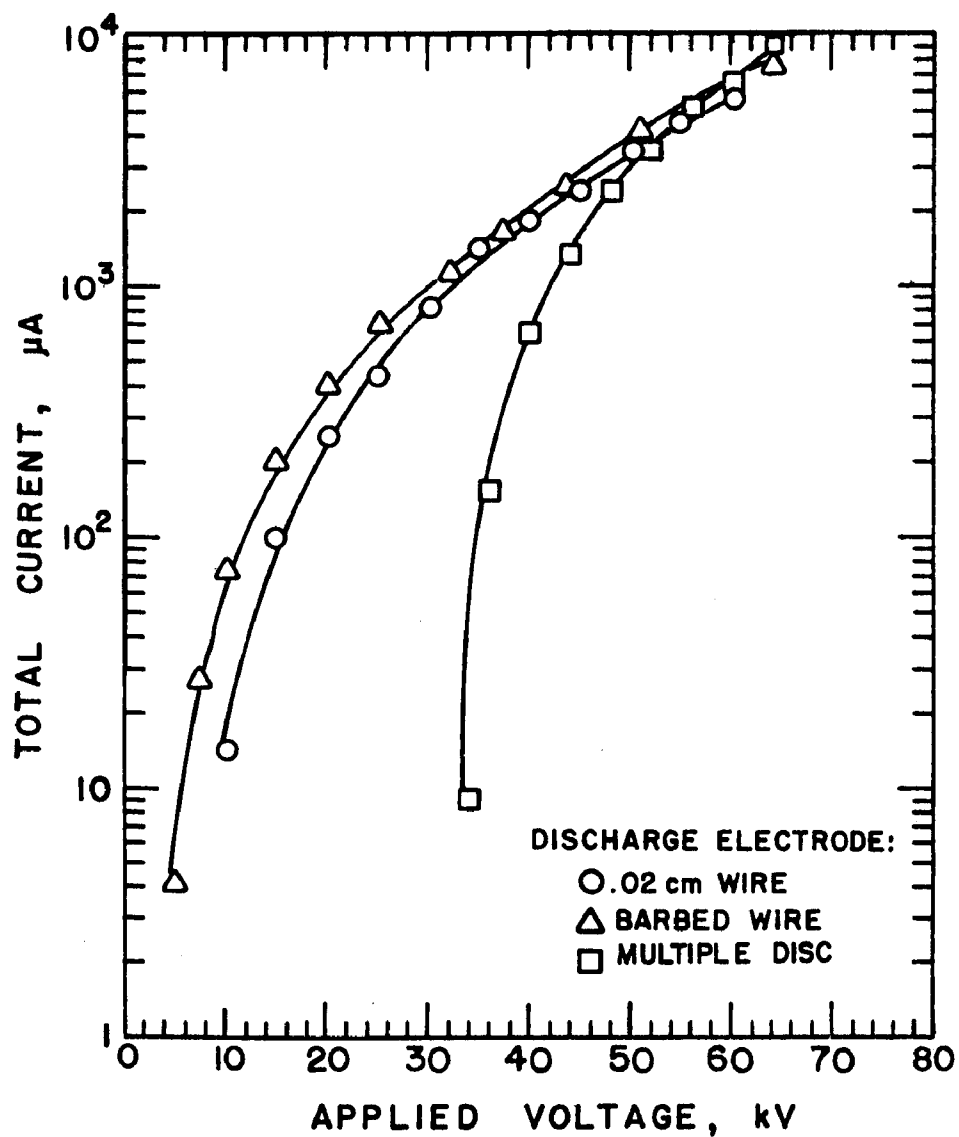


Figure 28. Comparison of I-V characteristics for a 0.02 cm wire, a barbed wire and an array of disc discharge electrodes. The passive electrode is a 14 cm diameter cylinder for all three curves.

SECTION 4

PILOT SCALE PRECHARGER

The results of the laboratory scale work were sufficiently encouraging to permit proceeding with the development of a pilot scale three-electrode pre-charger capable of handling a minimal gas flowrate of approximately $0.71 \text{ m}^3/\text{sec}$ (1500 acfm). Such a device was designed and fabricated by Southern Research Institute. Figure 29 is a photograph of the precharger lying on one side. The top of the precharger is shown at the left-hand side of the picture. The three thick rods protruding from the top of the device are rapping rods, which are welded to the top edge of the plate electrodes. A pair of spring-loaded supports can be seen flanking each of the rapping rods. The arrangement of the electrodes can be seen in more detail in Figure 30, which also shows the shape of the corona discharge electrodes. The discharge electrode-to-plate spacing is 9.2 cm and the screen electrode-to-plate spacing is 2.0 cm.

INITIAL PILOT TEST PROGRAM

The device was installed in the test section at the inlet of an existing conventional pilot scale ESP at SoRI. Current-voltage (I-V) characteristics for the charger at ambient conditions and at elevated temperature were determined (Figure 31). There is approximately a two-fold increase in current with elevated temperature and a 10kV decrease in breakdown voltage. This result is expected because of the increased ion mobility at higher temperatures.

Tests of precharger performance under conditions of high resistivity dust loading were undertaken using redispersed fly ash. Temperatures ranging from 75°C to 130°C were used, and measured values of dust resistivity were in the range of 10^{12} to 10^{13} ohm-cm. The fly ash was injected into the system by means of a sandblasting gun, at a rate controlled by the air pressure applied.

Impactor measurements were made to determine the size distribution of the redispersed fly ash. Operating the sandblaster at a pressure of 138 Pa (20 psi) injects approximately 1.88 g/m^3 into a $0.71 \text{ m}^3/\text{sec}$ (1500 ft^3/min) stream of gas. The particulate mass median diameter at the inlet of the precharger has been determined to be about $25 \text{ }\mu\text{m}$. Figures 32-35 show the results of particle size distribution measurements.

Preliminary tests were conducted to determine the effectiveness of the screen electrode in the prevention of back corona, using a particulate loading of 1.88 g/m^3 at a temperature of 130°C , and humidity controlled at 1.2% (by volume). Ash resistivity under these conditions was determined to be approximately 10^{13} ohm-cm. These tests were performed without plate rapping. Figures 36, 37, and 38 illustrate three back corona suppression tests. The

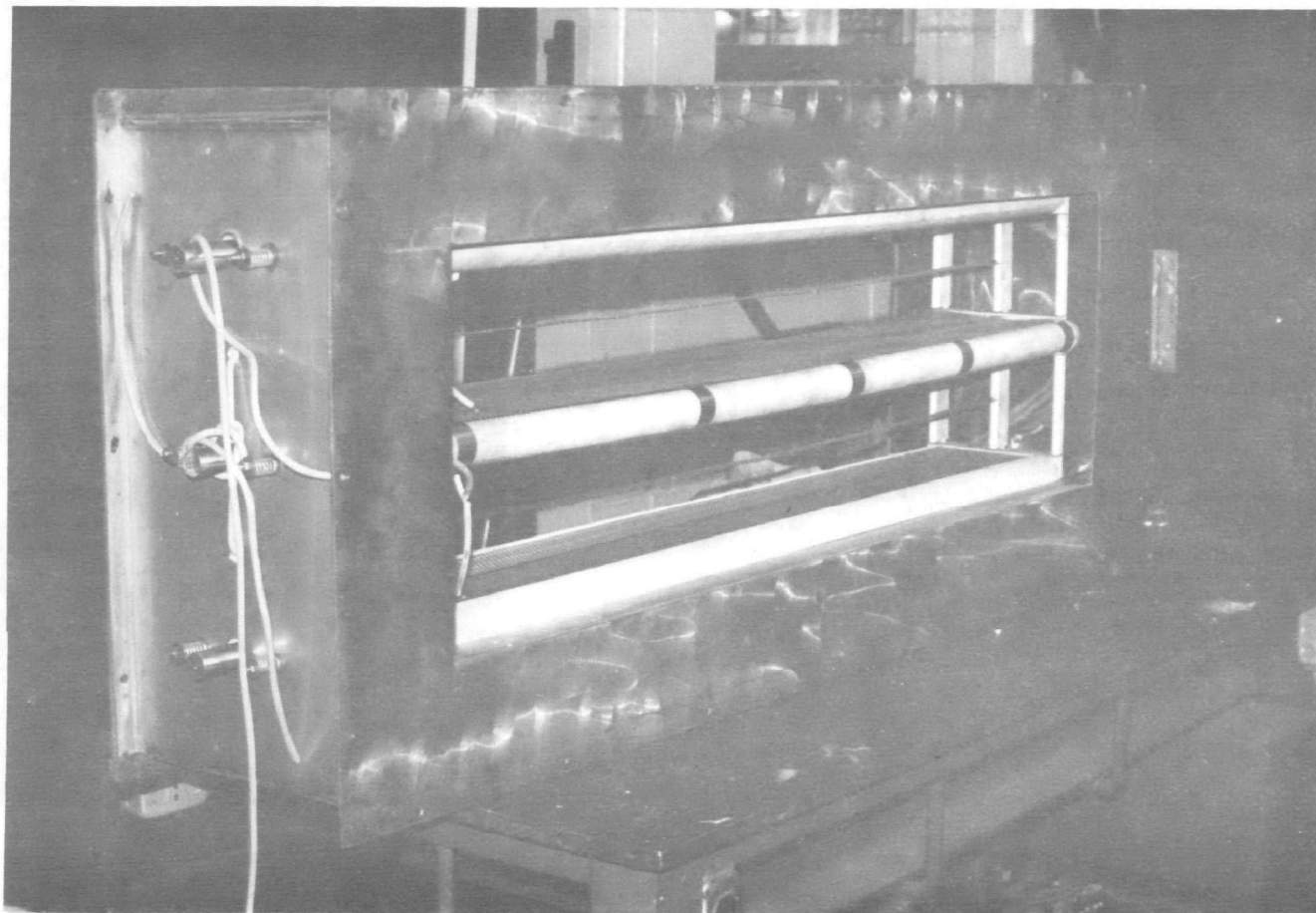
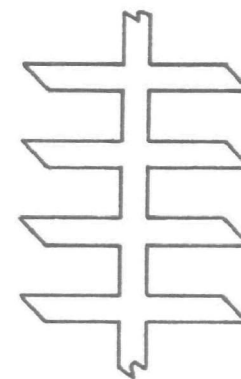
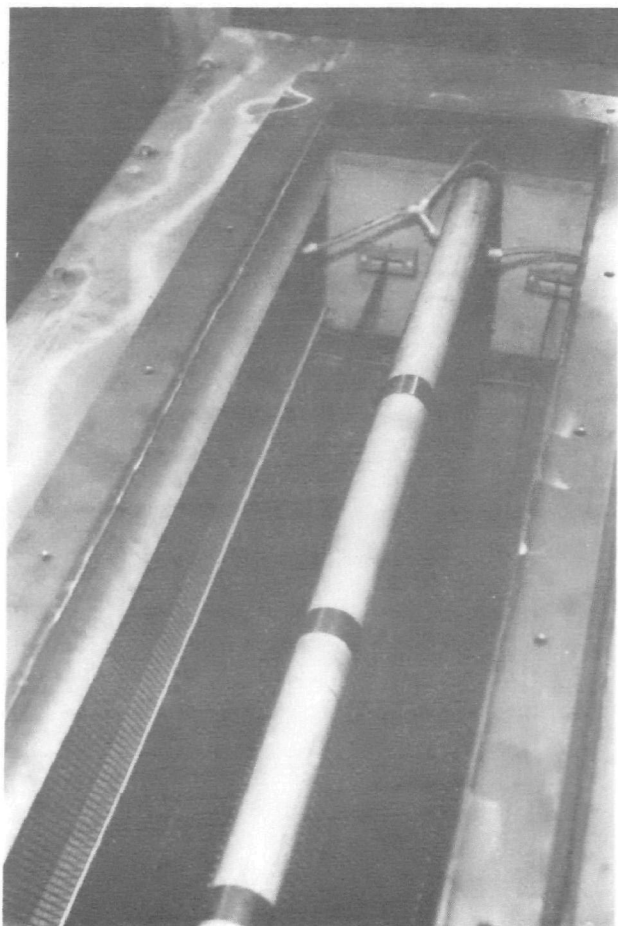


Figure 29. View of the pilot scale charger on its side.



(Full scale)

Detail of the Corona Discharge Electrode

Figure 30. View of the pilot scale charger electrode configuration.

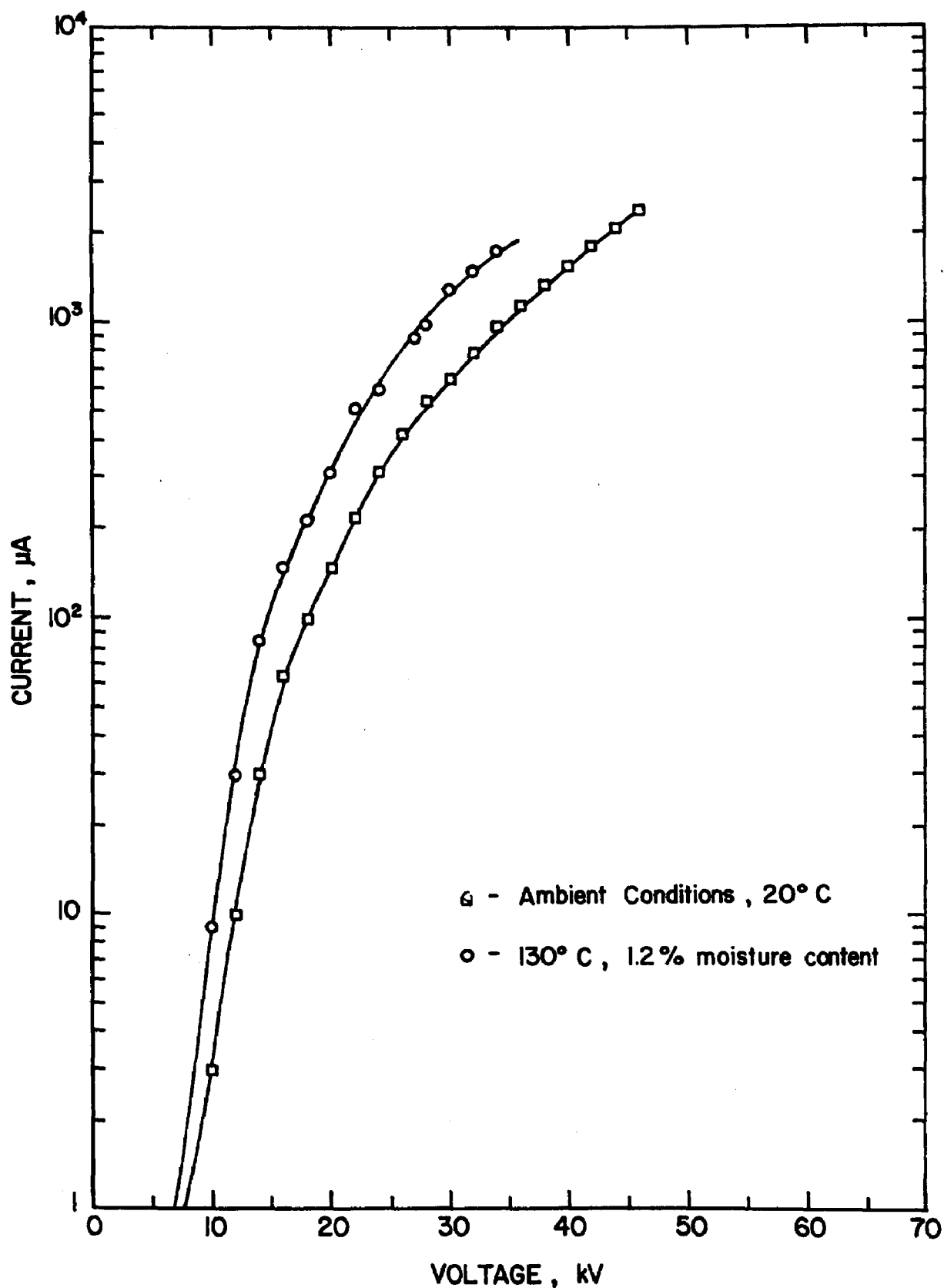


Figure 31. Corona current vs. corona voltage characteristics for the precharger with the screen voltage adjusted to maintain zero screen current.

INLET PRECHARGER TEST FEED RATE 20 PSI 10-25/26-77
 RHO = 2.47 GM/CC INCLUDE MASS LESS THAN .25 MICRONS

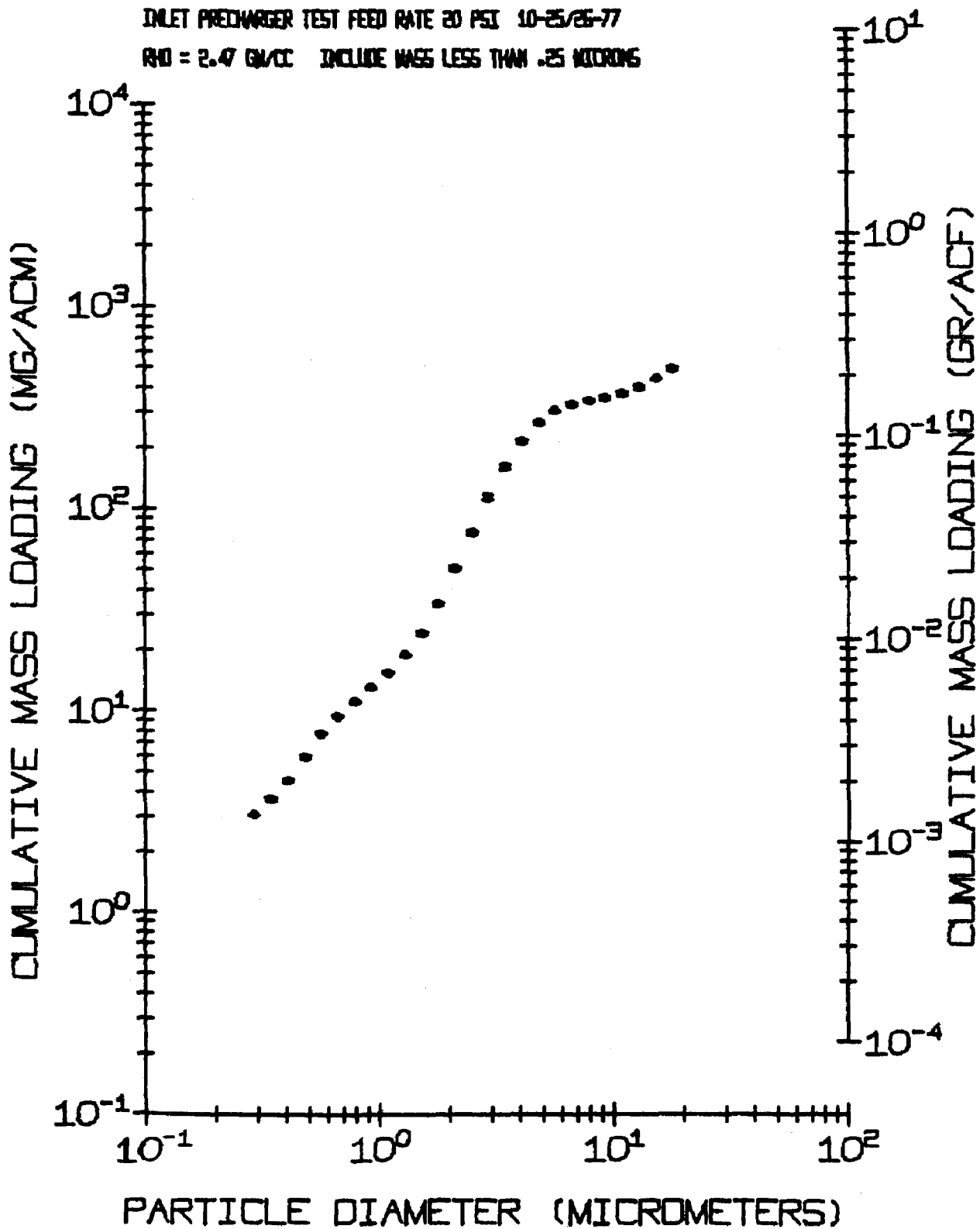


Figure 32. Results of the dust loading characterization at the precharger inlet with the sandblasting gun at 138 Pa (20 psi).

INLET PRECHARGER TEST FEED RATE 20 PSI 10-25/26-77

RHO = 2.47 GM/CC INCLUDE MASS LESS THAN .25 MICRONS

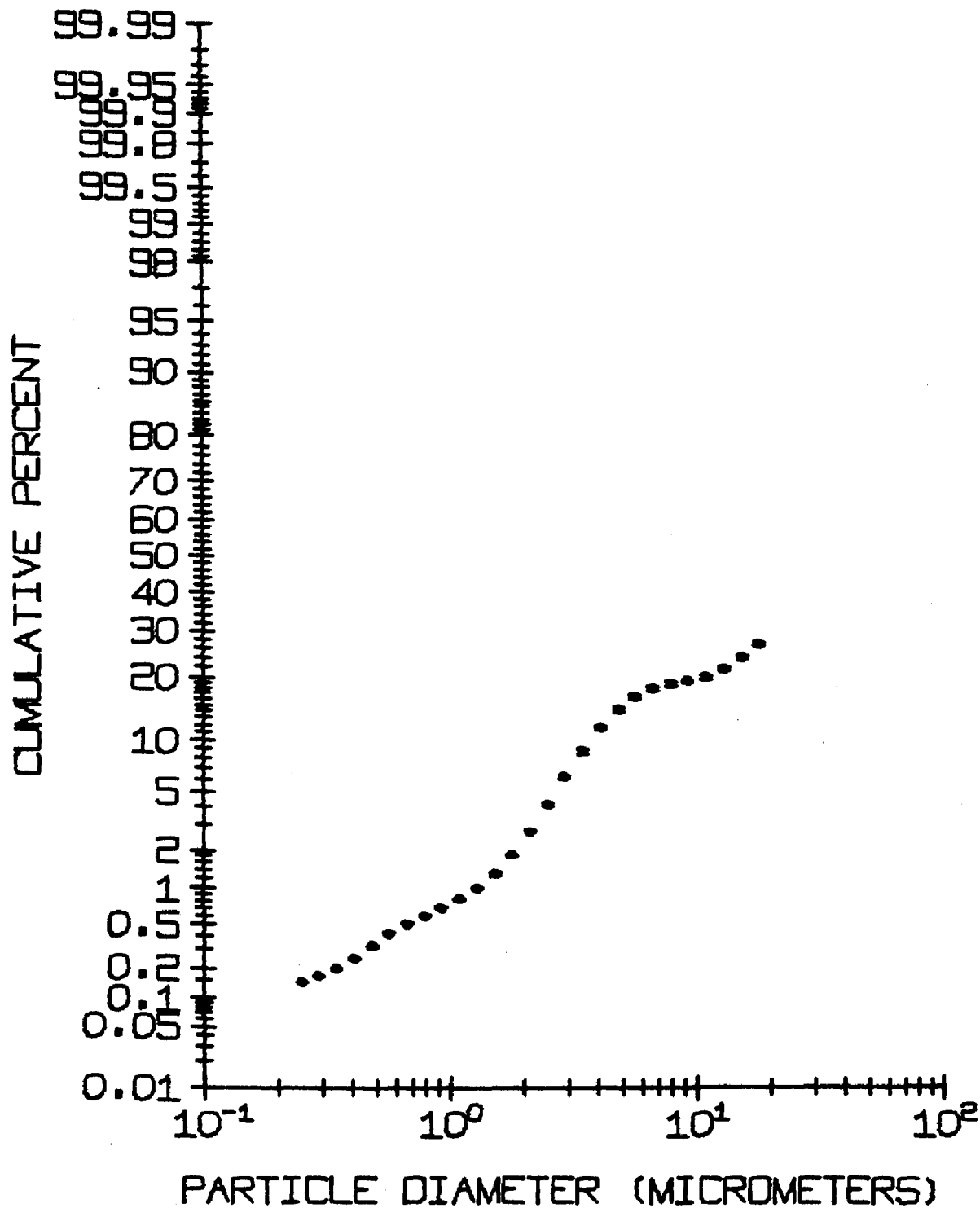


Figure 33. Results of the dust loading characterization at the precharger inlet with the sandblasting gun at 138 Pa (20 psi).

INLET PRECHARGER TEST FEED RATE 20 PSI 10-25/26-77

RHD = 2.47 G/CC INCLUDE MASS LESS THAN .25 MICRONS

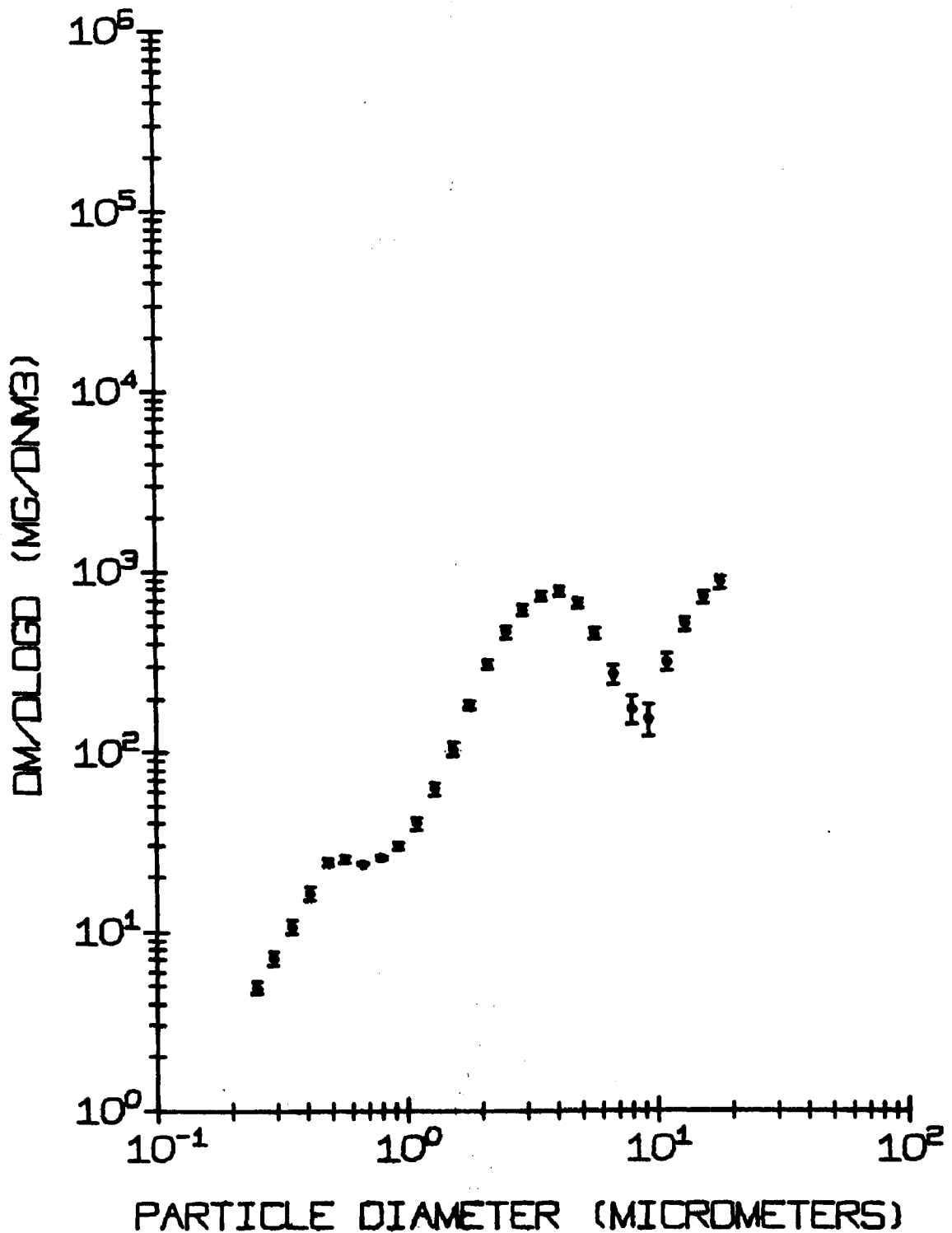


Figure 34. Results of the dust loading characterization at the precharger inlet with the sandblasting gun at 138 Pa (20 psi).

INLET PRECHARGER TEST FEED RATE 20 PSI 10-25/26-77

RHD = 2.4 G/CC INCLUDE MASS LESS THAN .25 MICRONS

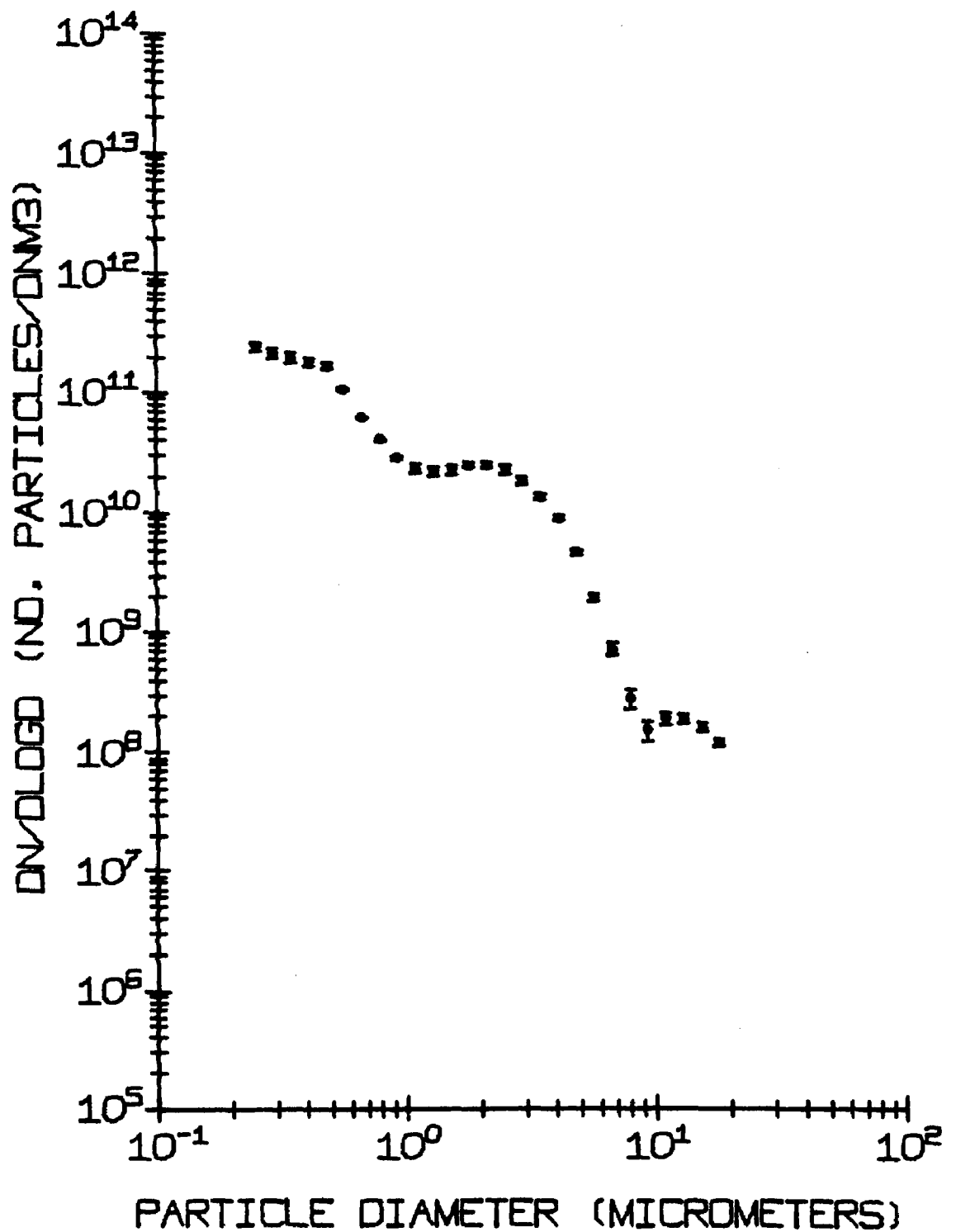


Figure 35. Results of the dust loading characterization at the precharger inlet with the sandblasting gun at 138 Pa (20 psi).

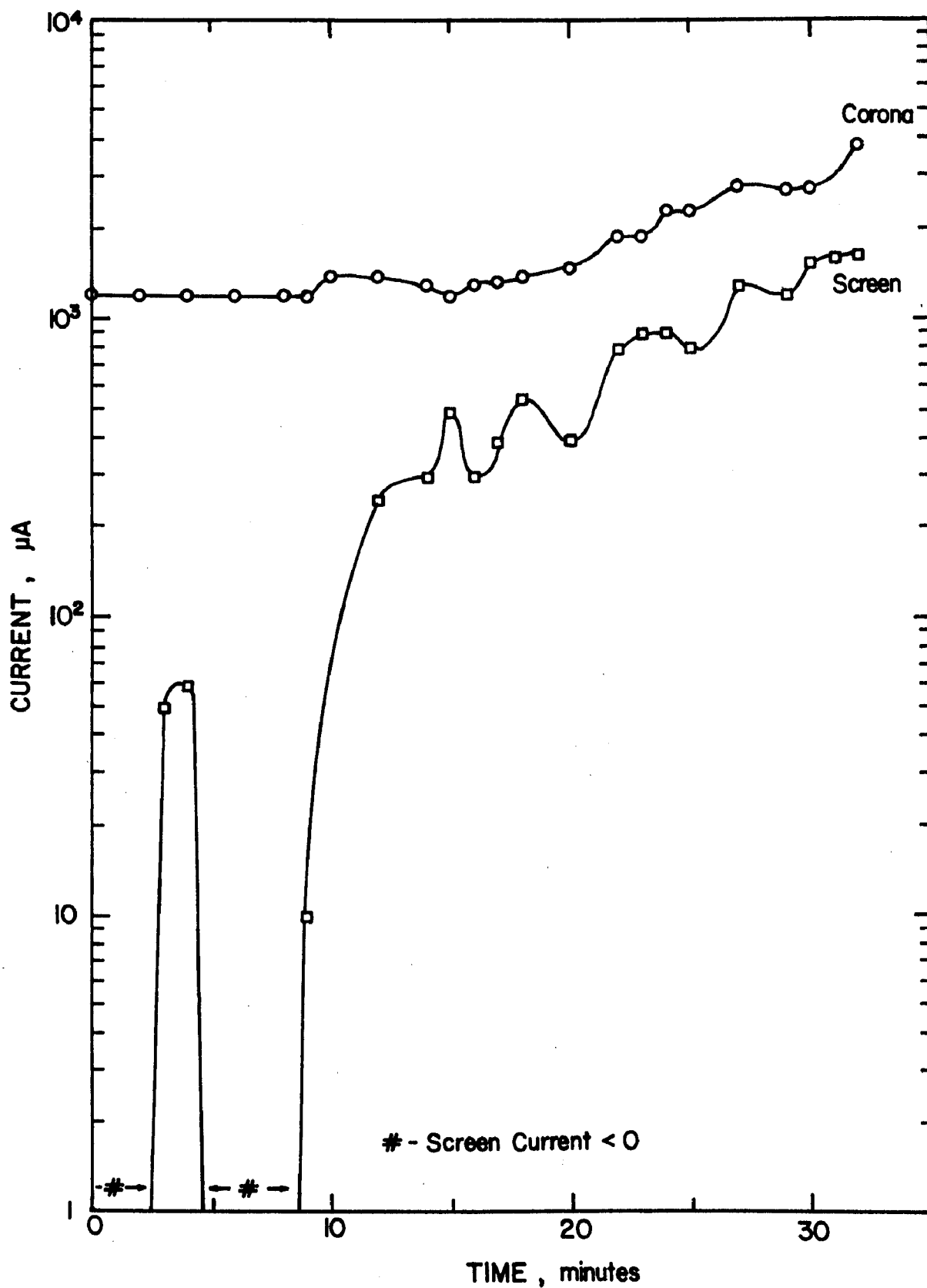


Figure 36. Back corona suppression test results. Test conditions were: $T = 130^{\circ}\text{C}$, $\%\text{H}_2\text{O} = 1.2$ (by volume), average gas volume flowrate = $.71 \text{ m}^3/\text{sec}$ ($1500 \text{ ft}^3/\text{min}$), dust loading = $1.88 \text{ g}/\text{m}^3$, $\text{MMD} = 25 \text{ }\mu\text{m}$, $E = 3.26 \times 10^5 \text{ V}/\text{m}$, and $Nt = 1.4 \times 10^{13} \text{ sec}/\text{m}^3$.

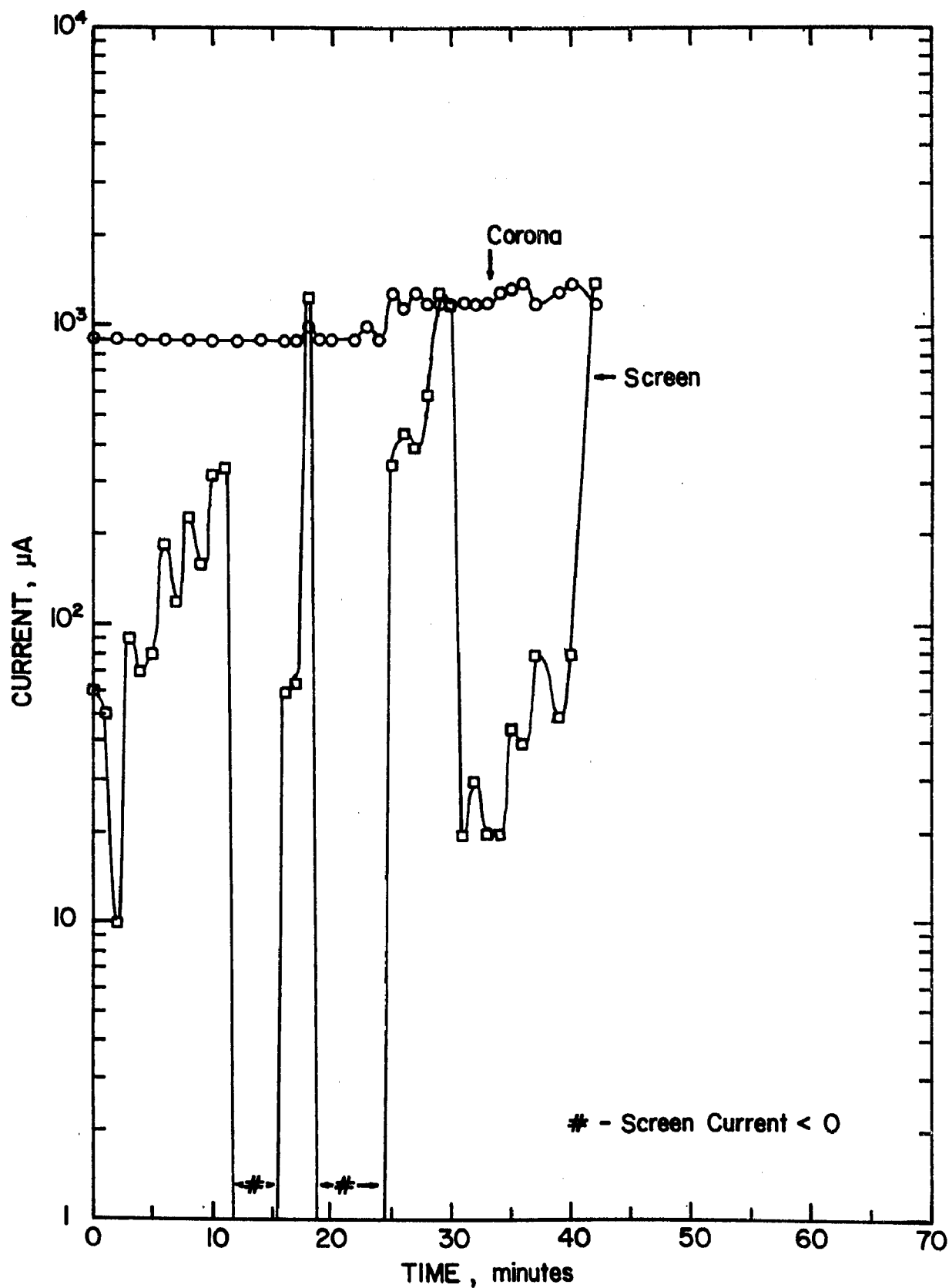


Figure 37. Back corona suppression test results. Test conditions were: $T = 130^\circ\text{C}$, $\%\text{H}_2\text{O} = 1.2$ (by volume), average gas volume flowrate = $.71 \text{ m}^3/\text{sec}$ ($1500 \text{ ft}^3/\text{min}$), dust loading = $1.88 \text{ g}/\text{m}^3$, $\text{MMD} = 25 \mu\text{m}$, $E = 2.72 \times 10^5 \text{ V}/\text{m}$, and $Nt = 1.3 \times 10^{13} \text{ sec}/\text{m}^3$.

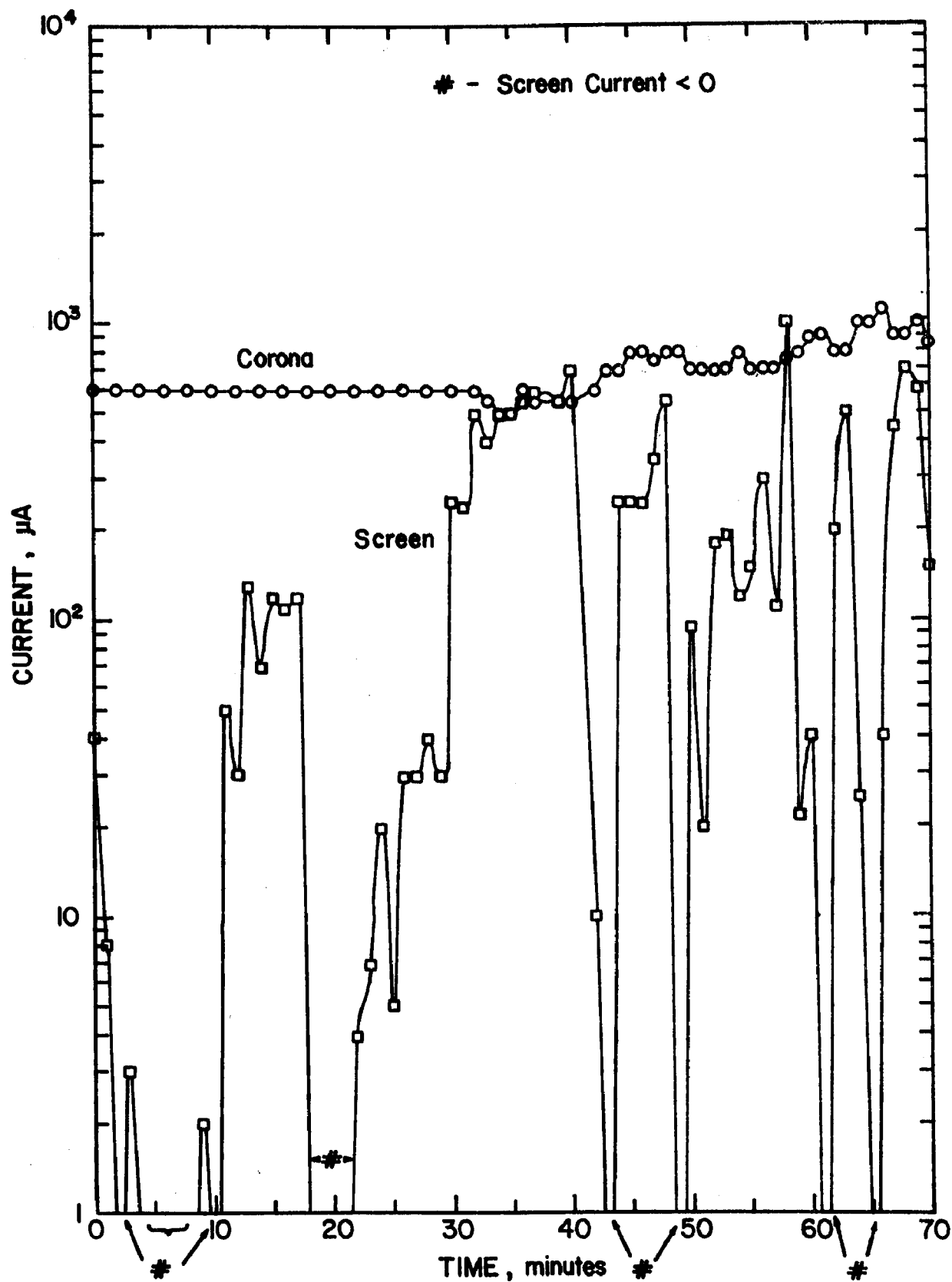


Figure 38. Back corona suppression test results. Test conditions were: $T = 130^{\circ}\text{C}$, $\% \text{H}_2\text{O} = 1.2$ (by volume), average gas volume flowrate = $.71 \text{ m}^3/\text{sec}$ ($1500 \text{ ft}^3/\text{min}$), dust loading = $1.88 \text{ g}/\text{m}^3$, MMD = $25 \mu\text{m}$, $E = 2.61 \times 10^5 \text{ V}/\text{m}$, and $Nt = 8.8 \times 10^{12} \text{ sec}/\text{m}^3$.

procedure in each of these experiments is as follows: 1) the voltage on the corona discharge electrodes is adjusted to give the total corona current corresponding to the desired current density with the screen electrodes voltage simultaneously adjusted to give zero screen current; 2) the ash injection system is turned on at time $t = 0$; and 3) the screen electrodes voltage is adjusted throughout the duration of the experiment in order to maintain the total corona current constant. In each of the tests shown, the total corona current could not be kept constant for the entire time due to excessive sparking at the screen electrodes' voltage required to hold the corona current down. When this condition occurred the corona current was held at the lowest stable value.

Further tests were performed to determine the charging effectiveness of the precharger, using the same general procedure described in the above paragraph to control the voltages on the precharger electrodes. The measure of charging effectiveness was taken to be the ratio of charge to mass, Q/m on a sample of particulate matter extracted downstream from the precharger. The particles are collected on a silver mesh filter mounted in an insulated plastic filter holder, fitted with a nozzle for isokinetic sampling. The filter is connected to an electrometer so that the charge accumulation can be monitored during the collection process. A foil shield, grounded through a 10 Megohm resistor, is wrapped around the body of the plastic filter holder to prevent a buildup of surface charge on the insulating material. The mass of the collected particulate is determined at the conclusion of the experiment and the Q/m value is calculated.

Tests of the precharger's back corona suppression capability and charging effectiveness were conducted with the gas stream temperature equal to 130°C , the moisture content in the gas stream equal to 1.2% (by volume), a dust loading of approximately $1.88\text{g}/\text{m}^3$, and an average volume flowrate of $0.71\text{ m}^3/\text{sec}$ ($1500\text{ ft}^3/\text{min}$). The fly ash used in the experiments under these conditions has a measured resistivity of $1.2 \times 10^{12}\ \Omega\text{-cm}$. The result of a typical test at these conditions is shown in Figure 39. The passive electrodes were rapped manually every five minutes during this experiment. The average value of Q/m obtained from four tests at 130°C is $3.8 \times 10^{-6}\text{ C/g}$. The current-voltage (I-V) characteristics of the precharger at 130°C with the electrodes clean and the electrodes dirty (Figure 40) show that back corona is being produced at the current level maintained during the experiments.

Additional tests of the precharger's performance were conducted at 75°C , with the other parameters constant. The fly ash used in these experiments had a measured resistivity of $1.4 \times 10^{12}\ \Omega\text{-cm}$ at test conditions. The passive electrodes were rapped manually every two minutes during the experiments. The result of one test at 75°C is shown in Figure 41. Control of back corona was achieved, as shown by the successful maintenance of the corona current at its initial value. An evaluation of charging effectiveness was made during the test, as indicated in the figure, and the Q/m value was measured to be $9.6 \times 10^{-6}\text{ C/g}$. Successful back corona suppression was maintained during another test at these conditions which lasted two hours.

The Southern Research Institute ultrafine particle sampling system with a Thermosystems, Inc. Electrical Aerosol Analyzer (EAA) was set up at the outlet test section of the EPA-SoRI pilot scale ESP. Table 1 shows the results

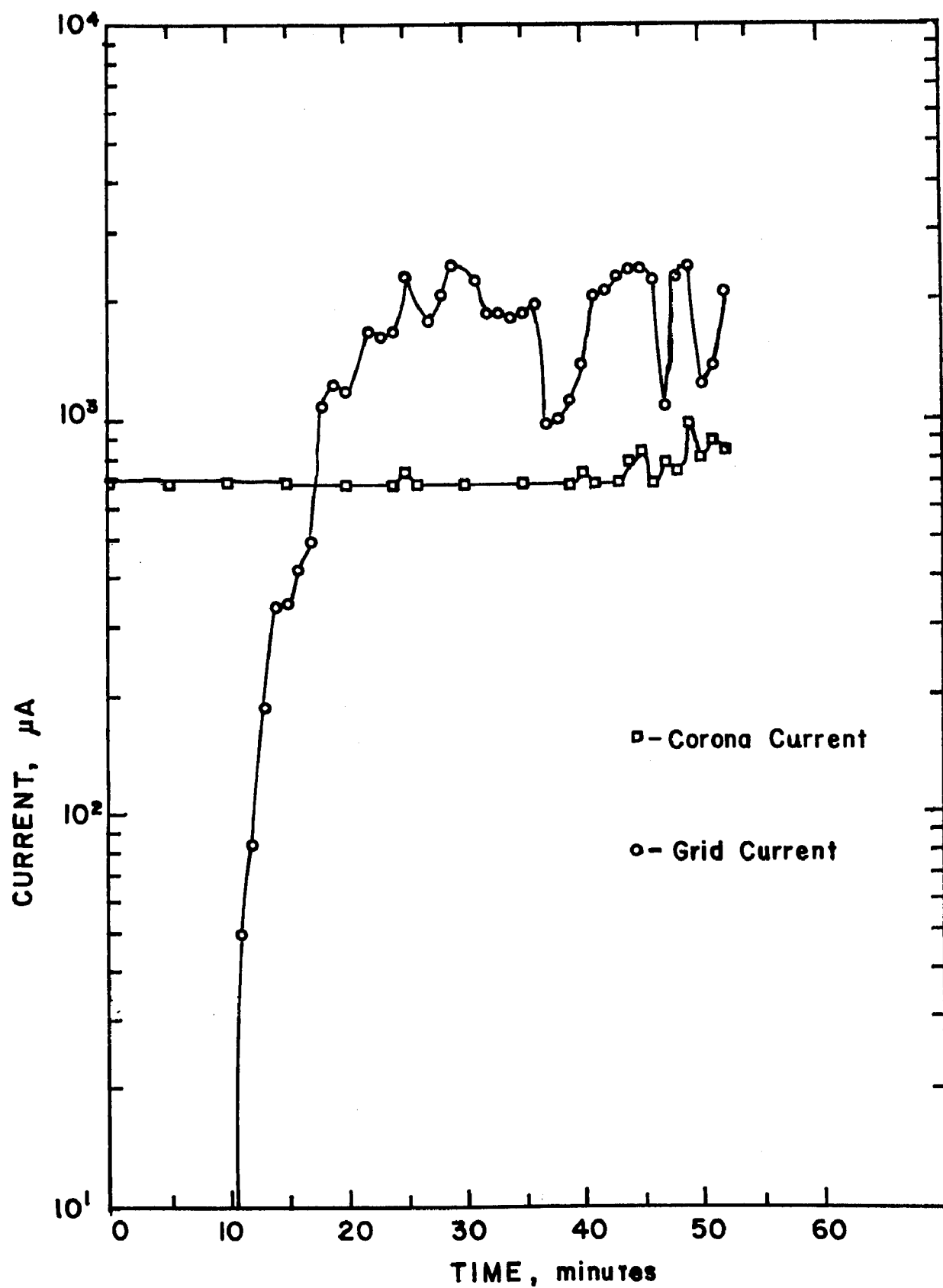


Figure 39. Back corona suppression test at 130°C , 1.2% H_2O , $\rho = 1.2 \times 10^{12} \Omega\text{-cm}$, $j = 9.4 \times 10^5 \text{ nA/m}^2$, and the dust loading = 1.88g/m^3 .

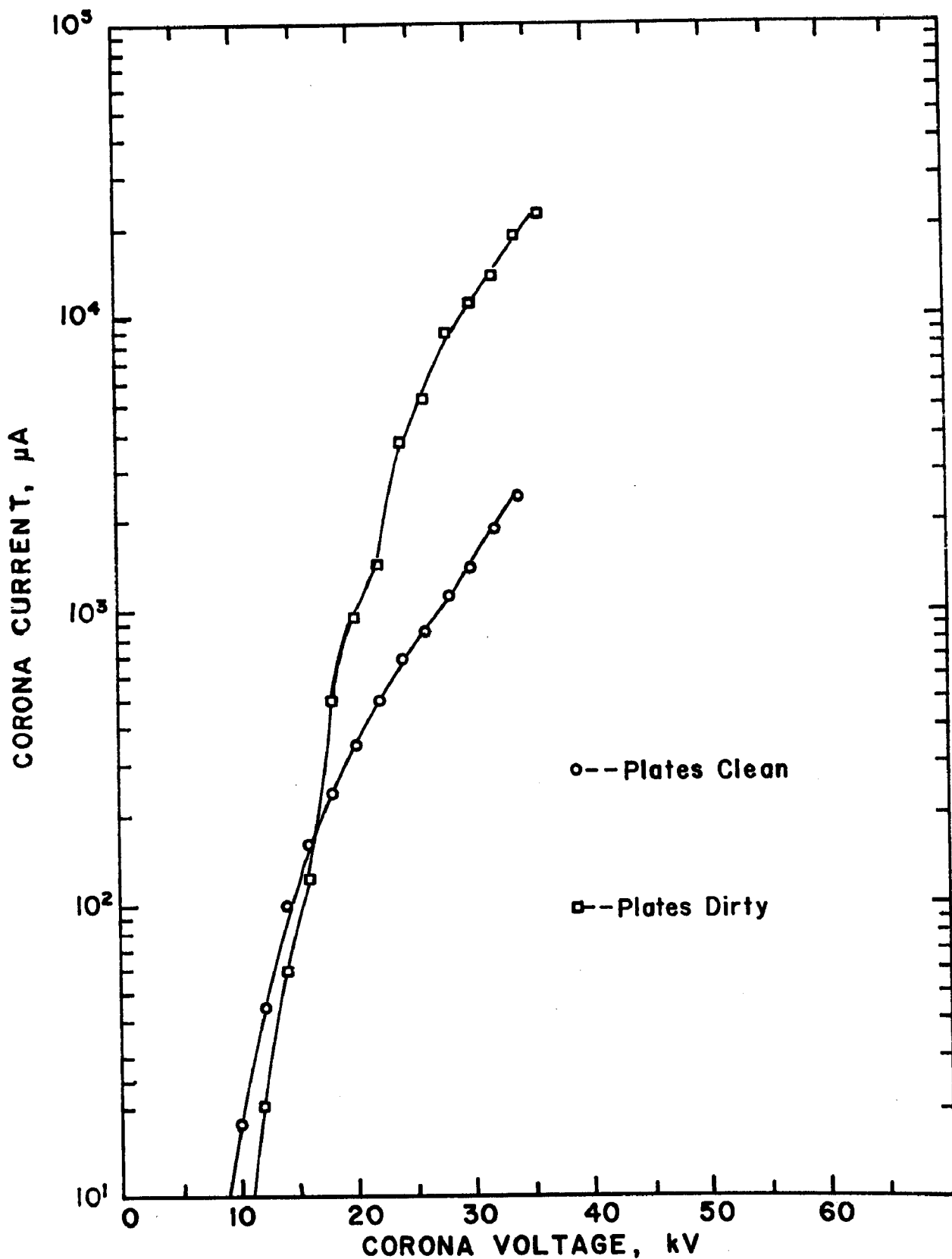


Figure 40. Corona current vs. corona voltage for clean and dirty electrodes at 130°C , 1.2% H_2O , and $\rho = 1.2 \times 10^{12} \Omega\text{-cm}$. Grid current was held to zero for these measurements.

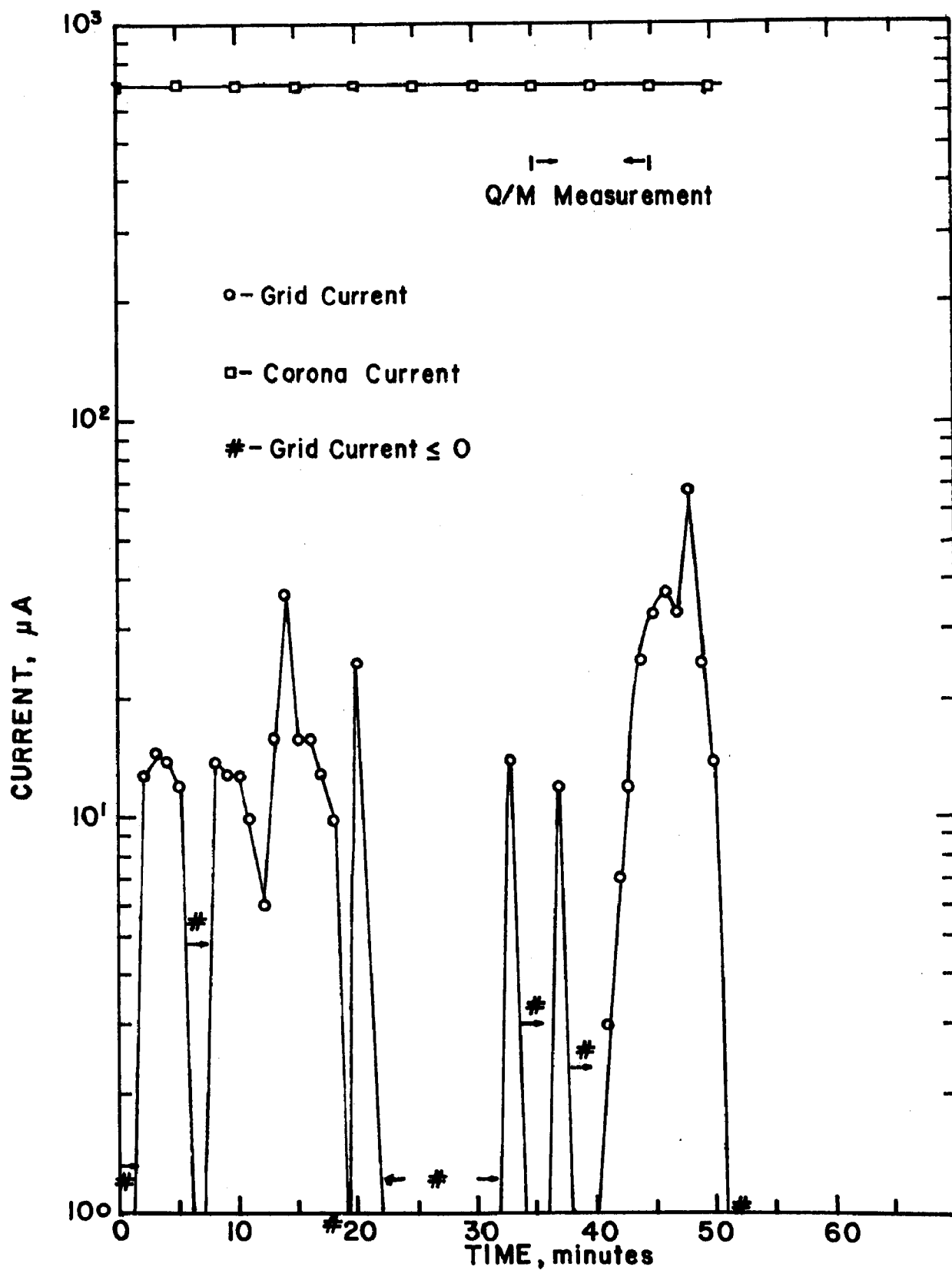


Figure 41. Back corona suppression test and Q/m measurement at 75°C , $1.2\% \text{H}_2\text{O}$, $\rho = 1.4 \times 10^{12} \Omega\text{-cm}$, $j = 9.4 \times 10^5 \text{ nA/m}^2$, dust loading = 1.88g/m^3 , and $Q/m = 9.6 \times 10^{-6} \text{ C/g}$.

Collection Efficiencies

Particle Diameter (μm)	Collector (%)	Precharger + Collector (%)
0.013 *	- 1.01	22.22
0.022 *	- 8.22	52.38
0.031	13.10	41.17
0.050	17.98	24.81
0.092	22.51	47.38
0.150	21.58	49.55
0.220	21.92	49.34
0.310	21.89	49.71

* Large standard deviations were recorded for the collection efficiencies corresponding to these two size ranges.

Table 1. EAA data analysis for the following test conditions:
 $T = 75^\circ\text{C}$, % $\text{H}_2\text{O} = 1.2\%$ (volume), $\rho = 1.4 \times 10^{12} \Omega\text{-cm}$,
 $j_{\text{precharger}} = 9.4 \times 10^5 \text{ nA/m}^2$, $E_{\text{collector}} = 2 \text{ kV/cm}$,
dust loading = 1.88 g/m^3 .

of the EAA data analysis for a test conducted at 75°C. The comparative efficiencies of the precharger-collector system and the collectors alone indicate a more than two-fold average increase in ESP performance with the addition of the precharger. Optical particle counter data were also acquired during the test documented above, showing a similar percentage of performance enhancement for particles of diameters greater than 0.3 micrometers.

The result of a back corona suppression test at 100°C is shown in Figure 42. In this case, the corona current was maintained constant throughout the test by momentarily turning off the screen and corona discharge electrodes' power supplies during rapping (the plates were rapped every two minutes). The absence of the electric field improves the rapping efficiency enough that sufficient fly ash is removed from the plates to allow continuous operation. The Q/m measured during this test was 3.0×10^{-6} C/g. The I-V characteristics of the precharger at 100°C with the electrodes clean and dirty show in Figure 43 that back corona is evident at the operating current level.

In further experiments a back corona control test was conducted with the gas stream temperature equal to 75°C and the moisture content equal to 1.2% by volume. The fly ash had a resistivity of 1.4×10^{12} Ω-cm at these conditions. The ash was injected with the sandblaster set at 276 Pa (40 psi) pressure, or twice the pressure used in previous tests. This corresponded to a dust loading of 5.97 g/m³. The precharger plates were rapped manually every two minutes. The results of this experiment are shown in Figure 44.

Automatic pneumatic rappers were installed on the precharger and placed in service. The test described in the above paragraph was repeated with this modification made to the system (Figure 45). The rappers were operated at 552 Pa (80 psi) air pressure (25 ft/lbs energy per impact). A charging effectiveness measurement was made during the test, yielding a Q/m value of 8.6×10^{-6} C/g. In addition, a Climet model 208B optical particle counter and a Tracor-Northern model TN-1705 pulse height analyzer were used to qualitatively evaluate the downstream collector efficiency enhancement with the precharger on. The collector was operated at -30 kV potential throughout the experiment. Data were taken for particles in the range .75 μm diameter to 3.3 μm diameter. The penetration for particles in this diameter range was decreased by 33.7% with the precharger turned on.

A back corona suppression test was then performed with the gas stream temperature equal to 100°C and the ash injected at the sandblaster setting of 414 Pa (60 psi) pressure. All other parameters remained the same as in the test described above. As can be seen in Figure 46, control of back corona is more difficult in this case. This is evidenced by the instability of the corona electrode current. The I-V characteristics of the precharger at 100°C before (clean) and after (dirty) this test indicate back corona is produced by the dust layer deposited on the passive electrodes (Figure 47).

Figure 48 illustrates a back corona suppression test with a gas temperature of 100°C and fly ash injected under 345 Pa (50 psi) pressure on the sandblaster. Other parameters, including moisture content and plate rapping were unchanged from the preceding test. The decrease in dust loading allowed more stable

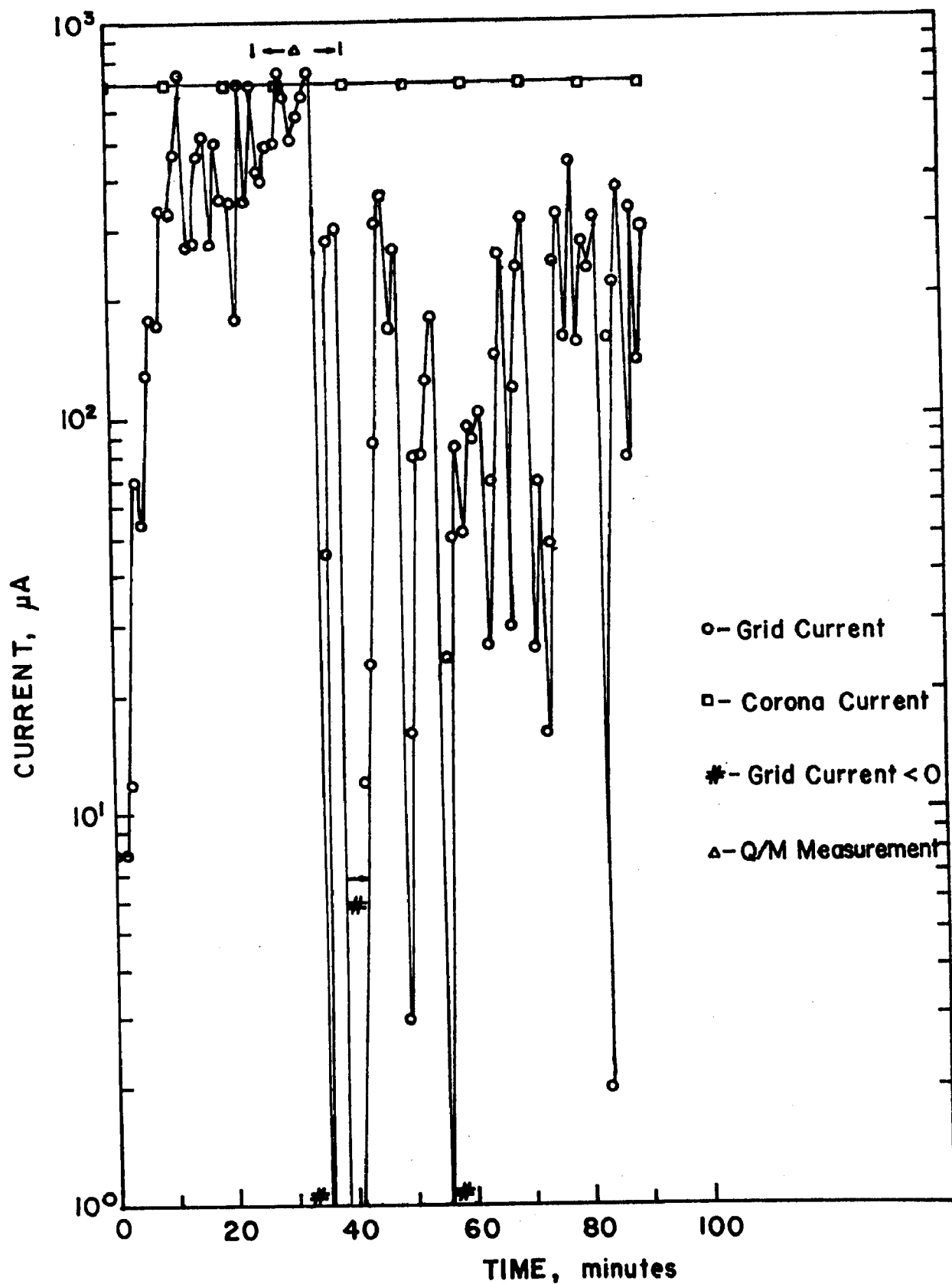


Figure 42. Back corona suppression test and Q/m measurement at 100°C , 1.2% H_2O , $j = 9.4 \times 10^5 \text{ nA/m}^2$, dust loading = 1.88g/m^3 , and $\text{Q/m} = 3.0 \times 10^{-6} \text{ C/g}$.

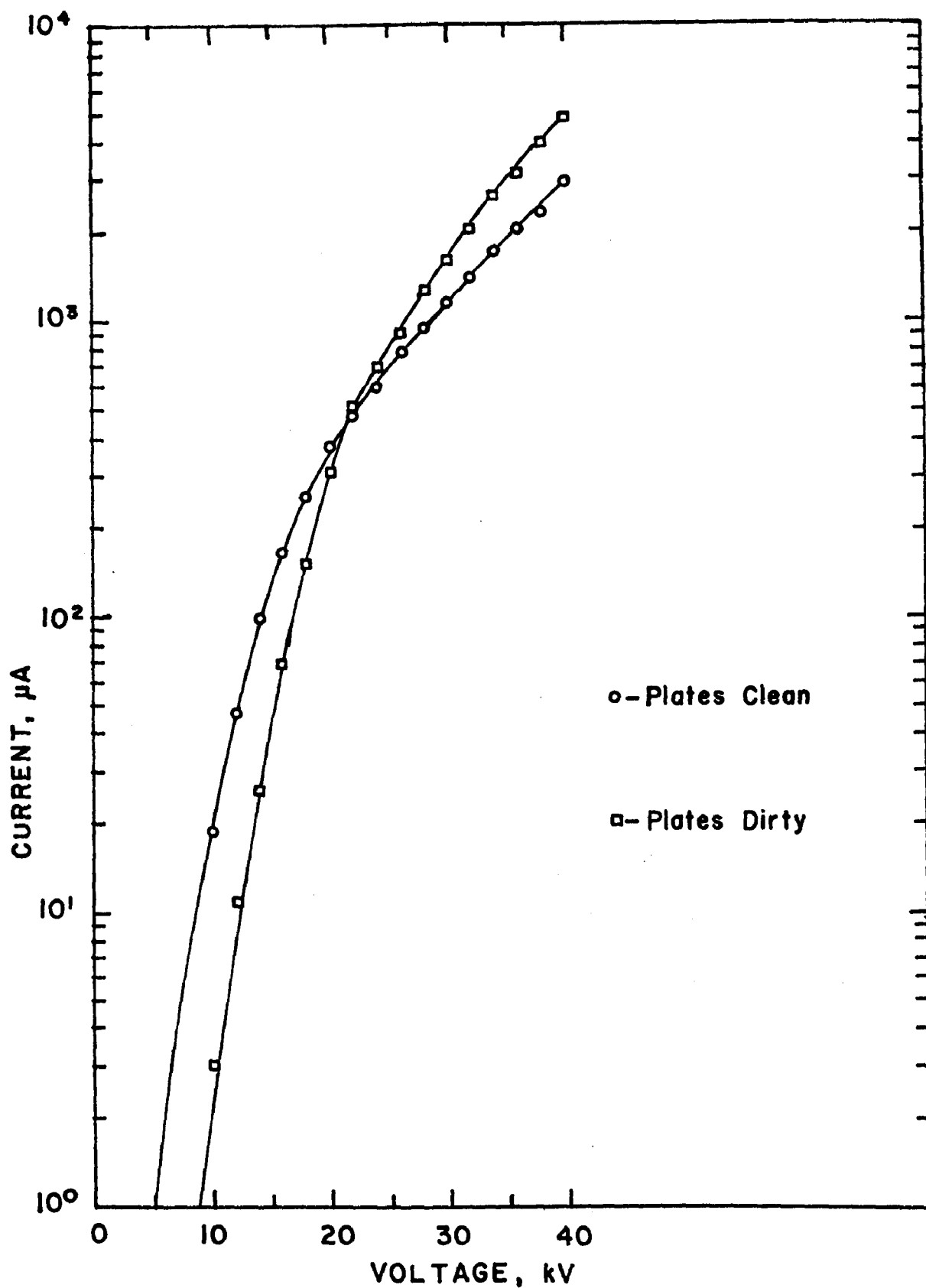


Figure 43. Corona current vs. corona voltage for clean and dirty electrodes at 100°C and 1.2% H_2O . Grid current was maintained at zero for these measurements.

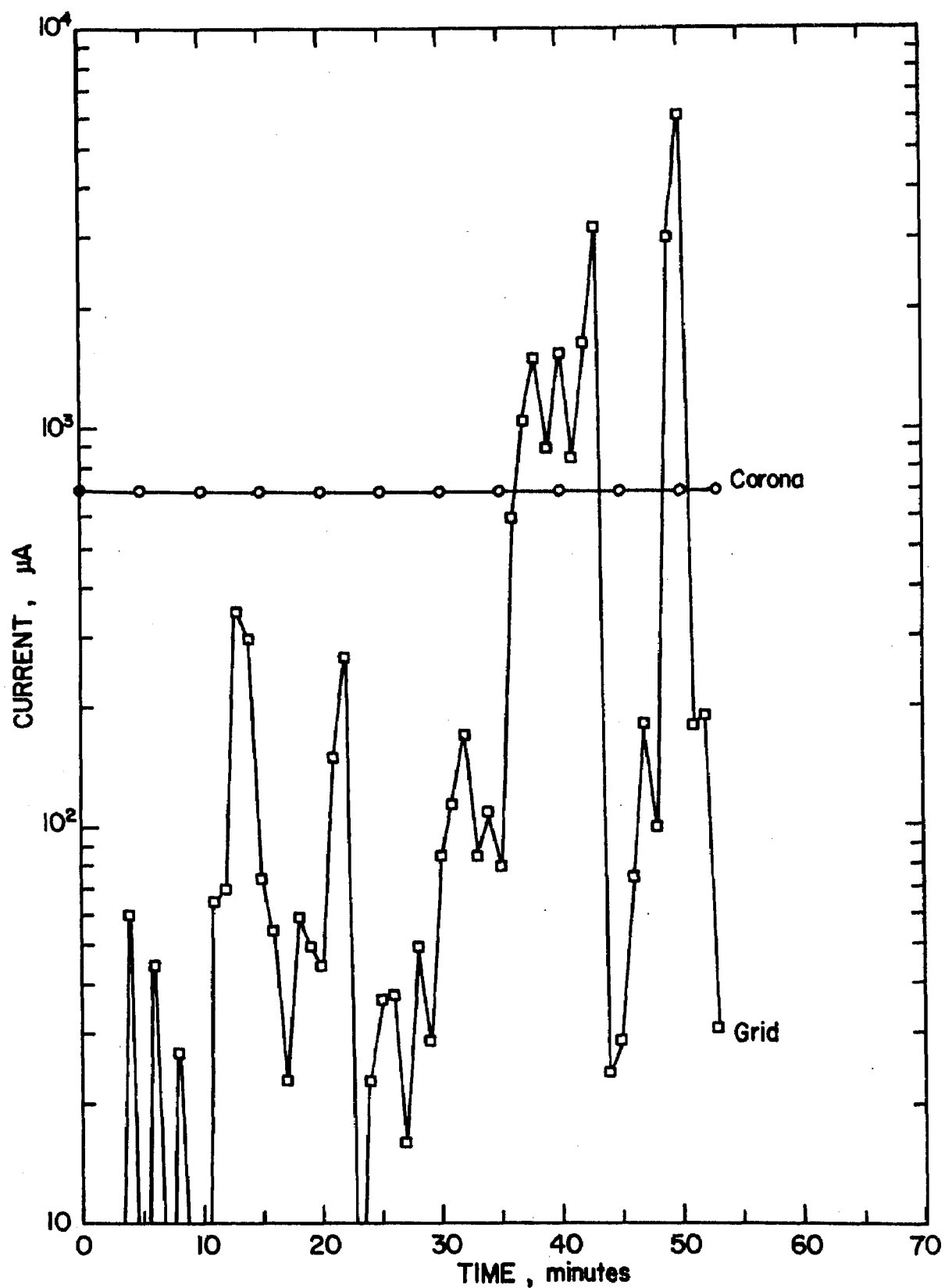


Figure 44. Back corona suppression test at 75°C , 1.2% H_2O , $\rho = 1.4 \times 10^{12} \Omega\text{-cm}$, $j = 9.4 \times 10^{-5} \text{ nA/m}^2$, ash injection at 276 Pa, and manual rapping

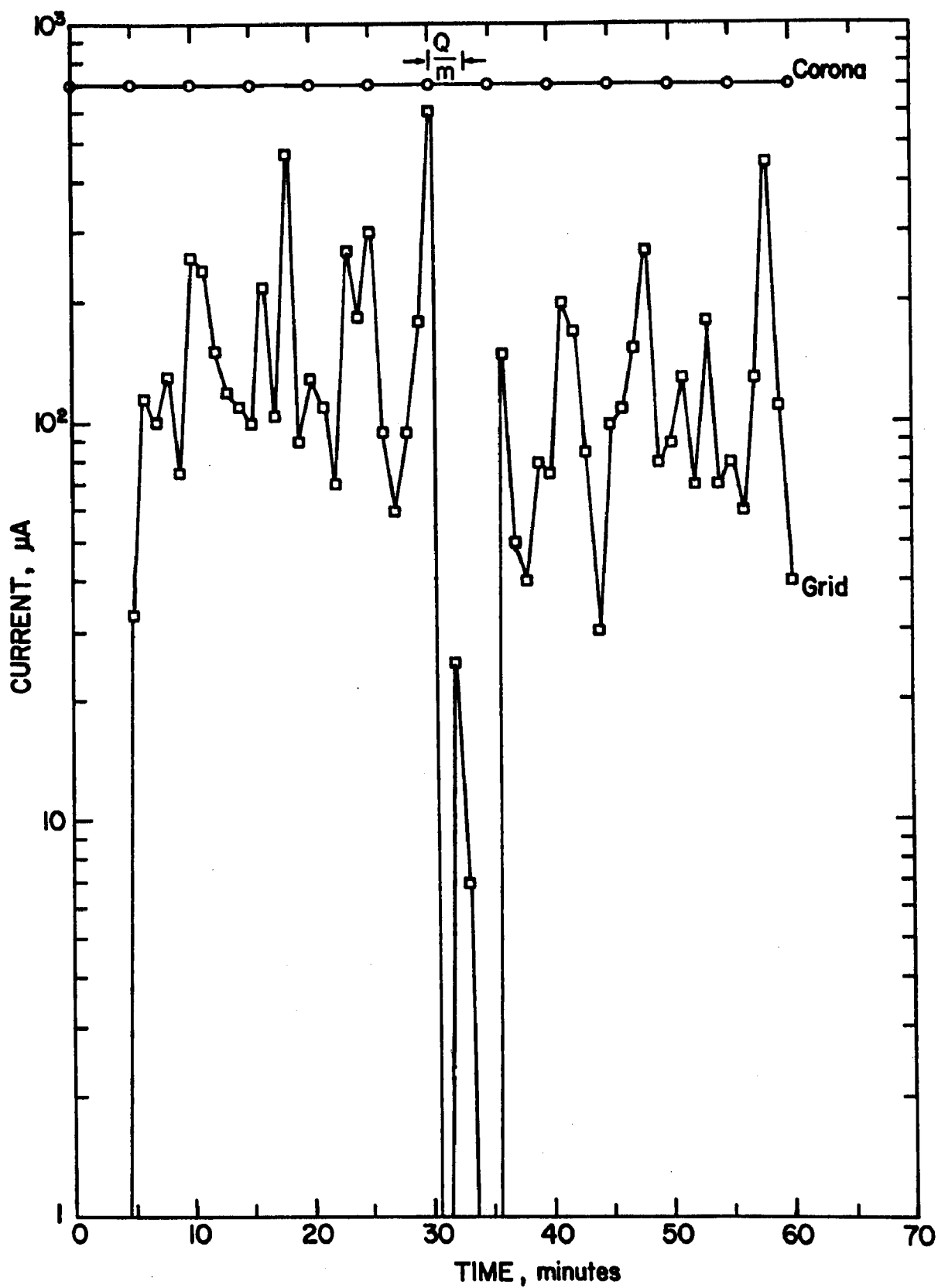


Figure 45. Back corona suppression test and Q/m measurement at 75°C, 1.2% H₂O, $\rho = 1.4 \times 10^{12} \Omega\text{-cm}$, $j = 9.4 \times 10^{-5} \text{ nA/m}^2$, ash injection at 276 Pa, pneumatic rapping at 552 Pa, and $Q/m = 8.7 \times 10^{-6} \text{ C/g}$.

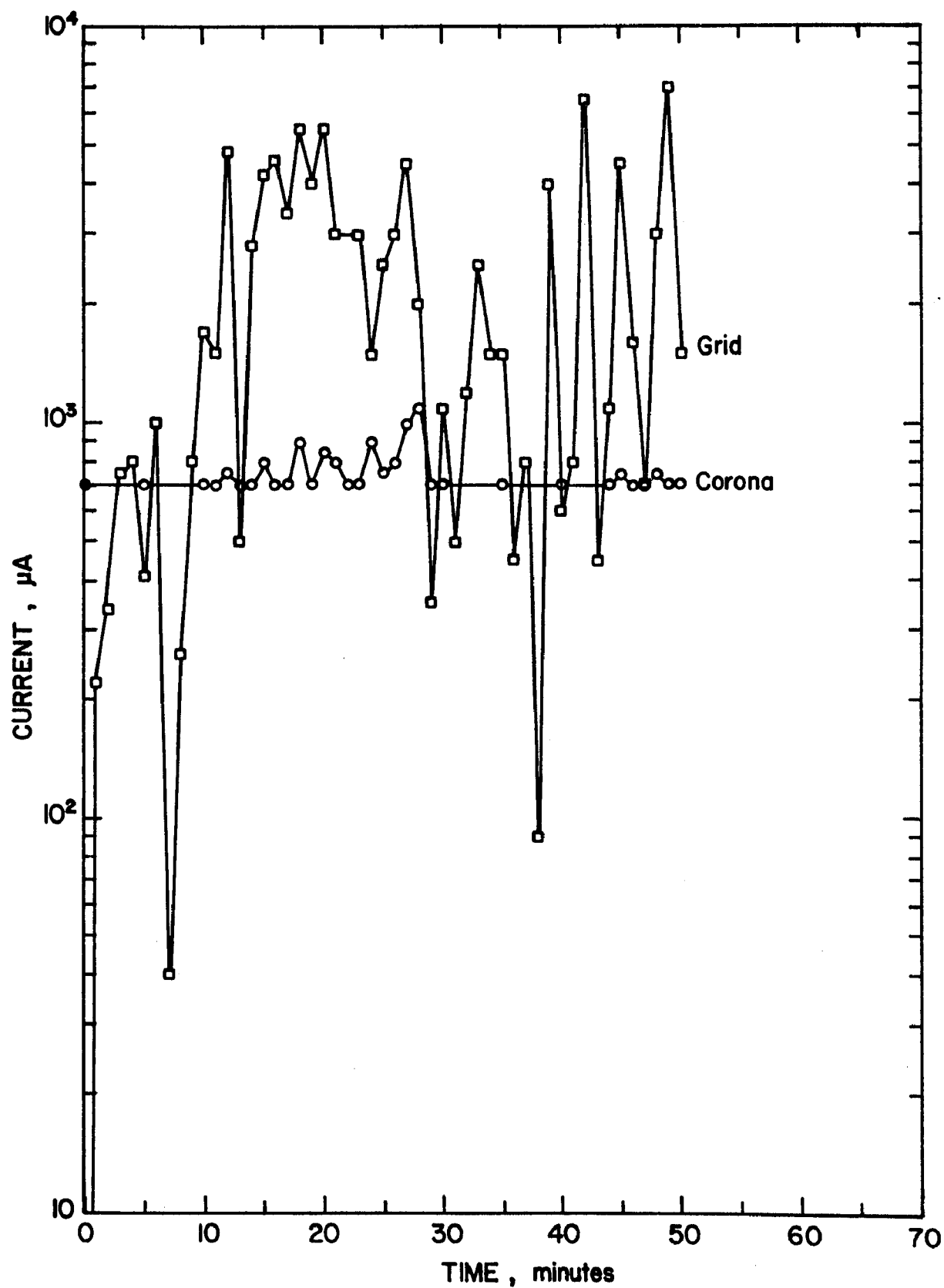


Figure 46. Back corona suppression test at 100°C, 1.2% H₂O, $j = 9.4 \times 10^{-5}$ nA/m², ash injection at 414 Pa, and pneumatic rapping at 552 Pa.

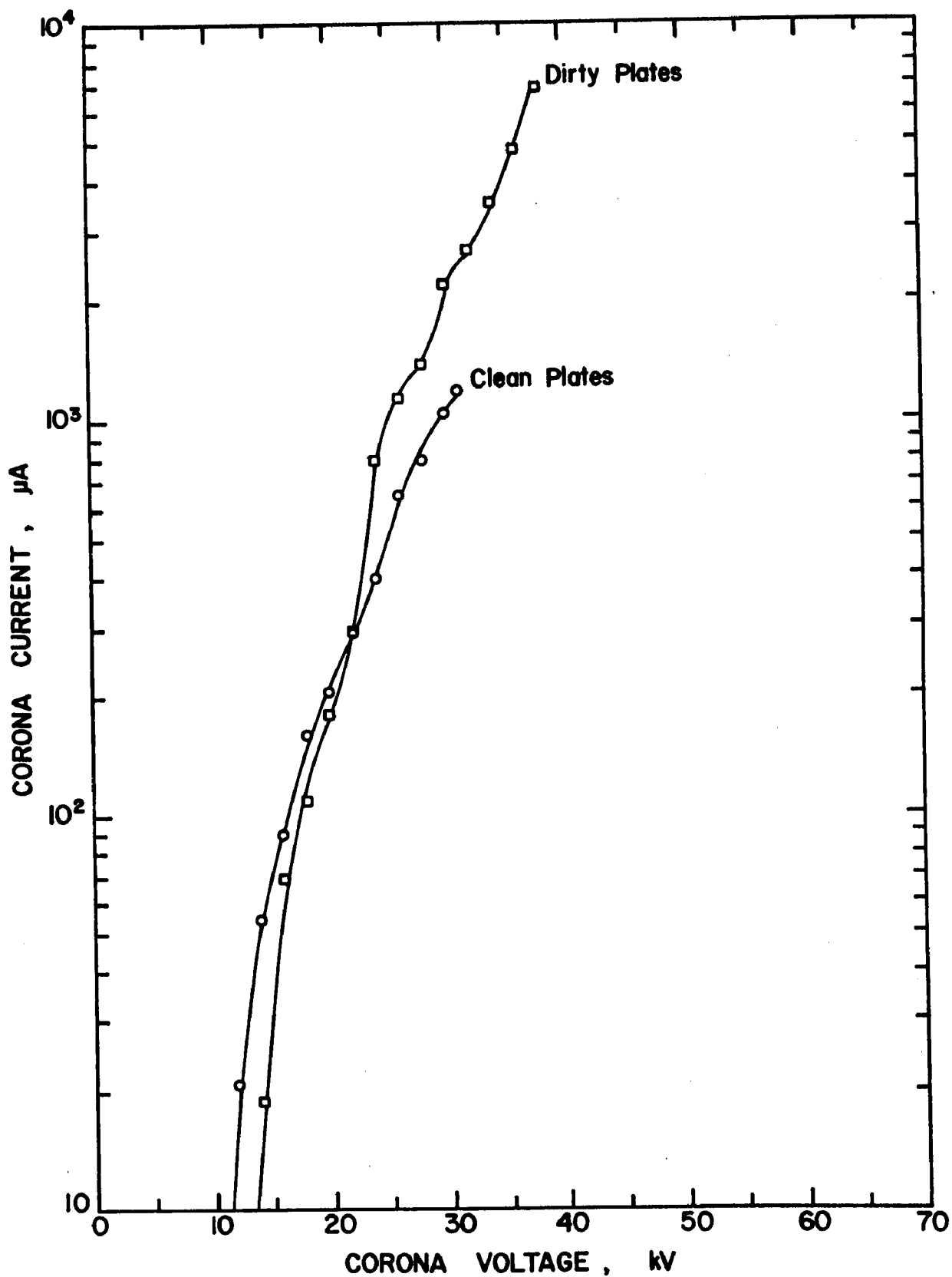


Figure 47. Corona current vs. corona voltage for clean and dirty electrodes at 100°C and 1.2% H₂O. Grid current was held to zero for these measurements.

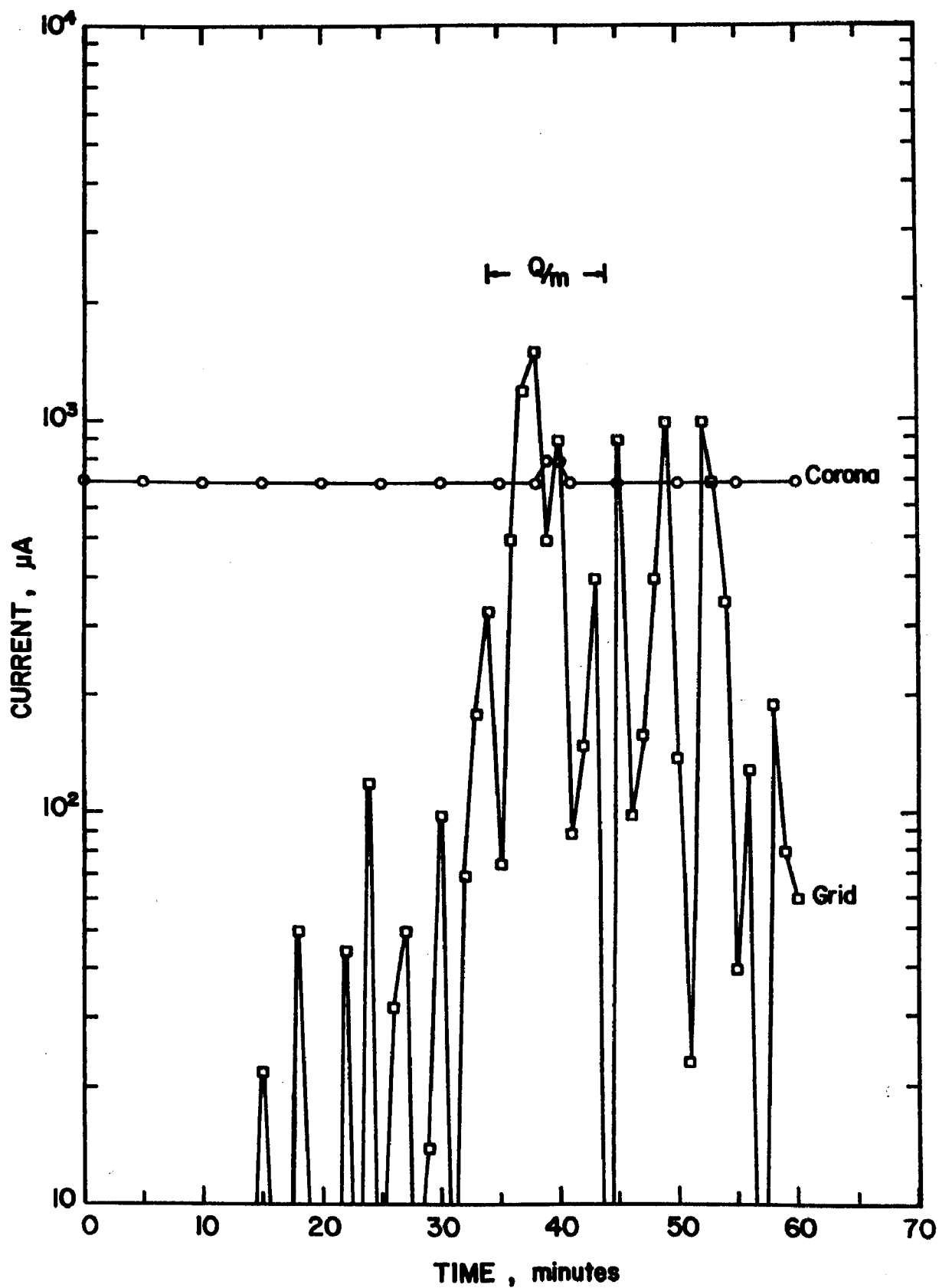


Figure 48. Back corona suppression test and Q/m measurement at 100°C, 1.2% H₂O, $j = 9.4 \times 10^{-5}$ nA/m², ash injection at 345 Pa, pneumatic rapping at 552 Pa, and $Q/m = 2.86 \times 10^{-6}$ C/g.

control of the back corona. A charging effectiveness measurement made during the test gave a Q/m value of 2.86×10^{-6} C/g.

The test conditions for successful back corona suppression experiments are summarized in Table 2. As in the case depicted in Figure 32, there were other conditions for which back corona control was marginal.

Stress cracks developed on the precharger's passive electrodes due to the rapping force applied during the experiments. Modifications were made to remedy this problem and prevent its reoccurrence.

INSTALLATION OF AUTOMATIC SCREEN VOLTAGE CONTROL

An automatic screen voltage control circuit was devised and built to enable "hands-off" operation of the precharger. Figure 49 is a schematic diagram of the electronic circuit used for controlling the screen voltage in response to fluctuations in the primary corona current. The output voltage of the screen power supply (Spellman model RHR15PN225/RVC/TP/FG) can be controlled over its entire range by applying a low voltage signal to pin 6 of the remote voltage control terminal board.

Since adjustments required in the screen voltage depend upon variations in the primary corona current, the input signal to the control circuit is derived from the ground return line on the corona power supply by means of a 4N25 opto-isolator. The signal is then amplified by a factor of ten by means of one section of an LM747 dual operational amplifier. The other section of the LM747 is used as an integrating circuit to even out rapid transient voltages in the control signal. A dc bias voltage, derived from a voltage divider network, is added to the control signal at the input of the integrating circuit.

In order to set the system for automatic control, both power supplies are turned on, and the screen supply is set in the automatic mode. The corona power supply is set at the desired voltage and current level for clean precharger operation. The 10k Ω potentiometer in the control circuit is then adjusted to the point where the screen current falls to zero. No further adjustments are necessary under normal operating conditions.

When high resistivity dust is injected into the precharger, the effects of back corona may tend to increase the primary corona current. Such a change is sensed by the automatic control circuit, which increases the screen voltage until the primary corona current returns to its original value. The screen voltage is thus caused to follow the fluctuations resulting from back corona in such a manner that the primary corona current remains constant.

The automatic control circuit was installed in the screen power supply cabinet and tested using two different types of corona power supplies. In both cases the circuit performed as described in the preceding paragraphs. The primary corona current was held at a very steady level as large fluctuations occurred in the screen current.

TEST CONDITIONS

Gas Stream Temperature (°C)	Fly ash Resistivity (Ω -cm)	Corona Current Density (nA/cm ²)	Air Pressure to Ash Dispersion Device (Pa)	Rapping Mechanism
130	1.2×10^{12}	94	138	manual
100	1.4×10^{12} @ 75°C	94	138, 276	manual
100	1.4×10^{12} @ 75°C	94	276, 345	pneumatic (552 Pa)
75	1.4×10^{12}	94	138, 276	manual
75	1.4×10^{12}	94	276, 414	pneumatic (552 Pa)
75	1.4×10^{12}	121	414	pneumatic (552 Pa)

Table 2. Test conditions for which successful back corona suppression was maintained.

Figure 49. Schematic diagram of the electronic circuit designed to provide automatic adjustment of the precharger screen voltage in response to changes in the primary corona current.

PILOT TESTS AT IERL/RTP

A series of tests was conducted at the Environmental Protection Agency Industrial Environmental Research Laboratory in Research Triangle Park, North Carolina. The pilot scale precharger was installed in the place of the inlet test section of the in-house precipitator for these tests. Telescoping duct sections with sampling ports had been fabricated and were used to fit the precharger into the ESP inlet test section space.

Tests were performed to make sure the precharger's behavior had not changed during transportation and/or set-up, and also to check the automatic screen power supply control circuit's ability to maintain the corona current constant. An example of a back corona suppression test conducted for these purposes is illustrated in Figure 50. This test was made with a gas temperature of 93°C (200°F), gas volume flow rate of 5.19 m³/sec (1100 ACFM), pneumatic rappers operated at about 310 Pa air pressure, and fly ash, having a resistivity $\rho \geq 1.4 \times 10^{12} \Omega\text{-cm}$, injected at a rate equivalent to 1.0 g/m³ (0.44 gr/ft³). The figure shows that despite large variations in the screen current, the corona current was held constant by the automatic controller. The screen current rise corresponds to increasing back corona activity on the plates. The presence of back corona is confirmed by the difference between clean and dirty plate current-voltage curves shown in Figure 51. A charge-to-mass ratio measurement was conducted during the back corona test illustrated in Figure 50 with the resulting value of $Q/m = 1.35 \times 10^{-6} \text{ C/g}$.

Another back corona suppression test is depicted in Figure 52. The gas temperature equalled 107°C (225°F) for this test (all other parameters remained the same as described in the above paragraph). Very large fluctuations in the screen current are evident with only two minor disturbances occurring in the Corona current.

Experiments were conducted in conjunction with the downstream collector in order to determine the efficiencies of the precharger, collector, and the precharger-collector system. Particles penetrating the device were extracted through a sampling nozzle inserted in a sampling port on the outlet test section of the ESP, reduced in number concentration with a diluter, and analyzed with a Climet optical particle counter. A Tracor-Northern multi-channel analyzer was used to count the particles and provide their size distribution. The information was then recorded on a DECwriter printer.

The first efficiency test was performed with the collector plates spaced 38 cm (15 in.) apart and the wire-to-wire spacing equal to 17.8 cm (7 in.). Other test parameters were fixed at the following values: gas temperature = 100°C (213°F), gas flow rate = 5.19 m³/sec (1100 ACFM), moisture content = 0.6%, and fly ash, ($\rho \geq 1.4 \times 10^{12} \Omega\text{-cm}$), injection rate = 1.0 g/m³ (.44 gr/ft³). The particle diameter range selected to provide the particle number counts for the efficiency computation was 1.8 to 5.0 μm . Three values of efficiency, or decrease in penetration of particles in the selected diameter range, were measured: 1) the collection efficiency of the precharger; 2) the collection efficiency of the precharger-collector system; and, 3) the collection efficiency of the collector. The results of this test and a repeat of this test are summarized beginning on page 75.

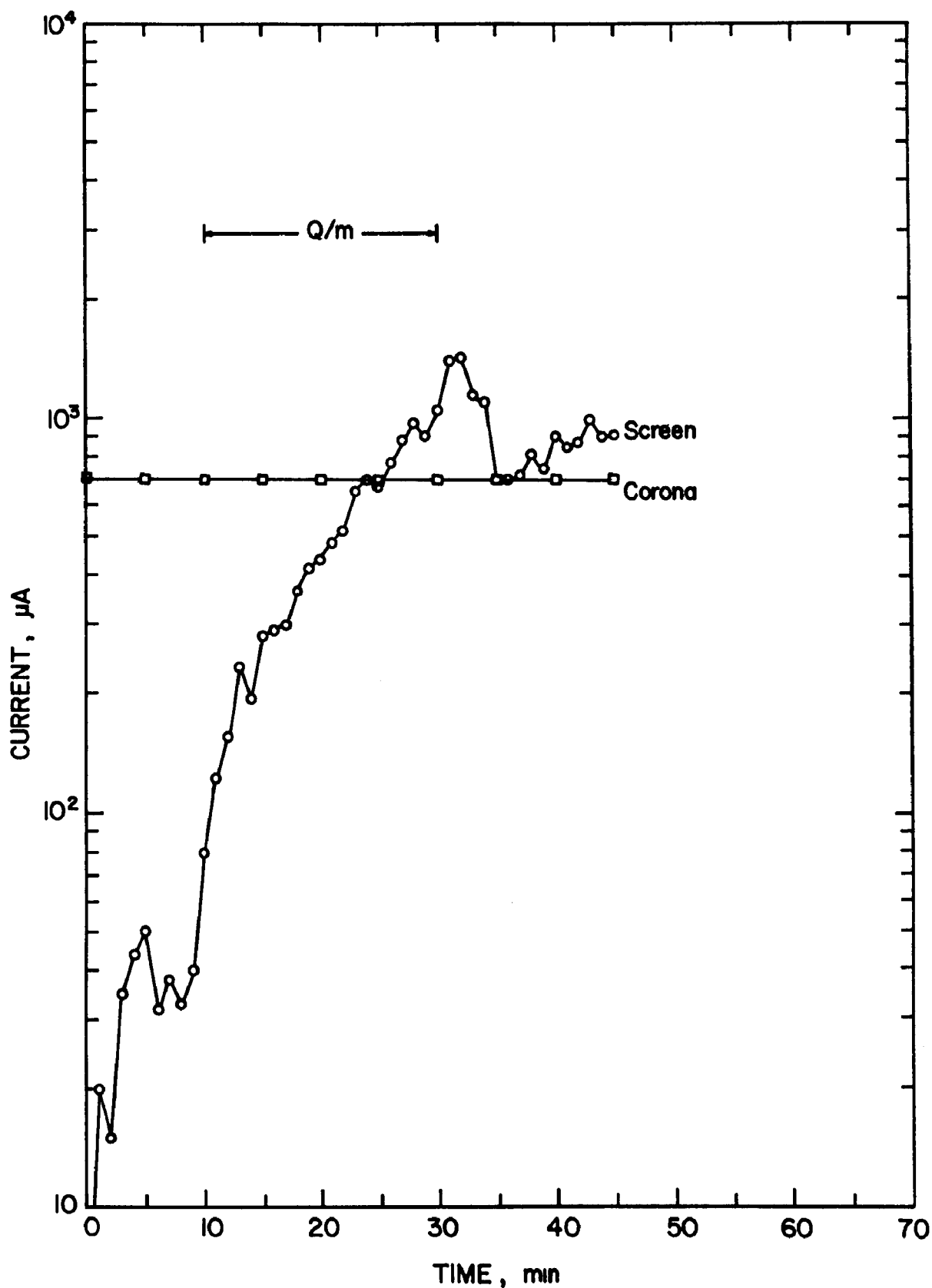


Figure 50. Back corona suppression test with $T = 93^{\circ}\text{C}$, flowrate = $5.19 \text{ m}^3/\text{sec}$, and mass loading = 1.0 g/m^3 . The Q/m value obtained in this test is $1.36 \times 10^{-6} \text{ C/g}$.

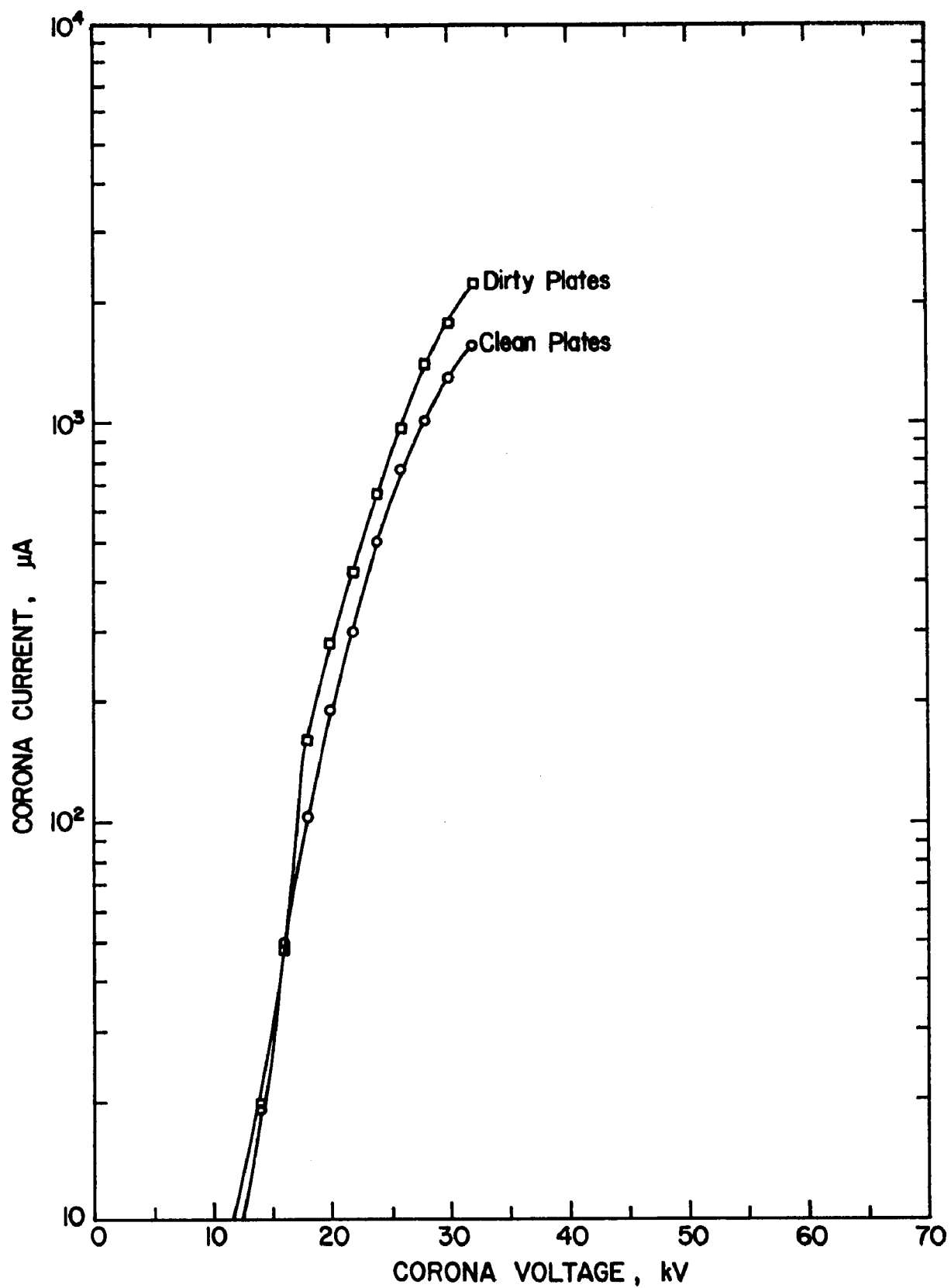


Figure 51. Current-voltage characteristics for the precharger clean and dirty at 93°C.

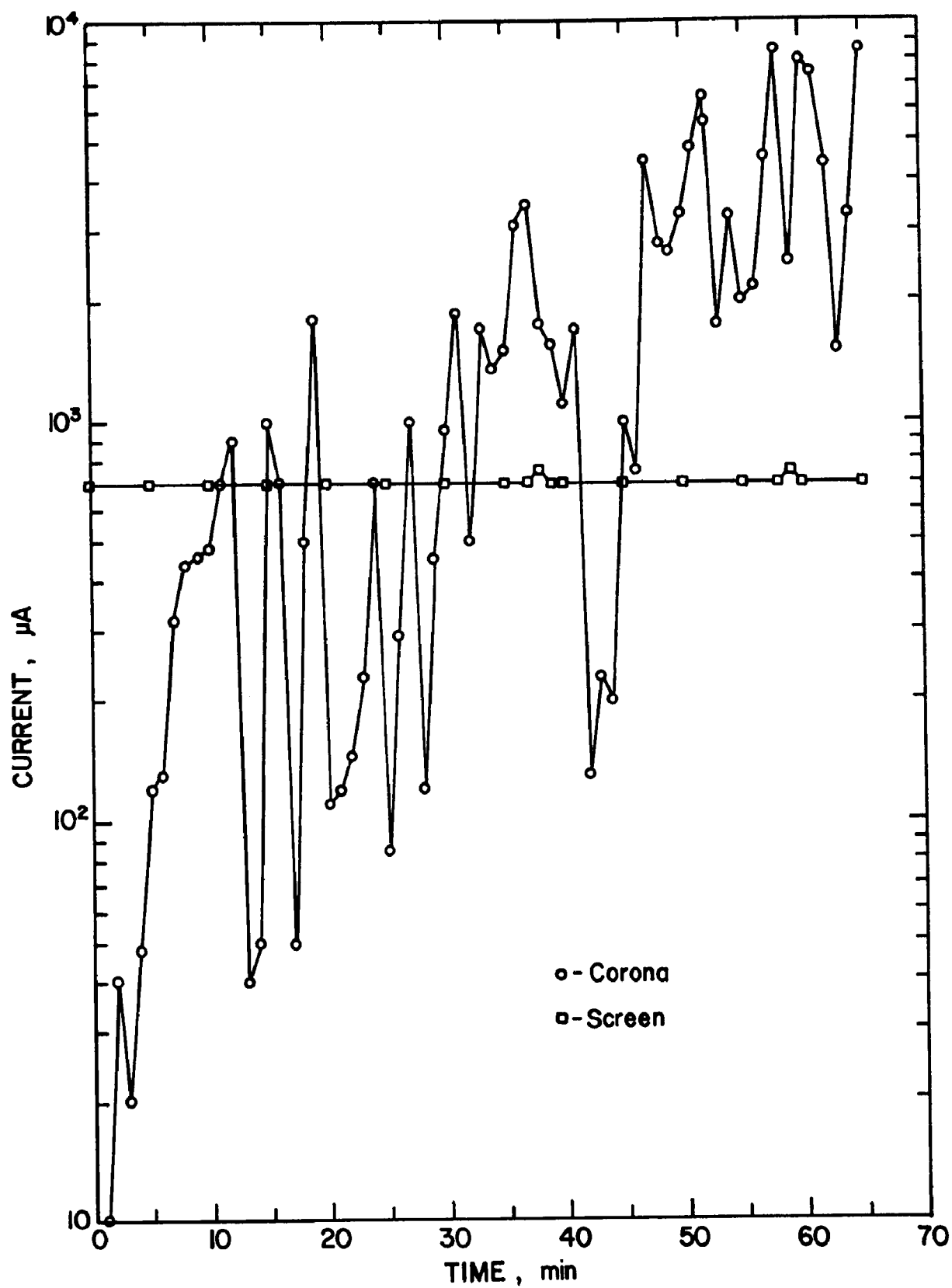


Figure 52. Back corona suppression test with $T = 107^\circ\text{C}$, flow rate = $5.19 \text{ m}^3/\text{sec}$, and mass loading = $1.0 \text{ g}/\text{m}^3$.

Another set of efficiency tests was performed with the collector plate-to-plate spacing = 30.5 cm (12 in.), wire-to-wire spacing = 17.8 cm (7 in.), gas temperature = 92°C (198°F), gas flow rate = 9.44 m³/sec (2000 ACFM), moisture content = 0.6%, and fly ash ($\rho \geq 1.4 \times 10^{12} \Omega\text{-cm}$) injection rate = 1.0 g/m³ (.44 gr/ft³). Again, the 1.8 - 5.0 μm diameter particle range was used to calculate the following efficiencies: 1) the collection efficiency of the precharger; 2), 3), and 4) the collection efficiencies of the precharger-collector system at three different collector field strengths; and 5), 6), and 7) the collection efficiencies of the collector at three different electric field strengths. The results of these measurements are also included in the summary.

A third set of experiments was made with a collector plate-to-plate spacing of 20.3 cm (8 in.). All other conditions remained the same as in the previous tests. The collection efficiencies of the precharger alone, the precharger-collector system at three different collector field strengths, and the collector alone at three different field strengths were calculated for the particle size range 1.8 - 5.0 μm diameters. The summary also includes these results.

As indicated by the tabulated results of the efficiency measurements, the relative electrode positions in the downstream collector have a marked effect on the system behavior. In the 38 cm plate-to-plate spacing case, the percentage of collection efficiency enhancement due to the precharger was found to be negligible. The 30.5 cm plate-to-plate condition showed a very significant improvement in collection when the precharger was on. The 20.3 cm plate-to-plate spacing yielded a significant enhancement due to the precharger, but less of a performance boost than with a 30.5 cm spacing. The differences in performance of the precharger-collector system at the three plate-to-plate spacings was possibly due to anomalous electric field effects as the ratio of plate-to-plate to wire-to-wire separation was varied. These data indicate that additional experiments on the effects of plate-to-plate and wire-to-wire spacing are needed.

A trend in the efficiencies is evident. The percentage enhancement due to the precharger is less on the second, or repeat experiment at each plate-to-plate spacing. This is probably caused by the absence of rapping in the collector and the resultant degradation of performance by the deposited dust layer on the plates.

It should be noted that the collection efficiencies given in the tables were calculated from comparisons of dust concentration at the outlet of the precipitator with the precharger on and off, and collectors on and off. The real system collection efficiency, i.e., outlet concentration versus inlet concentration, was determined by collecting a mass sample at the ESP outlet and comparing the dust loading to the predetermined fly ash feed rate. This measurement was made with the collector plate-to-plate spacing of 20.3 cm. The decrease in particulate penetration resulting from action of the precharger, with the collectors operated at ~40 kV was 22% and 9% for the two tests, which agrees with the number concentration percentages. The overall system collection efficiency was determined to be 92% and 86% respectively at these conditions.

SUMMARY OF TESTS RESULTS

I. Plate-to-plate spacing	= 0.38 m (15")	
Gas temperature	= 100°C (212°F)	
Gas flow rate	= 5.19 m ³ /sec (1100 acfm)	
Moisture content	= .6 v/o	
Dust loading	= 1.0 g/m ³ (0.44 gr/ft ³)	
Particle size range observed	= 1.8 - 5.0 µm dia.	
a. Collection efficiency of precharger (27 kV, 700 µA)		= 9.8%, 3.1%
b. Collection efficiency of precharger (27 kV, 700 µA) plus collectors (38-41 kV, 0.00-0.04 mA)		= 33.9%, 35.8%
c. Collection efficiency of collectors (36-41 kV, 0.00-0.08 mA)		= 32.4%, 37.1%
d. Percentage decrease in penetration due to precharger		= 2.3%, -2.2%
II. Plate-to-plate spacing	= 0.305 m (12")	
Gas temperature	= 92°C (198°F)	
Gas flow rate	= 944 m ³ /sec (1000 acfm)	
Moisture content	= .6 v/o	
Dust loading	= 1.0 g/m ³ (0.44 gr/ft ³)	
Particle size range observed	= 1.8 - 5.0 µm dia.	
a. Collection efficiency of precharger (28 kV, 700 µA)		= 18.0%, 10.3%
b. Collection efficiency of precharger (28 kV, 700 µA) plus collectors (29.8 - 30.3 kV, 0 mA)		= 28.9%, 23.2%
c. Collection efficiency of precharger (28 kV, 700 mA) plus collectors (29.6 - 40.6 kV, 0.00 - 0.03 mA)		= 39.7%, 29.9%
d. Collection efficiency of precharger (28 kV, 700 µA) plus collectors (44.0 - 46.0 kV, 0.05 - 0.18 mA)		= 50.8%, 35.4%
e. Collection efficiency of collectors (29.9 - 30.3 kV, 0 mA)		= 13.0%, 9.4%
f. Collection efficiency of collectors (40 kV, 0.00 - 0.01 mA)		= 25.4%, 21.3%
g. Collection efficiency of collectors (43.8 - 45.1 kV, 0.03 - 0.29 mA)		= 26.8%, 23.9%
h. Percentage decrease in penetration due to precharger		
1) with collectors at 30 kV		= 18.0%, 15.2%
2) with collectors at 40 kV		= 19.5%, 10.9%
3) with collectors at 45 kV		= 32.7%, 15.1%
III. Plate-to-plate spacing	= 20.3 cm (8")	
Gas temperature	= 92°C (198°F)	
Gas flow rate	= 9.44 m ³ /sec (2000 acfm)	
Moisture content	= .7 v/o	
Dust loading	= .44 g/m ³ (1.0 gr/ft ³)	
Particle size range observed	= 1.8 - 5.0 µm dia.	
a. Collection efficiency of precharger (27.8 kV, 700 µA)		= 19.9%, 8.8%
b. Collection efficiency of precharger (27.8 kV, 700 µA) plus collectors (30.0 - 30.3 kV, 0 mA)		= 24.9%, 23.2%

- | | |
|---|----------------|
| c. Collection efficiency of precharger (27.8 kV, 700 A)
plus collectors (34.8 - 35.1 kV, 0.05 - 0.35 mA) | = 26.8%, 19.2% |
| d. Collection efficiency of precharger (27 kV, 700 A)
plus collectors (36 - 40 kV, 0.5 - 2.25 mA) | = 45.5%, 28.3% |
| e. Collection efficiency of collectors (30.0 - 30.1 kV,
0.00 - 0.04 mA) | = 11.4%, 12.7% |
| f. Collection efficiency of collectors (34.8 - 35.0 kV,
0.08 - 0.63 mA) | = 13.6%, 16.3% |
| g. Collection efficiency of collectors (31.0-40.0 kV,
0.93 - 2.25 mA) | = 30.3%, 19.0% |
| h. Percentage decrease in penetration due to precharger | |
| 1) with collectors at 30 kV | = 15.3%, 12.0% |
| 2) with collectors at ~35 kV | = 15.2%, 3.5% |
| 3) with collectors at ~40 kV | = 21.7%, 11.4% |

The test results detailed in the above summary show that the use of the precharger can produce a substantial improvement in the collection efficiency of the system. The overall values of collection efficiency were, however, quite low. It was concluded from these results that improved performance of the system would require optimizing the electrical configuration of the pilot scale ESP that served as the downstream collector.

SECOND GENERATION PILOT PRECHARGER

Although the electrical performance of the prototype pilot scale precharger was good, there were some design problems that required correction if adequate performance was to be expected in a field environment. The spacers holding the screen electrodes were fabricated of glass-filled Teflon. Because these spacers were located in the gas stream, they became coated rapidly with fly ash, which tends to degrade the insulating properties of the material. Teflon is also susceptible to heat damage.

A redesign of the precharger was undertaken with the objective of removing all insulating materials from the gas stream and providing a generally more rugged structure. The design features of the precharger are shown in Figure 53. The gas flow baffles serve to inhibit gas sneaking around the precharger electrodes. The passive electrodes, supported and edged all around by .95 cm (.375 inch) diameter rod, are rapped with pneumatic springless impactors. The screen electrodes are made of .635 cm (.25 inch) hexagonal opening, 79% open area perforated sheet steel and are framed and mounted on tubular supports. The corona discharge electrodes are barbed wire with a 2.5 cm (1.0 inch) barb-to-barb spacing.

The precharger was taken to the IERL precipitator facility, at Research Triangle Park, where it was installed, along with a sampling section, in the test section location of the in-house ESP. The objectives of the tests conducted with the system were to examine various downstream collector electrode geometries for their potential application, to evaluate the precharger's charging effectiveness, and to determine the effect of the precharger on the collection efficiency of the precipitator.

The precipitator sections were set up with 22.86 cm (9 in.) plate-to-plate spacings. Section 1 was initially configured with .3175 cm (1/8 in.) diameter wires spaced 22.86 cm apart. Section 2 had a 2.54 cm (1 in.) mesh

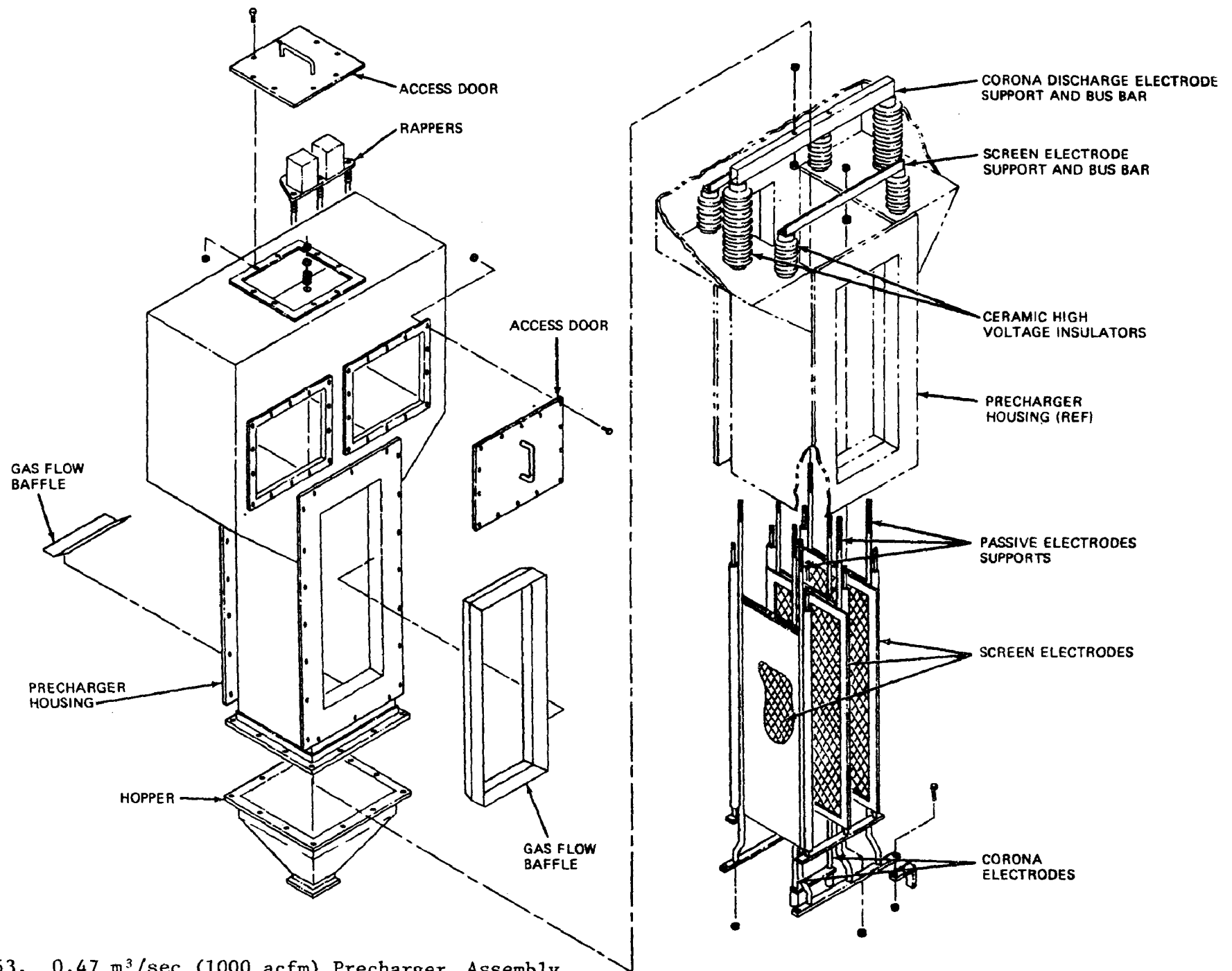


Figure 53. 0.47 m³/sec (1000 acfm) Precharger Assembly.

discharge electrode. Section 3 was set up with .3175 cm diameter wires spaced 2.54 cm apart. Section 4 was arranged with .635 cm (1/4 in.) diameter wires with a 5.08 cm (2 in.) wire-to-wire spacing. This variety of collector discharge electrode configurations was selected so that comparisons between the voltage-current characteristics of the different designs might contribute to the determination of the most appropriate discharge electrode for the collector section. The I-V curves for the four sections are shown in Figure 54.

The discharge electrodes in Section 1 were replaced with a 2.54 cm mesh discharge electrode. The mesh electrode provides the high electric field and low current density combination desirable in the collector of a two-stage precipitator. The small wire diameter and large wire-to-wire spacing configuration is clearly inferior in this respect. Figures 55 and 56 show the I-V curves of the downstream collector sections as configured for the collection efficiency tests and at the operating temperature.

The current-voltage characteristic of the precharger is shown in Figure 57. The alignment of the screen and passive electrodes required several adjustments before problems with the relative spacing of the electrodes were eliminated as operating limitations.

The precharger-collector system was operated at 150°C (302°F) for the tests. Steam injection was not used and the moisture content measured at the operating conditions was 1.14% by volume. These values of temperature and moisture content of the gas stream contribute to a resistivity of the redispersed fly ash of approximately 5×10^{12} ohm-cm. The fly ash was injected into the system at a rate of approximately 1.15 g/m³ (.5 gr/ft³). The total gas volume flowrate through the system was held to 0.47 m³/sec (1000 ACFM) for the tests.

The precharger charging effectiveness was tested under the conditions described above. The precharger was operated with corona voltage = 21 kV, corona current = 700 μ A, grid voltage = 7.2 to 8.2 kV, and grid current = 2500 to 20,000 μ A. The fluctuations in the grid voltage and current were the result of intense back corona from the passive electrodes. The passive electrodes were rapped 21 times per minute with 5.6×10^4 kg/m² (80 psi) air pressure on the pneumatic impactors. Sparking from the grids to the passive electrodes occurred throughout the charging test. A charge/mass ratio was determined under these conditions to be -1.89×10^{-6} C/g.

Another test of particle charging was made with continuous sparking on the grid; 6-11 kV applied voltage on the grid, 10-25 mA grid current, 16 kV corona voltage, and 1000 μ A corona current. The Q/m value measured in this case was -2.06×10^{-6} C/g and -2.46×10^{-6} C/g. These values of charge-to-mass ratio have an average of -2.1×10^{-6} C/g, which is equivalent to the Q/m values obtained in tests with the original 0.47 m³/sec precharger.

The next phase in the precharger evaluation was to determine the effect of the precharger on the efficiency of the downstream collector-precharger system. The collector sections were set up as described earlier and operated with a total current of 0.01 - 0.05 mA per section. This current setting corresponded to an applied voltage of 20-35 kV per section.

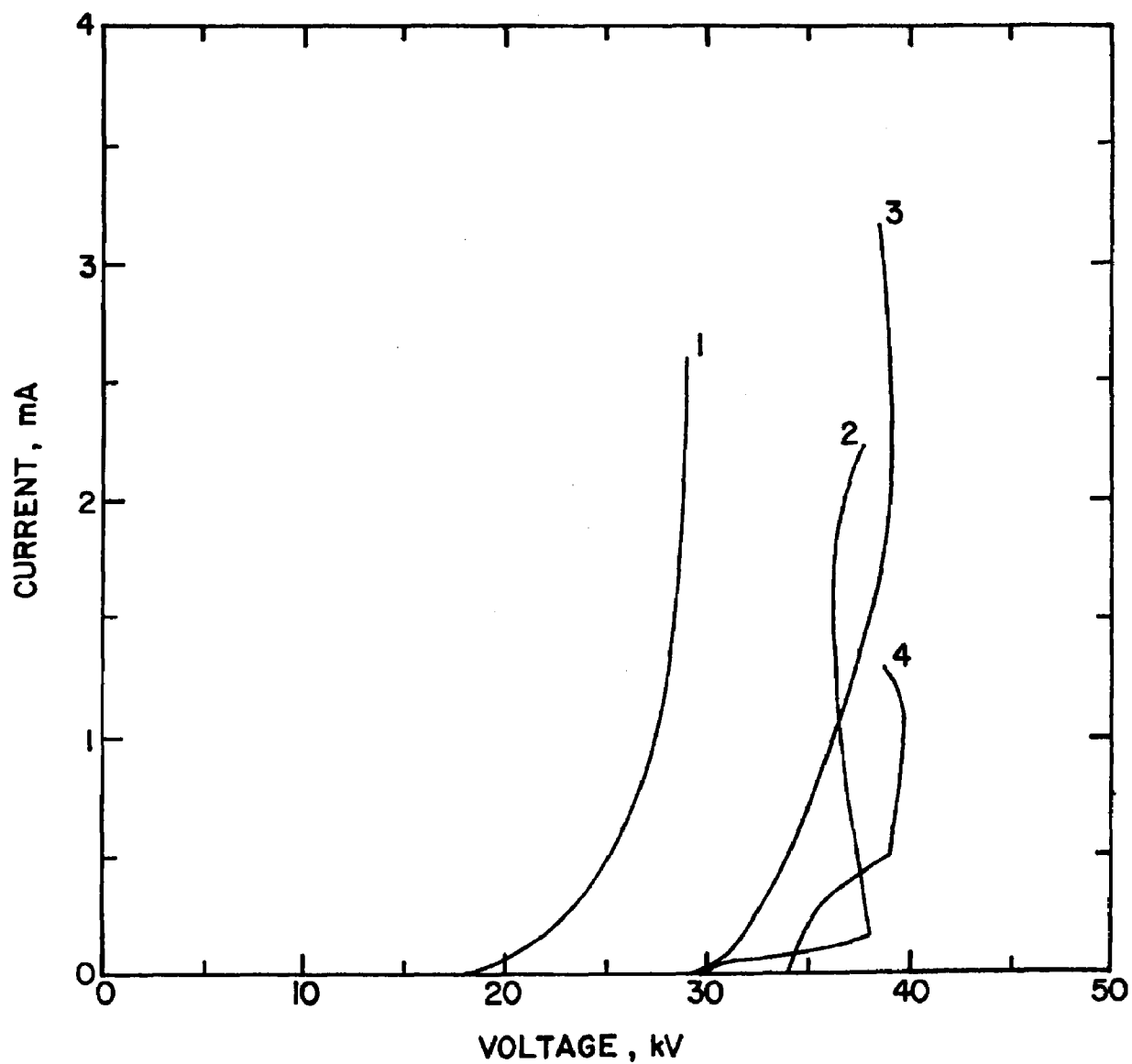


Figure 54. I-V curves of the downstream collector section with dirty wires and plates, no dust flow, and 300°F.

- 1) 0.312 cm diameter wires spaced 22.9 cm apart
- 2) 2.54 cm mesh
- 3) 0.312 cm diameter wires spaced 2.54 cm apart
- 4) 0.635 cm diameter wires spaced 5.08 cm apart

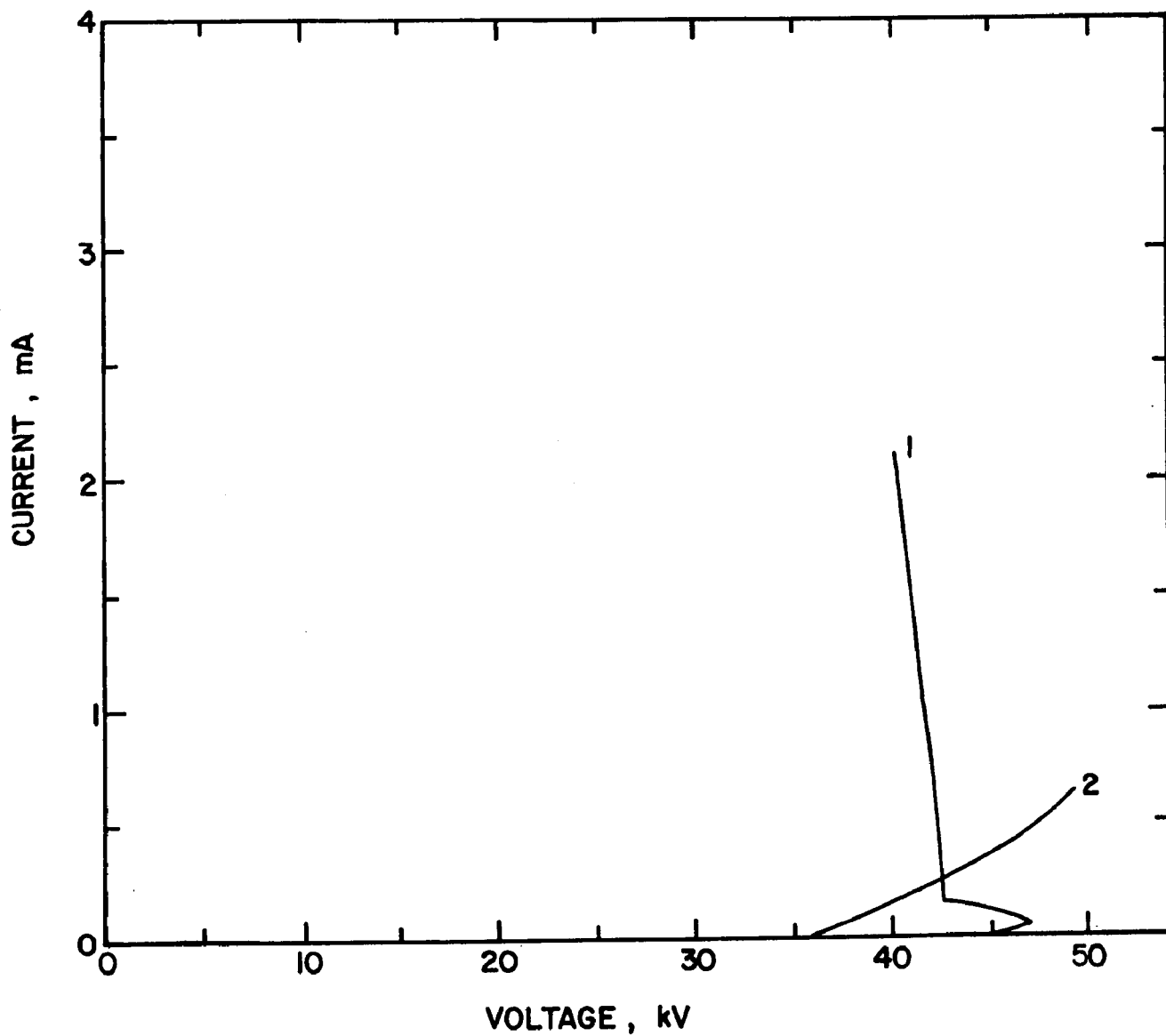


Figure 55. I-V curves of sections 1 and 2 of the downstream collector with dirty 2.54 cm mesh discharge electrodes, dirty plates, no dust flow, and 149°C.

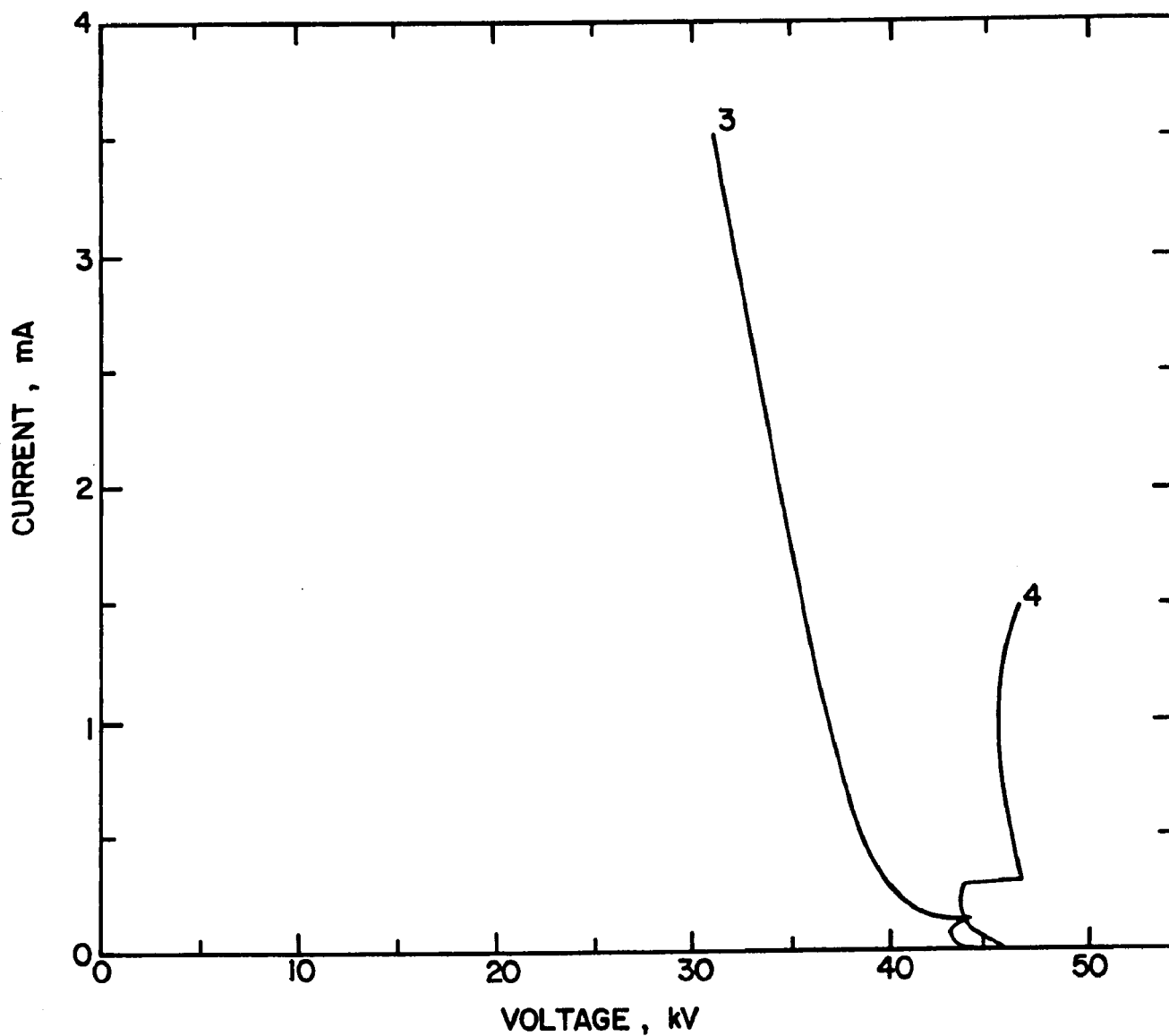


Figure 56. I-V curves of sections 3 and 4 of the downstream collector with dirty wires, dirty plates, no dust flow, and 149°C.
3) 0.318 cm wire diameter and 2.54 cm wire spacing
4) 0.635 cm wire diameter and 5.08 cm wire spacing

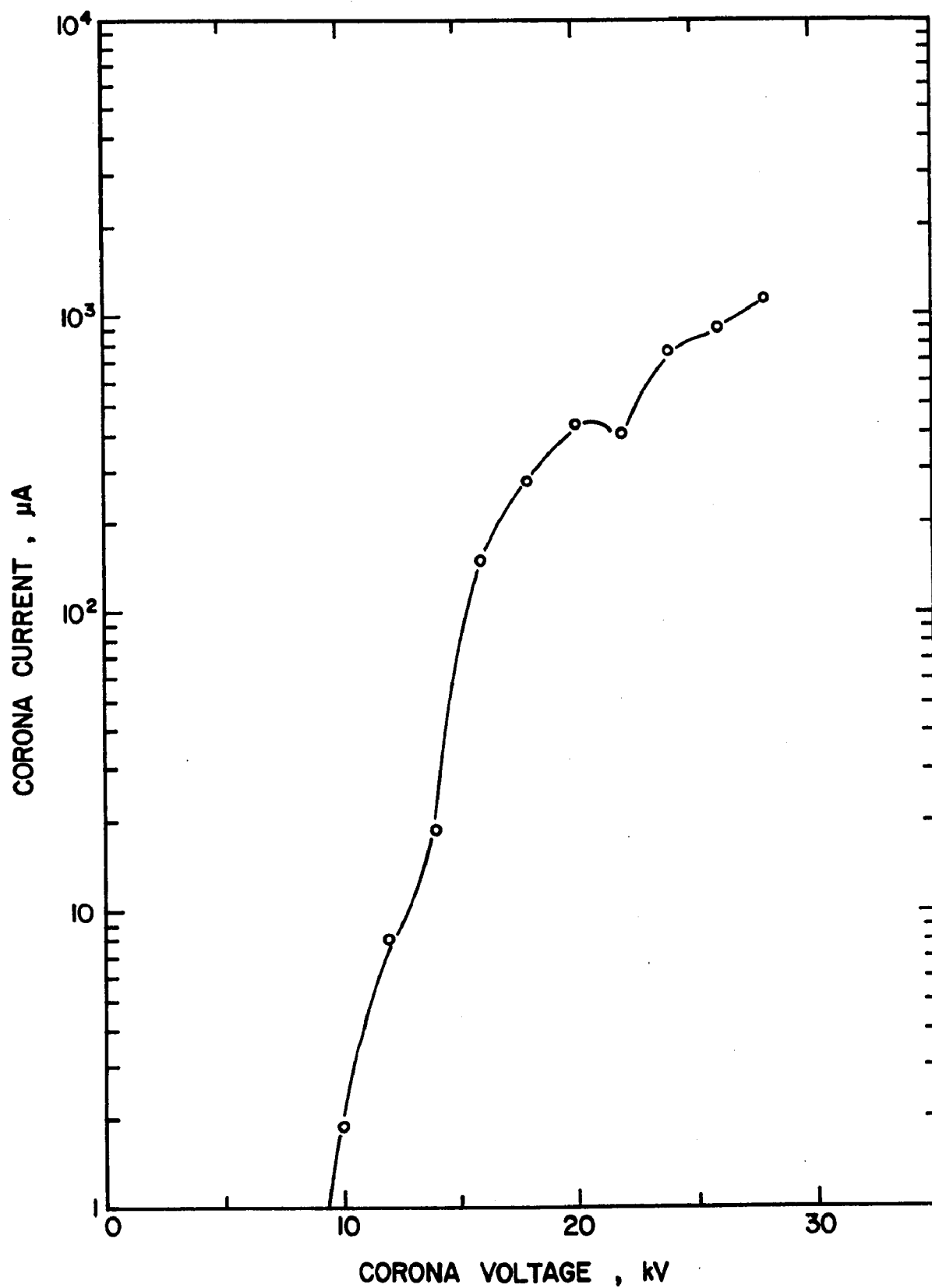


Figure 57. Precharger corona electrode I-V curve with the grid current held at zero, temperature = 158°C, and gas flowrate = 0.47 m³/sec.

An optical particle counter system (OPCS) was used to monitor the particle concentration as a function of particle diameter at the outlet of the precharger-collector system. The measurement system is shown schematically in Figure 58. The concentrations of particles in the range of 1.5 to 5.0 μm diameters were monitored during the efficiency tests.

The first attempt to evaluate the precharger-collector system was made by monitoring the particle concentration for the particle diameter region of interest with the precharger on and off and the collector sections held to 0.01 - 0.05 mA current in both cases. An average of 7234 particles/sec was observed with the collector on and the precharger off. With the collector on and precharger on the number of particles/sec measured was 2566. Therefore, the precharger effectively decreased the penetration of particles in the 1.5 - 5.0 μm diameter range by 64.5%.

The results of another test of particle concentration vs. particle diameter for the precharger-collector system is shown in Figure 59. The curves indicate concentration vs. diameter for particles in the range of 1.5 to 5.0 μm diameters for three conditions: 1) precharger off/collector off, 2) precharger off/collector on, and 3) precharger on/collector on. The differences in particle concentration for the three conditions are consistent for all particle diameters in the region of interest. Condition 1 measurements yielded an average value of 15,936 particles/sec for the entire particle diameter region of interest. The average for condition 2 tests was 6,632 particles/sec. From these two values, the collector alone accounts for a decrease in penetration of particles in the range of interest of 58.4%. The addition of the precharger in condition 3 measurements further decreased the particle concentration in the region of interest to 2,797 particles/sec. This corresponds to an overall system penetration decrease of 82.4% over the condition 1 case, or an improvement in performance attributable to the precharger of 57.8%.

It should be emphasized that the measurements of particle concentration in condition 1 tests were taken at the outlet end of the collector. Therefore, the decreases in penetration due to the collector and the collector with precharger do not necessarily represent collection efficiencies. Mass train measurements taken at the outlet and inlet of the precipitator indicated a mass collection efficiency of approximately 70% for the collector alone. Assuming this is directly related to the particle concentrations measured with the OPCS, an additional 12% collection efficiency due to settling can be added to the OPCS measured penetration decrease of 58.4% for the collector. Further, adding the settling percentage to the penetration data for precharger with collector gives a system collection efficiency of 94%.

The tests of the 0.47 m^3/sec precharger in conjunction with the IERL in-house precipitator show a significant precipitator enhancement capability for the precharger. The extremely high fly ash resistivity (5×10^{12} ohm-cm), very low collector S.C.A ($25.6 \text{ m}^2/\text{m}^3/\text{sec}$, or $130 \text{ ft}^2/1000 \text{ acfm}$), and the non-uniformity of the collector sections' discharge electrodes would tend to degrade the performance of the two-stage system below the normal operation expectations. Even so, a collection efficiency greater than 90% was obtained with this non-ideal two-stage system; with a contribution to the overall efficiency of approximately 60% directly attributable to the action of the precharger.

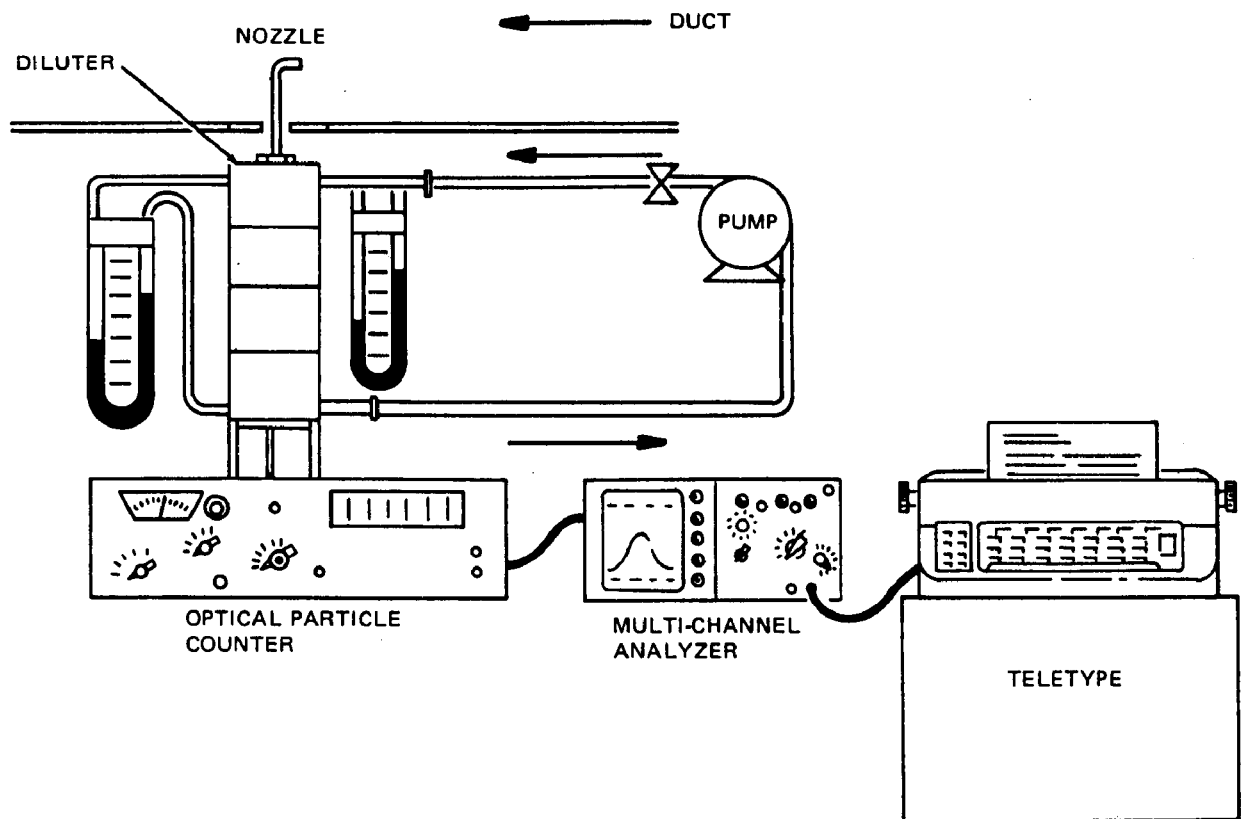


Figure 58. Optical particle counter measurement system.

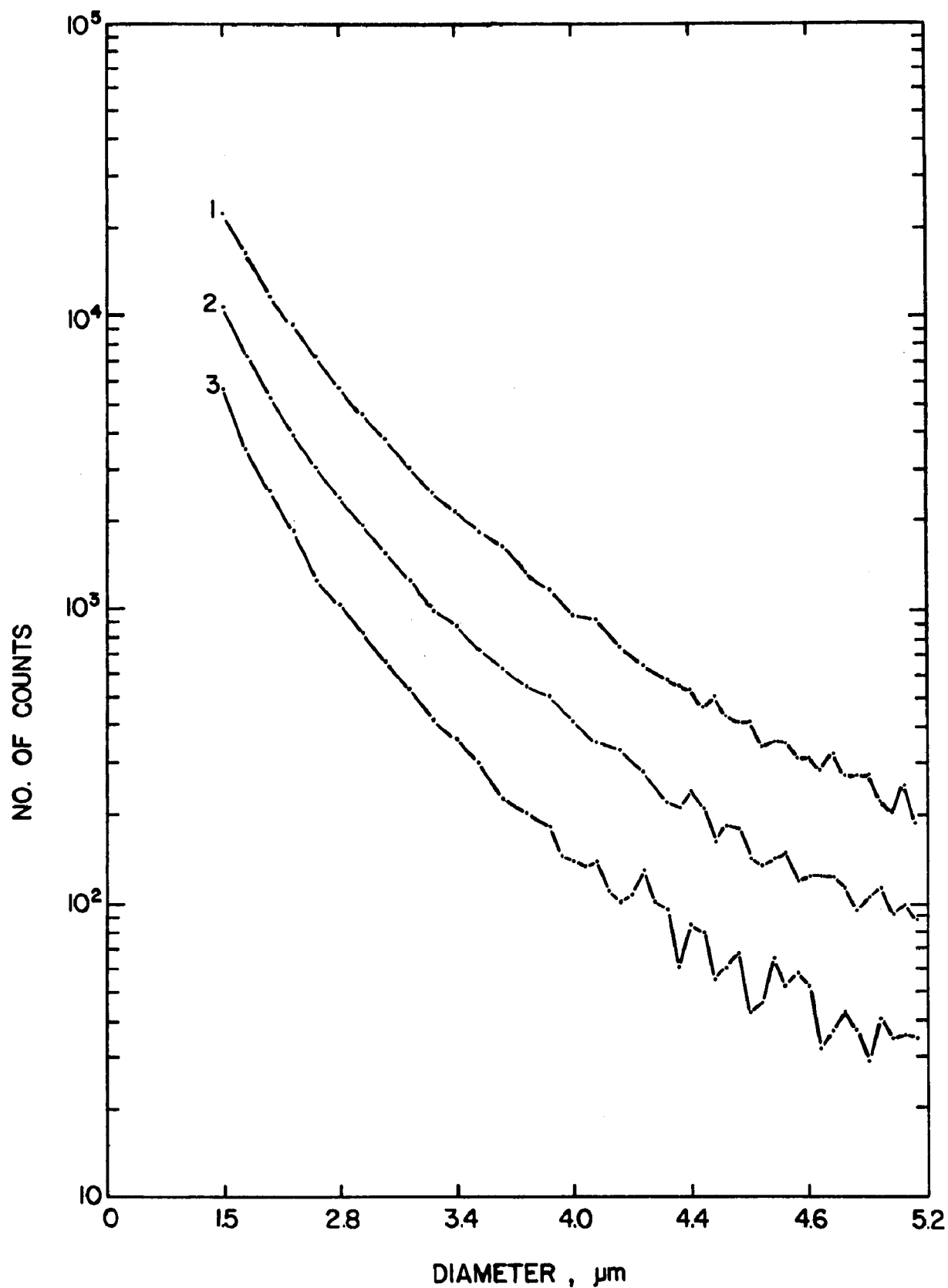


Figure 59. No. of counts vs. particle diameter as observed with the Climet optical particle counter for the three conditions:
1 - precharger off and collector off,
2 - precharger off and collector on, and
3 - precharger on and collector on.

SECTION 5

CHARGED PARTICLE COLLECTOR

In order to complete the precipitation process it is necessary to provide a suitable mechanism for collecting the charged particles emerging from the precharger. Since high resistivity particles may be encountered the problem of back corona must again be dealt with. It is not necessary, however, to maintain a high number density of ions in the downstream collector, because the particles are already charged. On the other hand, if the current density in the collector were reduced to zero, particles reentrained into the gas stream by rapping might not be recollected due to loss of charge during contact with the grounded collecting surfaces. It is thus assumed that the optimum current density in the collector should be slightly less than that which would bring about back corona.

The electric field strength in the collector should be as high as can be achieved within the constraints imposed by limiting the corona current density. The maximum field strength would result from the use of a parallel plate arrangement of electrodes in the collector, but that would produce, ideally, no corona current at all. A conventional wire-plate configuration would have to be operated at a relatively low applied voltage because of the limit on current density imposed by the presence of high resistivity materials. A wire-plate system could be modified from conventional practice, however. By the use of large diameter corona wires or by a much reduced spacing between wires the current-voltage characteristics can be adjusted to provide more desirable operating parameters.

Because a rectangular geometry offers significant advantages in flexibility and convenience in design and fabrication as compared to cylindrical or other type configurations, emphasis in this investigation was placed on a model employing parallel plate passive electrodes with corona discharge electrodes arranged in the plane midway between adjacent passive electrodes. The discharge electrodes could be parallel wires, an array of sharp points in the plane, a screen, or any of several other conceivable constructions. The screen and parallel wire arrangements were considered most attractive from an engineering and economic viewpoint.

Computer models of several corona wire diameters and wire-to-wire spacings in the conventional wire-plate precipitator configuration were executed. Further, a series of bench-scale experiments was performed to evaluate various corona electrodes. Corona wires of 0.65 cm and 0.32 cm diameters were tested at several wire-to-wire spacings (see Figures 60 and 61). Also tested were 2.54 cm and 1.27 cm square mesh, and 2.54 by 5.08 cm rectangular mesh.

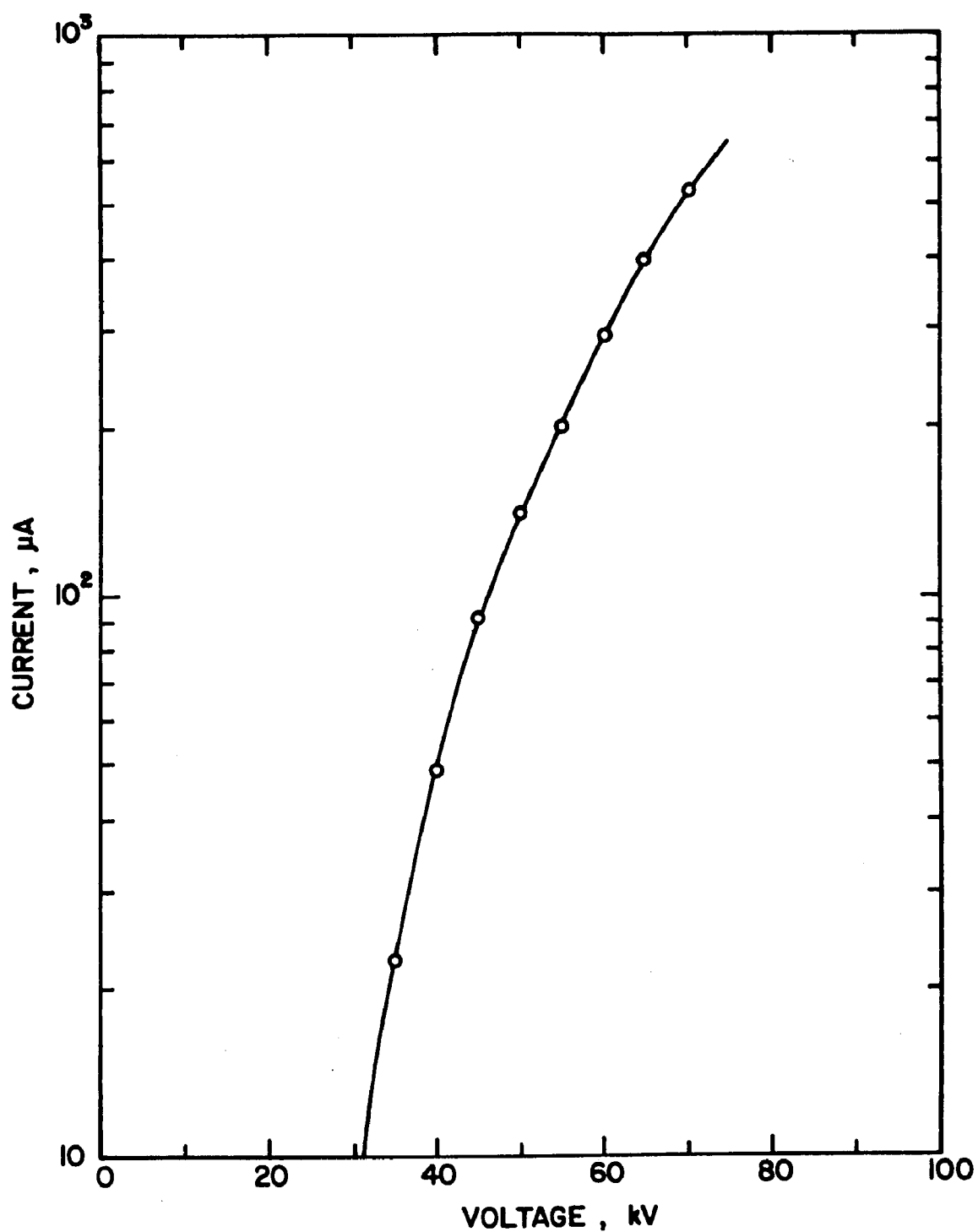


Figure 60. The current-voltage characteristic of five 0.64 cm diameter wires spaced 9.5 cm from a grounded plate with a wire-to-wire spacing = 3.81 cm.

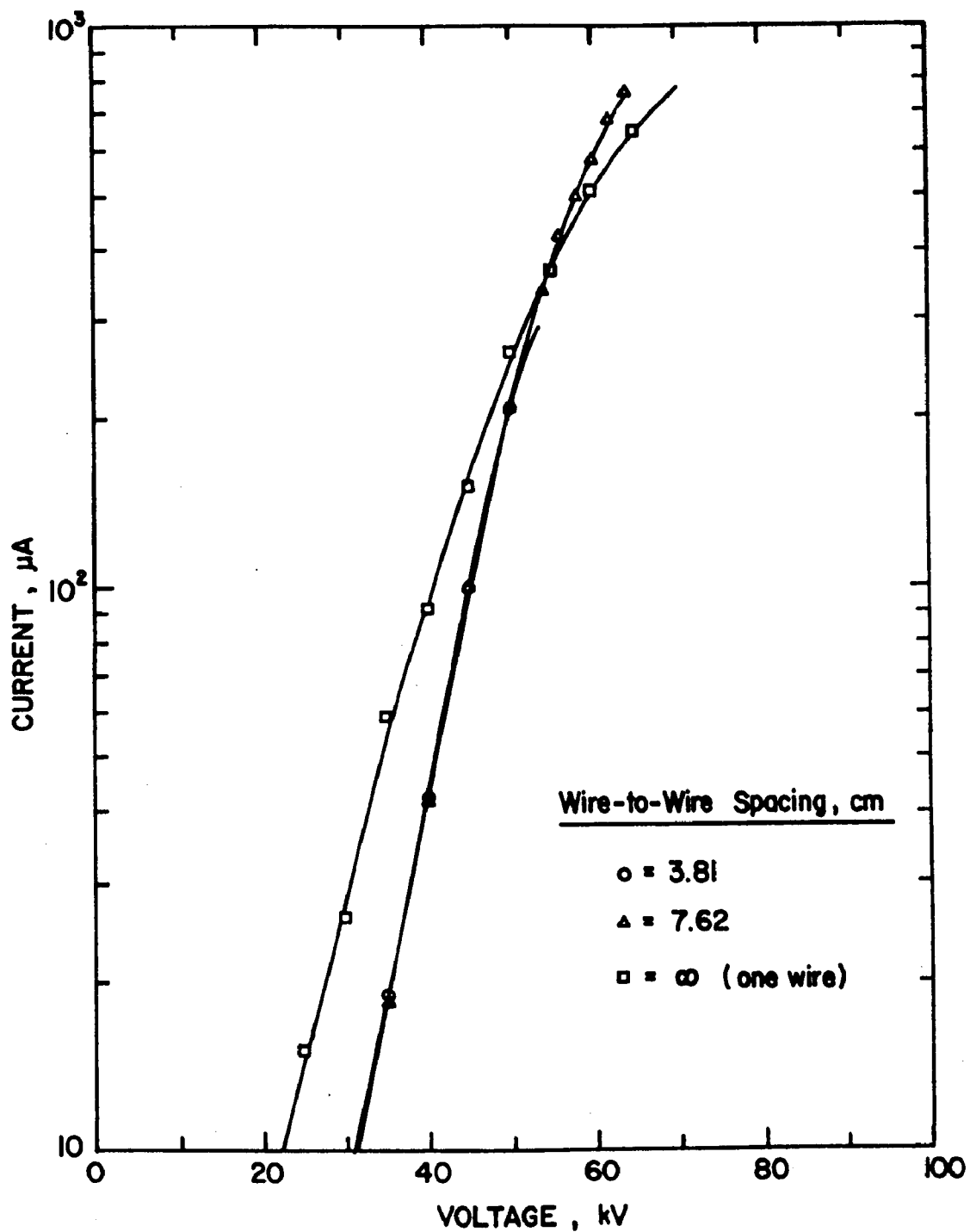


Figure 61. The current-voltage characteristics of 0.32 cm diameter wires spaced 9.5 cm from a grounded plate at three wire-to-wire spacings.

Figure 62 shows a comparison of current density as a function of spacing between active and passive electrodes for several wire and screen electrode configurations. It was found that the 2.54 cm square mesh screen electrode performed at the highest attainable electric field strength, at a low, controllable current density.

The use of a screen-type discharge electrode provides a periodic structure for corona activity. It tends to avoid a potential problem that might exist for closely spaced wires -- the development of localized regions of enhanced corona discharge spaced unpredictably, and unevenly, along the wire, resulting in an overall poor distribution of corona current.

In preparation for testing the two-stage concept a downstream collector was designed for use with the pilot scale precharger. An assembly drawing of the collector is shown in Figure 63. Discharge electrodes were 2.54 cm square mesh screen.

The device was fabricated and subjected to a preliminary testing program. Current-voltage relationships for the four collector sections were made. The two parallel gas passages in each section were independently energized to check the electrical, and thus the mechanical consistency of the electrodes in each section. Discrepancies between the I-V characteristics of two gas passages or two sections could be due to the existence of local surface discontinuities on the electrodes, electrode misalignment, or the varying proximity of the discharge electrodes to hopper baffles or other structural grounds. All of the I-V characteristics taken in this set of tests were at ambient conditions.

The current-voltage curves corresponding to the two gas passages in section 1 are shown in Figure 64. A maximum of nearly fivefold difference in current values between the two gas passages occurs in the mid-range of the voltage values (7.2 μ A to 34 μ A at 32 kV applied). In the projected operating range of 50-60 kV applied the difference is markedly less. Careful attention to smoothing the electrode surfaces may alleviate this inconsistency. Also, some exposed ends of the wire mesh discharge electrode may be present (in gas passage 2 especially) and leading to atypical I-V characteristics.

Figure 65 shows the current-voltage curves for the two gas passages in section 2 of the downstream collector. The similarity between the two curves is much greater in this case.

The I-V curves for section 3 are shown in Figure 66. The agreement between gas passages is good with the exception of a large difference in breakdown values (12 kV difference). This disparity may be due to the same factors discussed in conjunction with section 1 curves. Section 4 I-V characteristics are shown in Figure 67. There is very good agreement between the curves of the two gas passages in this section.

Figure 68 shows the current-voltage curves for all four sections of the downstream collector where the two gas passages in each section were electrically connected, as will be the case in actual operation. The sections vary

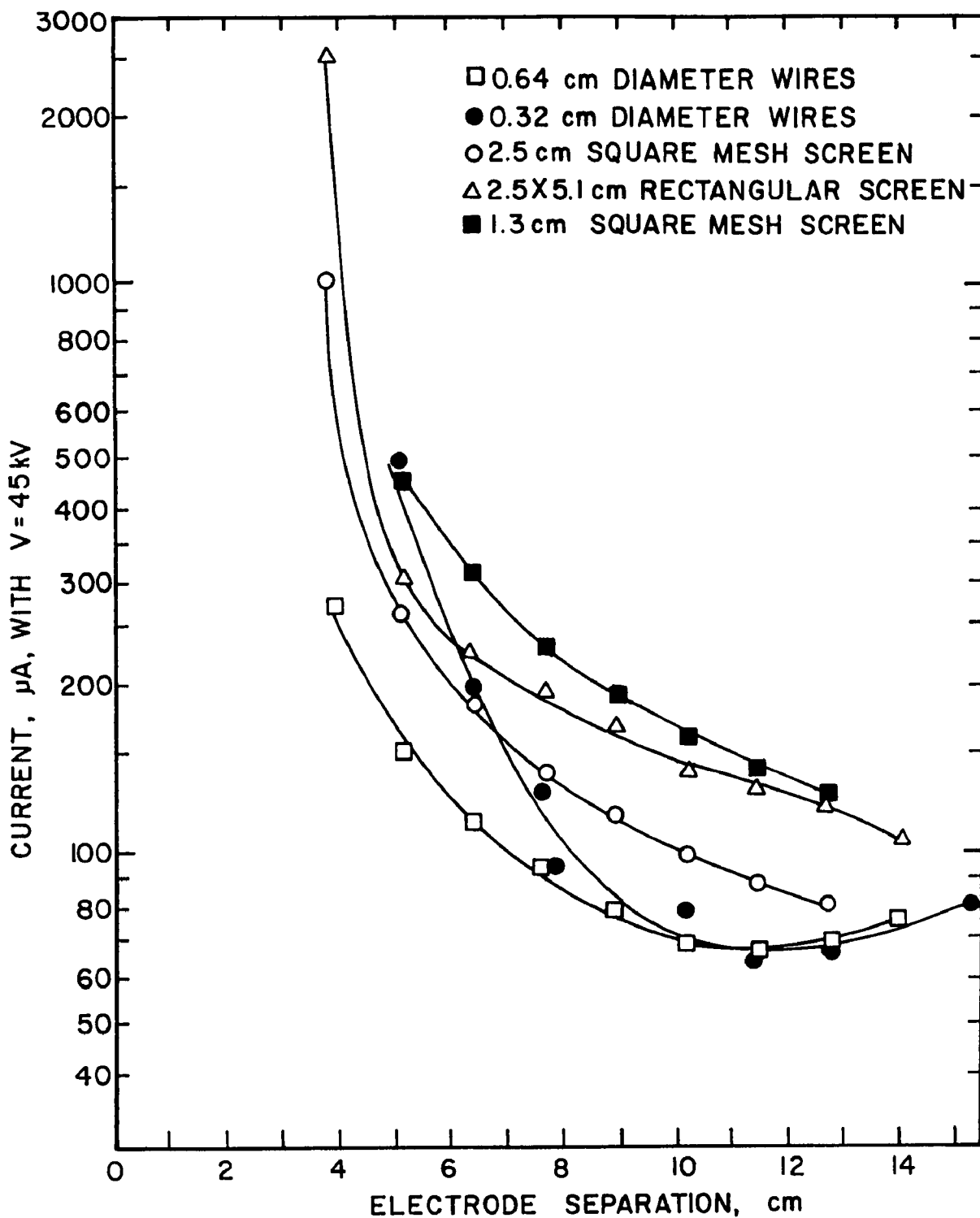
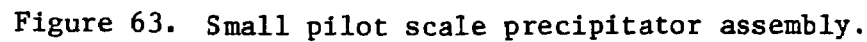


Figure 62. Comparison of electrical behavior for various types of corona discharge electrodes. The wires are in arrays of five in parallel, spaced at 3.8 cm.



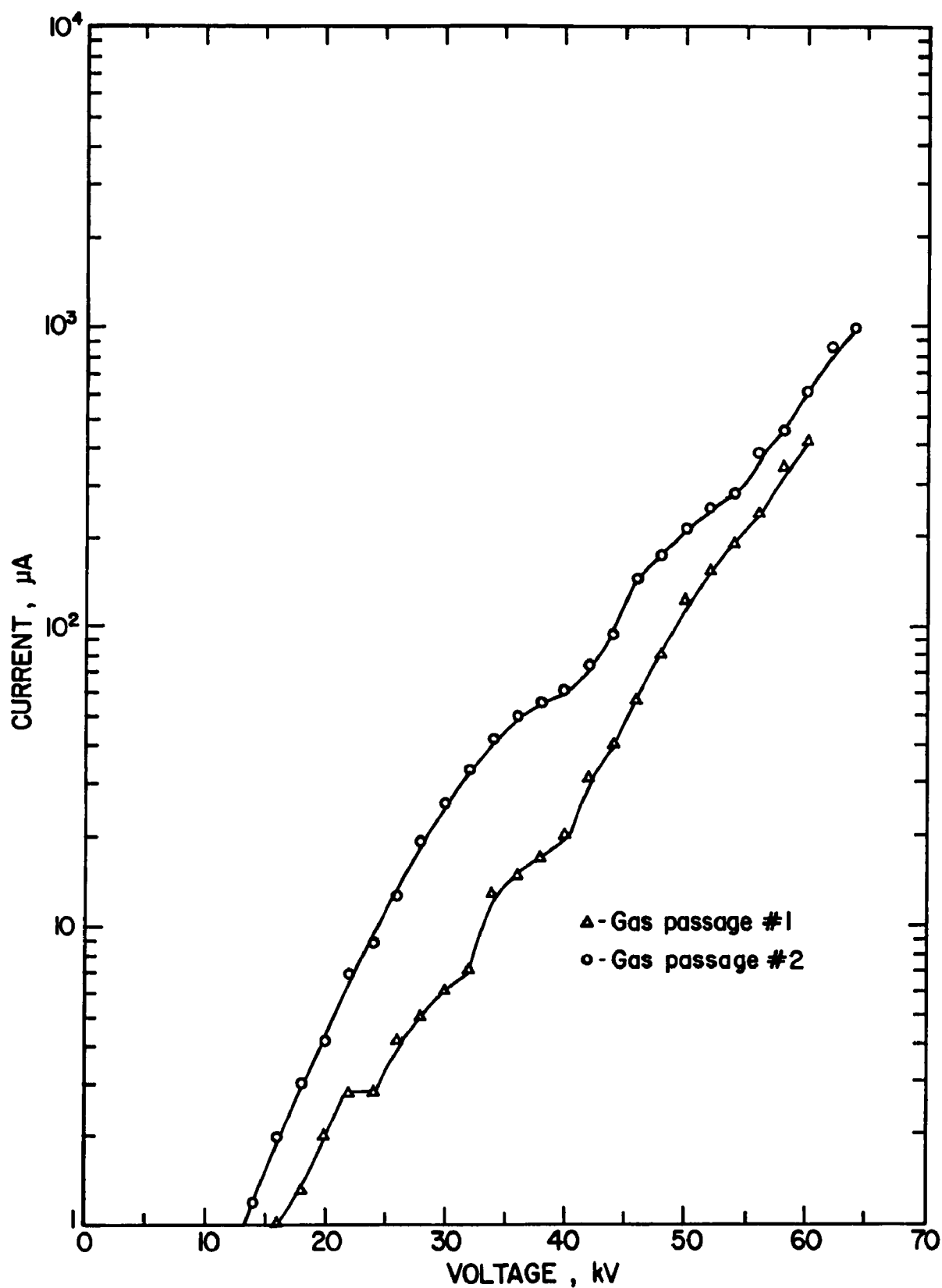


Figure 64. I-V characteristics of section 1 of the downstream collector with no gas flow and ambient conditions.

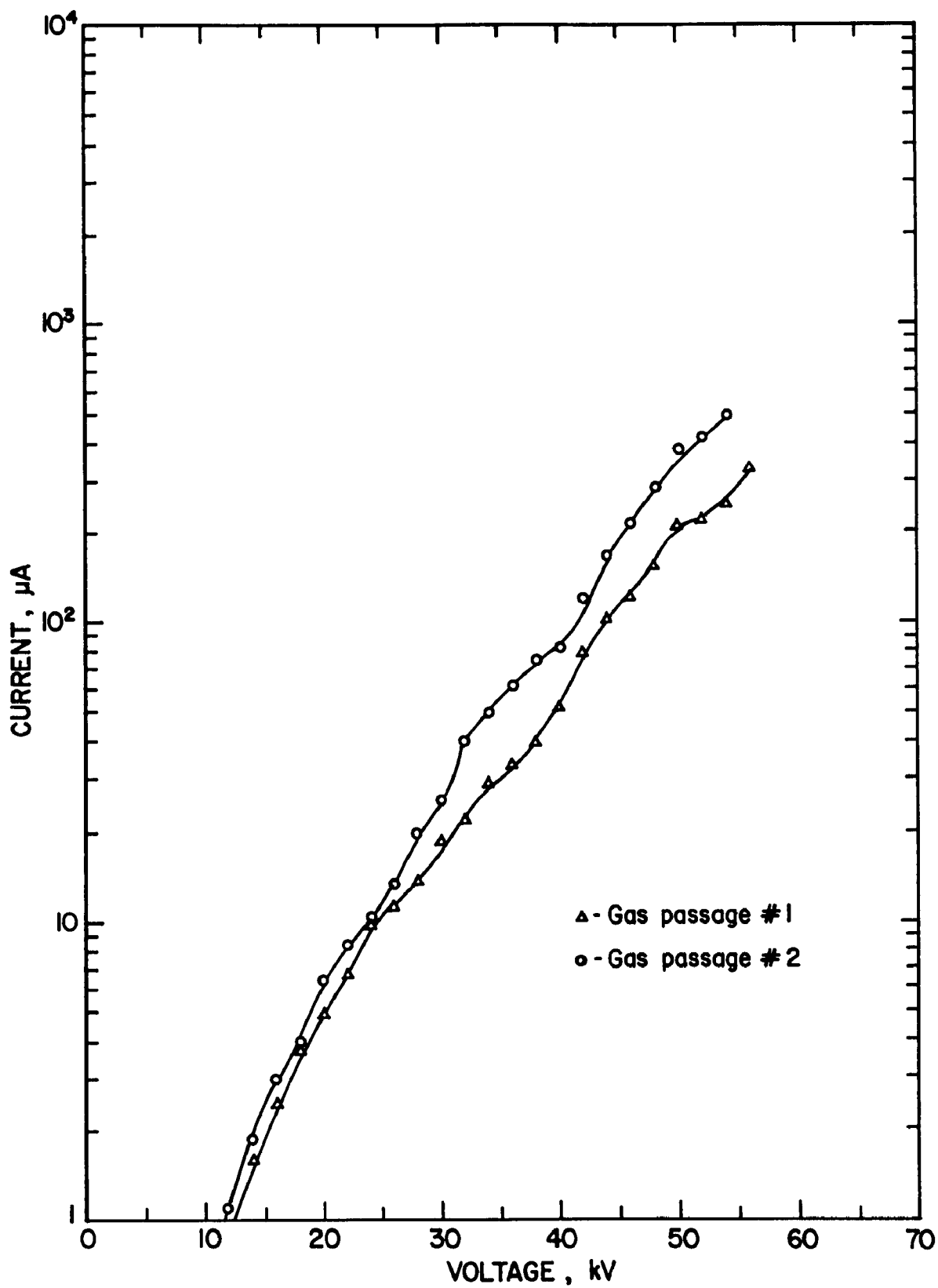


Figure 65. I-V characteristics of section 2 of the downstream collector with no gas flow and ambient conditions.

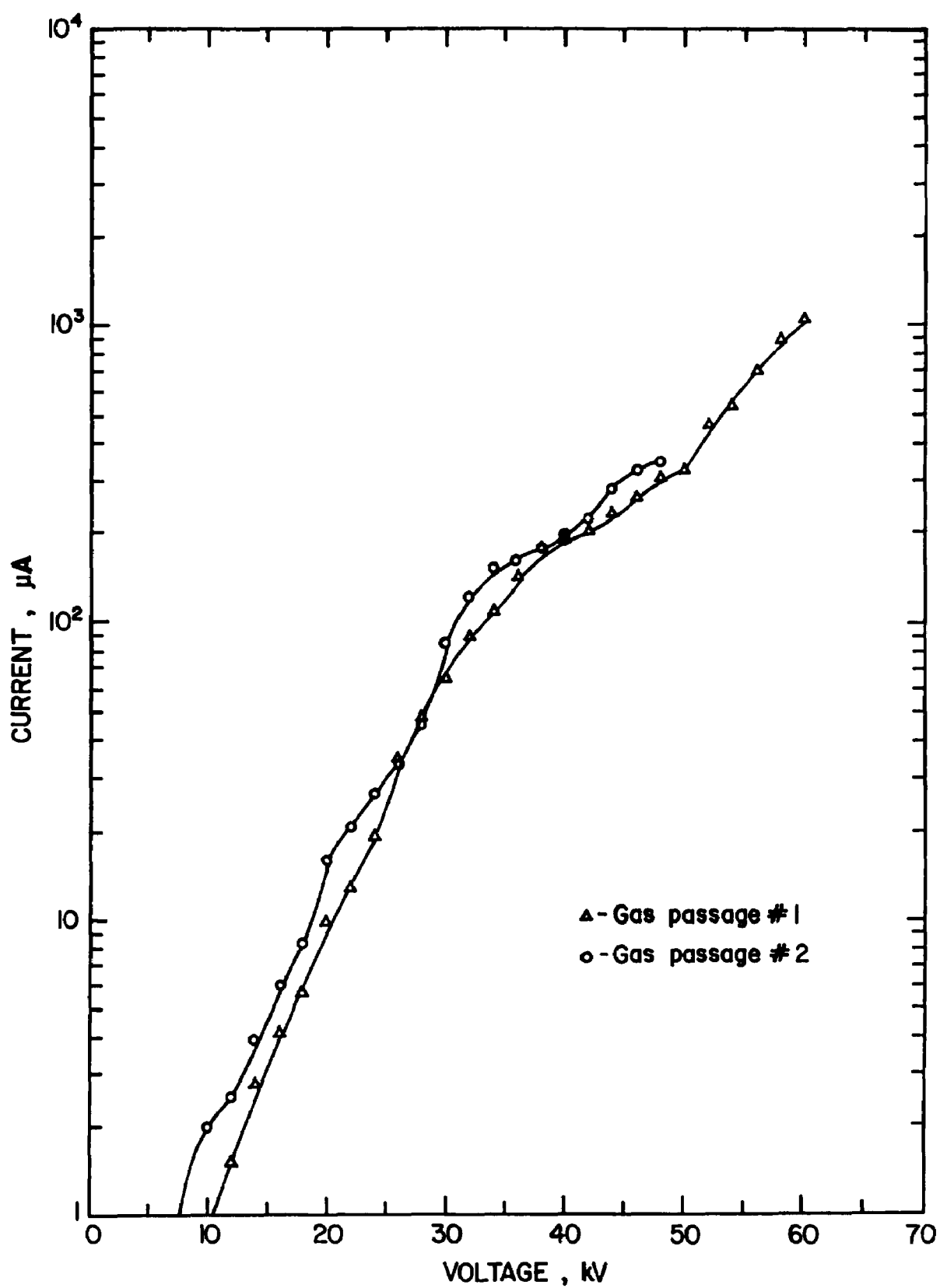


Figure 66. I-V characteristics of section 3 of the downstream collector with no gas flow and ambient conditions.

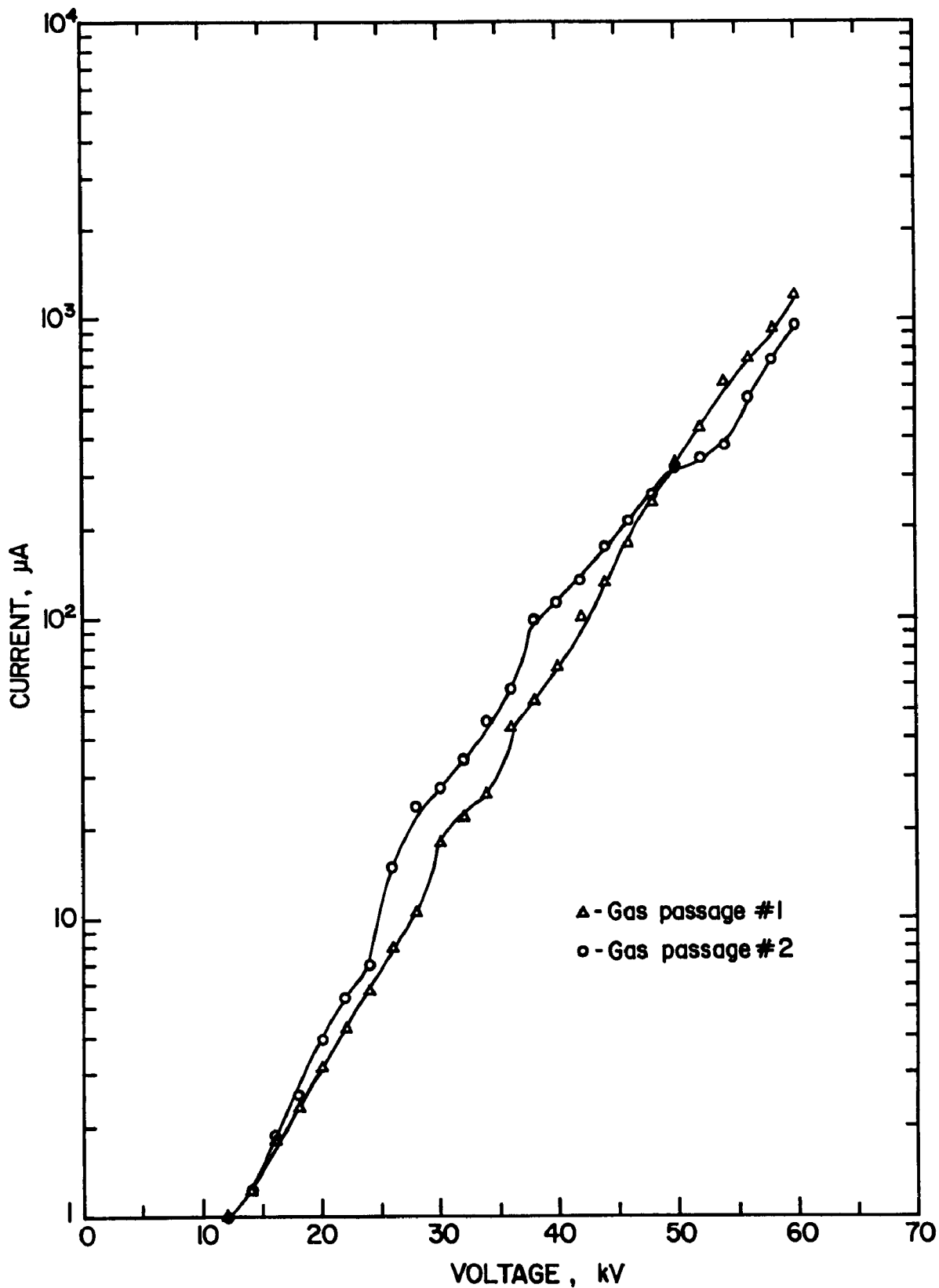


Figure 67. I-V characteristics of section 4 of the downstream collector with no gas flow and ambient conditions.

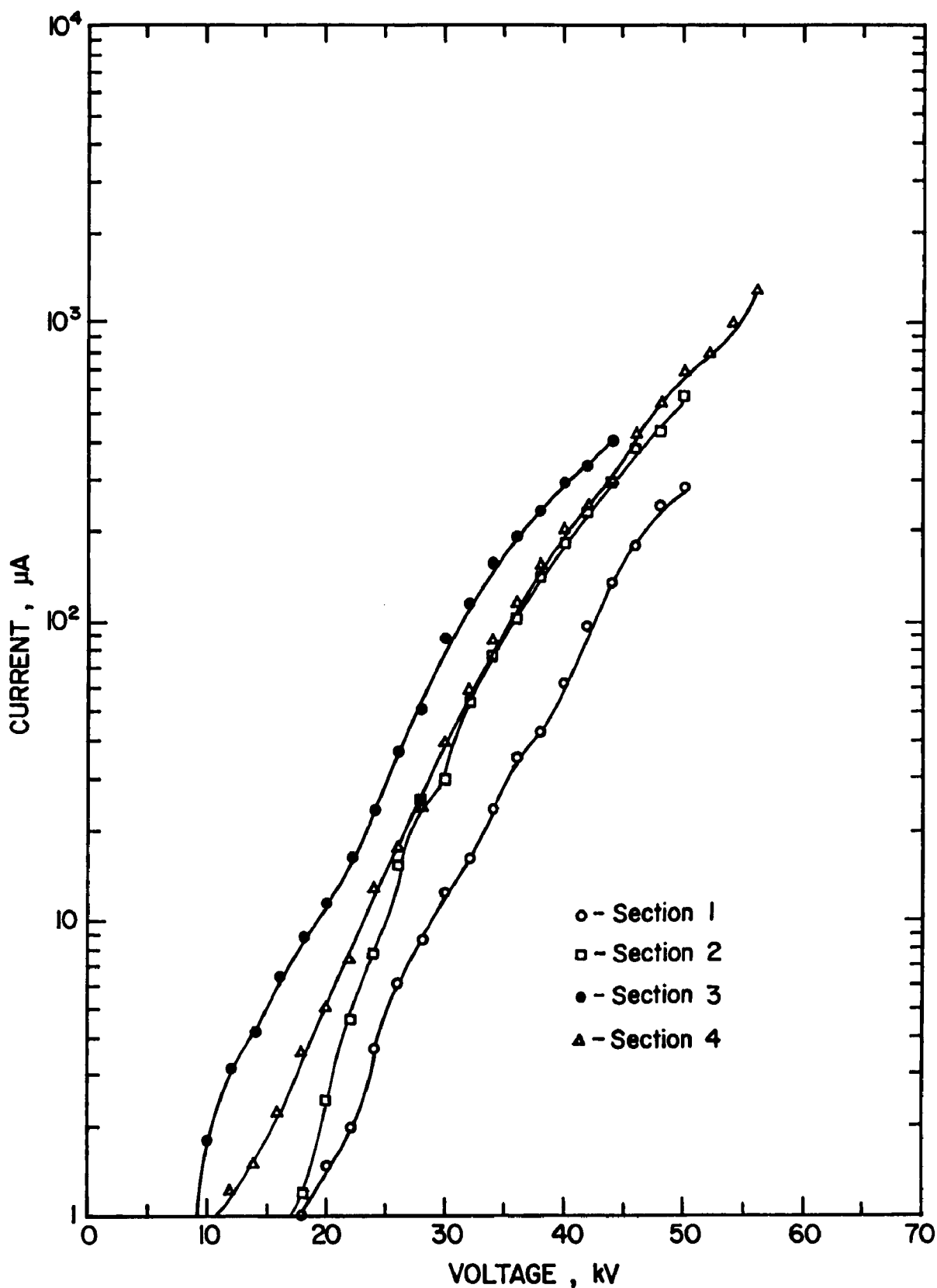


Figure 68. I-V characteristics of section 1 through 4 of the pilot scale downstream collector at ambient conditions. The two gas passages in each section were electrically connected for these tests.

considerably in their electrical characteristics. Mechanical differences between the four sections will be carefully eliminated, inasmuch as it is possible. This should normalize the electrical behavior of the sections.

The particle collector, in combination with the pilot scale precharger will be tested in the field, on a slip-stream taken from the exhaust ducting upstream of existing control devices at a coal-fired electric power plant. That test program will be carried out in connection with a separate research project under EPA Contract No. 68-02-2683, which supports work leading toward optimization of the downstream collector design.

SECTION 6

ENGINEERING AND COST ANALYSIS

ESTIMATED COSTS OF FULL SCALE PRECHARGER - COLLECTOR SYSTEMS

The criterion commonly used to estimate the cost of electrostatic precipitators is the number of square feet of collecting surface required to meet the design efficiency. Although the cost of the collection electrodes generally represents only 15-20 percent of the total precipitator cost, it is a reliable yardstick for estimating the capital investment required for a conventional precipitator installation. In order to approximate the cost of a full scale precharger-collector system the same criterion will be used as a base cost factor with additional factors added to estimate the extraordinary expenses required by the hybrid system.

The determination of the collecting surface area required in a full scale hybrid ESP is made using the data acquired in the pilot scale precharger performance tests and the collector study. The corona current densities maintained in all of the experiments are greater than found in the range of current densities ($5\text{--}75\text{ nA/cm}^2$) used in conventional full-scale fly ash precipitators operating under best conditions. The effect of ash resistivity on the current-voltage characteristics of conventional precipitators has been described by White.¹ He indicates that the current density would have to be reduced from .1% to .01% of clean plate values in the presence of a 2 mm thick deposited layer of high resistivity fly ash ($10^{11}\text{--}10^{13}\text{ }\Omega\text{-cm}$) to prevent breakdown, i.e., before back corona formation. Thus, the current densities maintained in the pilot scale charger tests are 2 to 4 orders of magnitude greater than could be expected in a conventional precipitator handling $10^{12}\text{ }\Omega\text{-cm}$ resistivity fly ash.

To determine whether valid theoretical estimates of particle charging behavior could be obtained with the data from the pilot scale experiments, a calculation of charge to mass ratio, Q/M , (see Appendix B) for a polydisperse aerosol simulating the particle size distribution encountered in the experiments was made and the theoretical value compared with experimental Q/m values. A log-normal particle size distribution was assumed, although this was only an approximation to the actual size distribution with which the charger was tested. A MMD, or D_{50} , of $19\text{ }\mu\text{m}$ was used, and a geometric standard deviation, σ_g , of 3.0 was derived from the particle size distribution obtained from actual impactor data, with the approximation $\sigma_g \approx D_{50}/D_{16}$. The physical conditions used in the Q/m calculations correspond to those in the precharger test where the gas stream temperature = 75°C , dust loading = 7.65 g/m^3 , fly ash resistivity = $1.4 \times 10^{12}\text{ ohm-cm}$, corona current density = 94 nA/cm^2 , and $Nt =$

8.63×10^{12} sec/m³. An ion mobility of 2.2×10^{-4} m²/V-sec, mean thermal velocity of 500 m/sec, particle relative dielectric constant of 5, and particle density equal to 2.47 g/cm³ were assumed. The theoretical Q/m calculated for this set of conditions equals 2.90×10^{-6} C/g. This compares to an average measured value of $Q/m = 2.69 \times 10^{-6}$ C/g at these conditions, or a difference of approximately 7%. Since there is adequate agreement between theoretical and experimental charging values, estimates of expected performance for the pilot scale precharger-collector system can be drawn from the experimental values of physical parameters and theoretical values of particle charge.

The predicted performance of a pilot scale system with a given collecting surface area was determined. In order to give a conservative evaluation of performance, the particle diameter which gives the poorest charging characteristic, .2 μ m diameter, was used in calculating the expected efficiency of the precharger-collector system. A calculation of the efficiency of collection of 19 μ m diameter particles was also made.

In order to determine the collection efficiency of the pilot scale precharger-collector system the following calculations were made:

- 1) charge on .2 μ m and 19 μ m diameter particles,
- 2) mobility of charged .2 μ m and 19 μ m diameter particles,
- 3) migration velocity of .2 μ m and 19 μ m diameter particles at four different collector field strengths, and
- 4) efficiency of collecting .2 μ m and 19 μ m diameter particles with the migration velocities determined in 3).

The charge on the particles was determined from the combined theoretical field and diffusional charging effects and is given by

$$q(a) = \pi a 4 \epsilon_0 \left\{ \frac{\mu a E_p N t}{\mu N t + \frac{4 \epsilon_0}{e}} \left[1 + 2 \frac{(k-1)}{(k+2)} \right] + \frac{KT}{e} \ln \left(\frac{\bar{v} N t}{\frac{4 \epsilon_0}{e} \frac{KT}{e}} + 1 \right) \right\}, \quad (1)$$

where Nt = ion concentration-time product (sec/m³),
 E_p = electric field strength in the precharger (V/m),
 a = particle radius (m),
 ϵ_0 = permittivity of free space (fd/m),
 e = electronic charge (C),
 k = particle dielectric constant,
 μ = ion mobility (m²/V-sec),
 T = temperature (°K),
 K = Boltzman's constant (j/°K),
 \bar{v} = mean thermal ion speed (m/sec), and
 $q(a)$ = charge on a particle of radius a (C).

Values of charging parameters from the pilot scale charging experiments used in the calculation were $Nt = 8.63 \times 10^{12}$ sec/m³, $E = 3.15 \times 10^5$ V/m, and

$T = 348^\circ\text{K}$. Other values used were $k = 5$, $\mu = 2.2 \times 10^{-4} \text{ m}^2/\text{V-sec}$, and $\bar{v} = 500 \text{ m/sec}$. The charge accumulated on the particles was determined to be $q(0.1 \times 10^{-6}) = 2.09 \times 10^{-18} \text{ C}$ and $q(9.5 \times 10^{-6}) = 6.49 \times 10^{-15} \text{ C}$.

After determining the charge on the particles, their mobility was calculated using the expression

$$M(a) = \frac{q(a)C}{6\pi\eta a}, \quad (2)$$

where $q(a)$ = charge on a particle of radius $a(\text{C})$,
 η = viscosity of the gas (kg/m-sec),
 C = Cunningham slip correction factor, and
 $M(a)$ = particle mobility ($\text{m}^2/\text{V-sec}$).

The value of viscosity, $2.1 \times 10^{-5} \text{ kg/m-sec}$, is that for air at 348°K . The mobilities for the two particle sizes of interest at these conditions are $M(.1 \times 10^{-6}) = 9.86 \times 10^{-8} \text{ m}^2/\text{V-sec}$ and $M(9.5 \times 10^{-6}) = 1.74 \times 10^{-6} \text{ m}^2/\text{V-sec}$.

The mobility is related to the particle migration velocity by the following relationship:

$$W = ME_c, \quad (3)$$

where E_c = electric field strength in the collector (V/m),
 M = particle mobility ($\text{m}^2/\text{V-sec}$), and
 W = particle migration velocity (m/sec).

The migration velocity was calculated for four values of E_c corresponding to applied voltages of 30, 40, 50, and 60 kV and an electrode spacing of 9.5 cm (19 cm duct width) in the collector. The values of the migration velocity for .2 μm and 19 μm diameter particles at these four conditions are listed in Table 3.

Now that the migration velocity is known, predicted values of efficiency for monodisperse particles can be determined from the Deutsch-Anderson equation.

$$\eta = 1 - e^{-(SCA)W}. \quad (4)$$

In this equation W = particle migration velocity (m/sec),
 $SCA = A/V$ (sec/m),
 A = effective collection surface area (m^2),
 V = gas flowrate (m^3/sec), and
 η = fractional efficiency.

The collection surface area of the pilot scale collector is given to be 23.78 m^2 . Assuming a gas volume flowrate of $.71 \text{ m}^3/\text{sec}$ ($1500 \text{ ft}^3/\text{min}$), the SCA used in the calculations of efficiency is 33.62 sec/m ($170 \text{ ft}^2/1000 \text{ ACFM}$). The collection efficiencies for the various calculated migration velocities are given in Table 3. The projections of collection efficiency were expanded in detail over the range of particle diameters between 0.1 and 10 μm . Figure 69 shows collection efficiency curves for two values of collecting field

PILOT SCALE PRECHARGER-COLLECTOR SYSTEM
PERFORMANCE PREDICTION

Particle diameter (μm)	E_p (V/m)	Nt (sec/m ³)	q (C)	M (m ² /V-sec)	SCA (sec/m)	E_c (V/m)	W (m/sec)	Collection Efficiency %
.2	3.15×10^5	8.63×10^{12}	2.09×10^{-18}	9.86×10^{-8}	33.62	3.16×10^5	3.12×10^{-2}	65.0
						4.21×10^5	4.15×10^{-2}	75.2
						5.26×10^5	5.19×10^{-2}	82.5
						6.32×10^5	6.23×10^{-2}	
19	3.15×10^5	8.63×10^{12}	6.49×10^{-15}	1.74×10^{-6}	33.62	3.16×10^5	5.50×10^{-1}	~100
						4.21×10^5	7.33×10^{-1}	~100
						5.26×10^5	9.15×10^{-1}	~100
						6.32×10^5	1.10×10^0	~100

Table 3. Estimated performance of the pilot scale precharger-collector system.

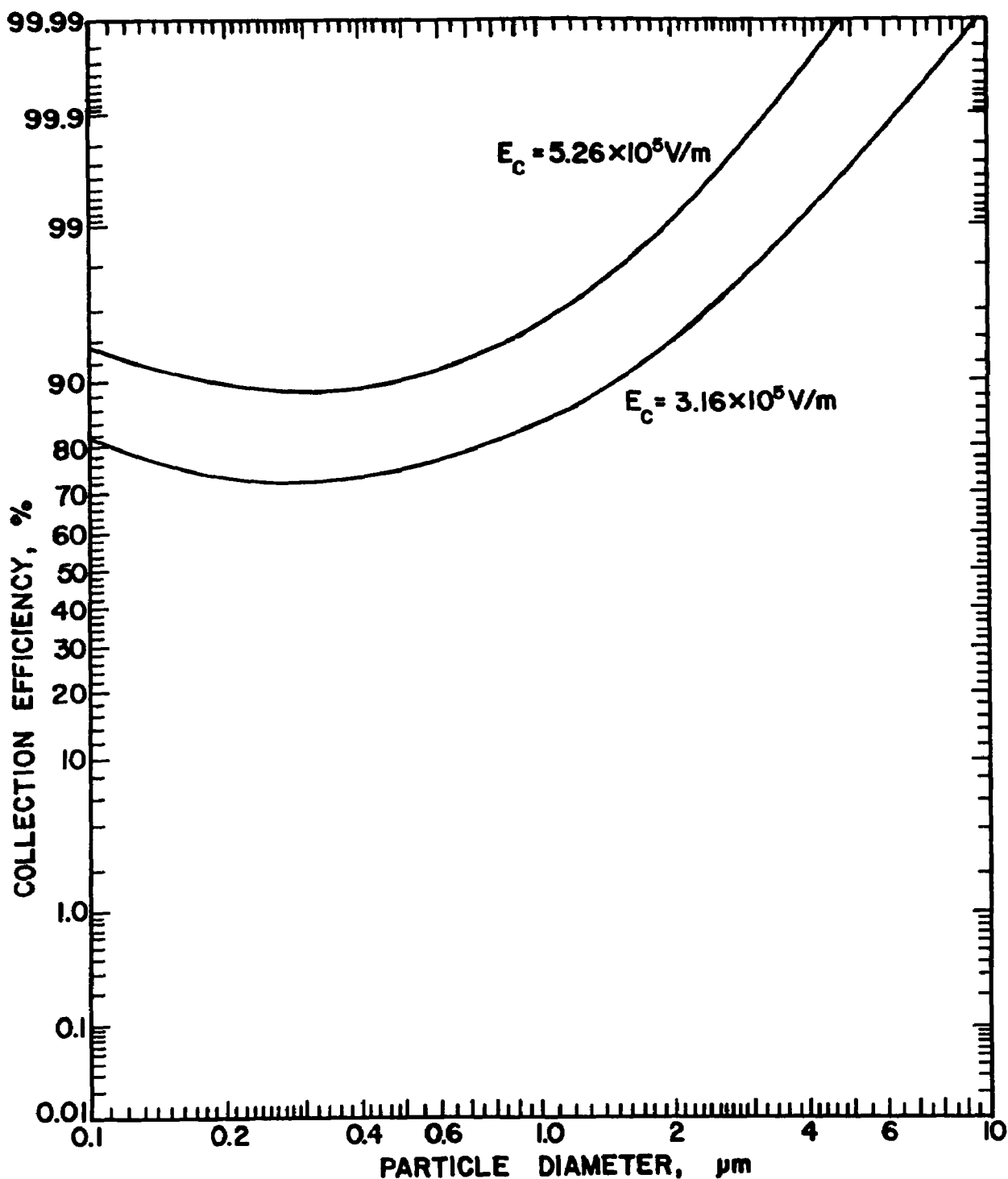


Figure 69. Theoretical collection efficiency of the pilot scale precharger-collector combination, plotted as a function of particle diameter. Charging parameters are $Nt = 8.63 \times 10^{12} \text{ sec/m}^3$, $E_c = 3.15 \times 10^5 \text{ V/m}$ and $T = 348^\circ \text{K}$. These data^p correspond to charging experiments where the dust resistivity was greater than $10^{11} \Omega \text{cm}$.

strength: $3.16 \times 10^5 \text{ V/m}$, corresponding to an applied voltage of 30 kV, and $5.26 \times 10^5 \text{ V/m}$ for 50 kV applied voltage. These curves cover the region of minimum particle mobility. For particles greater than $10 \mu\text{m}$ in diameter the theoretical collection efficiency is above 99.99%.

If a collection efficiency requirement is specified, the effective collection surface area needed to meet the design efficiency can be determined from Equation 4 by using the particle migration velocity obtained with the pilot scale precharger data and the design gas volume flowrate. Values of $E_p = 3.15 \times 10^5 \text{ V/m}$ and $N_t = 8.63 \times 10^{12} \text{ sec/m}^3$ for the precharger can be used to determine the charge acquired by a $2 \mu\text{m}$ diameter particle. This diameter particle is chosen to give an estimated effective migration velocity for the particles passing through the precharger-collector system. The charge is calculated using Equation 1 to be $q = 9.3 \times 10^{-17} \text{ C}$.

With an operational field strength in the downstream collector of $E_c = 4.0 \times 10^5 \text{ V/m}$, the particle migration velocity is given by Equations 2 and 3 to be $W = 1.02 \times 10^{-1} \text{ m/sec}$. The average gas velocity in the collector is $V_c = 1.5 \text{ m/sec}$ and the total gas volume flowrate is given to be $940 \text{ m}^3/\text{sec}$ ($2.0 \times 10^6 \text{ acfm}$). The collection surface area required in order to give 99.95% collection efficiency for $2 \mu\text{m}$ diameter particles can be determined to be $7.0 \times 10^4 \text{ m}^2$ ($7.6 \times 10^5 \text{ ft}^2$). This corresponds to an SCA of $74 \text{ m}^2/\text{m}^3/\text{sec}$ ($380 \text{ ft}^2/1000 \text{ cfm}$).

For a collection efficiency of 99.5% the collection surface area required, with all other conditions the same, is reduced to $4.9 \times 10^4 \text{ m}^2$ ($5.3 \times 10^5 \text{ ft}^2$). This is an SCA of $52 \text{ m}^2/\text{m}^3/\text{sec}$ ($265 \text{ ft}^2/1000 \text{ cfm}$).

Although costs among precipitator vendors vary greatly, an average for the erected cost of conventional precipitators as a function of collecting surface area is $\$108/\text{m}^2$ ($\$10/\text{ft}^2$) collecting area^{2,3}. Using a conservative value of SCA of $59 \text{ m}^2/\text{m}^3/\text{sec}$ ($300 \text{ ft}^2/1000 \text{ cfm}$) for a design efficiency of 99.5% and a gas volume flowrate of $9.4 \times 10^2 \text{ m}^3/\text{sec}$ gives a total collection surface area of $5.55 \times 10^4 \text{ m}^2$ ($5.97 \times 10^5 \text{ ft}^2$). The basic cost for an erected precipitator of this size is approximately $\$6 \times 10^6$.

It is necessary to add to this base cost the extraordinary expenses incurred by having as the first electrical section the three-electrode precharger geometry, and by using an unusual discharge electrode in the collector sections of the precipitator. The estimates of these extra costs are based on the detailed proposal for fabrication and erection of a $14.2 \text{ m}^3/\text{sec}$ ($30,000 \text{ cfm}$) version of a two-stage precipitator of this design made by Lodge-Cottrell Division of Dresser Industries. The precharger costs represented approximately 5% of the erected precipitator total cost. A very conservative adjustment to the base cost of the hybrid system to account for the precharger is 20%. The discharge electrodes in the collector are expected to cost less than 1% more than conventional electrodes. These adjustments in the base cost of $\$6 \times 10^6$ yield a total capital investment estimate for a 99.5% efficient two-stage ESP using the SoRI precharger and high field, low current density collector treating $9.4 \times 10^2 \text{ m}^3/\text{sec}$ of flue gas of $\$7.26 \times 10^6$.

COMPARISONS OF COSTS WITH CONVENTIONAL PRECIPITATORS

In order to accurately determine the cost effectiveness of a full scale two-stage ESP using the three-electrode precharger concept, the costs of conventional electrostatic precipitators for use in the same application and with the required collection efficiency must be determined. Three sources have been relied upon to provide cost information for conventional ESPs.

A cost model for ESPs burning low sulfur Western coal was developed by David V. Bubenick of Research-Cottrell, Inc.⁴ Models for calculating capital investment and annual operating costs for cold, hot, and cold SO₃ conditioned ESPs were derived. The only parameters required for computation of costs are volume of gas treated and area of the collection electrodes. For the purposes of this analysis, the following conditions were applied: 1) low sulfur (.5 - .7%) coal, 2) gas volume = 940 m³/sec at 163°C (2,000,000 acfm at 325°F), 3) collection efficiency = 99.5%, and 4) a precipitation rate parameter of 4 cm/sec. These conditions and the Deutsch-Anderson equation

$$\eta = 1 - e^{-\frac{Aw}{Q}} \quad (5)$$

where η = collection efficiency,
A = area of collection surface,
Q = volume flowrate, and
w = migration velocity,

give a value for the collection surface of $A = 1.25 \times 10^5 \text{ m}^2$, or 2.25 times as large as predicted for the SoRI two-stage ESP. Note that this value for the collection area does not include such non-ideal effects as rapping, non-uniform gas flow, sneakage, and aerosol polydispersity. However, the cost models compensate for this inaccuracy.

Upon substituting $A = 1.25 \times 10^5 \text{ m}^2$ and $Q = 940 \text{ m}^3/\text{sec}$ into the cost model for cold electrostatic precipitators, the total capital investment and annual operating costs are \$13.6 million and \$2.5 million, respectively. This is consistent with the \$108/m² of collecting area cost estimate used in the two-stage ESP case. A detailed cost breakdown is shown in Table 4. The capital investment is 86 percent higher than is expected with the precharger-collector hybrid system. Annual operating costs for the two-stage system are not expected to be greater than the conventional ESP. The power consumption should be no more than equal to the conventional ESP due to the operating mode of the collecting sections.

In the case of the hot precipitator model, adjustments to the volume flowrate and collection area must be made. Due to the temperature increase from 163°C to 371°C there is a corresponding increase in the gas volume

treated: $Q_H = \frac{1160}{785} \times Q = 1386 \text{ m}^3/\text{sec}$. The Research-Cottrell model

also makes an allowance for the collection area of hot precipitators. A decrease in specific collection area, $SCA = A/Q$, of $\frac{1}{2}$ is achieved over that of a cold ESP. The collection area required by the hot ESP to achieve collection efficiency of 99.5% is thus determined to be $A_H = 9.22 \times 10^4 \text{ m}^2$. Substituting these values of A_H and Q_H into the hot precipitator cost model

TABLE 4. COLD ESP COST MODEL

Capital Investment, \$*

1. Complete collector, flange-to-flange	5.130 x 10 ⁶
2. Typical precipitator accessories	7.695 x 10 ⁵
3. Structural support	8.726 x 10 ⁵
4. Tax and freight	5.420 x 10 ⁵
5. Engineering	3.000 x 10 ⁵
6. Erection and installation	5.367 x 10 ⁶
7. Contingencies	6.490 x 10 ⁵
8. TOTAL CAPITAL INVESTMENT	13.63 x 10 ⁶

Annual Cost, \$*

9. Labor	8.88 x 10 ³
10. Maintenance	6.00 x 10 ⁴
11. Power	3.76 x 10 ⁵
12. Administration	8.88 x 10 ²
13. Overhead	4.45 x 10 ⁴
14. Capital charges	2.04 x 10 ⁶
15. TOTAL ANNUAL COST	2.53 x 10 ⁶

* 1977 dollars

yields an estimated total capital investment of \$11.4 million and an annual operating cost of \$2.2 million (see Table 5 for a detailed cost breakdown).

The cost model for a cold SO₃ conditioned ESP is calculated with an SCA credit allowance of $\frac{1}{3}$. That is, the collection surface area required in a gas conditioned precipitator is $\frac{1}{3}$ less than an unconditioned ESP requires. Therefore $A_G = 8.34 \times 10^4 \text{ m}^2$. A cost breakdown for a cold SO₃ conditioned ESP with this collection area, a gas volume flowrate of 940 m³/sec, and achieving a collection efficiency of 99.5% is shown in Table 6. The total capital investment is \$10.5 million and the annual operating expense is \$2.11 million.

Another estimate of the cost of conventional cold-side electrostatic precipitators was obtained from a report of the Electric Power Research Institute (EPRI).² Data from four ESP manufacturers describing ten large modern precipitators served as a base for cost estimates. The system parameters (the same as were used for the Research-Cottrell cold ESP model) and cost breakdown are shown in Table 7. Only initial capital investment is tabulated.

A third source of information concerning costs of electrostatic precipitators is a Southern Research Institute report³ which includes data for cold-side, hot-side, and flue gas conditioned precipitator costs. These data are for larger installations than references 4 and 2; however, comparisons can be drawn. The design parameters and cost information are shown in Table 8.

The costs of conventional electrostatic precipitators for handling high resistivity particulate matter, whether cold-side, hot-side, or SO₃ conditioned, are significantly higher, as reported from the sources quoted above, than the estimated cost of an SoRI precharger-collector hybrid precipitator designed for the same efficiency and same conditions. A very considerable savings in capital investment seems possible by installing the two-stage ESP where particles of high resistivity need to be efficiently collected. Specifically, there appears to be a very substantial advantage at large utility boiler installations burning low sulfur coal.

Based on the information compiled here, the EPA/SoRI precharger-collector electrostatic precipitator is very cost competitive with conventional technology in high resistivity particle collection. Tests of the two-stage system in the field will allow for more accurate estimates of the system's performance.

TABLE 5. HOT ESP COST MODEL

Capital Investment, \$*

1. Complete collector, flange-to-flange	4.536 x 10 ⁶
2. Typical precipitator accessories	6.804 x 10 ⁵
3. Structural support	6.605 x 10 ⁵
4. Tax and Freight	4.700 x 10 ⁵
5. Engineering	2.598 x 10 ⁵
6. Erection and installation	4.244 x 10 ⁶
7. Contingencies	5.425 x 10 ⁵
<hr/>	
8. TOTAL CAPITAL INVESTMENT	11.39 x 10 ⁶

Annual Cost, \$*

9. Labor	1.038 x 10 ⁴
10. Maintenance	8.850 x 10 ⁴
11. Power	3.509 x 10 ⁵
12. Administration	1.037 x 10 ³
13. Overhead	4.497 x 10 ⁴
14. Capital charges	1.709 x 10 ⁶
<hr/>	
15. TOTAL ANNUAL COST	2.20 x 10 ⁶

* 1977 dollars

TABLE 6. COLD SO₃ CONDITIONED ESP COST MODEL

Capital Investment, \$*

1. Complete collector, flange-to-flange	3.578 x 10 ⁶
2. Typical precipitator accessories	5.368 x 10 ⁵
3. Structural support	5.893 x 10 ⁵
4. Tax and freight	3.763 x 10 ⁵
5. Engineering	2.084 x 10 ⁵
6. Erection and installation	3.713 x 10 ⁶
7. Contingencies	4.501 x 10 ⁵
8. Total SO ₃ conditioning system investment	<u>1.043 x 10⁶</u>
9. TOTAL CAPITAL INVESTMENT	10.495 x 10 ⁶

Annual Cost, \$*

10. Labor	8.880 x 10 ³
11. Maintenance	6.000 x 10 ⁴
12. Power	2.497 x 10 ⁵
13. Labor (SO ₃ conditioning)	3.000 x 10 ⁴
14. Maintenance (SO ₃ conditioning)	3.129 x 10 ⁴
15. Utilities (SO ₃ conditioning)	3.880 x 10 ⁴
16. Sulfur (SO ₃ conditioning)	6.600 x 10 ⁴
17. Administration	3.888 x 10 ³
18. Overhead	4.847 x 10 ⁴
19. Capital charges	<u>1.574 x 10⁶</u>
20. TOTAL ANNUAL COST	2.111 x 10 ⁶

* 1977 dollars

TABLE 7. DETAILED AVERAGE COSTS FOR NEW COLD ESP

<u>Item</u>	<u>Cost (\$*)</u>
High-voltage power	838,925
Control panels	698,961
Ext. high-voltage system	206,082
Electrical devices	2,576
Casing	1,608,298
Hoppers	1,037,279
Collecting system	1,403,934
High-voltage system	589,051
Rapper system	861,251
Inlet plenum	283,363
Outlet plenum	266,189
Internal Access	55,814
External Access	121,932
Superstructure	356,350
Ventilation system support	23,184
Operating floor insulation	76,422
Hopper dust control	75,563
Safety interlocks	81,574
Support structure	1,078,725
Access facilities	501,237
Contingencies	2,033,342
TOTAL	12,200,052

*Cost corrected to 1977 dollars by assuming 7% inflation for 1975 and 1976.

TABLE 8. COMPARISON OF AVERAGE COSTS FOR ELECTROSTATIC PRECIPITATORS
COLLECTING HIGH RESISTIVITY FLYASH

Design Factors	Hot-side	Cold-Side	Flue-Gas Conditioned
Gas volume, 10^3 ACFM	3,640	2,500	2,500
Temperature, °F	750	300	300
Migration velocity, cm/sec	8.5	4.75	8
Collection area, 10^3 ft ²	1,169	1,411	848
SCA, ft ² / 10^3 ACFM	321	564	339
Plant area required for site, 10^3 ft ²	28	35	19
<u>Cost, 10^3 \$*</u>			
Base, accessories, and plenum	6,420	6,420	4,280
Flues	1,051	396	368
Support structure	708	842	499
Erection	6,146	7,013	4,302
Insulation	2,806	2,248	1,388
Gas conditioning			1,872
Ash handling @ \$5350/hopper	257	289	193
Power (\$856/kW)	2,009	2,977	2,310
Land @ \$10,700/acre	6	9	4
TOTAL INVESTMENT	19,403	20,194	15,216
<u>Annual Cost, 10^3 \$*</u>			
Fixed charges @ 18% investment	3,493	3,635	2,739
Heat loss @ \$1.75/ 10^6 Btu	306		
Energy loss @ \$.02/kwh	304	282	367
SO ₃			535
Maintenance	82	90	104
TOTAL ANNUAL COST	4,185	4,007	3,745

* Cost corrected to 1977 dollars by assuming 7% inflation for 1976.

REFERENCES

1. Pontius, D. H., L. G. Felix, J. R. McDonald, and W. B. Smith. Fine Particle Charging Development. Southern Research Institute, EPA, Research Triangle Park, N.C., 1977. 239 pp. EPA-600/2-77-173.
2. Air Pollution Systems, Inc. Development Program for an Ionizer-Precipitator Fine Particle Dust Collection System as Applied to Coal-Fired Utility Steam Generators: Final Report, Volume 1: Technical and Economic Summary. EPRI FP-291. Palo Alto, CA. October 1976, p. 3-6.
3. Southern Research Institute. A Review of Technology for Control of Fly Ash Emissions from Coal in Electric Power Generation. SORI-EAS-77-243, Birmingham, AL. July 1977. p. 32-
4. Bubenick, D. V. Economic Comparison of Selected Scenarios for Electrostatic Precipitators and Fabric Filters. J. of APCA, 28(3): 279-283. 1978.
5. Browne, W. R., and E. E. Stone. Sulfur Dioxide Conversion Under Corona Discharge Catalysis. PH 86-65-2, U.S. Department of Health, Education and Welfare. 1965. 21 pp.
6. Matteson, M. J., A. L. Stringer, and W. L. Busbee. Corona Discharge Oxidation of Sulfur Dioxide. Environmental Science and Technology. 6(10): 895-901, 1972.
7. Parker, J. D., J. H. Boggs, and E. F. Blick. Introduction to Fluid Mechanics and Heat Transfer. Addison-Wesley Publishing Co., Reading, Mass. 1974. 612 pp.
8. Melcher, J. R., and K. S. Sachar. Charged Droplet Technology for Removal of Particulates from Industrial Gases. Final Report to Air Pollution Control Office, Durham, N. C. Contract No. 68-002-0018, Task 8. August 1971.
9. White, H. J., Industrial Electrostatic Precipitation. Addison-Wesley Publishing Co., Reading, Mass. 1963. pp. 322-324.

APPENDIX A

INVESTIGATION OF ALTERNATE METHODS

Limited theoretical studies and laboratory tests were applied to the evaluation of various techniques for controlling back corona and space charge effects in a high current density corona field. Practical and economic factors led to the development of the three-electrode system as described in detail in the text of this report. Since the alternative methods explored were not pursued beyond the preliminary tests, and therefore did not contribute substantially to the principal goals of the project in a direct manner, the results of these investigations are included in this appendix rather than in the main text.

INJECTION OF CONDITIONING REAGENTS

A method for control of high resistivity fly ash by means of injecting conditioning reagents directly into an electrical corona at the discharge electrode was investigated. The rationale behind this technique is as follows: In a charging device, both current density and electric field strength must be high in order to provide adequate particle charging. In the presence of high resistivity fly ash, back corona problems are most severe where the current density at the passive electrode is greatest. Any method used to control back corona must therefore be most effective in the precharging section of a two stage precharger-ESP system. A controlled amount of conditioning material injected through the corona region would become highly charged and driven by the electric field to the passive electrode. The greatest amount of conditioning agent would naturally be applied to the region of highest current density on the passive electrode. Conditioning against high resistivity would thus be limited principally to the particulate material actually collected in the precharging section. The total amount of conditioning material required should therefore be much smaller than that required to treat the entire influx of particles.

Experiments were done in the laboratory to test the injection technique with the application of various reagents of both liquid and gaseous types. The theoretical considerations and experimental results are presented in the following paragraphs.

Gas Injection

Initial experiments involved the introduction of a mixture of SO_2 and O_2 into the corona region. The high electric field strength in the corona should

provide the most favorable environment for conversion to SO_3 . Furthermore, the ionization of SO_3 molecules would provide for their transport to the passive electrode. The SO_3 ions would also be directly involved in the charging process.

Previous studies of the conversion of SO_2 to SO_3 and the effects of this reaction on high resistivity fly ash have dealt with the SO_2 as a constituent of the gas stream.^{2,3} The present study is based upon the premise that more efficient use of the reagent can result from direct injection into the corona region.

Theory of Ion Injection:

In order to provide enough gas to account for a corona current made up entirely of SO_3 ions the minimum requirement of SO_2 is that which would provide one molecule for each elementary unit of charge in the corona current. Thus for a corona current I the required number of moles per second of SO_2 is

$$n = \frac{I}{eA} \quad , \quad (1)$$

where e is the electron charge in coulombs, and A is Avogadro's number. Since one mole of gas occupies 22.4 liters under standard conditions, the required volume flowrate is

$$U = \frac{22.4}{273} \frac{nT}{p} \quad ,$$

where T is the temperature (K), and p is the pressure in atmospheres. Thus, from equation (1)

$$U = \frac{22.4}{273} \frac{IT}{eAp} \quad ,$$

or

$$U = 8.501 \times 10^{-7} \frac{IT}{p} \text{ liters/sec} \quad (2)$$

In previous pilot scale particle charging experiments a precharger was used to charge particles in a total gas flow of about 400 cfm (189 l/sec) while operating at a total current of approximately 15 mA. The minimum SO_2 gas injection in such a device at 300K and one atmosphere is, from equation (2), $U = 3.83 \times 10^{-6}$ l/sec. Comparing this value with the total gas flow U_g , we have

$$U/U_g = 2.02 \times 10^{-8} \quad ,$$

or about 20 parts per billion. This is an extremely small amount compared to a level of several parts per million used in conventional conditioning methods with SO_3 .

The feasibility of applying an ion injection scheme such as that described in the above paragraphs depends upon SO_2 conversion to SO_3 , ionization and transport in the corona current, as well as the nature of the effect of SO_3 on the conduction mechanism in a deposited layer of fly ash. Although the amount of SO_2 injected would be extremely small, almost all of it would be restricted to the precharger section of a two stage precipitator, where dust accumulation would be minimized by aerodynamic design or continuous rapping.

Experimental Verification

A simple point-plane corona apparatus was set up in order to test the theoretical concepts discussed in the above. The discharge electrode was designed to admit a flow of gas into the corona region. A length of 0.2 mm nichrome wire was secured to the inside of a piece of 2.4 mm i.d. dielectric tubing so that the wire extended about 2 mm beyond the end of the tube. The gas flowing through the tube thus drifts directly into the corona region surrounding the end of the wire. During operation a mixture of two parts SO_2 to one part O_2 was forced through the tube at a controlled rate with a syringe pump.

In order to measure the amount of injected material carried over by the corona current, a petrie dish containing distilled, deionized water was used as a collecting electrode. A platinum wire immersed in the water served as a connection to the system ground.

In each experimental run a corona current was established and gas was injected into the corona region. After typically 100 min. running time the water used as the collecting electrode was analyzed chemically for sulfates by titration against a barium perchlorate solution.

Two experiments were run with the total gas flowrate set at 0.06 ml/min at room temperature. According to our theoretical interpretation the excess gas would remain un-ionized and drift out of the system. After each experiment two aliquots of the solution produced were analyzed for sulfate content. In addition, control experiments were run under three conditons: (1) corona current on with no gas flow, (2) corona current on with ambient air replacing the mixture of SO_2 and O_2 , and (3) injection of SO_2 and O_2 with the corona current turned off. Only trace amounts of sulfates were found in the control experiments. The experimental results shown in Table A-1 indicate fairly effective transport of the selected ion in the corona current. Measured sulfate concentrations were 74 to 84 per cent of the theoretical values.

Preliminary tests of fly ash conditioning were made using this system, but with a flat metal plate used as a collecting electrode. The system was enclosed in an oven to produce conditions favoring high resistivity in fly ash. An experiment was run to compare the operation of the system with and without gas injection at the discharge electrode. First, the clean plate I-V characteristic was determined for a 2.5 cm electrode spacing. Oven temperature was maintained at 150°C. The result is shown in Figure A-1. The system was then set to operate at a total current of approximately 300 μA , and a mixture of two parts SO_2 and one part O_2 was injected at a flowrate of 0.33 $\mu\text{l/sec}$.

TABLE A-1. COMPARISON OF THEORETICAL AND
EXPERIMENTAL DETERMINATIONS OF
SULFATE ION TRANSPORT

<u>Corona Current</u>	<u>Solution Volume Recovered</u>	<u>Calculated Normal Sulfate Concentration</u>	<u>Measured Normal Sulfate Concentration</u>
50 μ A	25 ml	2.48×10^{-4} N	1.92×10^{-4} N
50 μ A	25 ml	2.48×10^{-4} N	2.08×10^{-4} N
100 μ A	40 ml	3.11×10^{-4} N	2.43×10^{-4} N
100 μ A	40 ml	3.11×10^{-4} N	2.32×10^{-4} N

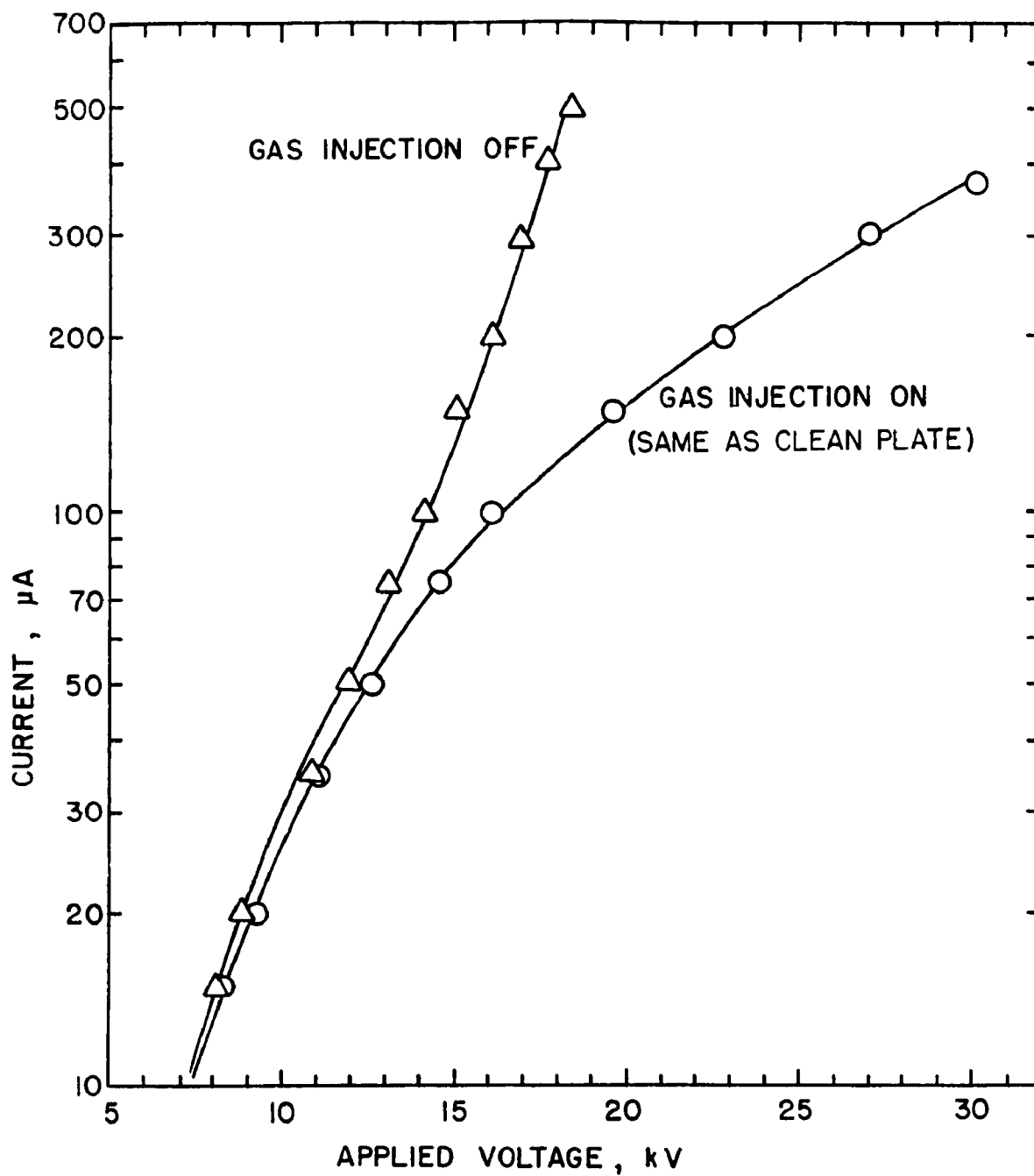


Figure A-1. Comparison of I-V characteristics for a corona system under dust loading conditions with gas injection on and similar conditions with gas injection turned off.

Fly ash was blown into the system in puffs through a tube by an elutriator. When changes in the current occurred after a puff a brief period, about five to fifteen seconds, was allowed before the next puff so that the conditioning effect of the gas could restore the original operating condition. Continuing this procedure for several minutes it was possible to deposit a total of 323 mg of ash on the grounded electrode with essentially no change in the I-V characteristic. There was no indication that the procedure could not be continued to deposit still more ash without producing back corona effects. After the gas flow was turned off and no further ash was applied the I-V characteristic remained unchanged.

The procedure was begun again with a clean plate, but with no gas injection. After the first few puffs of flyash the current rose sharply. The current was left on, but application of fly ash was suspended. No tendency toward a drift in current at a fixed voltage was observed over a period of fifteen minutes; the change in electrical behavior was permanent. The I-V characteristic was measured for comparison with the previous result. The curve, shown in Figure A-1, exhibits a rapid rise in current with a voltage above approximately 12 kV, indicating the presence of back corona. The total ash accumulated was 67.5 mg, about one fifth of the amount in the previous run.

Further experiments were run after modifications in the apparatus were made in order to provide a continuous flow of ash laden air and to control the humidity in the oven containing the corona system.

A mixture of SO₂ and O₂ was injected by syringe pump into the corona region as previously described. An elutriator, operated by a continuous flow of air, was used to introduce fly ash into the system when required. Humidity was controlled in the oven by circulating air from an external bubbler or desiccator source.

The general procedure used was to operate the corona system as a precipitator while observing any changes in current or voltage. Onset of back corona is normally accompanied by an abrupt increase in corona current.

Injection of a mixture of SO₂ and O₂ had little effect on back corona when desiccated air was circulated in the system. A measurable conditioning effect was observed, however, when moisture was present.

In a particular experiment the moisture level in the oven was maintained at approximately 10% by volume, and the corona current was held at 50 μ A with an electrode spacing of 5 cm. Air, loaded with approximately 4.3 g/m³ redispersed fly ash, was blown into the interelectrode space at a rate of 1.2 l/min. The experiment was run for 20 min. with a mixture of two parts SO₂ to one part O₂ injected at the corona discharge electrode at a rate of 0.02 ml/min. No change in electrical behavior was observed. The I-V characteristic measured at the end of the experimental run is presented in Figure A-2. A total of 103 mg of fly ash was precipitated during this run.

The experiment was repeated, starting with a clean plate, but without injection of gas at the corona electrode. After operating for 20 min. the I-V characteristic was measured, and the precipitated dust was weighed. The

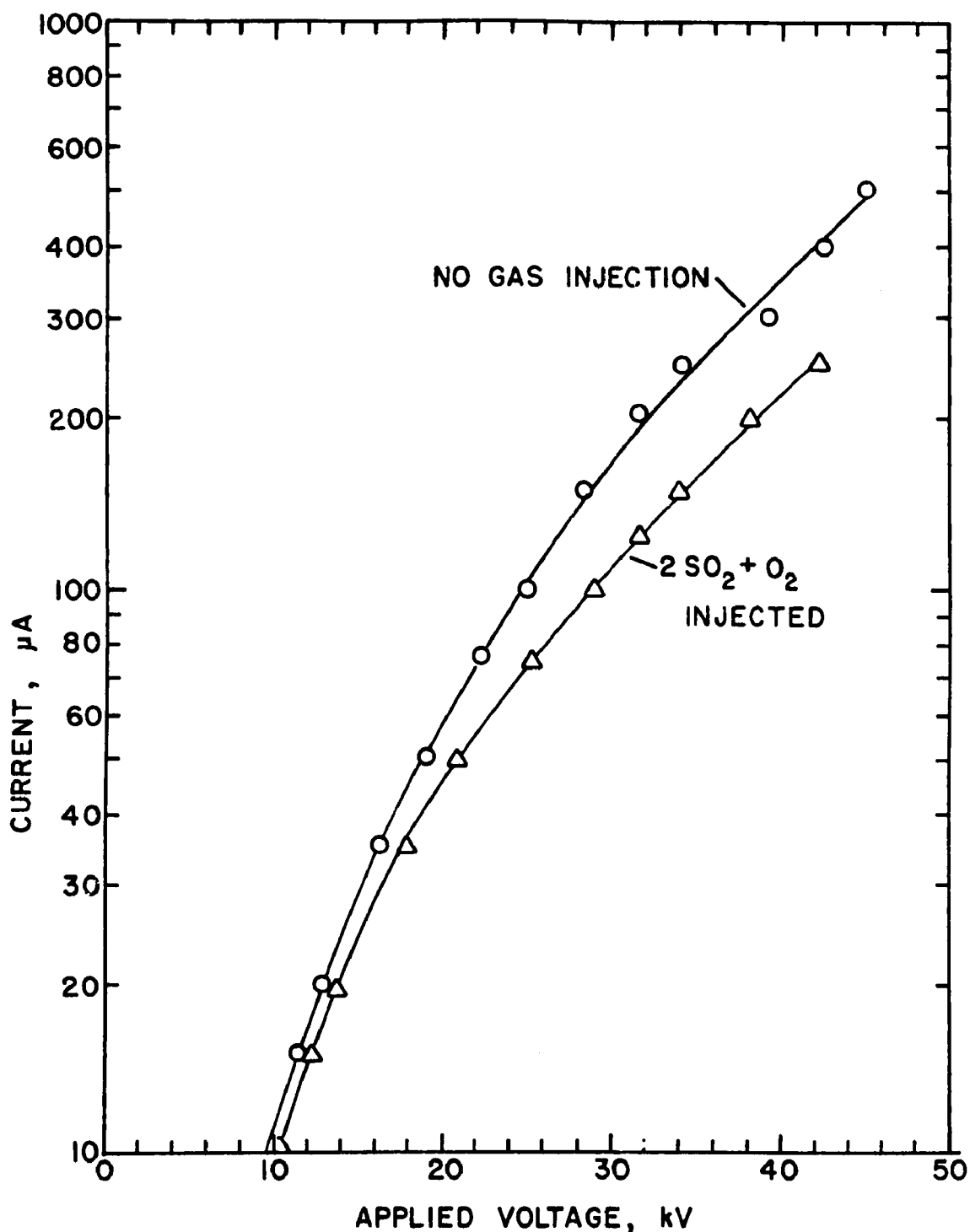


Figure A-2. Comparison of I-V characteristics of a point-plate electrode system under two conditions with high resistivity ash deposited on the plate electrode. For the lower curve a mixture of SO₂ and O₂ is injected into the corona region. The upper curve represents the case for no gas injection. The higher current in the latter case is taken to be a result of back corona.

I-V characteristic, shown in Figure A-2 displays substantially higher current values than the curve representing the experiment with gas injection. The mass of fly ash precipitated in the experiment without gas injection was 79 mg.

In this experiment it has been demonstrated that at least some conditioning against back corona can be accomplished by injecting SO_2 and O_2 into the ionizing region of a corona electrode system in the presence of moisture.

Liquid Reagent Injection

Theory

It has been demonstrated that the injection of a gaseous conditioning reagent into a corona region can provide at least some control of high resistivity fly ash in an electrical corona system. There is, however, a fundamental limitation on the rate at which a reagent in the gaseous state can be delivered to the passive electrode. That limitation is based on the fact that no more than one ionized molecule of the conditioning agent can be delivered to the passive electrode for each elementary unit of charge in the corona current. If, on the other hand, a liquid were injected into the corona region the formation of fine charged droplets might be expected to provide a greater quantity of conditioning reagent at the passive electrode.

The formation of fine, charged liquid droplets in an electrical corona has been termed electrohydrodynamic spraying. Investigation of the phenomenon with regard to various applications has led to an explanation of the mechanisms for droplet formation. Melcher and Sachar⁵ have presented a discussion of the phenomenon, summarized in the following paragraphs:

Consider a simple system consisting of a tube with small bore diameter through which a liquid may be passed at a slow flowrate, opposite a conducting plate electrode. A voltage is imposed between the tube and plate electrodes. At low voltages, large drops are formed at the end of the tube, as shown in Figure A-3(a). With the onset of corona, sporadic spitting from the tip of the liquid stream begins. As the field is increased the droplets become smaller, but still remain within about a factor of ten of the diameter of droplets formed with no applied field.

As the voltage is raised still further a significant change in the flow configuration occurs. Dripping and spitting cease, and a steady stream appears, which narrows to a very fine jet at the tip of the stream. Figure A-3(b) illustrates the shape of the flow configuration with a large field applied. This stream has been observed to be as small as one micrometer in diameter.

The shape of the stream with a high voltage applied may be explained in terms of the tangential component of electric field at the liquid surface, resulting from an electrical current through the stream. When electrical corona occurs, charge conservation requires an electrical current to flow through the liquid stream. The field direction in the stream is the same as the direction of current flow, hence a tangential component of the field exists

(a) NO CORONA CURRENT



(b) CURRENT DRIVEN STREAM



Figure A-3. (a) Liquid droplet formation at the tip of a tube with no corona current present, and
(b) stream formed by current passing through liquid to corona point at tip.

at the liquid surface. The presence of electrical charge at the liquid surface produces an acceleration which draws the stream out into a fine jet. It can also be shown that the polarization forces in the presence of an electrical current tend to stabilize the stream.

At the point where the stream becomes sufficiently fine, electrical breakdown occurs and the resulting corona discharge carries away the stabilizing current. The jet then breaks up into highly charged droplets which are driven by the electric field to the passive electrode. The current-driven jet is a source of both ions and charged droplets. The droplets are, generally, in the range of 1 to 50 μm diameter.

An orifice is not required to produce a spray of droplets. They may even be formed from a liquid film on a discharge electrode. Since the corona activity occurs at the air-liquid interface, clogging and deterioration of the discharge electrode may be avoided.

Experimental Work

Several different liquid reagents were used in experiments where injection at the corona discharge electrode was tested for conditioning effects on fly ash. Because some of the liquids used were electrical conductors the corona discharge electrode and the associated reagent injection system were connected to electrical ground, and the plate electrode was connected to the high voltage terminal of the corona power supply.

The reagents used in the experiments included distilled water and aqueous solutions of H_2SO_4 , NaOH , NH_4OH and Na_2CO_3 . Solution concentrations between 0.1 and 1.0 Normal were used. In all experiments the temperature of the system was maintained at 150°C .

The initial tests of conditioning effects on fly ash were done by first precipitating a quantity of ash onto the passive electrode without application of a reagent. The operating voltage was then adjusted to a level where strong back corona was evidenced by a current much greater than that which occurred with a clean plate at the same voltage. The conditioning agent was then injected through the discharge electrode at a continuous, controlled rate, and, with the corona voltage held constant, the current was monitored. A decrease in current at a fixed voltage is interpreted as a decrease in back corona current.

Solutions of H_2SO_4 more than 0.5 N produced detectable reduction of corona current when applied at the rate of 0.04 ml/min for several minutes. A 0.1 N solution required approximately 30 min. to produce a similar effect at the same flowrate. The total amount of dust treated in these tests was 50-100 mg. Desiccated air was circulated through the oven during the experiments.

Corrosive effects of H_2SO_4 were noted on both electrodes following experimental runs. Formation of a residue at the end of the discharge electrode tended to cause clogging, and the surface of the passive electrode was etched. Lining the discharge electrode with teflon tubing prevented the clogging, but the problem of erosion at the passive electrode remains.

Solutions of NaOH and NH₄OH, in concentrations of 0.3 to 1.0 N produced conditioning effects similar to those observed with H₂SO₄, but with much less corrosive effect.

Experiments run with H₂O and a 1.0 N solution of NaCl produced no conditioning effect. In the latter test back corona became more pronounced as salt crystals formed in the passive electrode. These tests confirmed that the mere presence of water or an electrically conductive solution is not sufficient to produce the desired reduction of back corona.

Further experiments were done using dust injection at a continuous flow-rate. An elutriator operated by air from a continuous supply served as the source of particulate matter. A settling chamber in the line between the source and the oven removed most of the larger particles. At an air supply rate of 1.2 l/min the system supplied approximately 5 g/m³ of redispersed fly ash. Microscopic examination showed few particles greater than 5 μm in diameter.

Using 0.5 N H₂SO₄ injected at 0.04 ml/min back corona was controlled throughout a 60 min. test. I-V characteristics taken at the conclusion of the experiment were similar to the clean plate characteristic, but with a reduced sparkover voltage. Solutions of less than 0.5 N H₂SO₄ were not successful in preventing back corona in similar tests. With a 0.1 N solution back corona began within 5 min. after dust injection was started.

A 0.3 N solution of NH₄OH also reduced the effects of back corona in tests similar to those run with H₂SO₄. The I-V characteristic was nearly the same as the clean plate characteristic except for a reduction in sparkover voltage.

The general result of these experiments indicates that a conditioning procedure based on injection of reagents at the corona discharge electrode may be feasible as a method for controlling back corona in a precharger system.

HEATED PASSIVE ELECTRODE

In general, the resistivity of fly ash increases as temperature rises up to a maximum resistivity value. Further increases in temperature result in decreased resistivity.

Experiments done by White⁹ indicate that good particle charging performance can be accomplished by maintaining the ground electrode temperature near 300°C. The principal difficulty with this method is the requirement for a large amount of energy to heat the ground electrodes. White reports a value of about 4000 to 6000 joule/m³ of flue gas treated (2 to 3 kW/1000 cfm).

The amount of heat required to maintain an electrode at a given temperature depends principally upon the heat losses to the flue gas blowing past the electrode. Intuitively, it is clear that the electrode surface area in contact with the flue gas should be made as small as practicable in order to minimize heat losses. If the surface of the passive electrode is made too

small, however, the field adjacent to the electrode may become strong enough to support a corona discharge.

Let us consider, for example, a corona system consisting of parallel rods and wires with axes perpendicular to the direction of gas flow. The wires serve as corona discharge electrodes and the rods are at electrical ground. The rate at which energy must be supplied to the rod electrodes in order to maintain them at a given temperature above that of the flue gas may be estimated by calculating the rate of heat transfer from a rod to the gas. The radiative losses are small in comparison with conductive losses.

The heat transfer problem is treated in the standard texts.⁴ First, computing the Reynolds number associated with rod diameter D and gas velocity V , we have

$$R = \frac{DV}{\nu}$$

where ν is the kinematic viscosity. The rate of heat transfer per unit area, q'/A , from a rod at temperature T_r into a gas having temperature T is

$$\frac{q'}{A} = \frac{Ck}{D} R^n (T_r - T),$$

where k is the thermal conductivity of the gas, and C and n are empirical parameters depending upon the numerical value of R . Since $A = \pi D l$ for a rod of circular cross section, we can express the heat transfer per unit length of the rod as

$$\frac{q'}{l} = \pi C k R^n (T_r - T)$$

or

$$\frac{q'}{l} = \pi C k \left(\frac{DV}{\nu} \right)^n (T_r - T).$$

Now, using a temperature of 300°C at the surface of the rod, the thermal conductivity of the air is 4.5×10^{-2} joule/sec m°C, and the gas viscosity is approximately 5.4×10^{-5} m²/sec. For a gas velocity of 3 m/sec and rod diameter between 0.1 and 6 cm we may use $C = 0.615$ and $n = 0.466$. Inserting these values into the above equation yields

$$\frac{q'}{l} = 14.2 (T_r - T) D^{0.466}$$

In a practical device the surface of the grounded electrodes might be required to be 150°C or more hotter than the flue gas temperature. In order to provide sufficient passive electrode surface area to maintain a reasonable ion current without developing a corona discharge at the ground electrode, the cylinder

diameters must be several times greater than the corona wire diameter. It is unlikely that a cylindrical ground electrode less than about 1.5 cm in diameter would be useful. The required rate of energy input to maintain the ground electrode at approximately 300°C in the presence of a flue gas at 150°C would thus be above 300 watts per meter of electrode length.

If a wire-cylinder separation of 10 cm is used the total gas flow U in the space between a cylinder one meter long and the adjacent pair of corona wires at a velocity of 3 m/sec is

$$U = 2 \times 0.1 \text{ m} \times 1 \text{ m} \times 3 \text{ m/sec}$$

or

$$U = 0.6 \text{ m}^3/\text{sec}.$$

This flowrate is equivalent to about 1270 cfm. Dividing the power input per unit length of electrode by the gas volume flowrate we obtain a value of 500 joule/m³ (or approximately 240 watts/1000 cfm). The calculated value is about one tenth of the power input requirements indicated by White.⁹ These calculations, however, are based upon a minimal temperature differential between gas and electrode, and surface area of the electrode has been taken to be quite small. The calculated value thus represents an extreme lower bound to energy requirements for heating the passive electrode. It is thus concluded that probable energy expenditures are too great to make the technique feasible.

OTHER TECHNIQUES

Among the other approaches considered for control of back corona effects were the use of porous collection electrodes, semiconductor coatings on collection electrodes, and wet-wall methods. These methods were generally considered to provide a low probability of success because of associated technical complications.

Porous electrodes made of sintered metal or similar material could provide a means for delivering chemical conditioning agents into a deposited dust layer. Such chemicals, in gaseous or liquid form, would be forced through the porous plate into the collected high resistivity material. Problems with this concept include probable clogging of the porous plates and reduced strength of the collecting electrodes.

The use of a semiconductor layer might provide a ballasting mechanism to distribute current density more evenly in the presence of incipient breakdown of a high resistivity dust layer. It is likely, however, that the semiconductor layer would degrade quickly in the harsh flue-gas environment. This technique would also be very expensive in comparison with others considered.

Wet-wall methods offer a high probability of success in a precharger. There are, however, some undesirable aspects of such an approach. The liquid must be well dispersed over the collecting surfaces, leaving no dry areas.

Depending on the characteristics of the dust, concrete-like deposits might occur due to the additional moisture concentration in the precharger. For these reasons further consideration of wet-wall techniques were set aside against the eventuality that no more practicable methods could be found.

SUMMARY

The search for a practical method for controlling the effects of back corona in the presence of a large ion current density and high resistivity dust included a search of the literature, theoretical studies and small scale laboratory investigations. The most promising techniques evaluated included the following:

- A. Chemical conditioning
 - 1. Injection of chemicals into the active ionization region.
 - 2. Injection of chemicals through porous collection electrodes.
- B. Electrical methods
 - 1. Use of a screen electrode to remove ions resulting from back corona
 - 2. Application of ballasting by means of a semiconductor layer on collecting electrodes
- C. Wet-wall techniques
- D. Heated collecting electrodes

Each of these approaches was considered with regard to effectiveness in controlling back corona, technical feasibility and cost. As a result of these studies the method involving the use of a screen electrode (described fully in the text of this report) was developed. The other concepts are not considered valueless, however. It is possible that, for certain applications, one or more of these techniques may be worthy of further study.

APPENDIX B

THEORETICAL STUDY OF SPACE CHARGE EFFECTS

The electrical conduction properties of a corona discharge system depend very strongly upon the distribution of charge in the interelectrode space. The principal current carriers are ions derived from the gas molecules in the conducting region. If the corona discharge electrode is negative with respect to the passive electrode, a free electron contribution to the conduction process also exists. Because the electrical mobility of the ions and free electrons is very large and the electrical field strength is, generally, very high in a corona system, the effects of macroscopic motions of the gas can be ignored in determining ionic drift velocities.

When suspended particles are present in a corona system they become charged by ion attachment in accordance with well-known principles. If the number density of the particles in the interelectrode region is large the charge on the particles can make a significant contribution to the overall charge distribution. In contrast with the ions, however, the drift, or migration velocities of the particles, due to the forces exerted by the electric field, are ordinarily much smaller than the velocities associated with the motion of the gas. The motion, and hence the spatial distribution of particulate matter in an electrostatic precipitator is, therefore, strongly dominated by the presence of any turbulent motion of the gas. This conclusion is supported by empirical studies which show that the concentration of dust in an ESP decreases exponentially along the path of the gas flow through the system, as expressed by models of the form of the Deutsch equation.

An effect of gas turbulence in an ESP is to produce a constant mixing of the aerosol, which tends to promote a homogeneity in the spatial distribution of the particles. Statistically, the charging conditions for the particles may be taken to be uniform. Thus, to the extent that complete and continuous mixing of the aerosol can be assumed, the space charge associated with the charged particles can be considered to be uniform along a cross-section of an ESP. The overall charge distribution in the interelectrode region therefore consists of a superposition of the mobile ion charge distribution on the relatively fixed and nearly uniform (in a given cross-section) charge distribution associated with the particles.

PARTICULATE SPACE CHARGE CALCULATION

Given a particle size distribution and a set of physical conditions for charging, a calculation can be made to yield the ratio of charge to mass for a polydisperse aerosol. Let $T(a)$ be the probability amplitude of the distribution as a function of particle radius a , and let $q(a)$ be the charge per

particle of radius a , for given values of electric field strength, ion density, residence time, ion mobility, gas temperature and particle dielectric constant. The ratio of charge to mass for the aerosol is

$$Q/M = \frac{\int_0^{\infty} q(a)T(a)da}{\int_0^{\infty} \frac{4}{3}\pi a^3 \rho T(a)da} \quad , \quad (B-1)$$

where ρ is the mass density of the particles. Multiplying the ratio Q/M by the mass loading yields the space charge density due to the charged particles.

Equation B-1 cannot generally be evaluated in closed form, but will require the application of numerical integration techniques. The function $T(a)$ may itself be difficult to express algebraically for an actual aerosol. However, in order to demonstrate the application of Equation B-1 to find reasonable space charge characteristics, we will evaluate Equation B-1 for several log-normal particle size distributions, defined by

$$T(a) = \frac{1}{\sqrt{2\pi}\log\sigma_g} \exp \left[-\frac{1}{2} \left(\frac{\log a/a_{gN}}{\log\sigma_g} \right)^2 \right] \quad (B-2)$$

where a_{gN} is the geometric mean of the numerical distribution and σ_g is the geometric standard deviation. In those cases where the mass median radius a_{gm} is specified, a_{gN} is derived from

$$\log a_{gN} = \log a_{gm} - 6.908 \log^2 \sigma_g \quad . \quad (B-3)$$

There is a number of charging theories available for prediction of $q(a)$. A fair approximation is the sum of the classical field charging and diffusion charging expressions:

$$q_F(a) = \left(1 + 2 \frac{K-1}{K+2} \right) \frac{Ea^2}{4} \left(\frac{\pi N t e \mu}{1 + \pi N t e \mu} \right) \quad (B-4)$$

and

$$q_D(a) = \frac{akT}{2e} \ln \left(\frac{1 + \bar{v}\pi e^2 N t}{2kT} \right) \quad (B-5)$$

respectively, where

- e = electron charge
- E = electric field strength
- k = dielectric constant of the particulate material
- K = Boltzmann's constant
- N = number density of the ions
- t = residence time of the particles
- T = absolute temperature
- \bar{v} = mean molecular velocity
- μ = ion mobility.

Now, using $q(a) = q_F(a) + q_D(a)$ along with Equation B-2, we can evaluate the overall particulate space charge defined by Equation B-1. This has been done for several examples, using an HP-65 calculator to carry out the calculation. (HP-65 program listed at the end of this appendix.)

Figure B-1 shows values of Q/M calculated as a function of σ_g for four different values of mass median diameter. For all of the curves shown in Figure B-1 the electric field strength was taken to be $4 \times 10^5 \text{ V/m}$, the ion density-residence time product (Nt) was set at $1.0 \times 10^{13} \text{ sec/m}^3$, the ion mobility was $1.8 \times 10^{-4} \text{ m}^2/\text{Vsec}$, absolute temperature was 295K and the mean molecular velocity was 500 m/sec. The particles were assumed to have a relative dielectric constant of 5 and density of 2.25 g/cm^3 . As the distribution broadens from monodispersity ($\sigma_g = 1$) there is a monotonic increase in Q/M . The significance of the shape of a particle size distribution can be illustrated by the observation that the value of Q/M for a particle distribution with mass median diameter of $20 \mu\text{m}$ and $\sigma_g = 3$ is approximately the same as that of a monodisperse aerosol consisting of $5 \mu\text{m}$ diameter particles.

In Figure B-2 the ratio of charge to mass is plotted as a function of mass median diameter for log-normal distributions of particles. Five values of σ_g were used in the calculations.

EFFECTS OF PARTICULATE SPACE CHARGE IN AN ESP

The number density N of the ions in the interelectrode region of a corona system can be calculated in terms of the current density j , the electric field strength, and the ion mobility as follows:

$$N = \frac{j}{e\mu E} \quad (\text{B-6})$$

Because the drift velocity of the particles is much smaller than that of the ions the charged particle contribution to j can almost invariably be ignored, even though the space charge associated with the charged particles may be a substantial part of the overall charge distribution.

In order to compare the ion number density with the particulate space charge, we shall define the quantities ξ_i and ξ_p as the charge per unit volume in the conducting region due to ions and particles respectively. For singly-charged ions

$$\begin{aligned} \xi_i &= Ne \\ \text{or} \quad \xi_i &= \frac{j}{\mu E} \end{aligned} \quad (\text{B-7})$$

The value of ξ_p is the product of Q/M by the total mass of particulate material L per unit volume of aerosol,

$$\xi_p = \frac{Q}{M} L \quad (\text{B-8})$$

By way of example, let us consider a full-scale ESP operating at an average current density of $1.2 \times 10^{-3} \text{ A/m}^2$, and an electric field strength of $4 \times 10^5 \text{ V/m}$.

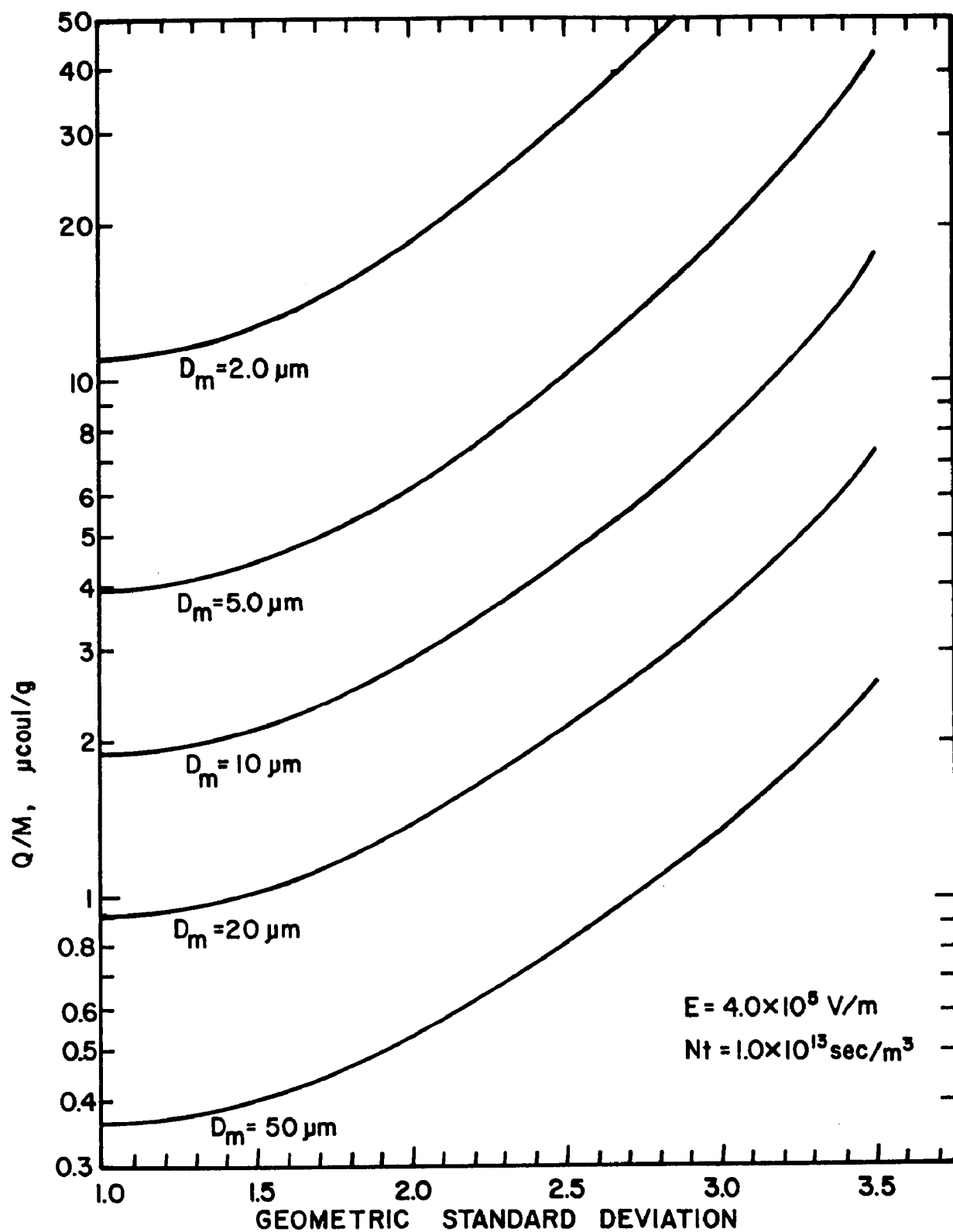


Figure B-1. Overall ratio of charge to mass for log-normal distributions of particles as a function of geometric standard deviation. All charging parameters were kept the same for all calculations. (D_m is mass medial diameter.)

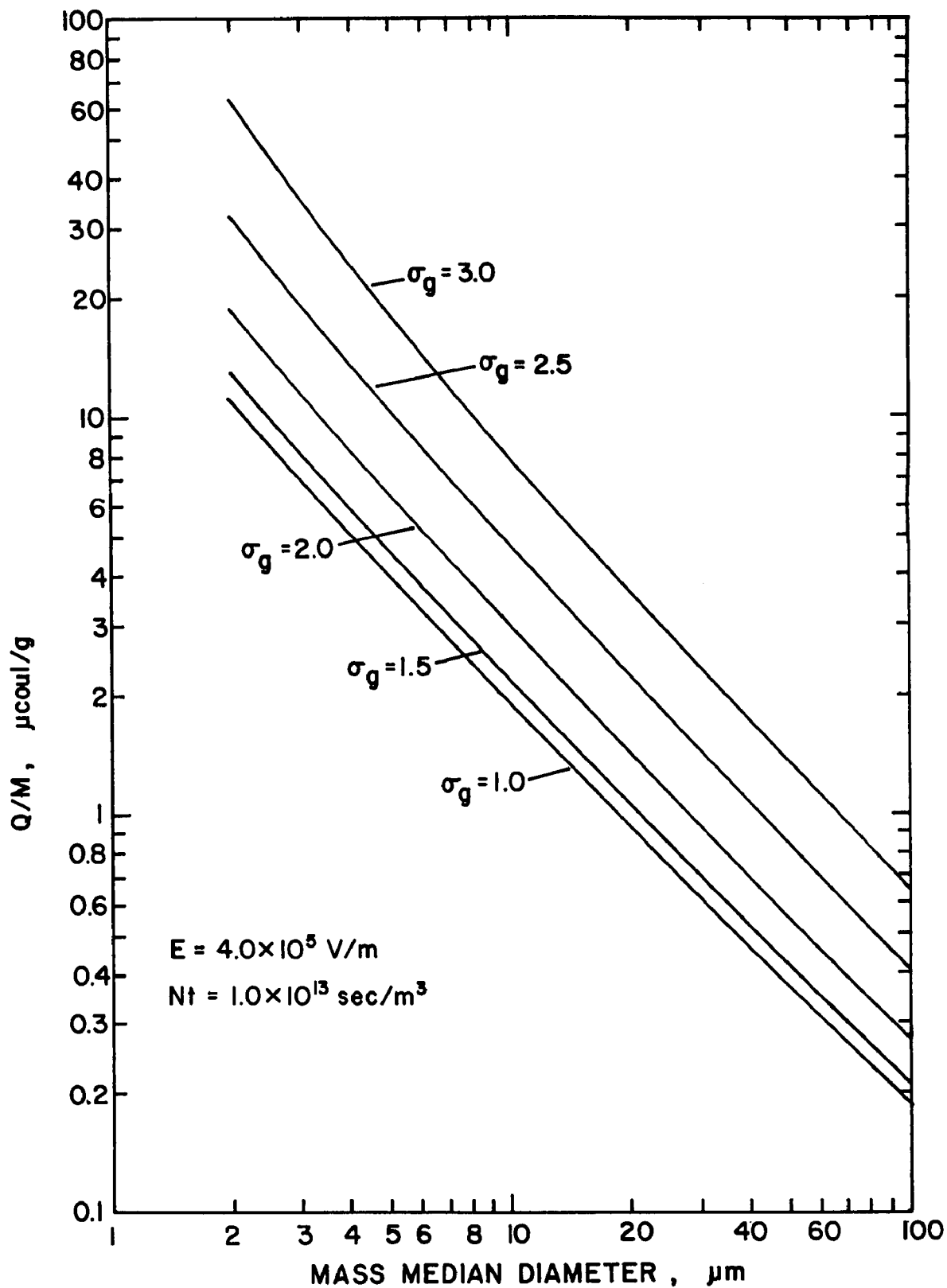


Figure B-2. Overall ratio of charge to mass for log-normal distributions of particles as a function of mass median diameter. All charging parameters were kept the same for all calculations.

Using a value of $1.8 \times 10^{-4} \text{ m}^2/\text{Vsec}$ for the ion mobility, we obtain from Equation B-7 an ionic charge density of $1.33 \times 10^{-5} \text{ C/m}^3$. These electrical quantities are consistent with those used for calculated values of particulate charge in Figures B-1 and B-2.

Suppose the aerosol passing through the ESP had a dust burden of 3 g/m^3 with mass median diameter of $10 \text{ }\mu\text{m}$ and $\sigma_g = 2.5$. Using Equation B-8 and reading $Q/m = 4.6 \times 10^{-6} \text{ C/g}$ from Figure B-1, we find that the space charge per unit volume due to the charged particles is $1.38 \times 10^{-5} \text{ C/m}^3$, or just slightly larger than the ionic space charge density.

In attempts to predict the behavior of an ESP on a theoretical basis a proper accounting of the space charge effects has proven difficult. One approach is to use an "effective mobility" derived by taking the measured current to be a sum of ion and particulate contributions. The effective mobility is then used in the computation of voltage-current relationships. This approach is based on the assumption that the motion of the particles depends principally upon the electrical forces, while ignoring the gas turbulence effects.

In the opposite extreme case the contribution to the measured current due to the presence of charged particles can be ignored. The space charge may then be calculated directly from the particle charging theory for a given or assumed particle size distribution. If the resulting particulate space charge is significant the electric field strength may have to be recalculated. Since the charging conditions depend upon the space charge, and vice versa, a self-consistent solution must ultimately be sought.

HP-65 PROGRAM: Q/M FOR LOG-NORMAL DISTRIBUTION OF PARTICLES

In order to determine the overall ratio of charge to mass in a log-normal distribution of particles, given the total particulate mass per unit volume of aerosol, the geometric mean radius a_0 , the geometric standard deviation σ_g , and the charging conditions as defined for Equations B-4 and B-5, a numerical integration scheme is applied. The particle distribution is divided into logarithmic increments, each defined by limits a_j and βa_j , where $\beta > 1$. The charge per particle is then computed for the midpoint in each increment ($a_j^* = \sqrt{\beta} a_j$) by

$$q_j = e\pi a_j^* C_1 \left\{ \frac{\mu a^* N t E}{\mu N t + C_1} \left[1 + 2 \left(\frac{K-1}{K+2} \right) \right] + C_2 T \ln \left[\frac{a_j^* \mu N t}{C_1 C_2} + 1 \right] \right\},$$

in accordance with Equations B-4 and B-5 (MKS units), where $C_1 = 4\epsilon_0/e$ and $C_2 = k/e$.

Now, the number of particles in increment j is

$$N_j = \gamma(a_j^*)(\beta-1),$$

where (a_j^*) is the amplitude of the distribution,

$$\gamma(a_j^*)^{-1} = \sqrt{2\pi} \log \sigma_g \exp \left[-\frac{(\log a_j^*/a_0)^2}{2(\log \sigma_g)^2} \right].$$

Thus, we have for the total contribution to the charge resulting from particles in the j increment,

$$Q_j = q_j (a_j^*) (\beta - 1)$$

The resulting values of Q_j are summed, as are the contributions to mass from each increment, and a ratio of the sums over the entire distribution is taken.

User Instructions

Part A

STEP	INSTRUCTIONS	INPUT DATA/UNITS	KEYS	OUTPUT DATA/UNITS
1	Enter dielectric constant	K	<input type="text" value="A"/> <input type="text"/>	
2	Enter ion density-time	Nt(sec/m ³)	<input type="text" value="R/S"/> <input type="text"/>	
3	Enter ion mobility	μ (m ² /V-sec)	<input type="text" value="R/S"/> <input type="text"/>	
4	Enter electric field strength	E(V/m)	<input type="text" value="R/S"/> <input type="text"/>	
5	Enter temperature	T(K)	<input type="text"/> <input type="text"/>	
6	Enter mean molecular speed	v(m/sec)	<input type="text"/> <input type="text"/>	
7	Enter mean particle radius	\bar{a} (m)	<input type="text"/> <input type="text"/>	
8	Enter geo. standard deviation	σ_g	<input type="text"/> <input type="text"/>	
9	Read in Part B	new card	<input type="text"/> <input type="text"/>	

Part B

STEP	INSTRUCTIONS	INPUT DATA/UNITS	KEYS	OUTPUT DATA/UNITS
1	Read in Program B		<input type="text" value="A"/> <input type="text"/>	
2	Go to Part C		<input type="text"/> <input type="text"/>	

Part C

STEP	INSTRUCTIONS	INPUT DATA/UNITS	KEYS	OUTPUT DATA/UNITS
1	Enter particle density	ρ (kg/m ³)	<input type="text" value="A"/> <input type="text"/>	
2	Read Q/M		<input type="text"/> <input type="text"/>	Q/M (Coul/kg)

Program Listing

Part A

CODE	KEYS
23	LBL
11	A
41	ENT
41	ENT
01	1
51	-
35 07	$g, x \Rightarrow y$
02	2
61	+
81	\div
02	2
71	x
01	1
61	+
33 01	STO 1
02	2
83	.
02	2
01	1
00	0
07	7
43	EEX
08	8
33	STO
09	9
33	STO
71	x
01	1
08	8
83	.
06	6
01	1
07	7
43	EEX

CODE	KEYS
42	CHS
05	5
33 08	STO 8
84	R/S
33 07	STO 7
84	R/S
71	x
41	ENT
41	ENT
81	R/S
71	x
35 07	$g, x \Rightarrow y$
34	RCL
09	9
61	+
81	\div
33	STO
71	x
01	1
35	θ
02	π
33	STO
71	x
01	1
01	1
83	.
06	6
00	0
02	2
42	EEX
42	CHS
01	1
09	9

CODE	KEYS
33	STO
71	x
01	1
35	θ
02	π
71	x
34 08	RCL 8
71	x
34	RCL
09	9
71	x
84	R/X
33 06	STO 6
71	x
33 02	STO 2
34 07	RCL 7
34 06	RCL 6
81	\div
34 08	RCL 8
81	\div
34	RCL
09	9
81	\div
84	R/S
71	x
33 03	STO 3
00	0
33 08	STO 8
84	R/S
33 05	STO 5
35 08	$g \downarrow$
33 06	STO 6
24	RTN

Part B

CODE	KEYS
23	LBL
11	A
00	0
33	STO
09	9
33 08	STO 8
33 07	STO 7
34 05	RCL 5
03	3
42	CHS
35	g
05	y ^x
34 06	RCL 6
71	x
33 04	STO 4
23	LBL
12	B
34 04	RCL 4
34 05	RCL 5
83	.
01	1
35	g
05	y ^x
71	x
33 04	STO 4
34 06	RCL 6
81	$\frac{\div}{\cdot}$
31	f
08	log
34 05	RCL 5
31	f
08	log
81	$\frac{\div}{\cdot}$
41	ENT

CODE	KEYS
71	x
02	2
81	$\frac{\div}{\cdot}$
42	CHS
32	f ⁻¹
07	ln
34 05	RCL 5
31	f
08	log
81	$\frac{\div}{\cdot}$
41	ENT
34 05	RCL 5
83	.
01	01
35	g
05	y ^x
01	1
51	-
71	x
41	ENT
41	ENT
34 04	RCL 4
03	3
35	g
05	y ^x
71	x
33	STO
61	+
08	8
35 08	g, R ⁺
41	ENT
34 04	RCL 4
34 03	RCL 3

CODE	KEYS
71	x
01	1
61	+
31	f
07	ln
34 04	RCL 4
71	x
34 02	RCL 2
71	x
34 04	RCL 4
41	ENT
71	x
34 01	RCL 1
71	x
61	+
71	x
33	STO
61	+
07	7
34 05	RCL 5
03	3
35	g
05	y ^x
34 06	RCL 6
71	x
34 04	RCL 4
35 22	g,x \Rightarrow y
12	B
35 01	g, NOP
24	RTN

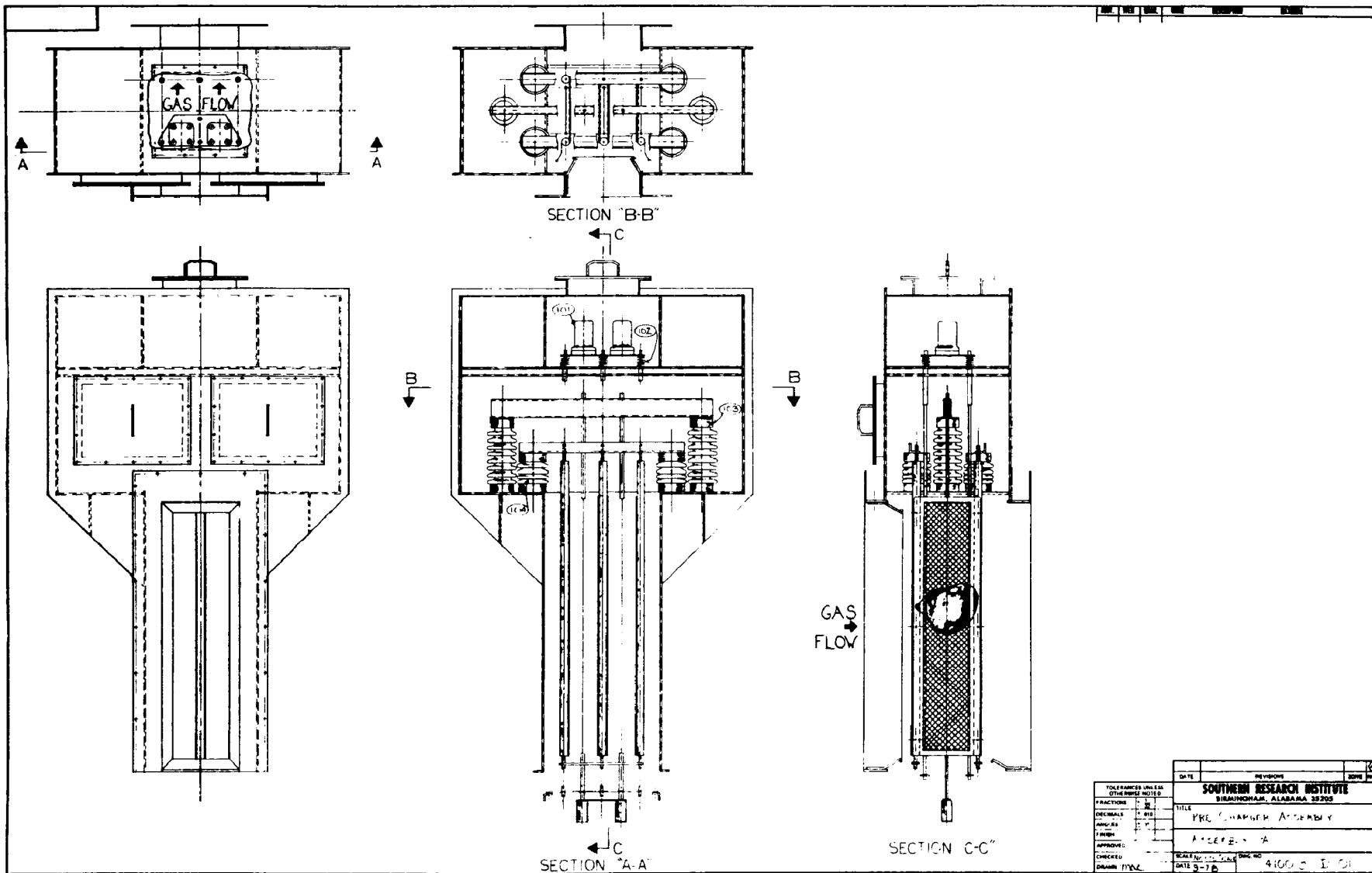
Part C

CODE	KEYS
23	LBL
11	A
41	ENT
35	π
02	π
71	x
04	4
71	x
03	3
81	\div
34 08	RCL 8
71	x
35	π
04	1/x
34 07	RCL 7
71	x
24	RTN

APPENDIX C

PRECHARGER

C-2



SECTION "D" (NO SCALE)

SECTION "B-B"

DETAIL "C"

DETAIL "D"

SECTION "A-A"

GENERAL NOTES

1. ALL MATERIAL SHALL BE 11 GAGE METAL SHEET, UNLESS NOTED.
2. ALL SHARP CORNERS, BURRS & WELD SPATTER MUST BE REMOVED.
3. TOLERANCES 6" AND BELOW ± .031" ABOVE 6" ± .063" ACCUMULATION ± .125".
4. ALL HOLES 3/16" DIA. UNLESS NOTED.
5. ALL CONNECTING FLANGES & ACCESSWAY FLANGES AS SHOWN TO BE 1 1/2" ± .125" ± .063" 11 GAGE BENT R. UNLESS NOTED.

BAFFLE 16 GAGE R.

BAFFLE 17 3/4" LONG 32" LONG BOTTOM ONLY THIS SIDE

GAS FLOW

DATE: _____

REVISIONS

SOUTHERN RESEARCH INSTITUTE
BIRMINGHAM, ALABAMA 35205

TITLE: GAS FURNACE ASSEMBLY

APPROVED: _____

CHECKED: _____

DRAWN: _____

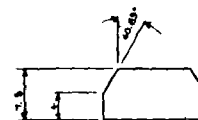
SCALE: 1/2" = 1'

DATE: 12-1-78

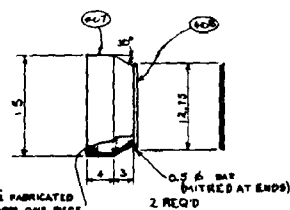
DRG NO: 410-5 D 02

	DATE	REVISIONS	ZONES
TOL FRANCES UNITS OF THE MODEL RICHES	SOUTHERN RESEARCH INSTITUTE BIRMINGHAM, ALABAMA 35202		
FRACTIONS	1	2	
DEFINITIONS	1	2	
ANALYSIS	1	2	
COMMENTS			
APPROVED	A. C. HARRIS - JCH		
CHECKED:			
DRAWN BY:	DATE: 9-7-68	ORIG NO:	410-2-D-02

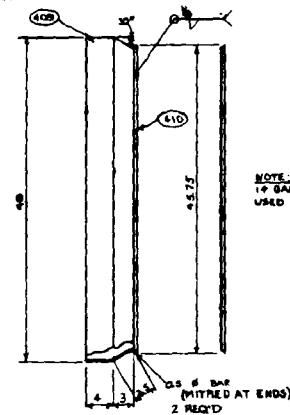
[illegible]



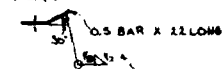
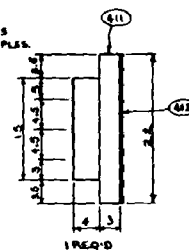
DETAIL 407:
DEVELOPED VIEW



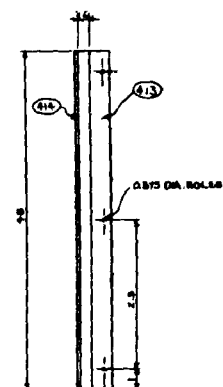
NOTE:
BAFFLE FABRICATED
TO FORM ONE PIECE
CORNER'S MITERED &
WELDED.



NOTE:
14 GAGE PLATES
USED FOR BAFFLES.

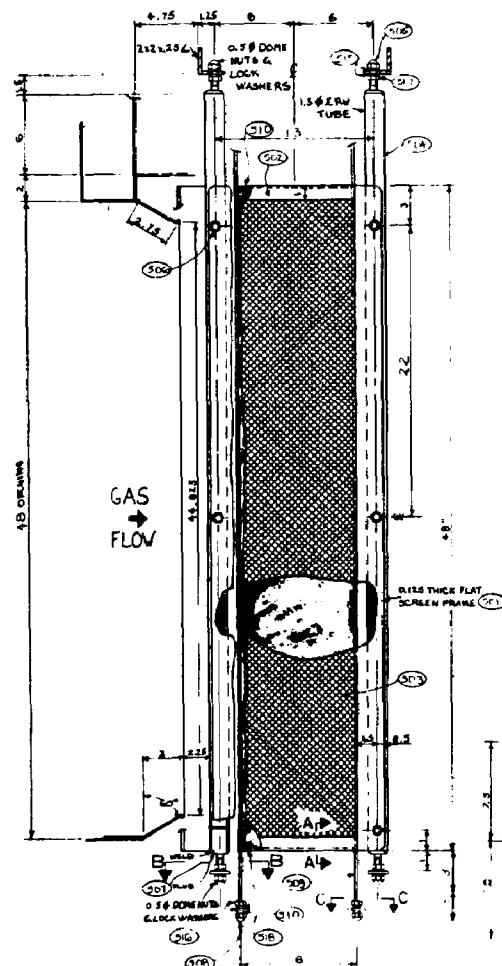


DETAIL 408:
DEVELOPED VIEW

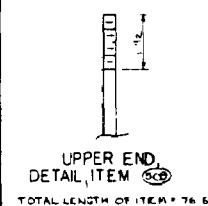
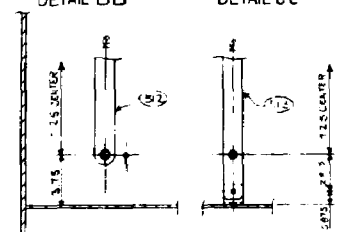
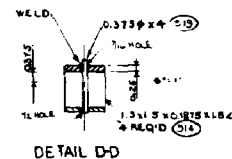
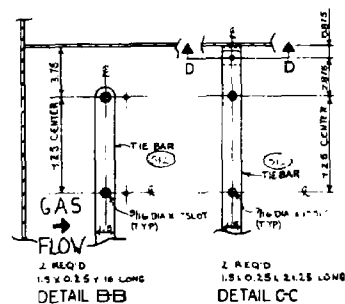


0.5 BAR X 12 LOM6
WELD
HIGHER PLATES
USED FOR BAFFLES
2 REQ'D

DATE	REVISION	BY	CHK
SOUTHERN RESEARCH INSTITUTE			
DURHAM, ALABAMA 35894			
TITLE			
PRE-CHARGER			
SUBJECT			
BAFFLES & HOPPER DETAILS			
PROJECT			
SCALE 1/2" = 1'			
DRAWING NO. 4100-31-D-04			

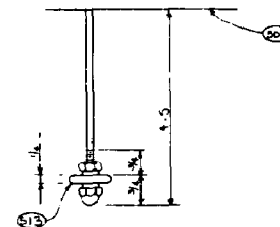


ELEVATION: SCREENS AND TUBES



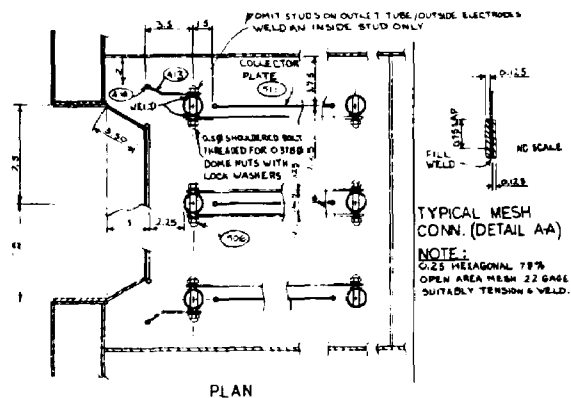
NOTES:

- ALL NUTS ON VIBRATED COMPONENTS (E.G. COLLECTORS) MUST BE TACK WELDED TO ADJACENT PART ON FINAL ASSEMBLY
- ALL SHARP CORNERS, BURRS AND WELD SPATTER MUST BE REMOVED
- TACK WELDED AND BE TACK WELDED ABOVE C AND ACCUMULATION 2.162

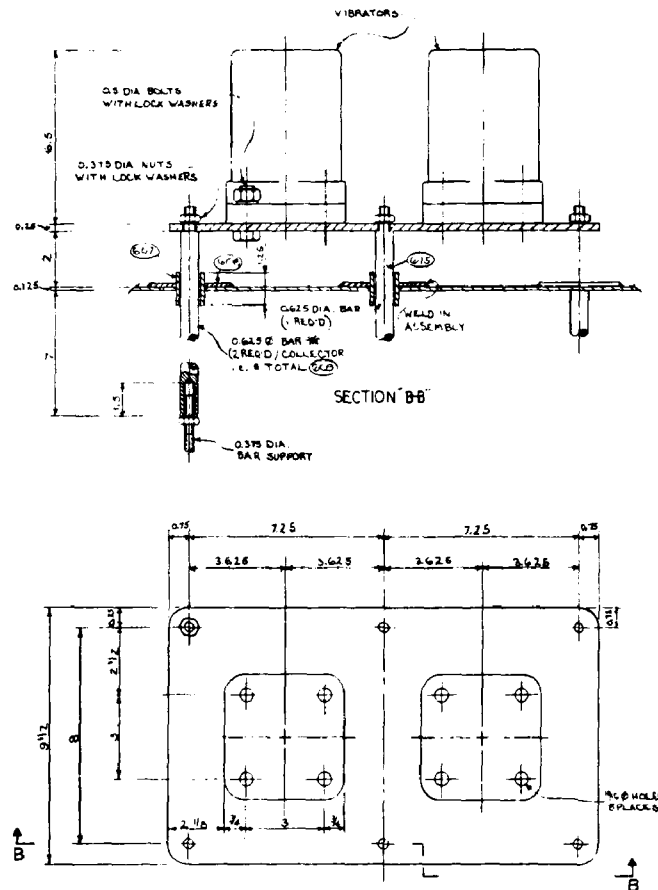
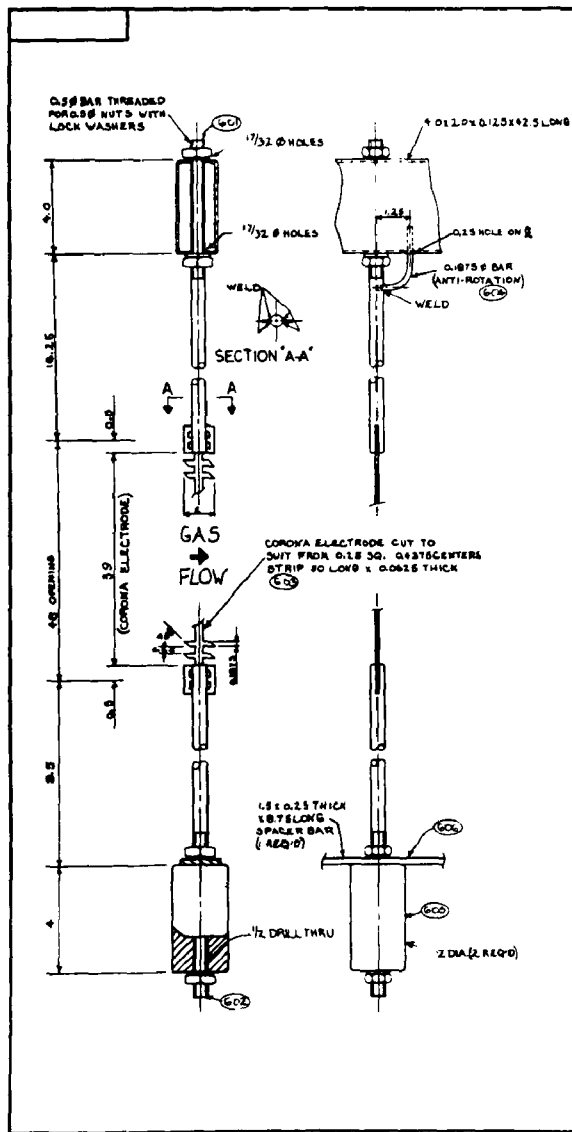


BOTTOM END, DETAIL, ITEM 125

- SLOT ITEM TO FIT IN HOSE PLATE (12)
- SLOT LENGTH = 4.8" BEGINNING 4.8" FROM BOTTOM END

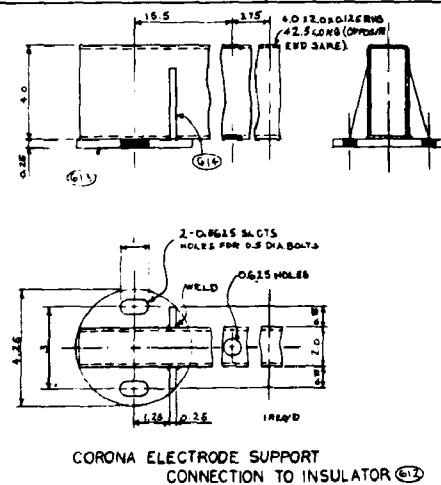
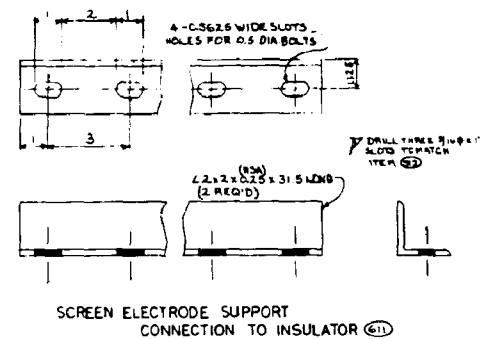


DATE	REVISION	16
SOUTHERN RESEARCH INSTITUTE BIHAMONIAH, ALABAMA 35205		
TITLE PRE-CHARGER		
SCREEN ELECTRODE SYSTEM		
DESIGNED BY FRACTIONS CHECKED BY FRACTIONS APPROVED BY FRACTIONS DATE FRACTIONS	SCALE 1/4" = 1'-0"	DATE 4-10-63



* NOTES:
SPRING ASSEMBLY SIMILAR FOR NON-VIBRATED SIDE
OF COLLECTOR WITH ARVIL REPLACED WITH
0.15 THICK CARB. PLATE(S) IS REQUIRED).

VIBRATOR PLATE



TELEPHONE UNIT OTHER NUMBER NOTED		DATE	RECEIVED	FILE
FRANCHISE <input checked="" type="checkbox"/> <input type="checkbox"/> DECEASED <input checked="" type="checkbox"/> <input type="checkbox"/> AVAILABLE <input checked="" type="checkbox"/> <input type="checkbox"/> FINGER <input type="checkbox"/> <input type="checkbox"/> APPROVED <input type="checkbox"/> <input type="checkbox"/> CHECKED <input type="checkbox"/> <input type="checkbox"/> OWNER SIGN <input type="checkbox"/> <input type="checkbox"/>		SOUTHERN RESEARCH INSTITUTE BIRMINGHAM, ALABAMA 35296 TITLE PRE-CLEARER R. L. T. DR. K. FORTS CYCLOTRON PLANT DATE 9-78 4100-31-2-06		

[illegible]

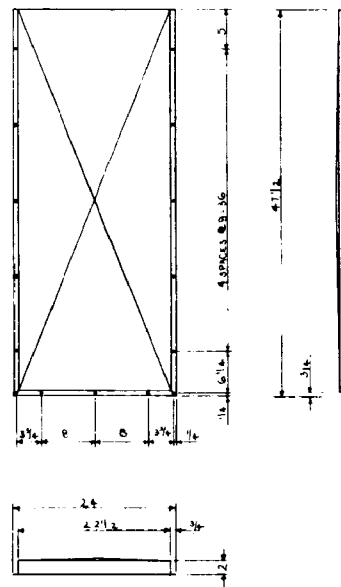
FOR TO GET DETAILS & DIMENSIONS OF SPRINGS

[illegible]

601	4	FLANGE & WALE - 12.51.77.78	3.5 - 11.00SG
602	4	FLANGE & WALE - 12.52.77.78	3.5 - 11.00SG
603	4	FLANGE & WALE - 12.51.7.78	3.5 - 11.00SG
604	4	FLANGE & WALE - 12.51.7.78	3.5 - 11.00SG
605	2	CONC FLANGE 12.51.77.78	4.2 - 10.00SG
606	4	CONC FLANGE 12.51.77.78	4.2 - 10.00SG
607	2	CONC FLANGE 12.51.77.78	3.5 - 10.00SG
608	2	BATTLE BAR - 12.51.77.78	3.5 - 10.00SG
609	2	BATTLE BAR	3.5 - 10.00SG
610	2	BATTLE BAR	3.5 - 10.00SG
611	1	BATTLE BAR - 12.52	3.5 - 10.00SG
612	1	BATTLE BAR - 12.52.77.78	3.5 - 10.00SG
613	2	BATTLE BAR (CONC) 12.51.78	3.5 - 10.00SG
614	2	BATTLE BAR - 12.51.78	3.5 - 10.00SG

IC1	2	VIBRATORS MODEL 200 SL CARVED VIBRATOR CONT.
IC2	6	AS USED IN VIBRATORS
IC3	2	INSULATED LAPP TYPE 7363351ATION PWT INHOM
IC4	4	INSULATED LAPP TYPE 7363351ATION PWT INHOM
IC5	3	COP PLATE 1/2 IN. 0.5 THT
A/R		THE VMC HEAD REPT. QNT SET 3.5.

TOLERANCES UNLESS OTHER INDICATED		DATE	REVISION	ZONE
FRACTIONS		TITLE		
DECIMALS	IN	PART CHARGER		
ANGLES	IN	ELECTRIC MATERIALS		
FINISH		SCALE	DWG. NO.	
APPROVED		DATE	3-7-72	
CHECKED		4100-31-D-07		
DRAWN	M. J.			

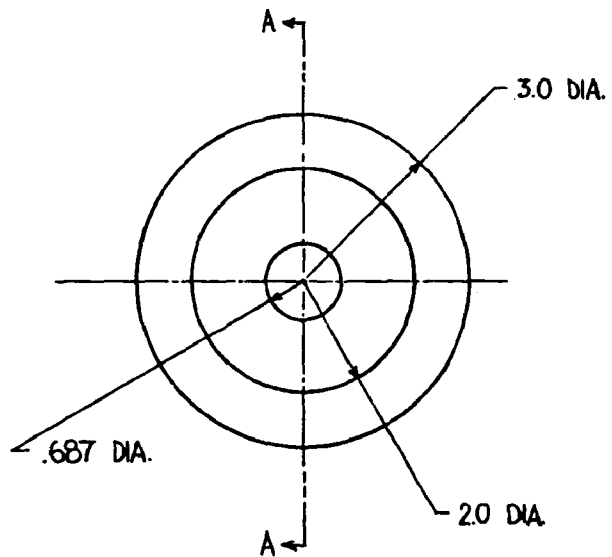


FORMING SEQUENCE

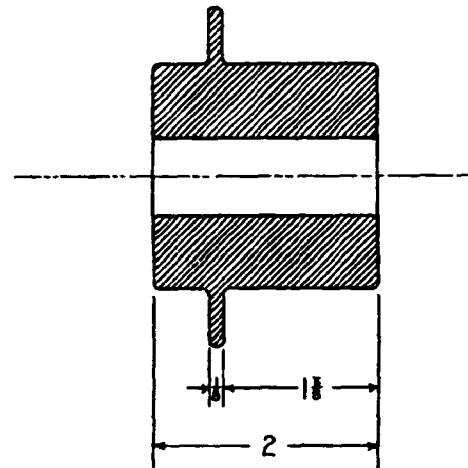
- ① DRILL $\frac{7}{16}$ " HOLES IN PLACES
- ② MAKE DIAGONAL BREAKS FOR STRENGTH
- ③ BREAK $\frac{7}{8}$ " FLANGES 30° UP.
- ④ BREAK 2 " FLANGES 90° DOWN
- ⑤ WELD CORNERS.
- ⑥ DRILL $\frac{7}{16}$ " HOLES IN CORNERS

COPIES OF THIS REPORT TO BE FORWARDED WITH ONE COPY BEING NOTED		DATE _____		REVISIONS _____		DRAWN BY _____		
FRACTIONS <input type="checkbox"/> 32		SOUTHERN RESEARCH INSTITUTE BIRMINGHAM, ALABAMA 35205						
DECIMALS <input type="checkbox"/> 010		TITLE PRE-CHARGER						
ANGLES <input type="checkbox"/> P		INSULATION COVER						
APPROVED _____		SCALE 1:10						
CHECKED _____		DATE 10-25-78						
DRAWN MAC		DWG NO. 4100-31-D-08						

C-10



ASSY.	ITEM	QTY	NAME	DESCRIPTION	MATERIAL
	1501	6	PLATE SUPPORT GUIDES	3" DIA. X 2" LONG	316 SS.



SECTION AA

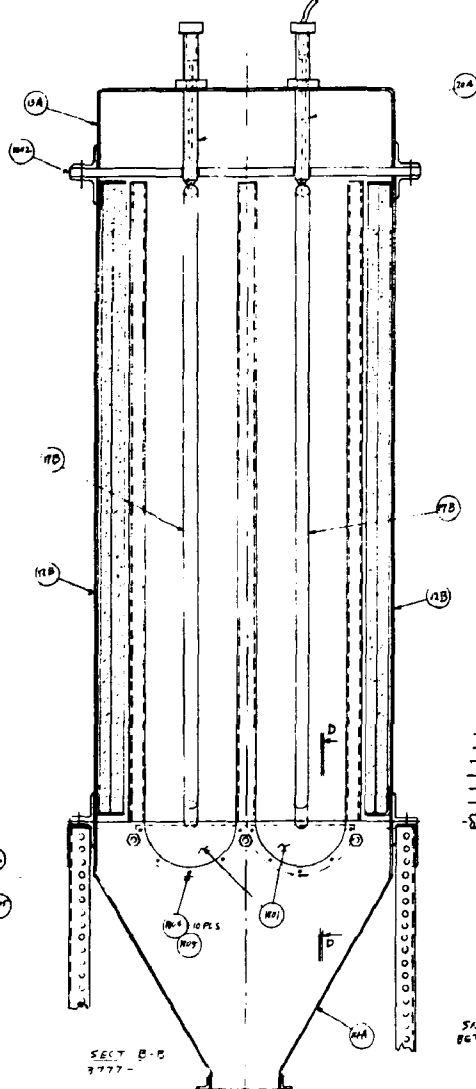
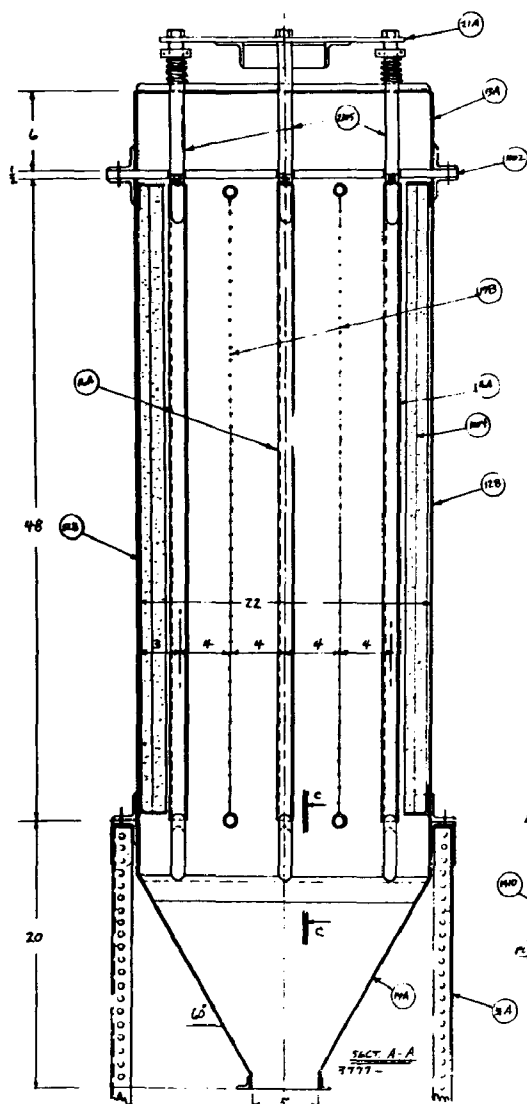
DATE		REVISIONS		ZONE	NO.
SOUTHERN RESEARCH INSTITUTE BIRMINGHAM, ALABAMA 35205					
TITLE					
PLATE SUPPORT GUIDES					
(REPLACES ITEMS 608 AND 609)					
APPROVED		SCALE FULL		DWG. NO.	
CHECKED		DATE 12-5-78		400-31 -B- 15	
DRAWN PVBUSH					

APPENDIX D

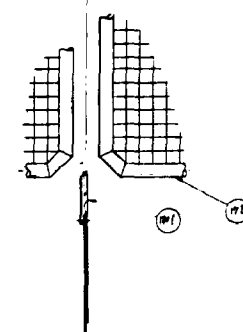
COLLECTOR

3777-D-10

D-2

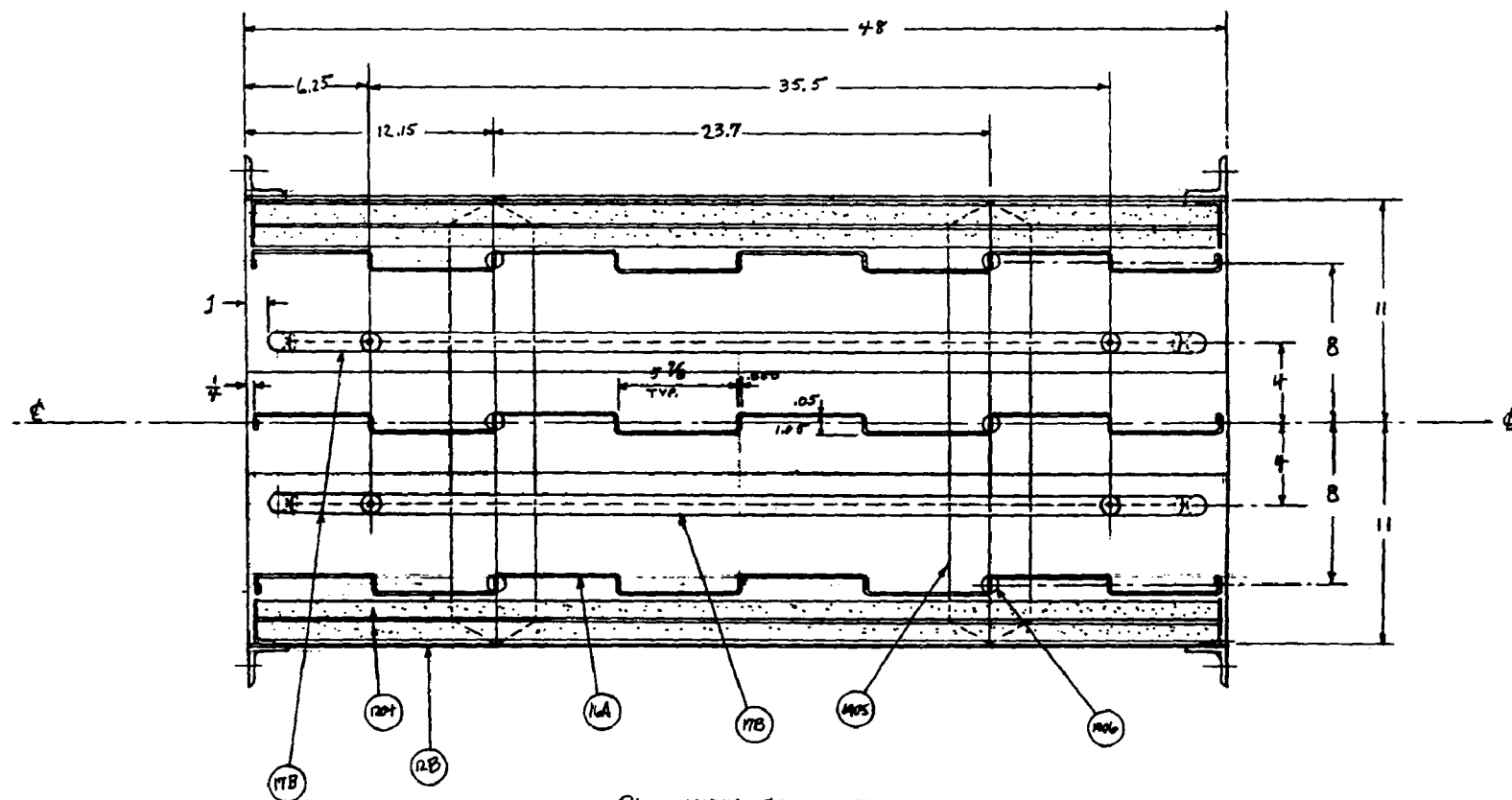


SEE ASSEMBLY DRAWING 3777-D-34
FOR MATERIAL LIST.



DESIGNER		DATE	
CHECKED		DATE	
LOUISIANA STATE UNIVERSITY BIRMINGHAM, ALABAMA 35202			
PROJECT PILOT PRECIPITATOR			
CROSS SECTIONS			
DRAWN APPROVED	DATE 12-11-77	SCALE 1/4" = 1'-0"	DRAWING NO. 3777-D-10

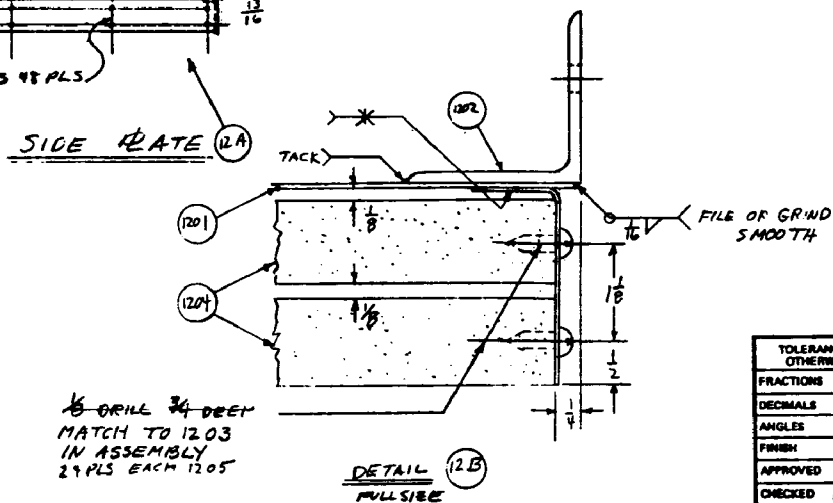
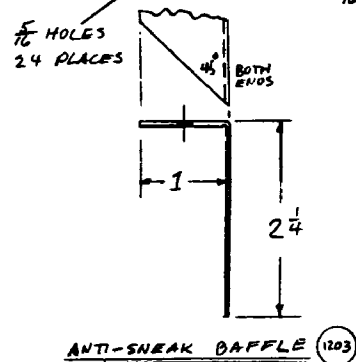
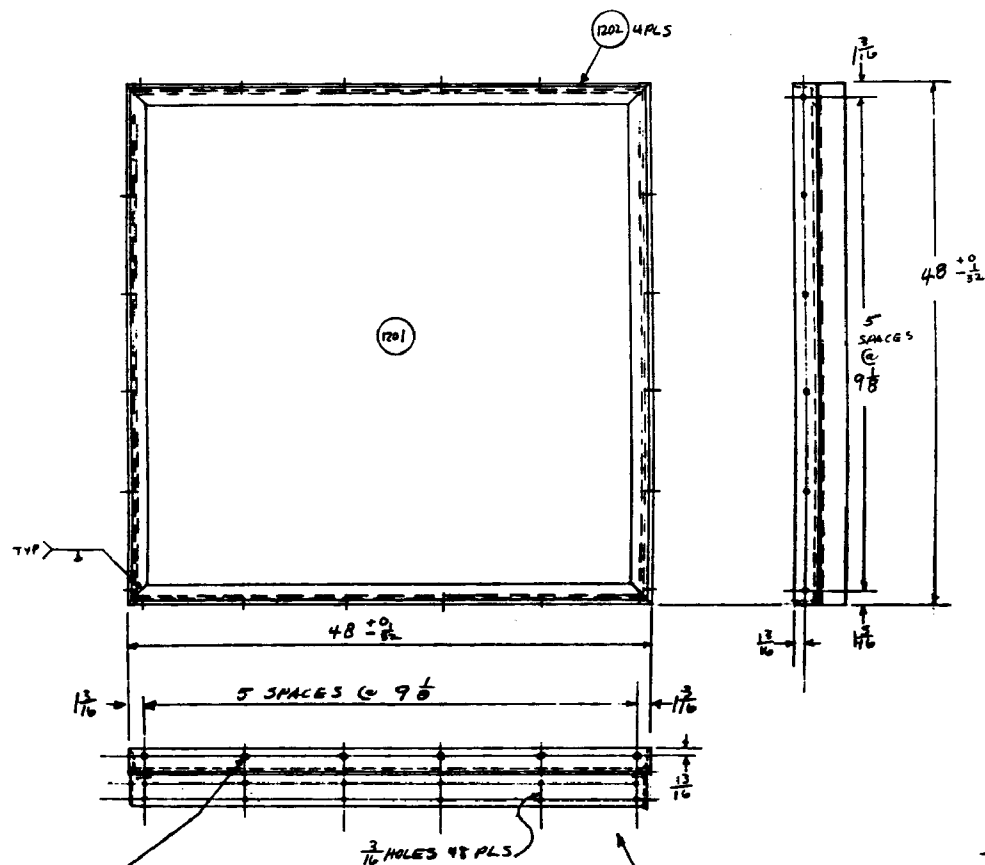
D-3



PLAN VIEW CROSS SECTION
1/4 X

SEE ALSO ASSEMBLY DRAWING 3777-D-34

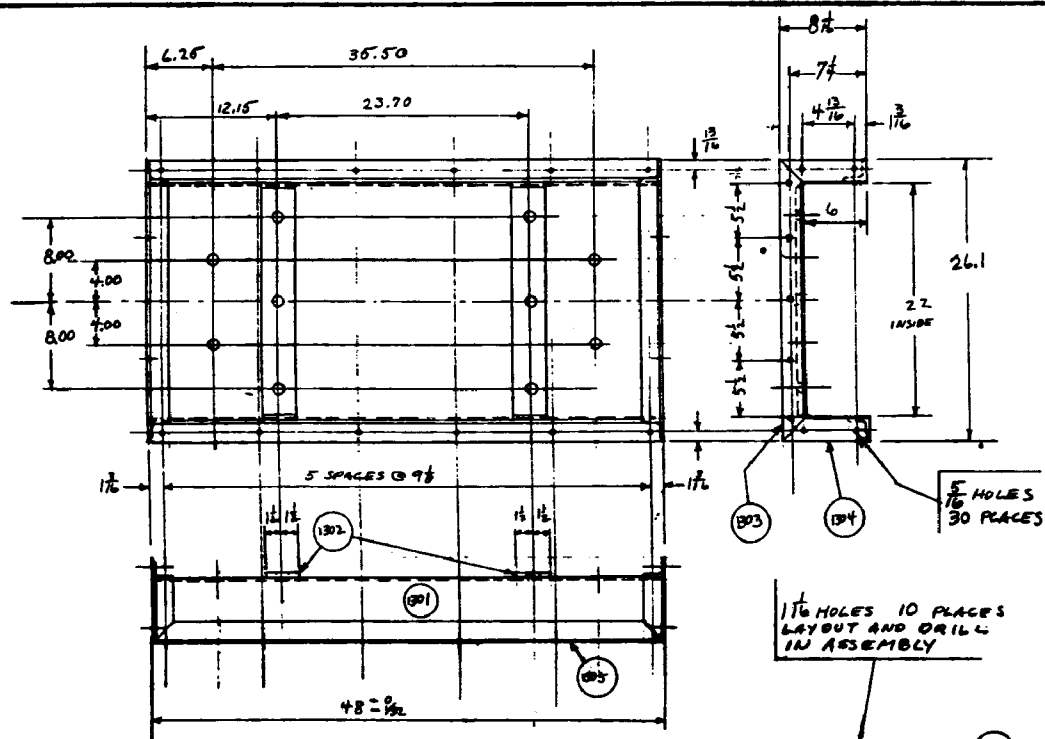
SOUTHERN RESEARCH INSTITUTE BIRMINGHAM, ALABAMA 35205	TITLE PILOT PRECIPITATOR
DRAWN (F.F.P./M.C.) DWG. NO. DATE 12-14-77	3777-C-11 PLAN VIEW CROSS SECTION



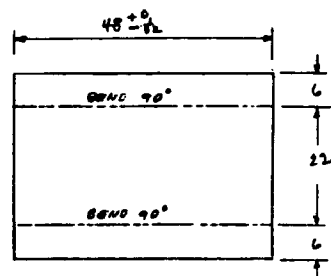
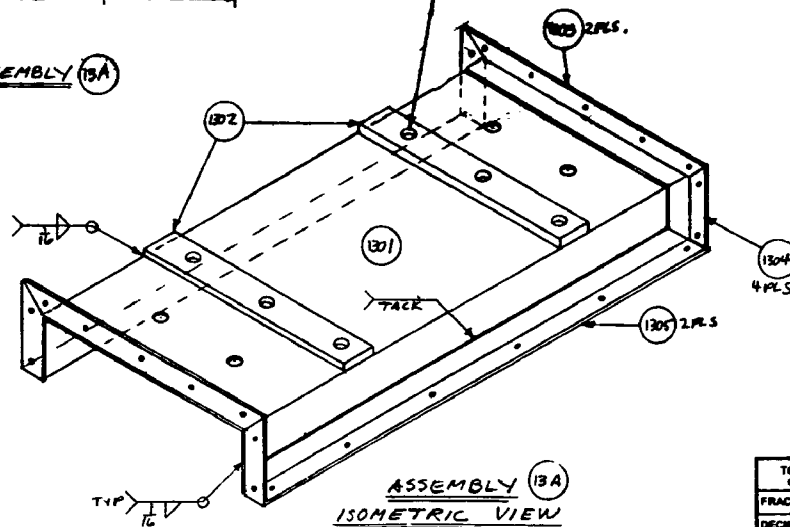
QTY.	REV.	QTY.	REV.	DESCRIPTION
		1201	8	PLATES, SIDE, 304 S.S., 48" X 48" X 1/8 GAGE (.050)
		1202	32	ANGLE FLANGE, 304 S.S., 2X2 X 1/8 X 48 LONG
A 8 REV'D	→	1		ITEM 1201
	→	4		ITEM 1202
	→	2		ITEM 1203
		1203	32	BAFFLE, ANTI-SNEAK, 304 S.S., 1/8 GAGE .050 X 36" X 47 1/2"
		1204	16	SHEETS, INSULATION, JOHNS-MANVILLE MARINITE 1" X 47 1/2" X 47 1/2"
		1205	384	SELF TAPPING SCREWS, 18-8 S.S. PAN HEAD CIRCLE POINT #8 (.164) X 3/4 LONG ALUMINUM CASE 91632A
B 8 REV'D	→	1		ASS'Y 12A
	→	2		ITEM 1204
	→	48		ITEM 1205

3-3-78	CORRECTION: ITEM 6 QUAN. REVERSE 0	12012
1-30-78	ADD SWEAT BAFFLE	1203
DATE	REVISIONS	ZONE

TOLERANCES UNLESS OTHERWISE NOTED		SOUTHERN RESEARCH INSTITUTE BIRMINGHAM, ALABAMA 35203	
FRACTIONS	$\pm \frac{1}{32}$	TITLE	PILOT PRECIPITATOR
DECIMALS	$\pm .010$		
ANGLES	$\pm 1^\circ$		
FINISH			
APPROVED		SIDE RATE DETAIL	
CHECKED	PVB	SCALE	1/8
DRAWN	FRANCIS	DATE	12-15-77
		DRG. NO.	3777 -C-12



COVER ASSEMBLY (13A)

DEVELOPED VIEW (1301)
1/16 SCALEASSEMBLY (13A)
ISOMETRIC VIEW

ITEM NO.	QTY	DESCRIPTION
1301	4	COVER PLATE, 304 SS, 1/8 GAGE 34 X 48
1302	8	STIFFENERS, 304 SS, 3/8 X 3 X 22
1303	8	CROSS ANGLES, S.S., 2 X 2 X 1/4 X 26.1 LONG
1304	16	VERTICAL ANGLES, S.S., 2 X 2 X 1/4 X 8 1/2, 89° L
1305	8	SIDE ANGLES, S.S., 2 X 2 X 1/4 X 48

A	→	1	ITEM 1301
	→	2	ITEM 1302
4	→	2	ITEM 1303
ROD	→	4	ITEM 1304 2R/2L
	→	2	ITEM 1305

TOLERANCES UNLESS
OTHERWISE NOTED

FRACTIONS	± 1/32
DECIMALS	± 0.010
ANGLES	± 1°
FINISH	

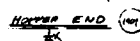
APPROVED

CHECKED D.P.

DRAWN N.FRANCIS

DATE	REVISIONS	ZONE NO.
SOUTHERN RESEARCH INSTITUTE BIRMINGHAM, ALABAMA 35205		
TITLE PILOT PRECIPITATOR		
COVER		
SCALE 1/8	DWG. NO.	3777-C-13
DATE 12-16-77		

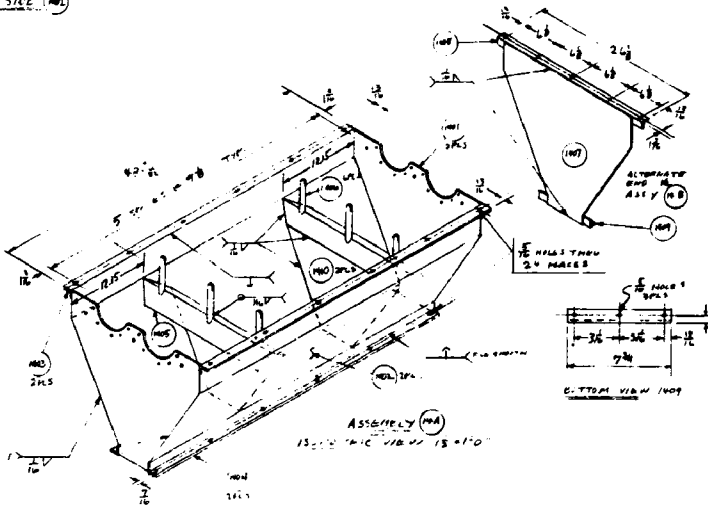
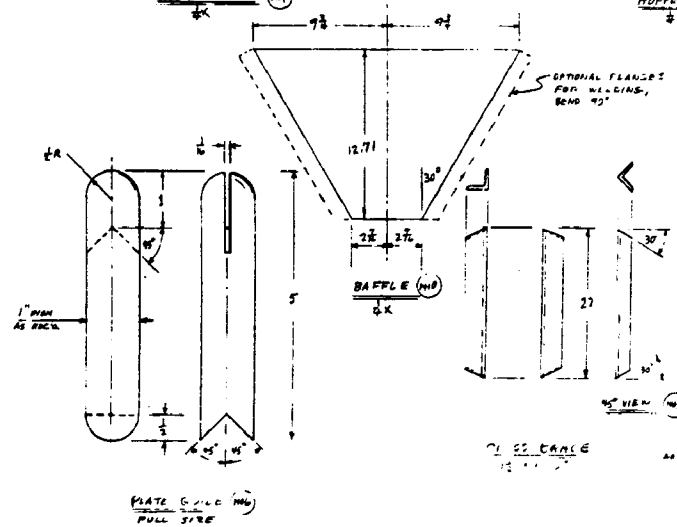
D-6



SIDE VIEW

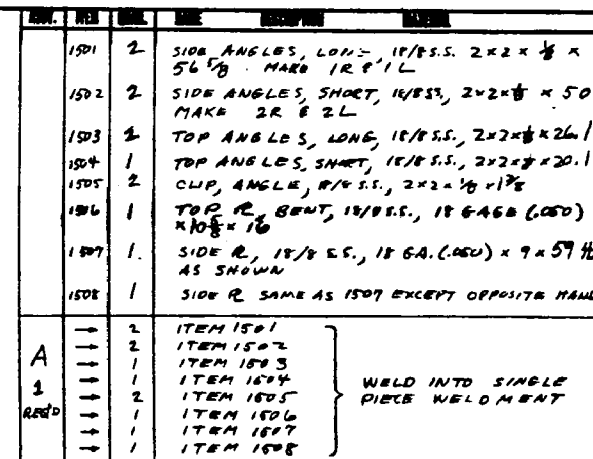
HOMER SIDE (M2)

DELETED COPY OF VIDEO

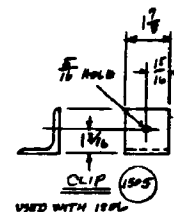


1901	9	HOPPER END, 304 STAINLESS STEEL, 18 GAUGE X 20 X 22
1901	10	HOPPER SUBS, 304 S.S., 18 GA. X 23 X 48
1943	18	PLAQUE, ANGLE, S.S., 2 1/2" W. X 10 L.G.
1943	19	PLAQUE, ANGLE, S.S., 1 1/2" W. X 10 L.G.
1905	8	WISS GASK, 1/2" ANGLE 3 X 3 1/2 X 22 G.
1904	24	GURDERS, S.S., 1" ANGLE 8" L.G.
A 4 SUB	→ 1	ITEM 1901 SUB
	→ 2	ITEM 1902 18"/L
	→ 3	ITEM 1903 TOP &
	→ 4	ITEM 1904 BOTTOM &
	→ 5	ITEM 1905 BRACE
	→ 6	ITEM 1906 GUIDE
B 1 SUB	→ 1	ITEM 1902 SIDE
	→ 2	ITEM 1903 TOP &
	→ 3	ITEM 1904 BOTTOM &
	→ 4	ITEM 1901 SUB
	→ 5	HOPPER AND PLAIN, S.S., 18 GA. X 20 X 22
	1907	1 ITEM 1901 SUB, 1/2" ANGLE AS ITEM 1901 WITHOUT BURNISHED OUT-DOTS AND WITHOUT HOLES
1908	1	END PLATE, S.S. ANGLE 2 1/2" X 12 L.G.
	2	ITEM 1901 SUB
	1	ITEM 1909, BOTTOM PLATE
C 1 END	→ 1	AS 1/2" 18 A
	→ 1	ITEM 1909, BOTTOM PLATE
	1908	2 PLATE, END, BOTTOM, S.S. ANGLE 1 1/2" W. X 7 1/2 L.G.
1910	10	SAMPLE, ANTI-SHOCK, 18" X 2 1/2", 18 GAUGE OPS. C. 12, 714 194

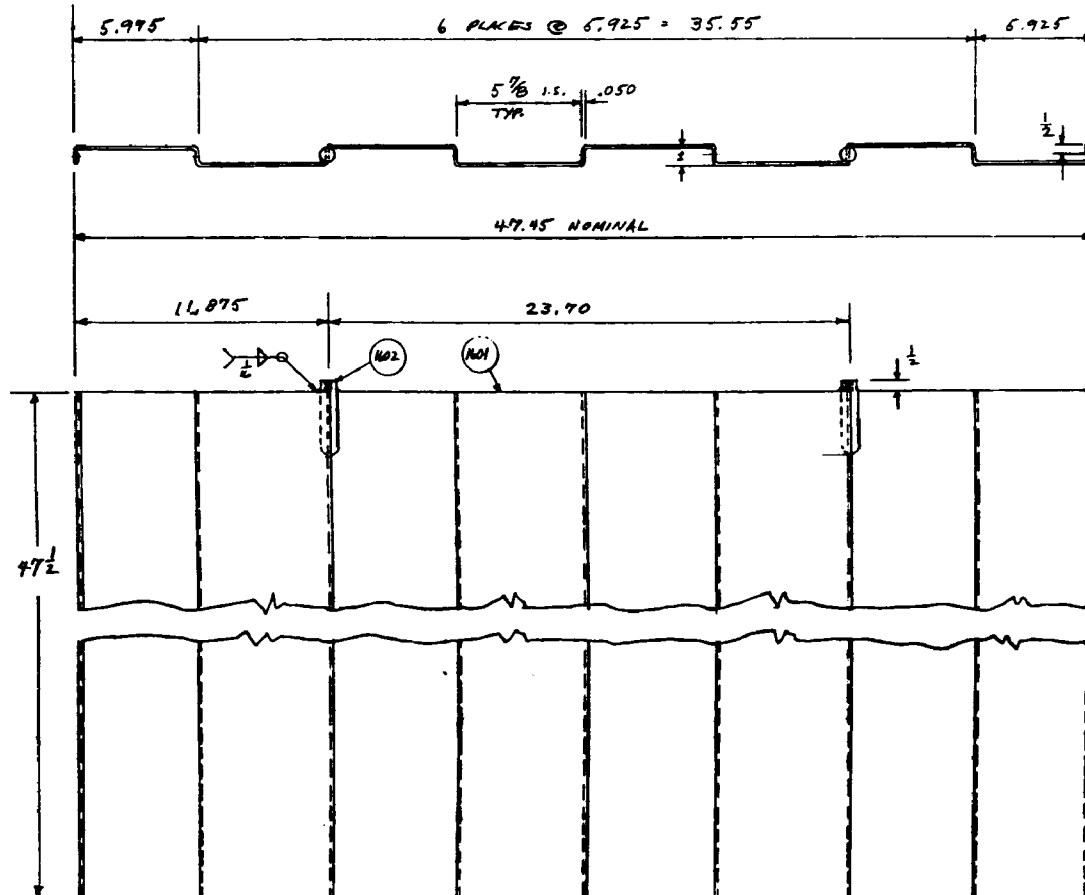
[illegible]



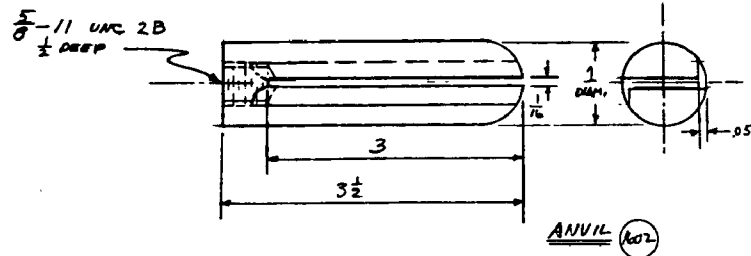
2. O.K. TO CHANGE DETAILS OF BRAKING AND WELDING TO SUIT SHOP METHODS.



3-3-78		ADD ACTG 2			
DATE		REVISIONS		ZONE	
SOUTHERN RESEARCH INSTITUTE BIRMINGHAM, ALABAMA 35205					
TITLE					
PILOT PRECIPITATOR					
OUTLET END SPACER					
TOLERANCES UNLESS OTHERWISE NOTED					
FRACTIONS	+	1	32		
DECIMALS	+	010			
ANGLES	+	5			
FINISH					
APPROVED					
CHECKED		PVB		SCALE 1/4	
DRAWN		NFRANCEIS		DATE 1-22-78	
				QMG. NO. 3777 -C-15	



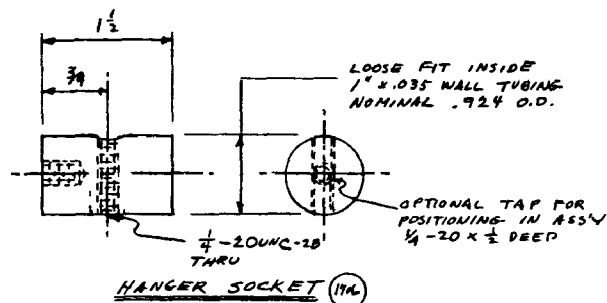
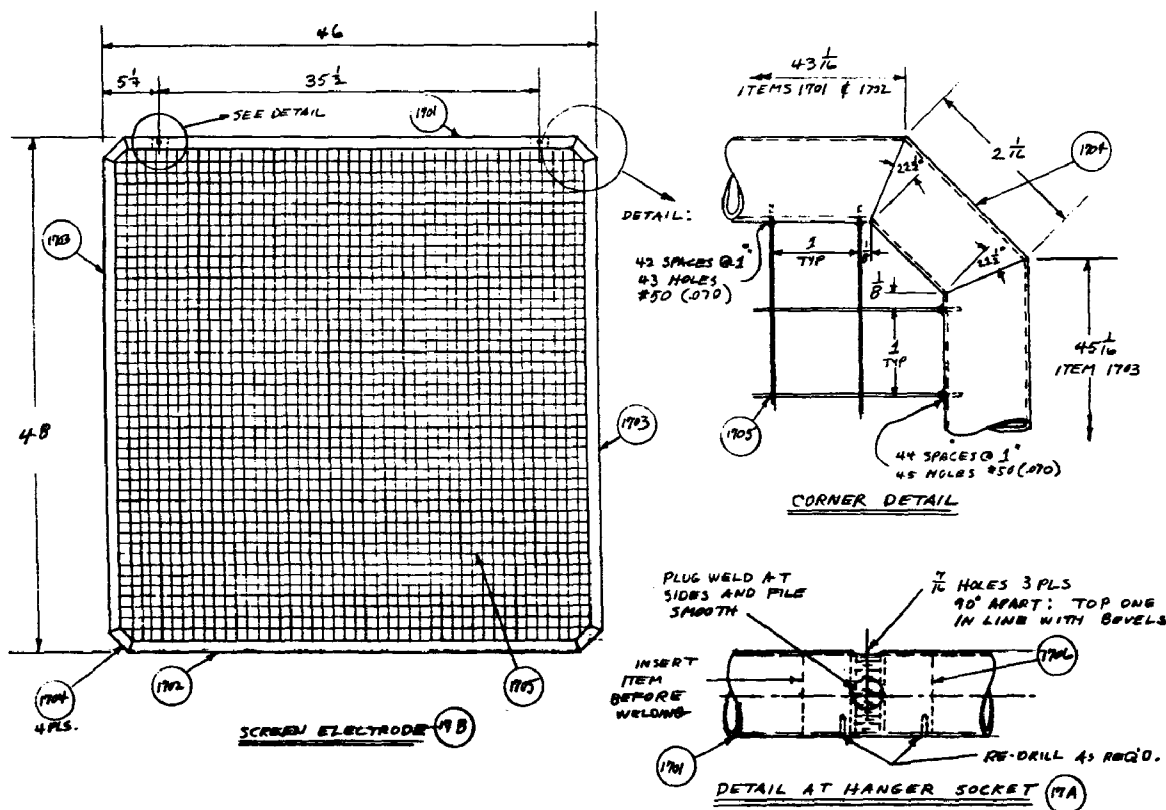
COLLECTION PLATE (14)



ANVIL (102)

REV.	DES.	DATE	DESCRIPTION	REVISION
1601	12		PLATE, COLLECTOR, ZIG-ZAG, 304 S.S., 10 GAGE, .050 X 4 7/8 X 57 LONG	
1602	24		ANVIL, 304 S.S., 1 DIA 1 3/4 LONG	
A	→	1	ITEM 1601	
12	→	2	ITEM 1602	
RRD				

DATE	REVISIONS	ZONE NO.
SOUTHERN RESEARCH INSTITUTE BIRMINGHAM, ALABAMA 35205		
TITLE PILOT PRECIPITATOR		
COLLECTION PLATE		
APPROVED		
CHECKED D.P.		
SCALE 1/8" = 1"		
DATE 12-27-77		
DRAWN N. FRANCIS		
DWG. NO. 3777-c-16-		

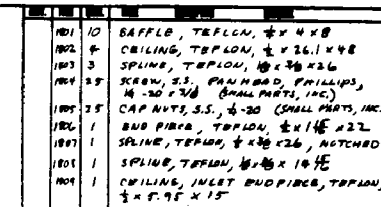


SEQUENCE OF ASSEMBLY

- (1) WELD HANGER BLOCKS 1706 INTO TOP RAIL 1701 & RE-DRILL BLOCKED WIRE HOLES 1/4" DEEP MIN.
- (2) WELD TWO CORNER PIECES 1704 ONTO TOP RAIL 1701.
- (3) SILVER SOLDER SCREEN 1705 INTO HOLES IN TOP RAIL 1701.
- (4) INSERT SCREEN WIRES INTO SIDE RAILS 1703 & SILVER SOLDER A FEW IN PLACE.
- (5) INSERT SCREEN WIRES INTO BOTTOM RAIL 1702 & SILVER SOLDER A FEW IN PLACE.
- (6) CLAMP RAILS SQUARE AND AT THE CORRECT DIMENSION AND WELD IN CORNER PIECES 1704.
- (7) COMPLETE SOLDERING OF WIRES.
- (8) REMOVE ALL SHARP CORNERS.

ASST.	ITEM	QTY	DESC.	UNIT
	1701	8	TOP RAIL, 304 S.S., 1" TUBE X .035 WALL X 43 7/8" LONG	
	1702	8	BOTTOM RAIL, SAME AS 1701 EXCEPT OMIT HANGER HOLES	
	1703	16	SIDE RAIL, 304 S.S., 1" TUBE X .035 WALL X 45 1/8" LONG	
	1704	32	CORNER PIECE, 304 S.S., 1" TUBE X .035 WALL X 2 1/8" LONG	
	1985	8	SCREEN PANEL, STAINLESS STEEL WIRE SCREEN 1" MESH .060 WIRE 44 1/2" X 46 1/2". CUT 1/4" BEYOND CROSS WIRES AND STRIP LAST CROSS WIRE ON ALL FOUR SIDES.	
	1706	16	SOCKETS, HANGER, 304 S.S., .924 DIAM. X 1 1/2" LONG	
A 8 REQD	→	1	ITEM 1701	} PLUG WELD PER DETAIL
	→	2	ITEM 1706	
B 8 REQD	→	1	ASS'Y 17-A	
	→	1	ITEM 1702	
	→	2	ITEM 1703	
	→	4	ITEM 1704	
	→	1	ITEM 1985	

TOLERANCES UNLESS OTHERWISE NOTED		DATE	REVISIONS	ZONE	IN
FRACTIONS	$\frac{1}{2}$ $\frac{3}{4}$	SOUTHERN RESEARCH INSTITUTE BIRMINGHAM, ALABAMA 35205 TITLE PILOT PRECIPITATOR SCREEN ELECTRODE			
DECIMALS	010				
ANGLES	1°				
FINISH					
APPROVED					
CHECKED	D. P.	SCALE $\frac{1}{8}$ 1"=1'-0"	DWG. NO.		
DRAWN	Francis	DATE 12-28-77	3777-C-17		

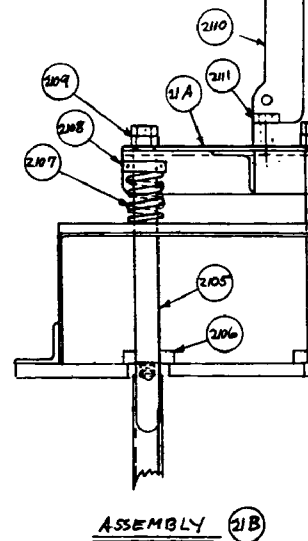
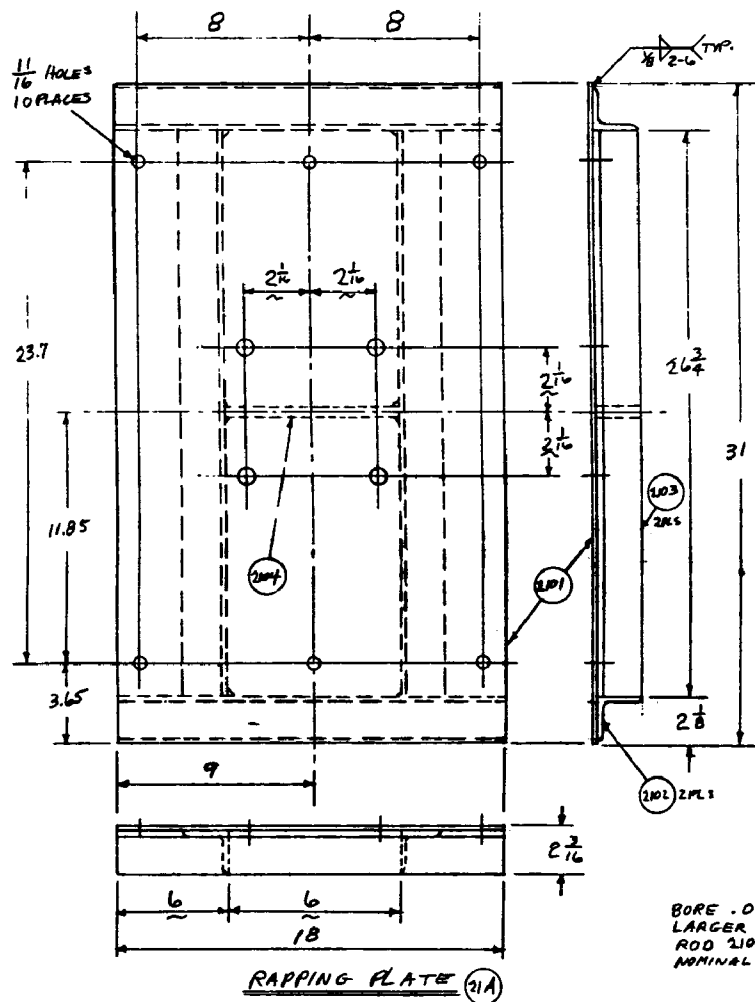


1-4-74		INCREASE THINGS ON SPINDS			
2-4-74		REDUCTION PHAS 2000			
DATE		REVISIONS		SHEET NO.	
<p>SOUTHERN RESEARCH INSTITUTE BIRMINGHAM, ALABAMA 35202</p>					
TITLE		PILOT PRECIPITATOR			
TEPLON BAFFLES					
CHECKED		DATE		SHEET NO.	
P4B		1-17-74		3777-0-10	
BY		DATE			
WHEELER		12-18-77			

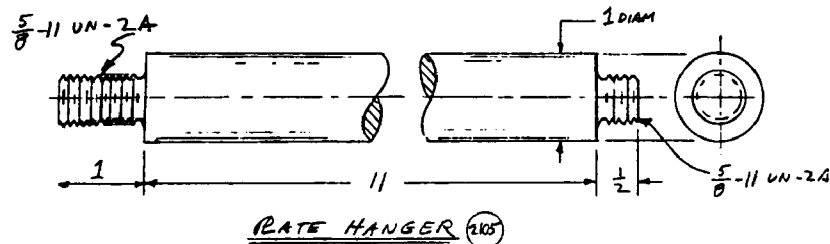
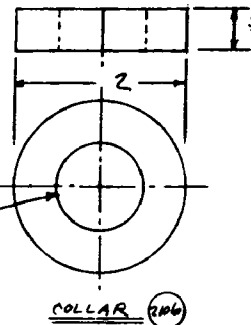
ASTY.	REIN.	QTY.	NAME	DESCRIPTION	REMARKS
		2001	20	BODY INSULATOR, GLASS FILLED TEFLON 1" DIAM. X 9" LONG (4 SPARES)	
		2002	5	CAP, PLAIN, TEFLON, 2" DIA X 3/4 LG. (1 SPARE)	
		2003	15	CAP, BORED, TEFLON, 2" DIA X 3/4 LG. (3 SPARE)	
		2004	20	HANGER, STAINLESS STEEL 304, .440 DIA X 5 3/8 LONG (4 SPARES)	
		2005	16	COLLARS, SEALING, TEFLON, 2" DIA X 1/2	
		2006	16	COLLARS, SPLIT CLAMP, 3/8 BORE X 1/2 THRU STAINLESS STEEL 303. STAFFORD MFG. CO., NORBURN, MASS. * SPL - 14 SS	
		2007	25	O-RING, RUBBER, 7/16 I.D. X 9/16 O.D. X 1/16 WIDE PARKER 2-013 OR EQUAL (13 SPARES)	
		2008	2	WRENCH, ASSEMBLY SPECIAL, STEEL, 3/16 DIA X 5 1/2 LONG (OK TO USE 1/2 TUBE)	
		2009	2	HANDLE, WRENCH, T&B, STEEL, 3/16 DIA X 3 LONG, GRIND OR FILE CORNERS	
A	→	1	ITEM 2001 BODY		
12	→	1	ITEM 2003 CAP, BORED		
	→	1	ITEM 2004 HANGER		
4	→	1	ITEM 2006 CLAMP		
2007	→	1	ITEM 2007 O-RING		
B	→	1	ITEM 2001		
	→	1	ITEM 2002 CAP, PLAIN		
4	→	1	ITEM 2004		
2007	→	1	ITEM 2006		
					} SAME AS 20-A EXCEPT NO HV. LEAD WIRE
C	→	1	ITEM 2008		
2	→	1	ITEM 2009		
2007					

NOTE: SPARE PARTS PROVIDED FOR FIELD REPAIRS.

TOLERANCES UNLESS OTHERWISE NOTED		DATE	REVISIONS	ZONE	NO.
FRACTIONS	$\pm \frac{1}{32}$	SOUTHERN RESEARCH INSTITUTE BIRMINGHAM, ALABAMA 35205			
DECIMALS	$\pm .010$				
ANGLES	$\pm 1^\circ$	TITLE <i>PILOT PRECIPITATOR</i>			
FINISH					
APPROVED		<i>HIGH VOLTAGE INSULATOR</i>			
CHECKED	D.P.				
DRAWN	AFRANCIS	SCALE	FULL	DWG. NO.	3777-c-20
		DATE	1-3-78		



BORE .020
LARGER THAN
ROD 2105
NOMINAL 1.020



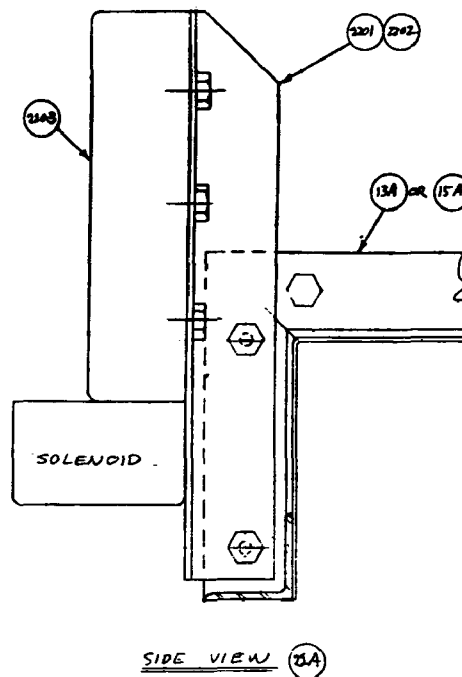
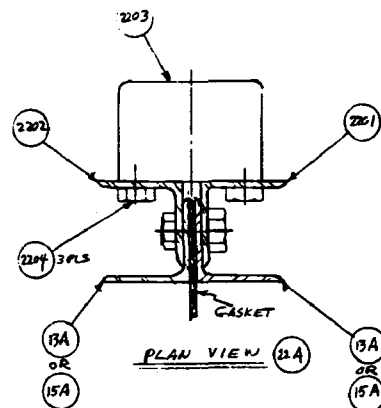
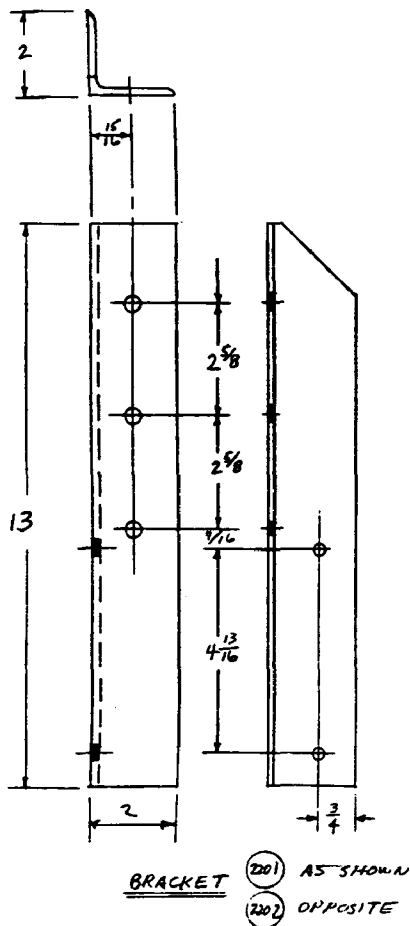
REV.	ITEM	QTY	DESCRIPTION
	2101	4	PLATE, RAPPING, 304 S.S., 3/16 X 18 X 31
	2102	8	STIFFENERS, CROSS, 304 S.S., 2 X 2 X 1/4 ANGLE X 18 LONG
	2103	8	STIFFENERS, LONG, 304 S.S., 2 X 2 X 1/4 ANGLE X 16 3/4 LONG
	2104	4	BAR, IMPACT, 304 S.S., 1/2 X 2 X 6
A	→	1	ITEM 2101
4	→	2	ITEM 2102
RECD	→	2	ITEM 2103
	→	1	ITEM 2104
	2105	32	HANGER, PLATE, 304 S.S., 1" ROD X 12 LONG (8 SPARES)
	2106	24	COLLARS, TEFLON, 2 DIAM X 1/2 THICK
	2107	32	SPRINGS, COMPRESSION, STEEL, 2 1/2 FREE LENGTH 1 1/2 X 1 1/2 PLAT WIRE ROUND EDGE, 1 1/2 SOLID HEIGHT 850 LB./IN. RATE MASTER-CARR 99624 K 53 (8 SPARES)
	2108	24	SPLIT COLLARS, STAINLESS STEEL, 1" BORE, 2" O.D., 1/2 WIDE, 1/4-28 SCREWS STAFFORD MFG. CO. # SPL-16 SS
	2109	100	NUTS, HEX, JAM, 5/8-11 UN, 18-8 SS MASTER-CARR 91851 D 035
	2110	4	IMPACTOR, PNEUMATIC, CVC MODEL 1350 S1 6 X 6 X 10, 39 LB., 172 FT. LB. IMPACT @ 90 PSI
	2111	25	BOLTS, 18-8 S.S., HEX HEAD, 5/8-71 X 1 1/2 MASTER-CARR 92198 A
B	→	1	ASSY 21-A
4	→	1	ITEM 2110
PRD	→	4	ITEM 2110
	→	8	ITEM 2109

TOLERANCES UNLESS OTHERWISE NOTED		DATE	REVISIONS	ZONE	NO.
FRACTIONS	± 1/16				
DECIMALS	± .010				
ANGLES	± 1°				
FINISH					
APPROVED					
CHECKED	D.P.	SCALE	1/4" = 1" 3" = 16"	DWG. NO.	3777-C-21
DRAWN	M.F.R.A.L.S.	DATE	1-7-78		

SOUTHERN RESEARCH INSTITUTE
BIRMINGHAM, ALABAMA 35205

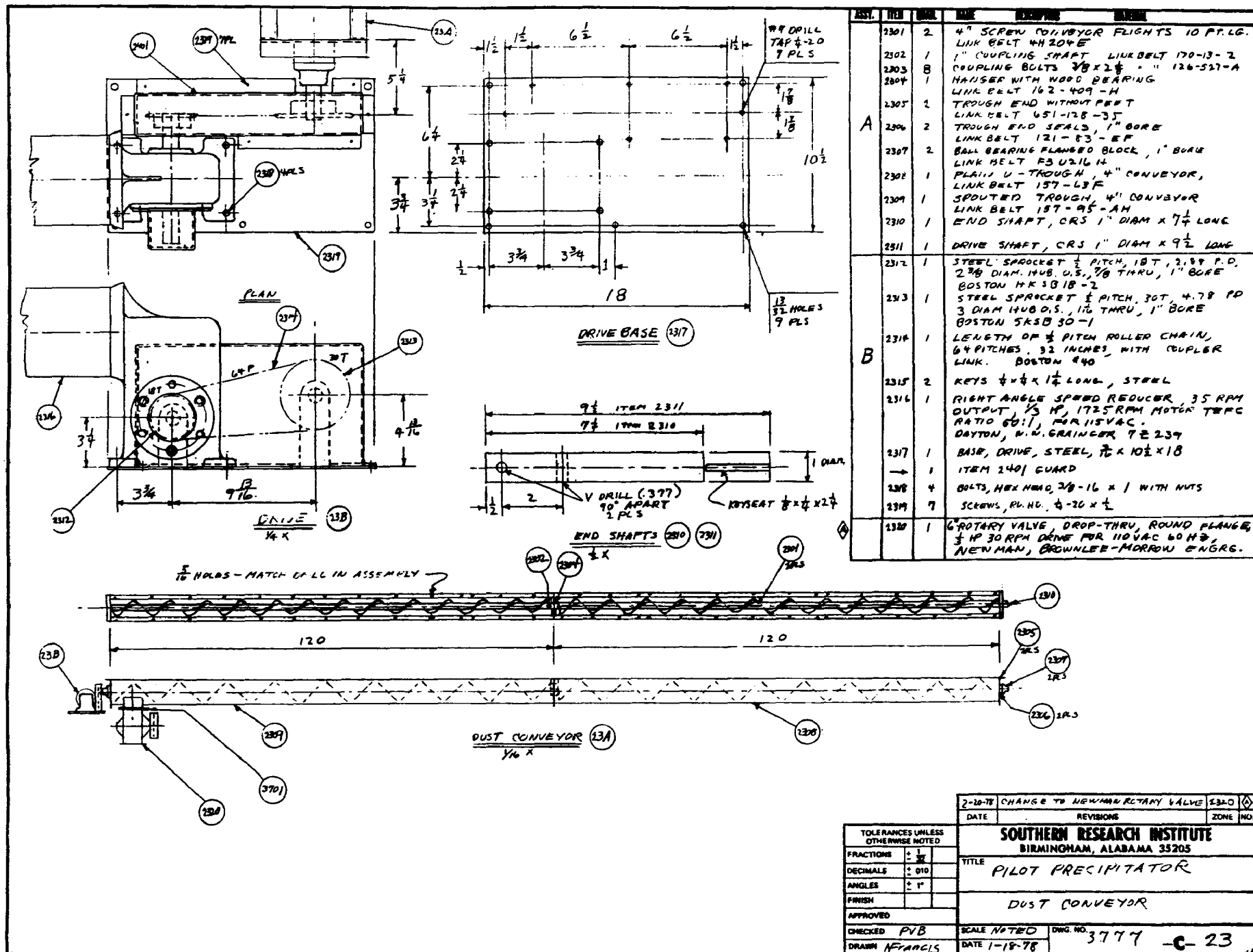
TITLE
PILOT PRECIPITATOR

RAPPING RATE



ASSY.	ITEM	QTY	DESC.	REVISION	DATE
	2201	4	BRACKET, ANGLE, AS SHOWN 304 SS. 2x2x1/8 ANGLE 13" LONG		
	2202	4	BRACKET, ANGLE, OPPOSITE TO SHOWN, 2x2x1/8 x 13 LONG		
	2203	4	VALVE, CONTROL AIR, 5 PORT, NOKEREN P71 LAJ1		
	2204	12	BOLT, HEX HEAD, S.S., 1/4-20x3 WITH NUTS AND FLAT WASHERS.		
A	→	1	ITEM 2201	BOLT TO JOINT BETWEEN 13A AND 13A OR 15A IN ASSEMBLY	
4	→	1	ITEM 2202		
REGD	→	1	ITEM 2203		
	→	3	ITEM 2204		

TOLERANCES UNLESS OTHERWISE NOTED		DATE		REVISIONS		ZONE NO.	
FRACTIONS	± 1/32	SOUTHERN RESEARCH INSTITUTE BIRMINGHAM, ALABAMA 35205					
DECIMALS	± .010	TITLE PILOT PRECIPITATOR					
ANGLES	± 1°	RAPPER VALVE BRACKET					
FINISH		APPROVED					
CHECKED	D.P.	SCALE	HALF	DWG. NO.	3777-C-22		
DRAWN	AFRANCIS	DATE	1-9-78				

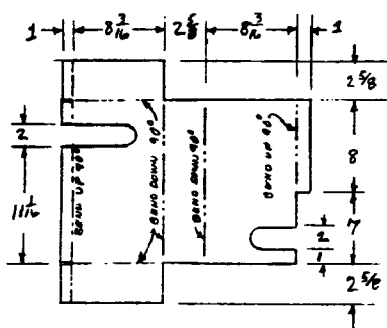


2-10-78	CHANGE TO NEWMAN ROTARY VALVE	2320	1
DATE	REVISIONS	ZONE	NO.

TOLERANCES UNLESS OTHERWISE NOTED	
FRACTIONS	± 1/32
DECIMALS	± 0.010
ANGLES	± 1°
FINISH	
APPROVED	
CHECKED PVB	SCALE NOTED
DRAWN NFRANCIS	DATE 1-18-78

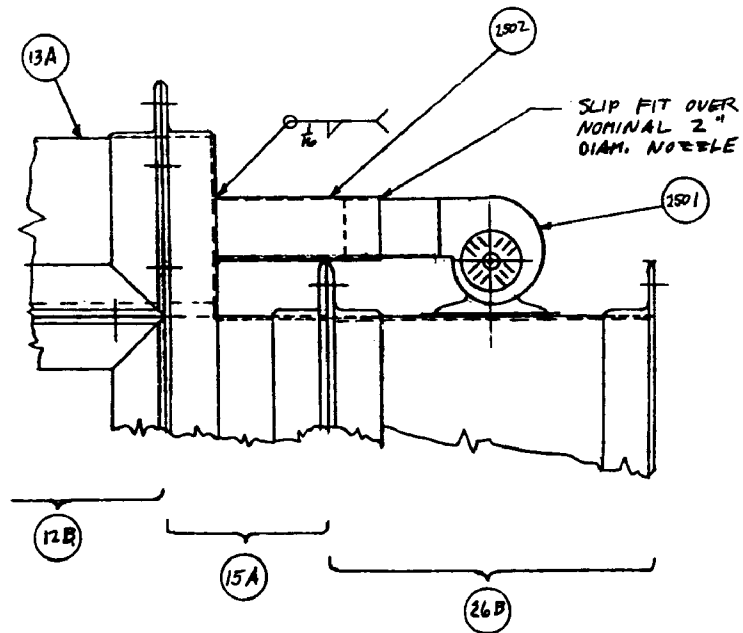
SOUTHERN RESEARCH INSTITUTE BIRMINGHAM, ALABAMA 35205	
TITLE PILOT PRECIPITATOR	
DUST CONVEYOR	
APPROVED	
CHECKED PVB	SCALE NOTED
DRAWN NFRANCIS	DATE 1-18-78

3777 -C-23



1 O.K. TO ADD TABS AND SPOT WELD OR SOLDER

TOLERANCES UNLESS OTHERWISE NOTED		DATE		REVISIONS		ZONE	
FRACTIONS $\frac{1}{16}$ $\frac{3}{16}$		SOUTHERN RESEARCH INSTITUTE BIRMINGHAM, ALABAMA 35205					
DECIMALS $\pm .010$							
ANGLES $\pm 1^\circ$		TITLE PILOT PRECIPITATOR					
FINISH							
APPROVED		GUARD					
CHECKED P.V.B.							
DRAWN A.F.R.N.E.L.S.		SCALE HALF		DWG. NO. 3777 -C-24			
		DATE 1-10-78					



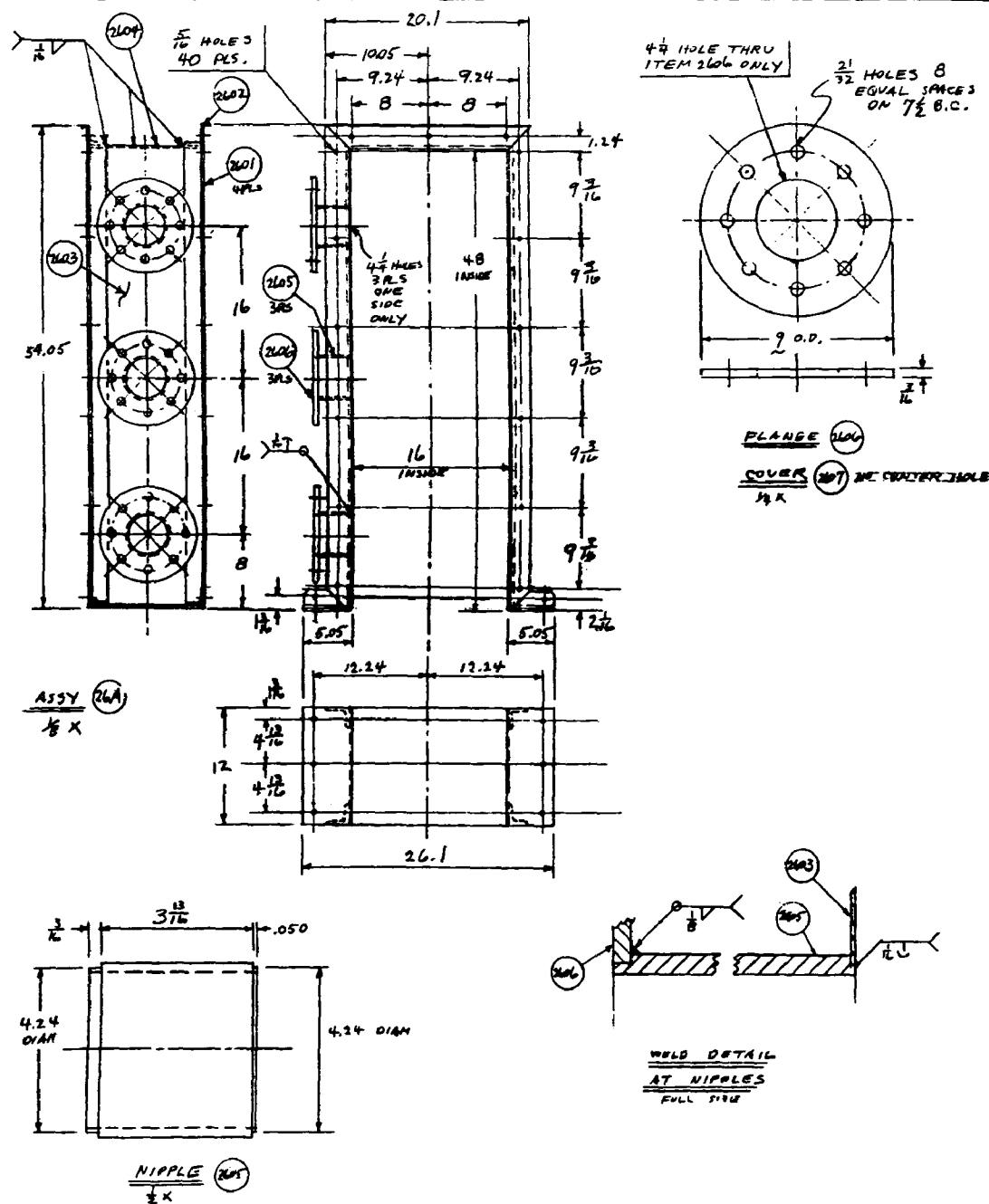
ASST.	ITEM	QTY.	NAME	DESCRIPTION	MATERIAL
	2501	1		DAYTON FLAMELESS HEAT GUN, 10 AMP AT 115 VAC, 300-500°F, 1600 FPM VEL, 2 NOZZLE, 40 CFM. W.N. GRANGER # 23788	
A	2502	1		PIPE, INLET, 18-8 S.S., 18 GAGE (.050) NOMINAL I.D. 2" x 6" LONG. FABRICATE FROM SHEET METAL .050 x 6 x 6 5/16. CUT HOLE IN ITEM 1505 TO MATCH LOCATION OF HEAT GUN AND DIAMETER OF INLET PIPE. WELD 2502 IN PLACE	

TOLERANCES UNLESS OTHERWISE NOTED			DATE	REVISIONS	ZONE	NO.
FRACTIONS	+ 1/32					
DECIMALS	+ .010					
ANGLES	+ 1°					
FINISH						
APPROVED						
CHECKED	P.V.B.		SCALE	1/4	DWG. NO.	3777-B-25
DRAWN	FRANCIS		DATE	1-19-78		

SOUTHERN RESEARCH INSTITUTE
BIRMINGHAM, ALABAMA 35205

TITLE
PILOT PRECIPITATOR

PURGE AIR SUPPLY



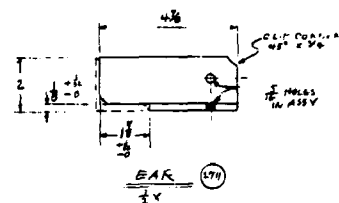
ITEM	QTY	DESCRIPTION	MATERIAL
2601	4	ANGLES, SIDE, 15/8 S.S., 2x2x1/8 x 50 (WAL)	
2602	2	ANGLES, TOP, 15/8 S.S., 2x2x1/8 x 10.1	
2603	2	SIDE R, 15/8 S.S., 10 GA (ASTM) x 12 x 48	
2604	1	TOP R, 15/8 S.S., 10 GA (ASTM) x 12 x 16	
2605	3	NIPPLES, PIPE, 15/8 S.S., SCHED. 10, 4" x 4.05	
2606	6	FLANGES, 15/8 S.S., 7/8 x 9 DIAM.	
2607	6	COVERS, 15/8 S.S., 3/16 x 9 DIAM.	
2608	98	BOLTS, HEX HEAD, STEEL, CADMIUM PLATED, 5/8 - 11 x 1 LONG WITH NUTS	
REVISIONS			
A	1	4	ITEM 2601
	2	2	ITEM 2602
	3	2	ITEM 2603 (ONE WITH HOLES)
	4	1	ITEM 2604
	5	3	ITEM 2605
B	1	1	ASSY 26-A
	2	3	ITEM 2607
	3	24	ITEM 2608
	4		

1 SEE 3777-C-2901 FOR FLOOR

2 WORK THIS DWG. WITH 3777-C-33

3-3-79	CHANGE TO SCHED 10	2607
DATE	REVISIONS	ZONE NO.
SOUTHERN RESEARCH INSTITUTE BIRMINGHAM, ALABAMA 35203		
TITLE PILOT PRECIPITATOR		
OUTLET SAMPLING SECTION		
APPROVED		
CHECKED PVB	SCALE NOTED	DWG. NO.
DRAWN H. FRANCIS	DATE 1-24-78	3777-C-26

TOLERANCES UNLESS OTHERWISE NOTED	
FRACTIONS	± 1/16
DECIMALS	± 0.010
ANGLES	± 1"
FINISH	

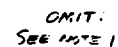


2701	5	ANGLE FLANGE, SHORT, 12-23, 13x20x30, 1
2702	1	SHORT LUG ANGLE, 12-23, CUT FROM 1/2" x 1/2" x 1/2" ANGLE LUG TO 1/2"
2703	1	SUPPORT ANGLE, 12-23, 2x3x8 x 1/2"
2704	7	TURNING ANGLE, LARGE R, 12-23, 18 GAGE, 240 x 132 x 16
2705	9	TURNING VARIOUS, LARGE R, 12-23, 18 GAGE, 180 x 120 x 16
2706	76	CLIPS, 12-23 15, 18 GAGE, 940 x 14 x 2 (CUT WELD TO VALVE)
2707	1	TURNING VARIOUS, SMALL R, 12-23, 18 GAGE, 180 x 10 1/2 x 16
2708	9	TURNING VARIOUS, SMALL R, 12-23, 18 GAGE, 180 x 10 1/2 x 16
2709	1	FLANGE ANGLE, 12-23 22 2x3 x 1/2 x 31.08
2710	2	SIDE R, 12-23, 18 GAGE DIA 17 3/4 x 2 (10/16)
2711	2	BAR, SUPPORT, ANGLE 180-23, 2 x 3 x 4
2712	1	FRUIT 12, 18-23, 18 GAGE DIA 4 x 1/2
2713	1	BACK R, 12-23, 18 GAGE 220 x 16 x 2 1/2
→	1	ITEM 2707 HUB
→	80	ITEM 2706 VALVE
→	7	ITEM 2706 VALVE
→	1	ITEM 2703 ANGLE
→	1	ITEM 2702 CLIPPER ANGLE
→	5	ITEM 2701 FLANGE 3

3 O.K. TO CHANGE DETAILS OF BRACING
AND WELDING TO SUIT SHOP METHODS.
O.K. TO SUBSTITUTE PIPE RIGIDS FOR SPCT
WELDING ON STOPS, 2706 & 2709.

1- ALSO USED ON 3777-C-354 & C-28A

[illegible]

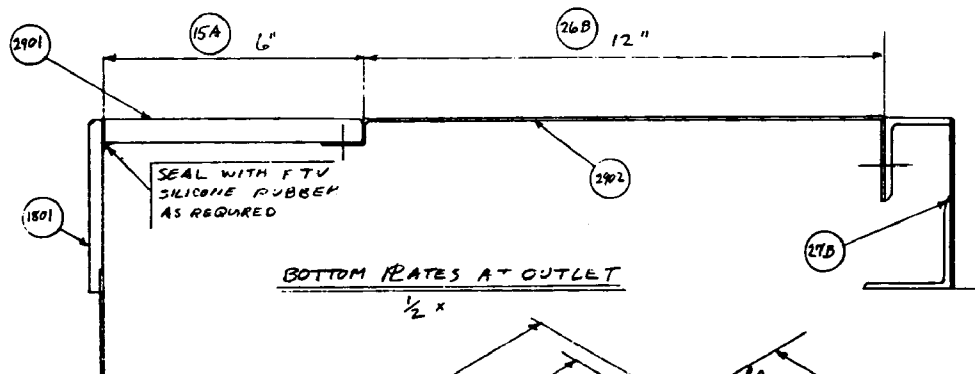


	QTY	NO	QTY	NO	QTY	NO	QTY	NO
A		2801	8	FLANGE, 18-8 S.S., ANGLE 2x2x $\frac{1}{2}$ x 19, 1				
		2802	2	SIDE RAKE, 18-8 S.S., 18 GAGE .050 x 19 x 19				
		2803	1	BACK RAKE, 18-8 S.S., 18 GAGE .050 x 15 x $\frac{3}{8}$, BEND 90° TO FORM 19 x 19 ANGLE 15° LONG				
		2804	1	INNER PLATE, 18-8 S.S., 18 GAGE .050 x 8 x 16, BEND 90° TO FORM 4 x 4 ANGLE 15° LONG				
	→	8	ITEM 2808 WAREZ } SPOT WELD					
	→	28	ITEM 2806 CLIPS }					
B		2805	4	FLANGE, 18-8 S.S., ANGLE 2x2x $\frac{1}{2}$ x 20				
		2806	1	TRANSFORM, ROUND 8° TO SQUARE 16", 24" LONG, 18-8 S.S. 18 GAGE				

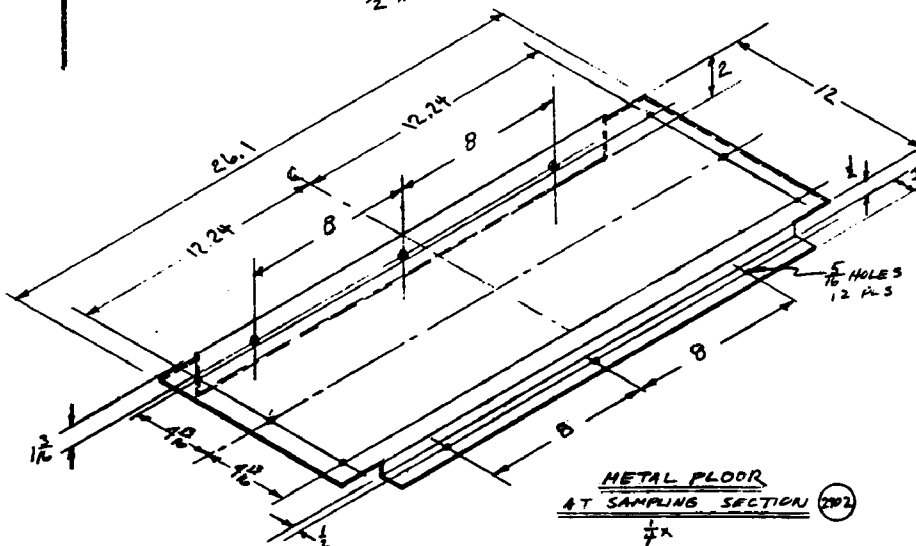
▷ OPTIONAL: USE WHEN PRECIPITATOR IS VERY CLOSE TO SOURCE



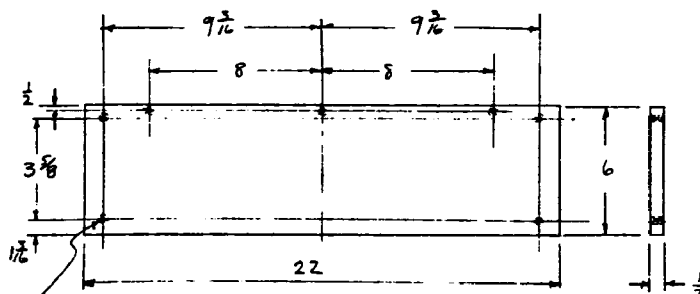
3-7-78		CANCEL ASSY 28-A, AIRCRAFT		16	
DATE		REVISIONS		ZONE INC	
TOLERANCES UNLESS OTHERWISE NOTED		SOUTHERN RESEARCH INSTITUTE			
		BIRMINGHAM, ALABAMA 35205			
FRACTIONS		TITLE			
DECIMALS		PILOT PRECIPITATOR			
ANGLES					
FINISH					
APPROVED		ELBOW & TRANSFORM			
CHECKED PVB		SCALE 1/8		DWG. NO.	
DRAWN N. FRANCIS		DATE 1-30-78		3777-C-28	



BOTTOM RATES AT OUTLET

 $\frac{1}{2}x$ 

METAL FLOOR
AT SAMPLING SECTION (202)
IX

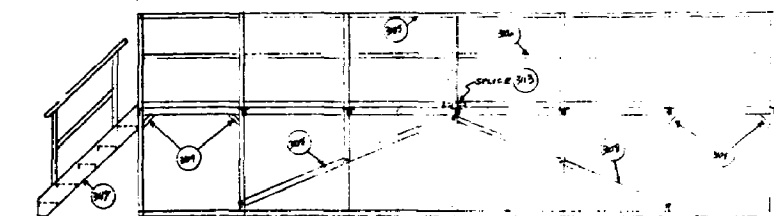


#7 TAP DRILL (.201)
TAP 1/4-20
7 PLS

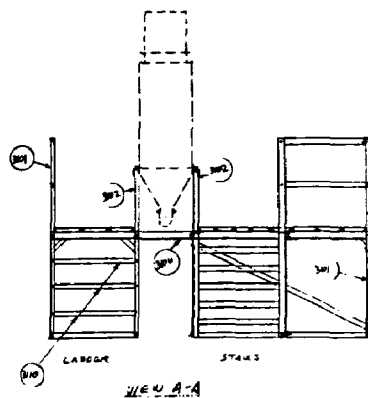
TEFLON FLOOR (2961)
AT FILLER
 $\frac{1}{4} \times$

TOLERANCES UNLESS OTHERWISE NOTED		DATE	REVISIONS	ZONE	NO.
FRACTIONS	1 2 32	SOUTHERN RESEARCH INSTITUTE BIRMINGHAM, ALABAMA 35205 TITLE PILOT PRECIPITATOR FLOOR AT OUTLET END			
DECIMALS	2 610				
ANGLES	2 1°				
FINISH					
APPROVED		SCALE	NOTED	DWG. NO.	
CHECKED	PVB	DATE	1-31-78	3777	-C-29
DRAWN	FRANCIS				

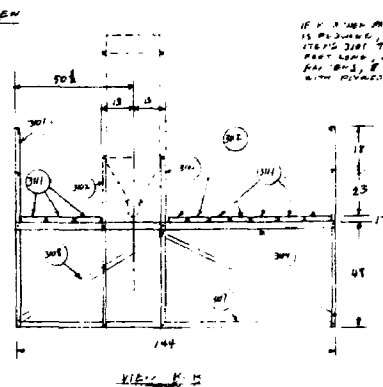
TOLERANCES UNLESS OTHERWISE NOTED		DATE	REVISIONS	ZONE	NO.
FRACTIONS $\frac{1}{2}$ $\frac{3}{4}$		SOUTHERN RESEARCH INSTITUTE BIRMINGHAM, ALABAMA 35205 TITLE PILOT PRECIPITATOR MODIFICATION OF PRE CHARGER			
DECIMALS $\frac{1}{10}$ $\frac{1}{100}$					
ANGLES 1°					
FINISH					
APPROVED					
CHECKED	PVB	SCALE	NOTED	DWG. NO.	
DRAWN <i>REYNOLDS</i>		DATE 2-2-78		3777-C-30	



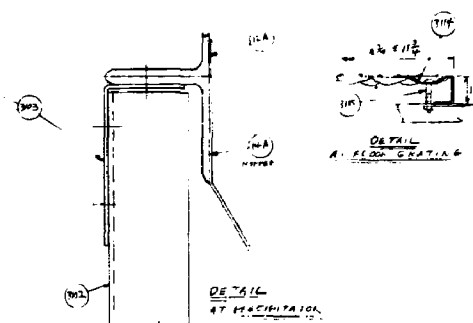
SIDE VIEW



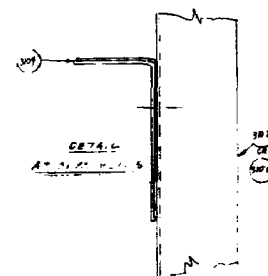
NEW A-A



Y1200 K. H.



DETAIL
AT PARTICIPATION



GE74.6
1974.5

340	16	POST, HALLWAY, SCOTTED ANGLE, GALV. 18" x 5" x .104 x 7'0" LONG
302	14	POST, HALLWAY, SCOTTED ANGLE, GALV., 18" x 5" x .104 x 7'0" LONG
401	4	PLATE, THICK, PL. 1/2" x 18" x 12" SET IN 1/2" x 12" x 12"
107	2	CHANNEL, 18" x 5" x .104 GALV. 18" x 5" x .104
308	4	TOP ANGLE, SCOTTED ANGLE, GALV. 2" x 2" x .080 x 12" F
306	4	BOTTOM RAILING, SCOTTED ANGLE GALV. 18" x 5" x .104 x 12" F
1007	12	SILL, SCOTTED ANGLE, GALV., 18" x 5" x .104 x 12" F
908	6	SUPERCAN, SCOTTED ANGLE, GALV. 18" x 5" x .104 x 12" F TO LENGTH IN ASS'Y TO SUIT.
307	16	GUEST, DOORWAY, 2 x 7 1/2" EGUPTO "4660
3105	9	RUNG, LADDER, SCOTTED ANGLE, 18" x 5" x .104 PL. 1/2" x 12" x 12"
3111	16	PLANK, STEEL PLATE GRATING, 18" x 18" x 1/2" (GALV.) STEEL x 1/4" x 1/4" LONG. EGUPTO 16172
3112	4	PLANK, STEEL PLATE GRATING, 18" x 18" x 1/2" (GALV.) x 1/4" x 1/4" EGUPTO 16172
3102	20	SPICERS, EGUPTO 5499-2
3104	50	CLAMP, GRATING, EGUPTO 10319
3105	50	16175, 30 MD. 5/16" x 12, EGUPTO 13194 WALNUTS
306	1	ANGLE CUTTER, EGUPTO 10213
107	1	REINFORCED STEEL 36" x 60" x 4" THICK, EGUPTO 936 F 61
308	1	SUPPORT FOR BRIDGE BASE, SCOTTED ANGLE 18" x 5" x .104 x 12" x 12" x 12" LENGTH ANGLE 18" x 5" x .104, BOLT TO FLOOR GRATING

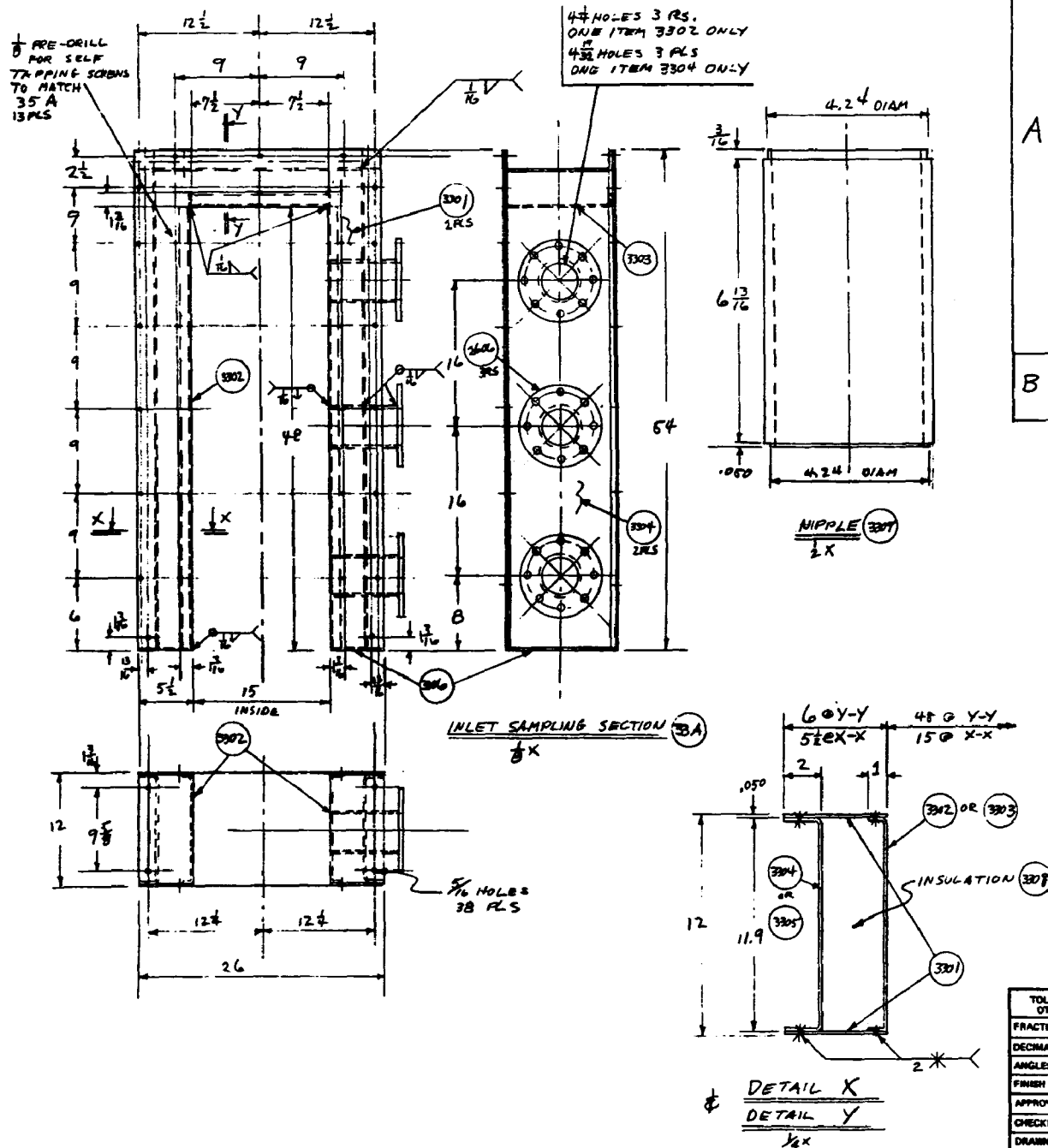
- ▶ PLOTTED ALGAE HANTS TO BE CUT FROM THE FOLLOWING
 - 5 BUNDLES OF 10 ANDES 14 3 IN ROW 4
 - 2 BUNDS OF 2 7 8 10
 - 3 BUNDLES OF 10 ANDES 14 3 IN ROW 4
 - 2 BUNDS OF 2 7 8 10
 - (5 BOLTS 4 WATS INCLUDED WITH EACH BUND)
- ▶ USE DOUBLE TENNANTS OF ANDES 3 AND AT ANY POINT HAVING A HEAVY LOAD.
- ▶ O.A. TO ASSEMBLE PER DEPT OF THE MANU O.A. CHARGE SECTION OF STAIRS AND SADDLES TO THE LOCAL CONDITIONS.

TELEFAXES UNLESS OTHER SOURCE NOTED		DATE		REVISED		DRAWN NO.	
FRACTIONS		SOUTHERN RESEARCH INSTITUTE BIRMINGHAM, ALABAMA 35202					
DECIMALS		TITLE		PLOT PRECIPITATOR			
ANGLES		PLOT					
FEET		SCALE					
APPROVED		SCALE 1" = 100'					
CHOSER		SCALE		DRAWN NO.		3777-D-31	
DRAWN		DATE		2-2-78			

NO.	QTY	UNIT	DESCRIPTION
3201	1		FACB RATE PRECIPITATOR SIDE, 18"-F.S. 1" GAGE .050 X 26 X 56 7/8
3202	1		FACB RATE PRECHARGED SIDE, 18"-F.S. 1" GAGE .050 X 20 X 54
3203	2		INNER SIDE RATE, 18"-F.S., 18 GAGE .050 X 7.9 X 53. BEND TO FORM CHANNEL 1 X 5.9 X 53 LONG
3204	2		OUTER SIDE RATE, 18"-F.S., 17 GAGE .050 X 7.9 X 53. BEND TO FORM CHANNEL 2 X 6.9 X 53 LONG
3205	1		TOP RATE, 18"-F.S., 18 GAGE .050 X 10.21 X 22. BEND TO FORM UNEQUAL LGE CHANNEL 1 X 3 1/2 X 6.9 X 22 LONG.
3206	1		CLIP, 18"-F.S., 18 GAGE .050 X 3 X 15. BEND TO FORM ANGLE .050 X 1 1/2 X 1 1/2 X 15 LONG
3207	2		BOTTOM RATE, 18"-F.S., 18 GAGE .050 X 5 1/2 X 6
3208	1.3		CUBIC FEET OF INSULATION MATERIAL. INSTALL DURING FABRICATION. O.K. TO USE FIBERGLAS, MINERAL WOOL, OR FIBERPRAX.
B	→	1	ITEM 1709 TEPLOW GAPPLE (REFER TO 3206)
	→	1	ASSY 32A
	3209	3	SELF TAPPING INSET METAL SCREWS, PAN HEAD, #8 X 3/8 LONG

1 O.K. TO CHANGE DETAILS OF BRAKING
AND WELDING TO SUIT SHOP METHODS

TOLERANCES UNLESS OTHERWISE NOTED		3-3-78 ADD NOTE 1 & FLANGE DIMENSIONS		DATE		REVISIONS		ZONE		NO.	
FRACTIONS		1/2		DECIMALS		0.010		ANGLES		1°	
FRESH				APPROVED				CHECKED		P.B.	
DRAWN		N. FRANCES		SCALE		NOTED		DWG. NO.		3777 - C - 32	
				DATE		2-14-78					

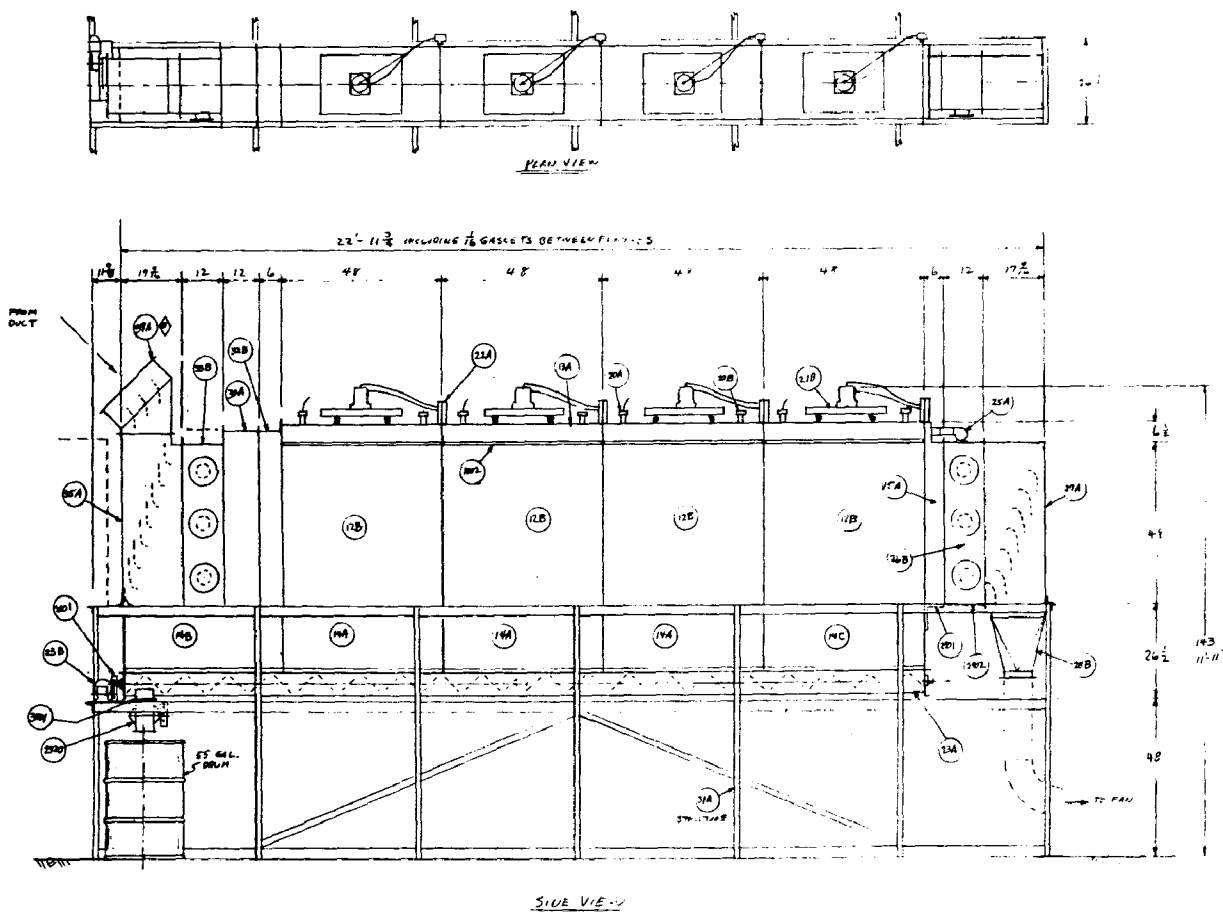


REV	DES	DATE	BY	DESCRIPTION
A	3301	2		FACE PLATES, 18-8 S.S., 18 GAGE .050 X 26 X 54
	3302	2		INNER SIDE PLATES, 18-8 S.S., 18 GAGE .050 X 13.8 X 48 BEND TO 11.9 X 1 CHANNEL
	3303	1		INNER TOP PLATE, 18-8 S.S., 18 GAGE .050 X 13.8 X 15 BEND TO 11.9 X 1 CHANNEL
	3304	2		OUTER SIDE PLATES, 18-8 S.S., 18 GAGE .050 X 15.8 X 52 BEND TO 11.9 X 2 CHANNEL
	3305	1		OUTER TOP PLATE, 18-8 S.S., 18 GAGE .050 X 15.8 X 22 BEND TO 11.9 X 2 CHANNEL
	3306	2		BOTTOM PLATE, 18-8 S.S., 18 GAGE .050 X 5 1/2 X 12
	3307	3		NIPPLE, 18-8 S.S. PIPE, 4" SCHED. 10, X 7.05 LONG
	3308	3 1/4		ITEM 2606 FLANGES CUBIC FEET OF INSULATION MATERIAL. INSTALL DURING FABRICATION, OK TO USE FIBERGLAS, MINERAL WOOL, OR FIBER FRAX.
B	3301	1		ASSY 33A
	3302	3		ITEM 2607 COVER
	3308	24		ITEM 2609 BOLTS

3-3-78	CHANGE TO XHEDIO	3307
DATE	REVISIONS	SOME NO.
SOUTHERN RESEARCH INSTITUTE BIRMINGHAM, ALABAMA 35205		
TITLE PLOT PRECIPITATOR		
INLET SAMPLING SECTION		
SCALE NOTED		
DATE 2-13-78		
3777-C-33		

TOLERANCES UNLESS OTHERWISE NOTED	
FRACTIONS	± 1/16
DECIMALS	± .010
ANGLES	± 1°
FINISH	
APPROVED	
CHECKED	PVB
DRAWN	NFWHLS

D-25



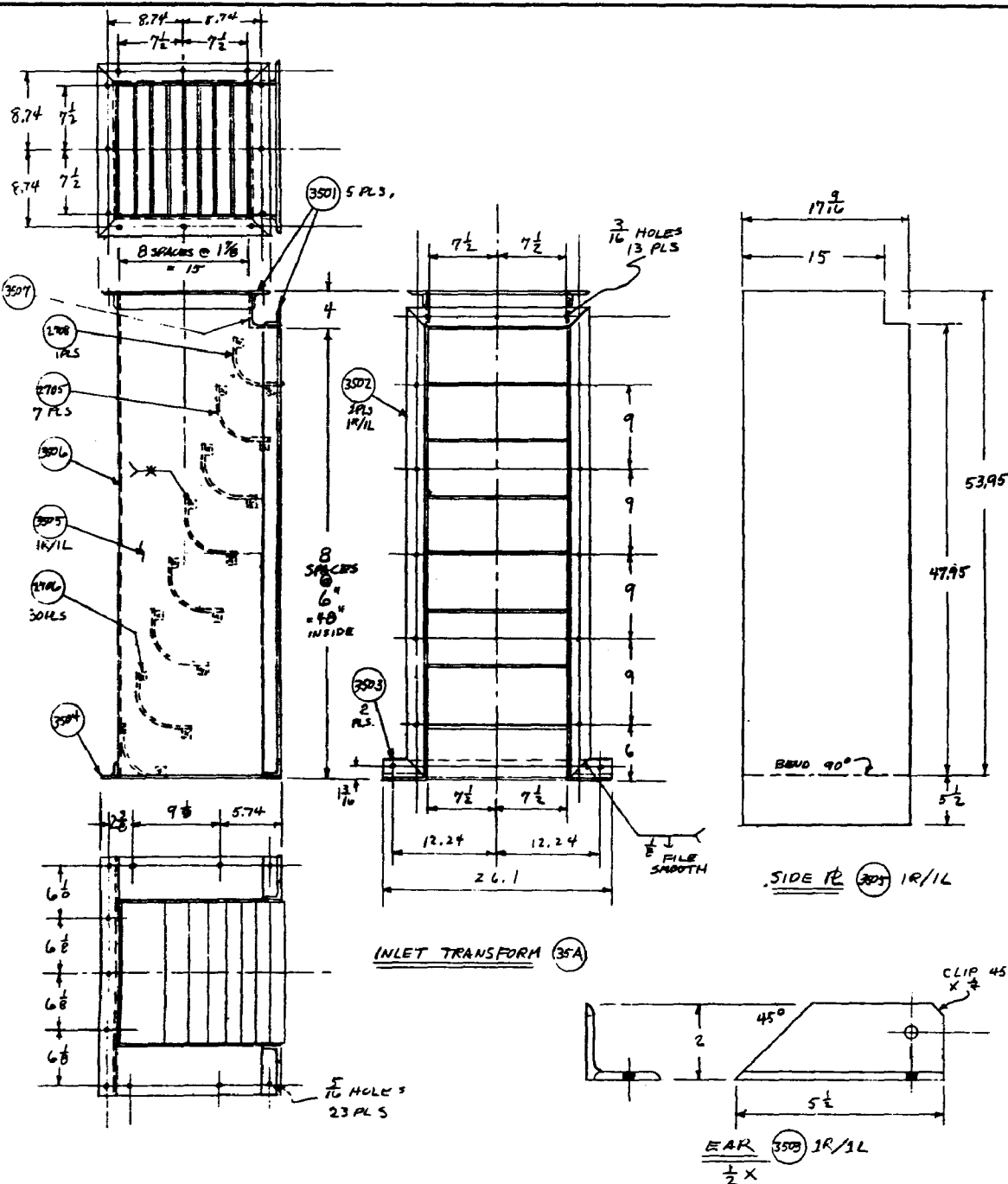
- | | | | |
|----|-----|-----------|------------------|
| 1 | 8 | A35V 12 A | END EC |
| 2 | 9 | A35V 12 A | COVER |
| 3 | 10 | A35V 12 A | TOPPER |
| 4 | 11 | A35V 14 B | INLET END PLUG |
| 5 | 12 | A35V 16 G | OUTLET AND PUMP |
| 6 | 13 | A35V 16 G | OUTLET AND PUMP |
| 7 | 14 | A35V 16 A | PULLEY/TIME GATE |
| 8 | 15 | A35V 17 D | SCREW ELYPTOR |
| 9 | 16 | A35V 17 D | SCREW ELYPTOR |
| 10 | 17 | A35V 18 G | TOP END PC |
| 11 | 18 | A35V 18 G | TOP END PC |
| 12 | 19 | A35V 18 G | TOP END PC |
| 13 | 20 | A35V 18 G | TOP END PC |
| 14 | 21 | A35V 18 G | TOP END PC |
| 15 | 22 | A35V 18 G | TOP END PC |
| 16 | 23 | A35V 18 G | TOP END PC |
| 17 | 24 | A35V 20 A | INSULATOR |
| 18 | 25 | A35V 20 A | INSULATOR |
| 19 | 26 | A35V 20 A | INSULATOR |
| 20 | 27 | A35V 20 A | INSULATOR |
| 21 | 28 | A35V 20 A | INSULATOR |
| 22 | 29 | A35V 20 A | INSULATOR |
| 23 | 30 | A35V 20 A | INSULATOR |
| 24 | 31 | A35V 20 A | INSULATOR |
| 25 | 32 | A35V 20 A | INSULATOR |
| 26 | 33 | A35V 20 A | INSULATOR |
| 27 | 34 | A35V 20 A | INSULATOR |
| 28 | 35 | A35V 20 A | INSULATOR |
| 29 | 36 | A35V 20 A | INSULATOR |
| 30 | 37 | A35V 20 A | INSULATOR |
| 31 | 38 | A35V 20 A | INSULATOR |
| 32 | 39 | A35V 20 A | INSULATOR |
| 33 | 40 | A35V 20 A | INSULATOR |
| 34 | 41 | A35V 20 A | INSULATOR |
| 35 | 42 | A35V 20 A | INSULATOR |
| 36 | 43 | A35V 20 A | INSULATOR |
| 37 | 44 | A35V 20 A | INSULATOR |
| 38 | 45 | A35V 20 A | INSULATOR |
| 39 | 46 | A35V 20 A | INSULATOR |
| 40 | 47 | A35V 20 A | INSULATOR |
| 41 | 48 | A35V 20 A | INSULATOR |
| 42 | 49 | A35V 20 A | INSULATOR |
| 43 | 50 | A35V 20 A | INSULATOR |
| 44 | 51 | A35V 20 A | INSULATOR |
| 45 | 52 | A35V 20 A | INSULATOR |
| 46 | 53 | A35V 20 A | INSULATOR |
| 47 | 54 | A35V 20 A | INSULATOR |
| 48 | 55 | A35V 20 A | INSULATOR |
| 49 | 56 | A35V 20 A | INSULATOR |
| 50 | 57 | A35V 20 A | INSULATOR |
| 51 | 58 | A35V 20 A | INSULATOR |
| 52 | 59 | A35V 20 A | INSULATOR |
| 53 | 60 | A35V 20 A | INSULATOR |
| 54 | 61 | A35V 20 A | INSULATOR |
| 55 | 62 | A35V 20 A | INSULATOR |
| 56 | 63 | A35V 20 A | INSULATOR |
| 57 | 64 | A35V 20 A | INSULATOR |
| 58 | 65 | A35V 20 A | INSULATOR |
| 59 | 66 | A35V 20 A | INSULATOR |
| 60 | 67 | A35V 20 A | INSULATOR |
| 61 | 68 | A35V 20 A | INSULATOR |
| 62 | 69 | A35V 20 A | INSULATOR |
| 63 | 70 | A35V 20 A | INSULATOR |
| 64 | 71 | A35V 20 A | INSULATOR |
| 65 | 72 | A35V 20 A | INSULATOR |
| 66 | 73 | A35V 20 A | INSULATOR |
| 67 | 74 | A35V 20 A | INSULATOR |
| 68 | 75 | A35V 20 A | INSULATOR |
| 69 | 76 | A35V 20 A | INSULATOR |
| 70 | 77 | A35V 20 A | INSULATOR |
| 71 | 78 | A35V 20 A | INSULATOR |
| 72 | 79 | A35V 20 A | INSULATOR |
| 73 | 80 | A35V 20 A | INSULATOR |
| 74 | 81 | A35V 20 A | INSULATOR |
| 75 | 82 | A35V 20 A | INSULATOR |
| 76 | 83 | A35V 20 A | INSULATOR |
| 77 | 84 | A35V 20 A | INSULATOR |
| 78 | 85 | A35V 20 A | INSULATOR |
| 79 | 86 | A35V 20 A | INSULATOR |
| 80 | 87 | A35V 20 A | INSULATOR |
| 81 | 88 | A35V 20 A | INSULATOR |
| 82 | 89 | A35V 20 A | INSULATOR |
| 83 | 90 | A35V 20 A | INSULATOR |
| 84 | 91 | A35V 20 A | INSULATOR |
| 85 | 92 | A35V 20 A | INSULATOR |
| 86 | 93 | A35V 20 A | INSULATOR |
| 87 | 94 | A35V 20 A | INSULATOR |
| 88 | 95 | A35V 20 A | INSULATOR |
| 89 | 96 | A35V 20 A | INSULATOR |
| 90 | 97 | A35V 20 A | INSULATOR |
| 91 | 98 | A35V 20 A | INSULATOR |
| 92 | 99 | A35V 20 A | INSULATOR |
| 93 | 100 | A35V 20 A | INSULATOR |


1 FAN AND DUCTWORK TO SUIT SITE.
SEE 3797-C-36 FOR PUMP ATTACHMENT.


2 SPECIAL TOOLS:
(1) ITEM 3116 ANGLE CUTTER
(2) ASSY 90-C INSULATOR ASSEMBLY WRENCH

3 DRAWING LIST: 377-C-10 THRU D-16 EXCEPT 19

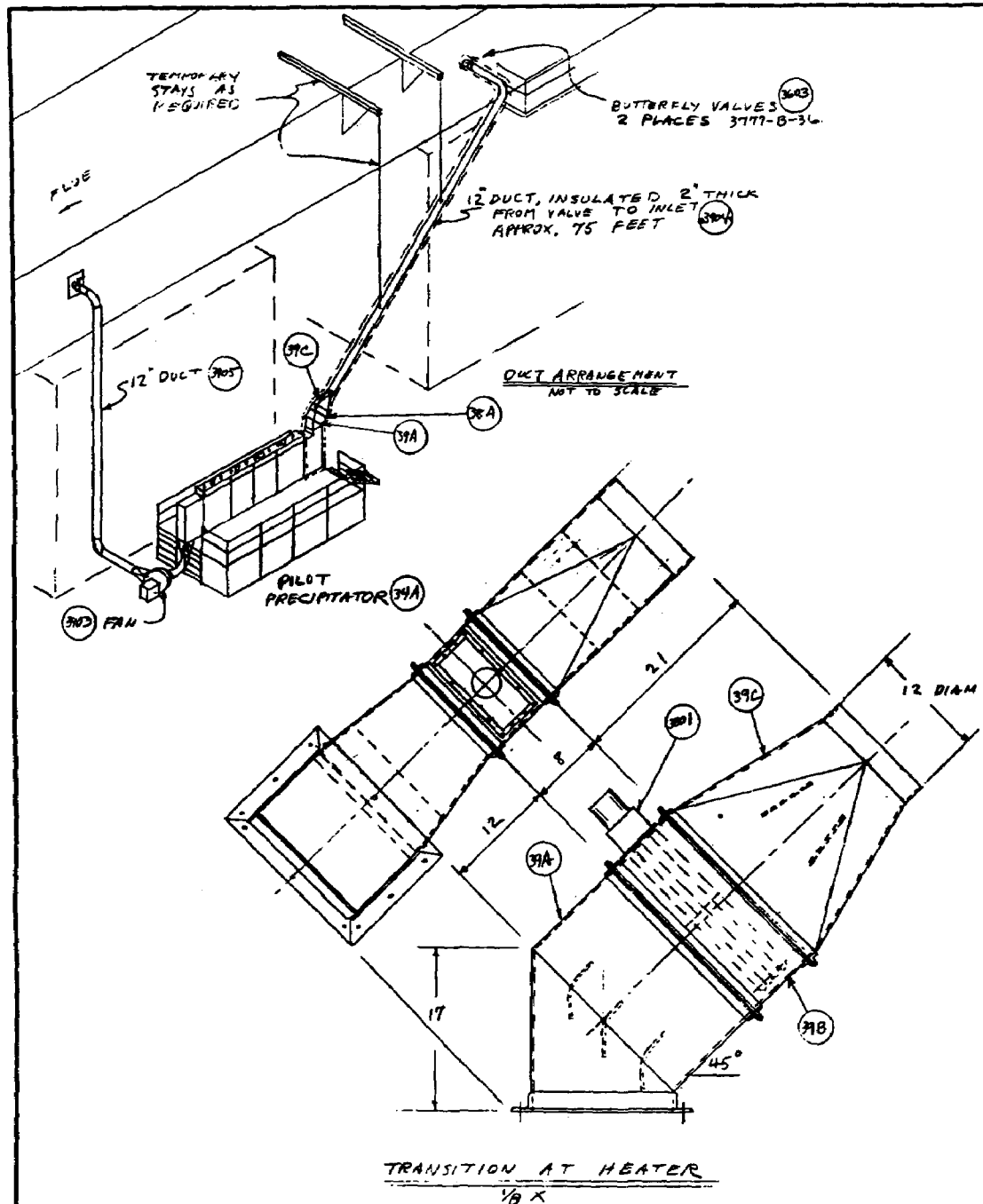
3-7-78	CHANGE GLOWN TO "A"	WFA
3-7-78	ADD AMMUNITION PLATES	WFA
DATE	REVISION	TIME
<p>SOUTHERN RESEARCH INSTITUTION BIRMINGHAM, ALABAMA 35203</p>		
TITLE		
PLOT PRECIPITATOR		
ASSEMBLY		
<p>APPROVED</p> <p>CHECKED WFA SCALE 1/2 DRG. NO. 3777-D-34</p> <p>QUANTITY 100 DATE 3-7-78</p>		



QTY.	ITEM	SIZE	DESCRIPTION	REMARKS
	3501	5	ANGLE FLANGE, SHORT, 18-8 S.S. 2x2x $\frac{1}{8}$ x 19.1 LONG	
	3502	2	ANGLE FLANGE, LONG, 18-8 S.S. 2x2x $\frac{1}{8}$ x 50 LONG, 1 R/1L	
	3503	2	EAK, 18-8 S.S. ANGLE 2x2x $\frac{1}{8}$ x 5 $\frac{1}{2}$ LG.	
	3504	1	SUPPORT ANGLE, 18-8 S.S., 2x2x $\frac{1}{8}$ x 26.1	
A	→	7	ITEM 2705	
	→	1	ITEM 2708	
	→	30	ITEM 2706	
	3505	2	SIDE RAKE, 18-8 S.S., 15 GAGE .050 x 17 $\frac{1}{16}$ x 57.45, MAKE 1 R/1L	
3506	1	BACK RAKE, 18-8 S.S., 18 GAGE .050 x 15 x 52		
3507	1	FRONT RAKE, 18-8 S.S., 18 GAGE .050 x 6.46 x 15, BEND INTO ANGLE 2.51 x 3.95 INSIDE LEGS.		
			WELD TOGETHER AIR TIGHT, SPOT WELD CLIPS & VANES	

1  O.K. TO CHANGE DETAILS OF DRAGING
AND WELDING TO SUIT SHOP METHODS.
O.K. TO SUBSTITUTE FOR RIVETS FOR SPOT
WELDING OF 2705, 2706 & 2708

3-5-78		ADD NOTE 1				DATE		REVISES		ZONE		MC	
TOLERANCES UNLESS OTHERWISE NOTED				SOUTHERN RESEARCH INSTITUTE BIRMINGHAM, ALABAMA 35205									
FRACTIONS		1/2		1/4		1/8		1/16		1/32		1/64	
DECIMALS		0.010		0.005		0.002		0.001		0.0005		0.0002	
ANGLES		1/2		1/4		1/8		1/16		1/32		1/64	
FINISH		1/2		1/4		1/8		1/16		1/32		1/64	
APPROVED				TITLE PILOT PRECIPITATOR									
				INLET TRANSFORM									
CHECKED		PVB		SCALE		1/8		DWG. NO.		3777 -C-35			
DRAWN		AFRANCIS		DATE		2-10-78							

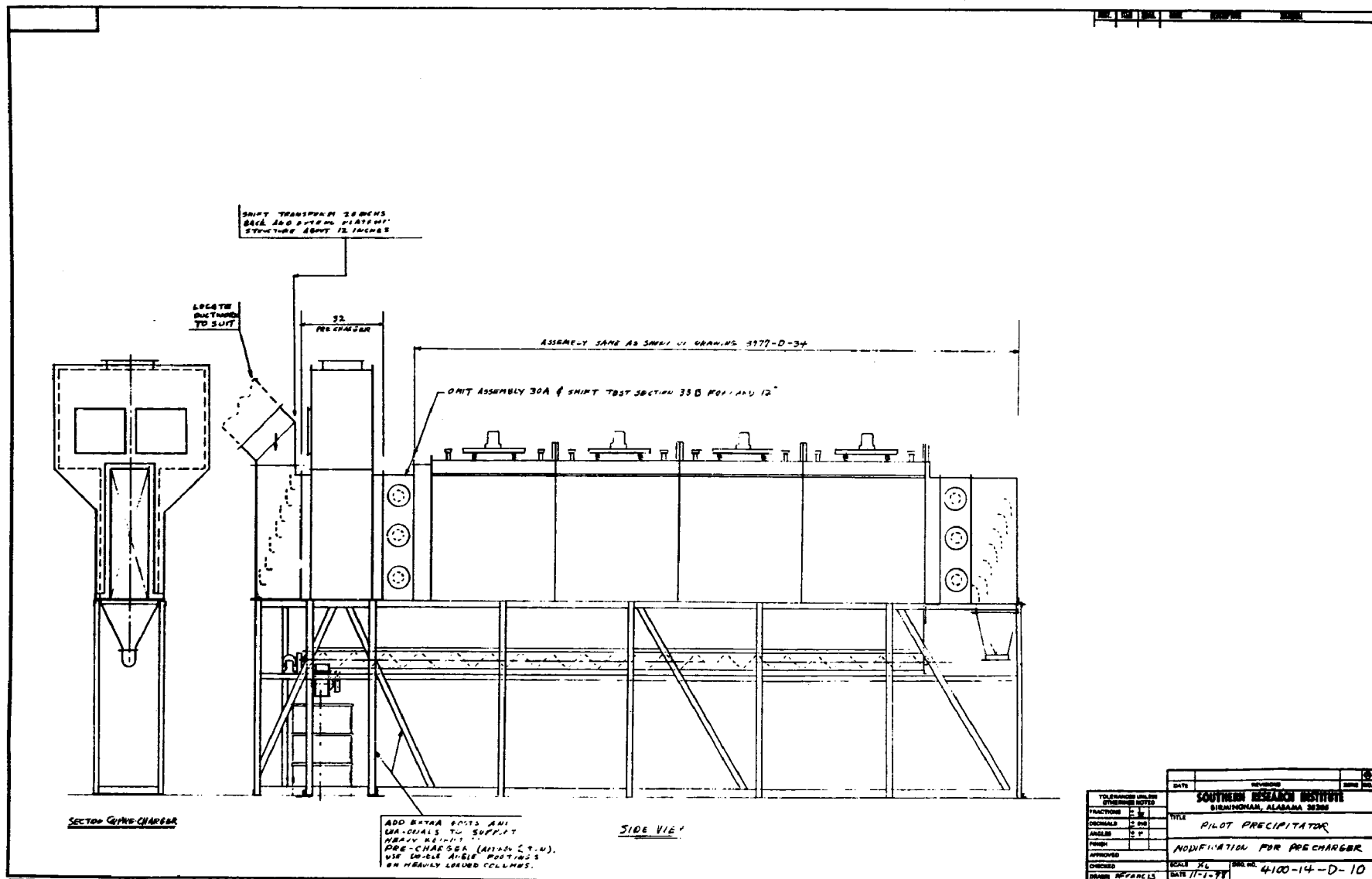


REV.	DATE	BY	DESCRIPTION
A	3801	1	HEATER, PROCESS DUCT, CHROMALOX TDH-6 C, 240 VOLT 3 PHASE 60 CYCLE, 6 KW AT 22 W/IN ² TO HEAT 3000 CFM OF AIR FROM 260°F TO 270°F
	3802	10	455'Y 39-B HOUSING, SCREWS, SHEET METAL, S.S., SELF TAPPING, GINLET POINT, PEN HEAD, #8 X 1/2 LONG. NC NUTS-CARR #91632 A
	3803	1	BLOWER FOR 3000 CFM AT 6 1/2" S.P. AT 270°F. NEWTON'S BLOWER PL 128 @ 3930 RPM 3/4" 3.1 HP NET / 4.3 HP GROSS OR EQUAL
	3804	1	ITEM OF DUCT WORK 12" DIAM. FROM FLUE TO PRECIPITATOR. INSULATE WITH 2" OF FIBERGLAS OR ROCK WOOL (BY LOCAL CONTRACTOR)
	3805	1	ITEM OF DUCT WORK 12" EQUIV. DIAM. FROM PRECIPITATOR TO FAN AND FROM FAN TO FLUE. NOT INSULATED (BY LOCAL CONTRACTOR)

4-278	REDRAWN		
DATE	REVISIONS		ZONE NO.
TOLERANCES UNLESS OTHERWISE NOTED			
FRACTIONS	± 1/32		
DECIMALS	± .010		
ANGLES	± 1°		
FINISH			
APPROVED			
CHECKED		SCALE NOTED	DWG. NO.
DRAWN	A. F. 115	DATE 4-2-78	3777-C-38

SOUTHERN RESEARCH INSTITUTE
BIRMINGHAM, ALABAMA 35205TITLE
PILOT PRECIPITATOR

DUCT ARRANGEMENT



TECHNICAL REPORT DATA

(Please read instructions on the reverse before completing)

1. REPORT NO. EPA-600/7-79-189		2.	3. RECIPIENT'S ACCESSION NO.	
4. TITLE AND SUBTITLE Electrostatic Precipitators for Collection of High Resistivity Ash			5. REPORT DATE August 1979	
			6. PERFORMING ORGANIZATION CODE	
7. AUTHOR(S) D. H. Pontius, P. V. Bush, and W. B. Smith			8. PERFORMING ORGANIZATION REPORT NO.	
9. PERFORMING ORGANIZATION NAME AND ADDRESS Southern Research Institute 2000 Ninth Avenue, South Birmingham, Alabama 35205			10. PROGRAM ELEMENT NO. EHE624	
			11. CONTRACT/GRANT NO. 68-02-2193	
12. SPONSORING AGENCY NAME AND ADDRESS EPA, Office of Research and Development Industrial Environmental Research Laboratory Research Triangle Park, NC 27711			13. TYPE OF REPORT AND PERIOD COVERED Final; 11/76 - 1/79	
			14. SPONSORING AGENCY CODE EPA/600/13	
15. SUPPLEMENTARY NOTES IERL-RTP project officer is Leslie E. Sparks, Mail Drop 61, 919/541-2925.				
16. ABSTRACT The report gives results of a research program to: (1) compare various electrode systems for charging fine high-resistivity dusts; (2) investigate techniques for charging the dusts in a high current density corona system; (3) perform a laboratory scale feasibility study of selected charging systems; and (4) design, fabricate, and test a 0.47 cu m/sec (1000 acfm) pilot-scale precharger for application to a two-stage system for electrostatic precipitation of high resistivity particulates. A literature review of previous attempts to control back corona caused by high resistivity dusts, and limited theoretical and experimental investigations: eliminated the impracticable and evaluated potentially useful approaches to the development of charging systems for high resistivity dust, and resulted in the derivation of a new three-electrode particle precharger, upon which further developments were based. The three-electrode concept, tested in a small laboratory device, charged high resistivity dusts to levels achievable only on low and moderate resistivity dusts in conventional systems. Charging results remained good for a pilot scale system designed, built, and tested at a gas volume flowrate of 0.47 cu m/sec. A rugged version of the pilot scale precharger was tested as a part of a two-stage system, where the collector was a modified pilot scale ESP. The new technique has economic potential.				
17. KEY WORDS AND DOCUMENT ANALYSIS				
a. DESCRIPTORS		b. IDENTIFIERS/OPEN ENDED TERMS		c. COSATI Field/Group
Pollution Coronas Electrostatic Precipitators Dust Ashes Electrical Resistivity Electrodes		Pollution Control Stationary Sources High Resistivity Dusts		13B 13I 11G 21B 20C 09A
18. DISTRIBUTION STATEMENT		19. SECURITY CLASS (This Report)		21. NO. OF PAGES
Release to Public		Unclassified		187
		20. SECURITY CLASS (This page)		22. PRICE
		Unclassified		